



## WATER OXIDATION WITH MONONUCLEAR RU COMPLEXES. BELOW THE TIP OF THE ICEBERG: THE OXO-BRIDGE SCENARIO

**Isidoro López Marin**  
Dipòsit Legal: T. 1505-2013

**ADVERTIMENT.** L'accés als continguts d'aquesta tesi doctoral i la seva utilització ha de respectar els drets de la persona autora. Pot ser utilitzada per a consulta o estudi personal, així com en activitats o materials d'investigació i docència en els termes establerts a l'art. 32 del Text Refós de la Llei de Propietat Intel·lectual (RDL 1/1996). Per altres utilitzacions es requereix l'autorització prèvia i expressa de la persona autora. En qualsevol cas, en la utilització dels seus continguts caldrà indicar de forma clara el nom i cognoms de la persona autora i el títol de la tesi doctoral. No s'autoritza la seva reproducció o altres formes d'explotació efectuades amb finalitats de lucre ni la seva comunicació pública des d'un lloc aliè al servei TDX. Tampoc s'autoritza la presentació del seu contingut en una finestra o marc aliè a TDX (framing). Aquesta reserva de drets afecta tant als continguts de la tesi com als seus resums i índexs.

**ADVERTENCIA.** El acceso a los contenidos de esta tesis doctoral y su utilización debe respetar los derechos de la persona autora. Puede ser utilizada para consulta o estudio personal, así como en actividades o materiales de investigación y docencia en los términos establecidos en el art. 32 del Texto Refundido de la Ley de Propiedad Intelectual (RDL 1/1996). Para otros usos se requiere la autorización previa y expresa de la persona autora. En cualquier caso, en la utilización de sus contenidos se deberá indicar de forma clara el nombre y apellidos de la persona autora y el título de la tesis doctoral. No se autoriza su reproducción u otras formas de explotación efectuadas con fines lucrativos ni su comunicación pública desde un sitio ajeno al servicio TDR. Tampoco se autoriza la presentación de su contenido en una ventana o marco ajeno a TDR (framing). Esta reserva de derechos afecta tanto al contenido de la tesis como a sus resúmenes e índices.

**WARNING.** Access to the contents of this doctoral thesis and its use must respect the rights of the author. It can be used for reference or private study, as well as research and learning activities or materials in the terms established by the 32nd article of the Spanish Consolidated Copyright Act (RDL 1/1996). Express and previous authorization of the author is required for any other uses. In any case, when using its content, full name of the author and title of the thesis must be clearly indicated. Reproduction or other forms of for profit use or public communication from outside TDX service is not allowed. Presentation of its content in a window or frame external to TDX (framing) is not authorized either. These rights affect both the content of the thesis and its abstracts and indexes.

UNIVERSITAT ROVIRA I VIRGILI

WATER OXIDATION WITH MONONUCLEAR RU COMPLEXES. BELOW THE TIP OF THE

ICEBERG: THE OXO-BRIDGE SCENARIO

Isidoro López Marin

Dipòsit Legal: T. 1505-2013

UNIVERSITAT ROVIRA I VIRGILI

WATER OXIDATION WITH MONONUCLEAR RU COMPLEXES. BELOW THE TIP OF THE

ICEBERG: THE OXO-BRIDGE SCENARIO

Isidoro López Marin

Dipòsit Legal: T. 1505-2013

# Water oxidation with mononuclear Ru complexes. Below the tip of the iceberg: the oxo- bridge scenario.

Ph.D. Thesis presented by

*Isidoro López Marín*

In candidacy for the degree of  
Doctor of Philosophy in Chemistry

Supervised by

*Prof. Antoni Llobet Dalmases*

2013



UNIVERSITAT ROVIRA I VIRGILI

UNIVERSITAT ROVIRA I VIRGILI

WATER OXIDATION WITH MONONUCLEAR RU COMPLEXES. BELOW THE TIP OF THE

ICEBERG: THE OXO-BRIDGE SCENARIO

Isidoro López Marin

Dipòsit Legal: T. 1505-2013



UNIVERSITAT ROVIRA I VIRGILI

FAIG CONSTAR que aquest treball, titulat “Water oxidation with mononuclear Ru complexes. Below the tip of the iceberg: the oxo-bridge scenario”, que presenta Isidoro López Marín per a l’obtenció del títol de Doctor, ha estat realitzat sota la meva direcció al Institut Català d’Investigació Química (ICIQ).

El director de la tesi doctoral

Prof. Antoni Llobet i Dalmases.

Tarragona, juliol de 2013

UNIVERSITAT ROVIRA I VIRGILI

WATER OXIDATION WITH MONONUCLEAR RU COMPLEXES. BELOW THE TIP OF THE

ICEBERG: THE OXO-BRIDGE SCENARIO

Isidoro López Marin

Dipòsit Legal: T. 1505-2013

UNIVERSITAT ROVIRA I VIRGILI

WATER OXIDATION WITH MONONUCLEAR RU COMPLEXES. BELOW THE TIP OF THE

ICEBERG: THE OXO-BRIDGE SCENARIO

Isidoro López Marin

Dipòsit Legal: T. 1505-2013

*A mi madre*



UNIVERSITAT ROVIRA I VIRGILI

WATER OXIDATION WITH MONONUCLEAR RU COMPLEXES. BELOW THE TIP OF THE

ICEBERG: THE OXO-BRIDGE SCENARIO

Isidoro López Marin

Dipòsit Legal: T. 1505-2013

## **Acknowledgments.**

I would like to thank to all the people that have helped me to carry out my thesis. I will do it in catalan as a simple tribute to Tarragona and Catalonia because I feel I owe to this city and this land.

Aquest treball no hagués sigut possible sense la intervenció, els savis consells i el suport de moltes persones. Serveixin aquestes poques línies per a agrair la seva invaluable aportació per a tirar endavant aquest projecte.

En primer lloc, vull agrair al Toni l'oportunitat que em va donar de fer investigació al seu grup durant tres mesos, que s'han convertit ja en més de cinc anys. Gràcies per la teva disponibilitat, els teus ànims i, per descomptat, per compatir el teu magisteri i la teva passió per la química amb mi.

Voldria també agrair a tots els companys del grup, als que hi són ara i als que ja han marxat. Tinc la sort d'haver coincidit amb molta gent amable, simpàtica i disposada a oferir-me la seva ajuda quan la necessitava. La llista és tan llarga que espero no oblidar a ningú: Carlo, Lydia, Nora, Xavi, Fernando, Stephan, Sophie, Laura, Pau, Lorenzo, Tomek, Roc, Joan, Craig, Carolina, Samuel, Serena, Thibaut, Miguel, Maria José, Tina, Paula, Josep, Francesca, Pablo i Edyta. Voldria destacar a la Chiara per introduir-me en el món de la investigació amb un somriure sempre a la cara, al Somnath per aconseguir culminar junts tants projectes lluitant amb mi braç a braç, a la Laia perquè a més de ser una bona amiga ha tingut la santa paciència de socórrer-me en les correccions d'aquestes gairebé tres-centes cinquanta pàgines. Gràcies també als visitants que hem tingut al grup com l'Arianna, la Stephanie, l'Ana i la Rebecca; particularment al Sven perquè hem compartit moltes alegries i malts de cap en el projecte en el que col·laborem. De tots ells me n'emporto a més de la seva contribució científica o administrativa, milers de moments agradables dels que

hem gaudit tant dins com fora del laboratori. A part de la gent del meu grup, agraeixo l'amistat de molts companys de l'ICIQ. No els enumeraré perquè em mancaria espai i de ben segur me'n deixaria una bona pila; llevat d'en Josep perquè és un monstre, i no perquè sigui capaç de menjar-se un kebab doble amb patates i una gerra gran de cervesa, sinó per tot els riures que hem fet. També vull mostrar la meva gratitud als departaments de suport a la recerca de l'ICIQ, que han manifestat el seu interès per la meva recerca i han estat prestos per donar-me un cop de mà. Gràcies al professor Peter Hildebrandt, a l'Uwe Kuhlmann i a l'Anke Keidel per acollir-me durant una setmana al seu grup, per dur a terme les mesures de rRAMAN i per les enriquidores discussions dels espectres.

Per altre banda, volia agrair a la gent del Màster: Núria, Moira, Míriam, Mercè, Oriol i Cristina. Vàrem formar una colla que farà enveja a les posteriors promocions durant anys. Gràcies Oriol, que et podria dir?, m'has fet sentir com si et conegués des de fa vint anys; has sigut i ets el meu millor amic a Tarragona. Brindo perquè aquesta amistat perduri per sempre.

Gràcies als meus "quimicuchos sevillanos": Jose, Luisca, Sergio, Ro, Fati, Eu, Toñi, Jose Manuel (quimicucho adoptat), Àguila (una altra catalanduza com jo) i María. Us porto al meu cor i em feu molt difícil tornar al nord després de baixar. Vull fer un agraïment especial al Jose perquè sense la teva il·lusió i el teu esperit aventurer científic mai hagués anat a parar a Tarragona, gràcies també per tot el que hem viscut aquí i allà, i el que ens queda per viure sap Déu on.

No puc deixar-me a quatre dels cinc magnífics *fuentecanteños* (jo sóc el cinquè!): Antonio, Javi, Colero i Bayón. Encara que la vida ens hagi escampat

per Espanya i més enllà, som una família i la vostra fe en mi m'ha recolzat durant aquest temps, malgrat que a vegades m'inundi la nostàlgia.

Agraeixo a la meva família el seu suport, el seu afecte i el seu encoratjament. Dono gràcies a Déu pels meus avis, que descansin en pau, perquè sense el seu sacrifici, la seva labor fatigosa de la terra allà a la serra nord de Sevilla i la seva humilitat mai hagués aspirat a fer un doctorat, veieu on he arribat avis? Gràcies als meus tiets, la Dolores i en Manolo, i a la meva cosina, la Paula, per la seva confiança i els seus ànims. Gràcies al meu pare per despertar en mi el *gusanillo de la curiosidad* i el seu zel pel meu benestar. Gràcies a la meva germana per la seva alegria, la seva tendresa i la seva energia. I a tu que et diré mamá? De tu neix la meva fortalesa, la meva persistència, la meva cultura, la meva manera de veure el món i la meva fe.

Vull agrair a la Maribel i a la seva família perquè cada cop que he anat a Salt m'han fet sentir com si estigués a casa meva i d'aquesta manera alleujar la pressió de la tesi. Gràcies Maribel per la teva vitalitat, el teu suport, la teva paciència amb mi i les teves atencions quan les he necessitat, mai m'has fallat. Fas que cada nou dia tingui una vida que mereix ser viscuda.

Finalment, voldria agrair a tots els químics honests que m'han precedit i que com jo, han volgut aportar el seu coneixement i el seu esforç en servei del progrés de la humanitat. Sense el seu llegat; la passió, la voluntat i la curiositat per explorar l'univers que sentim els que fem ciència no tindria cap sentit.

The work performed in the present doctoral thesis has been possible thanks to the funding of:

- ▣ Institut Català d'Investigació Química (ICIQ)
- ▣ Ministerio de Educación. Beca FPU: AP-2008-02350
- ▣ Ministerio de Ciencia e Innovación CTQ2010-21497
- ▣ AGAUR
- ▣ Ministerio de Ciencia e Innovación dentro del Programa Nacional de Internacionalización de la I+D (Proyectos y Acciones Internacionales )
- ▣ European Commission, SOLAR-H2



UNIVERSITAT ROVIRA I VIRGILI

WATER OXIDATION WITH MONONUCLEAR RU COMPLEXES. BELOW THE TIP OF THE

ICEBERG: THE OXO-BRIDGE SCENARIO

Isidoro López Marin

Dipòsit Legal: T. 1505-2013

UNIVERSITAT ROVIRA I VIRGILI

WATER OXIDATION WITH MONONUCLEAR RU COMPLEXES. BELOW THE TIP OF THE

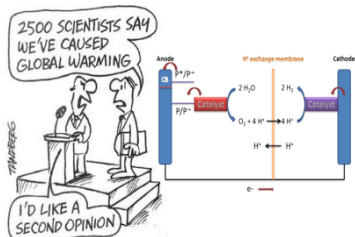
ICEBERG: THE OXO-BRIDGE SCENARIO

Isidoro López Marin

Dipòsit Legal: T. 1505-2013

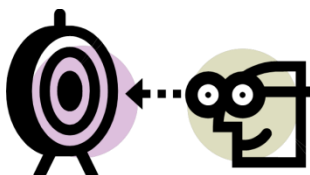
## Graphical Abstracts

### Chapter 1. General Introduction.

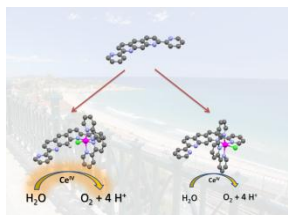


General introduction about the current environmental and energetic challenges that mankind faces. Solar fuels are a promissory solution and are based on Photosynthesis. In order to mimic it, an efficient and robust water oxidation catalyst (WOC) must be developed. Polypyridilic aquo Ru complexes are promissory candidates, although new systems based on other metals such as Ir, Mn, Co, Cu and Fe, even organocatalysts, are emerging.

### Chapter 2. Objectives.



### Chapter 3. New mononuclear Ru complexes containing the bipan ligand and their activity toward catalytic water oxidation.

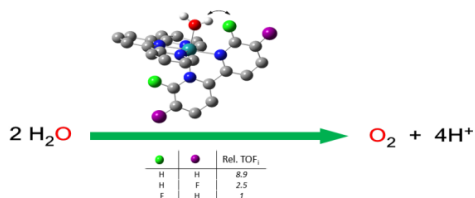


New mononuclear Ru complexes containing the ligand 2,7-bipyridil-1,8-diazaanthracene (bipan) have been synthesized and fully characterized. The compounds were evaluated as water oxidation catalysts. The *in*-isomer exhibits a good activity in the order of structurally related mononuclear complexes whereas the *out*-isomer is a poor catalyst due to its insolubility under catalytic conditions.



---

### Chapter 4. Mononuclear Ru water oxidation catalysts: Discerning between electronic and hydrogen bonding effects.

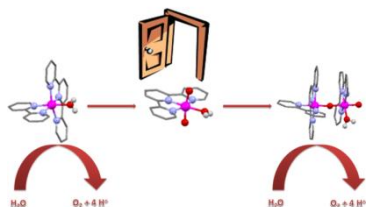


New mononuclear complexes of general formula  $[\text{Ru}(\text{trpy})(n,n'\text{-F}_2\text{-bpy})\text{X}]^{\text{m}+}$ , ( $n = n' = 5$ :  $\text{X} = \text{Cl}$ ,  $3^+$  and  $\text{X} = \text{H}_2\text{O}$ ,  $5^{2+}$ ;  $n = n' = 6$ :  $\text{X} = \text{Cl}$ ,  $4^+$  and  $\text{X} = \text{H}_2\text{O}$ ,  $6^{2+}$ ; trpy is 2,2':6',2''-terpyridine) have been prepared and thoroughly characterized. The 5,5'- and 6,6'- $\text{F}_2\text{-bpy}$  ligands allow exerting a remote

electronic perturbation to the Ru metal center that affects at the combination of species involved in the catalytic cycle. Additionally the 6,6'- $\text{F}_2\text{-bpy}$  also allows to interact through space with the Ru-O moiety of the complex via hydrogen bonding.

---

### Chapter 5. A Self Improved Water Oxidation Catalyst, Is One Site Really Enough?

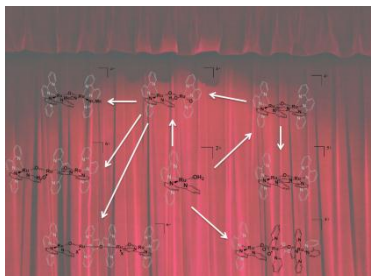


We show for the first time that highly active mononuclear Ru-aqua water oxidation catalysts are transformed into dinuclear complexes during oxygen evolution catalysis, even from the very beginning of the catalytic process. The new dinuclear species are much more robust than their mononuclear counterparts and remain active catalyst for the water oxidation, establishing the coexistence

of two different catalytic cycles in solution.

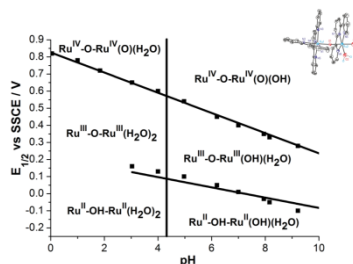
---

### Chapter 6. Behind Water Oxidation with Mononuclear Ru Complexes: The Oxo-bridge Scenario.



Water oxidation catalysts (WOCs) based on mononuclear Ru complexes related to  $[\text{Ru}(\text{trpy})(\text{bpy})(\text{H}_2\text{O})]^{2+}$  (where trpy is 2,2':6',2''-terpyridine and bpy is 2,2'-bipyridine) generate dinuclear oxo bridge complexes throughout or after the catalytic cycle which have remained unnoticed. The new dimer compound  $\{[\text{Ru}(\text{trpy})(\text{bpy})]_2(\mu\text{-O})\}^{4+}$  (**1-dm**<sup>4+</sup>) has been synthesized and completely characterized. The reactivity of this complex and previous known *O*-terminal dinuclear Ru complexes draws an oxo-bridge scenario of interconnected oxo bridge molecules with diverse nuclearity.

### Chapter 7. Exploring the properties of rugged oxo-bridge dinuclear water oxidation catalysts and its relationship with mononuclear catalysts.



The complete electrochemical and spectroscopic characterization of the dinuclear complexes  $[(\text{trpy})(5,5'\text{-X}_2\text{-bpy})\text{Ru}^{\text{IV}}(\mu\text{-O})\text{Ru}^{\text{IV}}(\text{trpy})(\text{O})(\text{H}_2\text{O})]^{4+}$  ( $\text{X} = \text{H}$ , **1-dn**<sup>4+</sup>;  $\text{X} = \text{F}$ , **2-dn**<sup>4+</sup>) has been accomplished. Additionally new rRAMAN spectroscopic studies evidence the conversion of the high oxidation states of the mononuclear complexes  $[\text{Ru}(\text{trpy})(5,5'\text{-F}_2\text{-Bpy})(\text{H}_2\text{O})]^{2+}$  ( $\text{X} = \text{H}$ , **1**<sup>2+</sup>;  $\text{X} = \text{F}$ , **2**<sup>4+</sup>) into its dinuclear counterparts, **1-dn**<sup>4+</sup> and **2-dn**<sup>4+</sup> respectively, *via* the formation of *trans*- $[\text{Ru}^{\text{VI}}(\text{trpy})(\text{O})_2(\text{H}_2\text{O})]^{2+}$  (**3**<sup>2+</sup>).

### Chapter 8. Conclusions.



UNIVERSITAT ROVIRA I VIRGILI

WATER OXIDATION WITH MONONUCLEAR RU COMPLEXES. BELOW THE TIP OF THE

ICEBERG: THE OXO-BRIDGE SCENARIO

Isidoro López Marin

Dipòsit Legal: T. 1505-2013

## **Table of Contents.**

Graphical Abstracts.	I
Tables of Contents.	V
Glossary of Terms and Abbreviations.	IX
<b>Chapter 1. General Introduction.</b>	<b>1-71</b>
1.1. <i>The dichotomy between energy demand and climate change.</i>	5
1.2. <i>Solar fuels.</i>	13
1.3. <i>Water Oxidation catalysis.</i>	24
1.4. <i>References.</i>	63
<b>Chapter 2. Objectives.</b>	<b>73-75</b>
<b>Chapter 3. New mononuclear Ru complexes containing the bipan ligand and their activity toward catalytic water oxidation.</b>	<b>77-116</b>
3.1. <i>Introduction.</i>	81
3.2. <i>Experimental Section.</i>	83
3.3. <i>Results and discussion.</i>	87
3.4. <i>Conclusions.</i>	98
3.5. <i>Acknowledgments.</i>	99

3.6. <i>References.</i>	99
3.7. <i>Supporting information.</i>	103
<b>Chapter 4. Mononuclear Ru water oxidation catalysts: Discerning between electronic and hydrogen bonding effects.</b>	<b>117-171</b>
4.1. <i>Introduction.</i>	121
4.2. <i>Results and discussion.</i>	122
4.3. <i>Conclusions.</i>	128
4.4. <i>Acknowledgements.</i>	128
4.5. <i>References.</i>	129
4.6. <i>Supporting information.</i>	131
<b>Chapter 5. A Self Improved Water Oxidation Catalyst, Is One Site Really Enough?</b>	<b>173-217</b>
5.1. <i>Introduction.</i>	177
5.2. <i>Results and discussion.</i>	179
5.3. <i>Conclusions.</i>	187
5.4. <i>Acknowledgements.</i>	187
5.5. <i>References.</i>	188
5.6. <i>Supporting Information.</i>	191

<b>Chapter 6. Behind water oxidation with mononuclear Ru complexes:</b>	<b>219-273</b>
<b>The oxo-bridge scenario.</b>	
6.1. <i>Introduction.</i>	223
6.2. <i>Experimental Section.</i>	225
6.3. <i>Results and discussion.</i>	229
6.4. <i>Conclusions.</i>	251
6.5. <i>Acknowledgements.</i>	252
6.6. <i>References.</i>	252
6.7. <i>Supporting information.</i>	257
<b>Chapter 7. Exploring the properties of rugged oxo-bridge dinuclear</b>	<b>275-320</b>
<b>water oxidation catalysts and its relationship with mononuclear</b>	
<b>catalyst.</b>	
7.1. <i>Introduction.</i>	279
7.2. <i>Experimental Section.</i>	282
7.3. <i>Results and discussion.</i>	285
7.4. <i>Conclusions.</i>	304
7.5. <i>Acknowledgements.</i>	306
7.6. <i>References.</i>	306

7.7. <i>Supporting information.</i>	309
<b>Chapter 8. Summary and Conclusions.</b>	<b>321-327</b>
<b>Appendix: Contributions to Congress.</b>	<b>329-333</b>

## Glossary of terms and abbreviations.

1D	Monodimensional
2D	Bidimensional
AcO <sup>-</sup>	Acetate
BBDE	Boron-doped diamond electrode
Bipan	2,7-bipyridil-1,8-diazaanthracene
Bpy	2,2'-bipyridine
COSY	Correlation spectroscopy
CPE	Controlled potential electrolysis
CV	Cyclic voltammetry
d	Doublet
$\delta$	Chemical shift
DCM	Dicloromethane
DFT	Density functional theory
dmso	Dimethyl sulfoxide
DOSY	Diffusion Ordered NMR Spectroscopy
DPV	Differential pulse voltammetry
E	Potential
E <sup>0</sup>	Standard potential
E <sub>1/2</sub>	Half wave potential
E <sub>p,a</sub>	Anodic peak potential
E <sub>p,c</sub>	Cathodic peak potential
ESI-MS	Electrospray ionization mass spectrometry
ET	Electron transfer
FTO	Fluorinated-doped Tin Oxide
GC	Glassy carbon



HOTf	Trifluoromethanesulfonic acid or triflic acid
ITO	Indium tin oxide
J	Coupling constant
j	Current density
$\lambda$	Wavelength
M	Molar
m	Multiplet
$\mu$	Ionic force
$\mu\text{A}$	Microampere
m/z	Mass-to-charge ratio
MLCT	Metal to ligand charge transfer
MS	Mass spectrometry
NADPH	Nicotinamide adenine dinucleotide phosphate
<i>n</i> -Bu <sub>4</sub> NPF <sub>6</sub>	Tetra( <i>N</i> -butyl)ammonium hexafluorophosphate
NHE	Normal hydrogen electrode
NMR	Nuclear magnetic resonance
NOESY	Nuclear Overhousser spectroscopy
OEC	Oxygen evolving center
Ortep	Oak Ridge thermal ellipsoid plot
PCET	Proton coupled electron transfer
Ph	Phenyl
Pic	2-picolinate
POM	Polyoxometalate
ppm	Parts per millon
PSI	Photosystem I
PSII	Photosystem II

PT	Proton transfer
Py	Pyridine
rds	Rate determining step
rRAMAN, RR	Resonance RAMAN spectroscopy
RT	Room temperature
s	Singlet, second
SSCE	Sodium saturated Calomel electrode
SPS	Solvent purification system
t	Triplet
TBAH	Tetra( <i>N</i> -butyl)ammonium hexafluorophosphate
TOF	Turn over frequency
TON	Turn over number
Trpy	2,2':6',2''-terpyridine
UV-vis	Ultraviolet-visible spectroscopy
V	Volt
WOC	Water oxidation catalyst
XRD	X-Ray diffraction

UNIVERSITAT ROVIRA I VIRGILI

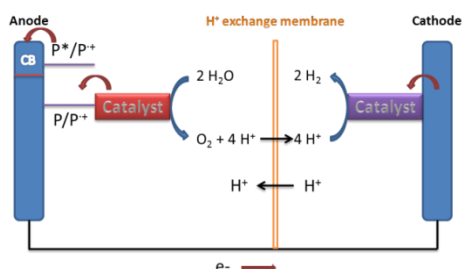
WATER OXIDATION WITH MONONUCLEAR RU COMPLEXES. BELOW THE TIP OF THE

ICEBERG: THE OXO-BRIDGE SCENARIO

Isidoro López Marin

Dipòsit Legal: T. 1505-2013

## Chapter 1. General Introduction.



The conversion of sunlight into solar fuels has become a promissory candidate for replacing carbon-based energy resources. The effective formation of  $\text{H}_2$  on the *cathode* of the simplest photoelectrochemical cell prototype requires that water oxidation to oxygen occurs quickly on the *anode*. This last process is difficult from a thermodynamic and mechanistic point of view. In nature, the reaction is catalyzed by the Oxygen Evolving Complex (OEC) sited in the Photosystem II (PSII). The core structure of OEC consists in an  $\text{CaMn}_4\text{O}_5$  cubane. In order to functionally mimic this cluster several metallic complexes have been prepared. It is worth noting the high and sustained activity achieved by polypyridilic Ru complexes. A few of them have been subjected to extensive mechanistic studies that have provided a description of the processes leading to oxygen at the molecular level. Other metallic complexes of Ir, Mn, Cu, Fe and Co have been prepared and studied, but there are doubts about the true nature of the catalytic species.

UNIVERSITAT ROVIRA I VIRGILI

WATER OXIDATION WITH MONONUCLEAR RU COMPLEXES. BELOW THE TIP OF THE

ICEBERG: THE OXO-BRIDGE SCENARIO

Isidoro López Marin

Dipòsit Legal: T. 1505-2013

## Table of Contents.

### Chapter 1. General Introduction.

<i>1.1. The dichotomy between energy demand and climate change.</i>	5
<i>1.1.1. Non carbon based energy resources.</i>	7
<i>1.2. Solar fuels.</i>	13
<i>1.2.1. Photosynthesis.</i>	13
<i>1.2.1.1. Thermodynamic and kinetic features of water oxidation.</i>	14
<i>1.2.1.2. Photosystem II (PSII).</i>	16
<i>1.2.1.3. The Oxygen Evolving Complex (OEC).</i>	17
<i>1.2.2. Artificial Photosynthesis.</i>	22
<i>1.3. Water oxidation catalysis.</i>	24
<i>1.3.1. Polypyridilic ruthenium catalysts.</i>	24
<i>1.3.1.1. Dinuclear Polypyridilic ruthenium catalysts.</i>	29
<i>1.3.1.2. Mononuclear Polypyridilic ruthenium catalysts.</i>	38
<i>1.3.1.3. Anchored Polypyridilic ruthenium catalysts.</i>	43
<i>1.3.2. Iridium catalysts.</i>	51

<i>1.3.3. Manganese catalysts.</i>	53
<i>1.3.4. Cobalt catalysts.</i>	56
<i>1.3.5. Copper catalysts.</i>	58
<i>1.3.6. Iron catalysts.</i>	59
<i>1.3.7. Polyoxometalates catalysts.</i>	60
<i>1.3.8. Organic catalysts.</i>	62
<i>1.4. References.</i>	63

## 1.1. THE DICHOTOMY BETWEEN ENERGY DEMAND AND CLIMATE CHANGE.

Mankind faces an energetic challenge because the increase of global population and economic growth. In 2008, the energetic demand was mostly supplied by fossil fuel resources<sup>1</sup> (Figure 1). Nuclear energy only contributed with a 2.0 % and renewable energies (RE) with a 12.9 %.

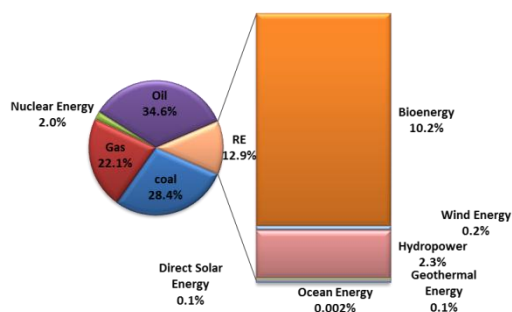


**Figure 1.** Contribution of resources to energetic demand in 2008. Source: International Panel of Climate Change.

Industrial revolution enabled the beginning of the widespread use of carbon based fuels, firstly as coal and later as oil and most recently as gas. The consumption of these resources has occasioned two global problems:

- Fossil fuels are Non-Renewable resources. For instance, in 1972 the discovery of additional conventional oil<sup>2</sup> was smaller than the consumed oil, which means conventional oil reserves have been diminishing from then (Figure 2). Depletion of conventional oil will force to turn to unconventional resources that will increase considerably the price of oil and will produce geopolitical conflicts. It is estimated that current reserves will only be able to cover up to one half of the oil demand in 2023.



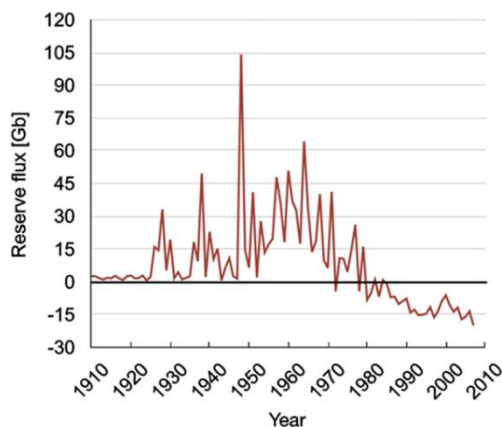


**Figure 2.** World conventional oil flux: additional discovered volume less consumed volume. Taken from reference 2.

- The burning of fossil fuels has been releasing  $\text{CO}_2$  and another greenhouse gases (GHG) to the atmosphere. GHG are responsible for global warming<sup>3</sup> and the consequent climate change. The Intergovernmental Panel on Climate Change (IPCC) has forecasted several scenarios and its consequences in the global surface warming (Figure 3). The mildest model B1 predicts a rise of the average temperature of 1.5 °C in 100 years. The less environmentally friendly scenario A1FI would produce an increase of 4 °C in the surface temperature, but the range of probable values is wide and the temperature could reach more than 6 °C.

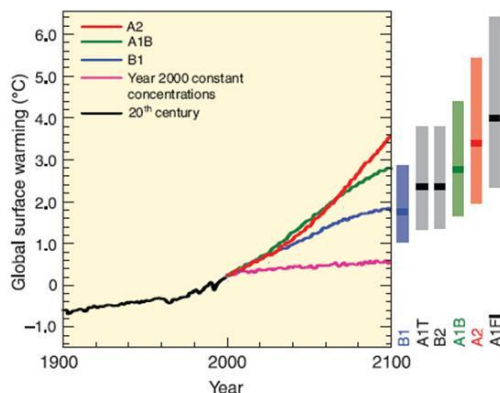


**Figure 3.** Prediction of the rise of global surface temperature according to several proposed scenarios. The bars at the right indicate the best estimate (solid line within each bar) and the likely range calculated for different scenarios.

The described problems with fossil fuels make desirable and important developing technology for more sustainable and clean resources. There are several alternatives, although the solution will be likely attained with a combination of different options. Some resources will be briefly considered below.

### 1.1.1. Non carbon based energy resources.

**Nuclear Fission.** It has been proposed to play an important role in the gradual replacement of carbon based resources. However there is a current controversy<sup>4,5</sup> about that. Proponents of nuclear energy argue that it is a clean resource, reduces the CO<sub>2</sub> emissions, is not intermittent and could reduce the dependence of Middle East imported fuels. Opponents argue that it is not safety because it can be the target of sabotage with terrorism goals. There is also a risk of nuclear weapon proliferation. Furthermore, several nuclear accidents (Mile Island, Chernobyl and Fukushima) question its safety despite the continuous improvement of the technology. Moreover, 1 GW<sub>e</sub> (gigawatt-

electric) nuclear power plant should be built every 1.6 days for the next 45 years in order to cover<sup>6</sup> the future energetic demand.

**Biomass.** It is a renewable resource that it is being thoroughly considered to help to cover the future energetic demands. The concept of biomass includes two different technologies: 1) the direct conversion of biomass in energy and 2) the transformation of biomass in biofuels as bioethanol.

A report<sup>7</sup> from the US Departments of Energy (USDOE) and agriculture (USDA) in 2005 estimated that biomass could provide a 30 % of its present energetic demand using non-arable agricultural land and maximizing forestry usage.

The most extended biomass-derived fuel<sup>7</sup> is ethanol produced from the fermentation of sugar or starches. Bioethanol can be currently mixing<sup>8</sup> in a 5-10 % with gasoline in normal cars. Special engines are needed to use bigger percentages (10-85%). In 2004, 30.000 millions of liters of bioethanol were produced as fuel,<sup>8</sup> what represents a 2 % of the gasoline consumption. However an improvement of the technology is still required in order to convert cereals in ethanol.

In spite of biomass is a good alternative to fossil fuels, it cannot supply by itself the future energetic demand because that would imply covering with the best known energetic crops<sup>7</sup> about 30 % of the land mass of Earth, which means almost three times all cultivable land currently used for agriculture. Skeptics about this resource usually put forward this argument. Moreover, they affirm<sup>9</sup> that the energetic balance is actually negative, that is, the production of 1 kcal of bioethanol needs more than 1 kcal of petroleum. Moreover, biomass is neither a CO<sub>2</sub> neutral resource, calculations indicate that

1 hectare of an energetic crop releases a net amount of 3100 kg of CO<sub>2</sub> equivalents.

**Wind Power.** It has an important role in the energetic supply in Spain since it provided<sup>10</sup> a 16% of the energetic demand in 2011. It is a renewable resource that is growing globally very fast because the price per unit of energy produced<sup>11</sup> is similar to the price for new +coal or natural gas installations. Although it will not be able to cover all the future energetic demand by itself, the European Commission has estimated<sup>7</sup> that the wind power will contribute a 30 % of the European energetic demand in a long term, an amount equal to the installed nuclear capacity. Intermittency<sup>12</sup> has been pointed as one of the most important drawbacks of wind power. However, this inconvenient can be mitigated by having the wind farm distributed<sup>7</sup> over a large geographical area. Issues as noise levels, effects on birds and the impact on landscape have been also considered. Some technological development is additionally required in the grid. Because, the present energy supply is thought to collect the current from a large-scale central generation of power and distribute it through the network, but wind power would distribute<sup>7</sup> the generation directly throughout the network. Nowadays the grid could accommodate a 20% of wind power penetration; larger penetration would require its reconfiguration.

**Photovoltaic.** The sun provides 100000 Terawatts (TW) to the Earth surface; this value is around 10000 larger than the world's present energetic demand. Photovoltaic (PV) cells could collect this energy and meet our present needs if a 0.5 % of the Earth's surface would be covered<sup>7</sup> with PVs with a conversion efficiency of 10%.

The most extended commercially PVs are made of silicon (94 % of market share). The world production of PVs has been experienced a continuous growing so far (Figure 4).

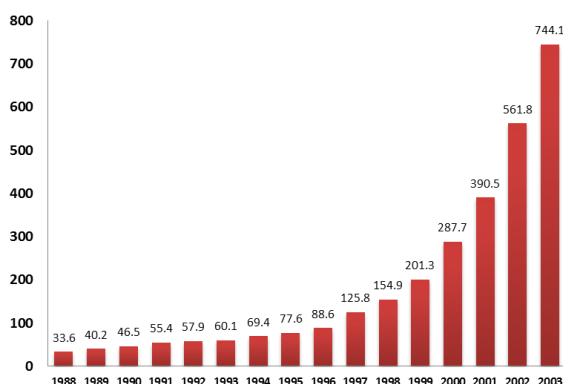


**Figure 4.** Growing of PVs production in the world. Source: reference 6.

Despite the growing market for PVs, the price of PV electricity is too high to be competitive with nuclear power and fossil fuels. The total cost of an installed PV system should be lower than 1 US\$/watt if PV wants to become competitive. The decrease of the cost seems even more difficult if we consider that the price of silicon is increasing a lot, 9 US\$ in 2000, 25 US\$ in 2004 and 60 US\$ in 2005. In fact, an increase of a 15% from the current value of PV is thought to be unavoidable, from 3.7 US\$/watt until 4.5 US\$/watt.

A second generation of PV could reduce the cost. The new kind of devices are formed by nanocrystalline  $\text{TiO}_2$  coated by a dye, which is a molecule than can absorb light. In this PVs, the process of light absorption and charge carrier transport are accomplished by two different elements of the cell. The PV is called dye sensitized cell (DSC). The special characteristics of DSC could lower the price of a module until 1 € while the outdoor efficiency of the

device would be even better than the one of first generation cell. Furthermore, a third generation of PV is currently being developed. These new devices are based in a quantum phenomenon: several excitations can be produced by the absorption of only one photon, if the energy of the photon is several times higher than the band gap.

On the other hand, solar energy can be also converted into electricity by the technology called concentrated solar power (CSP). The sunlight is concentrated in a small beam which is converted in heat. Then, the produced heat can be used for making electricity. It is a very promising technology, it has been estimated that it could provide<sup>13</sup> 12-25% of the world energetic demand in 2050. Spain is the world leader in CSP, more than 50 solar projects have been approved in this country and Spanish companies are exporting their technology around the world.

As in the case of wind power, intermittency is a drawback for this resource. Pro-nuclear associations<sup>14,15</sup> are very skeptic about the viability of non-hydro renewable energies to replace carbon based and nuclear energies because the intermittency. However, several authors<sup>16</sup> have suggested that intermittency can be overcome if solar and wind powers are combined. They are seasonally and geographically complementary, solar energy uses to peak in summer; in contrast, in many areas wind energy is lower in summer and higher in winter. Additionally, high pressure areas tend to have clear skies and low surface winds whereas low pressure areas tend to be windier and cloudier. Moreover, different energy storage technologies have been devised to supply the demand when this is very high. Pumped-storage hydroelectricity, rechargeable batteries, molten salts and paraffin wax are some of the proposed solutions. Solar fuels have been envisaged as the most practical

way<sup>17</sup> to store solar energy, sunlight is converted into chemicals which keep the solar energy as chemical bonds. These compounds are usually hydrogen or ethanol. Solar fuels will be considered in-depth below.

Other renewable resources exist, although they will not be described because it is out of the scope of this work. It can be mentioned that geothermal energy and wave and tidal power are being also exploited to help to supply the future energetic demand. On the other hand, fusion energy seems a non-realistic future alternative<sup>7</sup> to fossil fuels, at least in a medium term. The first fusion reactor (the international program ITER) will not work<sup>18</sup> before 2016 and recent setbacks could extend the date until 2022.

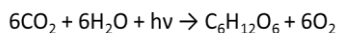
## 1.2. SOLAR FUELS.

Sunlight can be converted in several useful kinds of energy: heat, electricity and fuels. Solar fuels<sup>19</sup> are concentrated energy carriers with long term storage capacity produced from energy input from solar irradiation. Solar fuels are a very interesting option to store solar power. The energy density of traditional reservoirs<sup>17</sup> like pumped water ( $\approx 0.001$  MJ/Kg at 100 m), compressed air ( $\approx 0.5$  MJ/Kg at 300 atm) and batteries ( $\approx 0.1$ - $0.5$  MJ/kg) is modest, in contrast, current liquid fuels have an energy density 100 times bigger ( $\approx 50$  MJ/Kg) and in the case of hydrogen is even larger (140 MJ/Kg). Therefore, the conversion of sunlight into a solar fuel like hydrogen would enable to save a great amount of energy in a small space, ready to be used when it is needed. In this way, the intermittency issue would be resolved.

The conversion of sunlight into solar fuels is known nowadays as “Artificial Photosynthesis” because it is similar to the natural occurring process photosynthesis, where the reaction of sunlight, water and CO<sub>2</sub> produces the organic molecules that the plant needs for growing. Before “artificial photosynthesis” is described in detail, the principles and key points that operate in photosynthesis will be presented.

### 1.2.1. Photosynthesis.

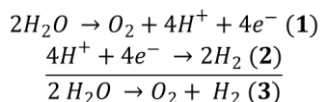
Photosynthetic organisms collect sunlight as an energy source to synthesize carbohydrates from CO<sub>2</sub> and H<sub>2</sub>O (Scheme 1). The side product of the reaction is O<sub>2</sub> which is released into the atmosphere.



**Scheme 1.** Photosynthesis equation.



At the heart of photosynthesis is the splitting of water by sunlight in  $O_2$  and  $H_2$  (Scheme 2 **(3)**), although hydrogen is not produced as such, it is actually incorporated in the final sugars by means of some intermediates like  $NADPH_2$ .



**Scheme 2.** Water splitting reaction **(3)** and its two constituent half-reactions: water oxidation **(1)** and proton reduction **(2)**.

If a mechanistic approach to water splitting is addressed, the process can be divided into two half-reactions (Scheme 2 **(1)** and **(2)**). The mechanistic approach<sup>20</sup> is useful since photosynthesis in green plants takes place in the thylakoid membrane and occurs in two physically separated molecular assemblies: light driven water oxidation in Photosystem II (PSII) and  $CO_2$  reduction in Photosystem I (PSI) and Calvin cycle.

The water oxidation reaction and PSII will be considered in-depth in the next sections.

### 1.2.1.1. Thermodynamic and kinetic features of water oxidation.

The oxidation of water has different thermodynamic barriers that depend<sup>21</sup> on the number of removed electrons. The more electrons released, the lower the thermodynamic potential (Table 1).

**Table 1.** Standard potentials for water oxidation at pH=1 and pH=7.

Redox Process <sup>a</sup>	E <sup>0</sup> / V (vs. SSCE)	
	pH = 1	pH = 7
$\cdot\text{OH} + 1\text{H}^+ + 1\text{e}^- \rightarrow \text{H}_2\text{O}$	2.50	2.15
$\text{HO-OH} + 2\text{H}^+ + 2\text{e}^- \rightarrow 2\text{H}_2\text{O}$	1.48	1.13
$\text{HO-O}\cdot + 3\text{H}^+ + 3\text{e}^- \rightarrow 2\text{H}_2\text{O}$	1.37	1.02
$\text{O}=\text{O} + 4\text{H}^+ + 4\text{e}^- \rightarrow 2\text{H}_2\text{O}$	0.94	0.58

<sup>a</sup>The formal oxidation state of the O-atoms are labeled according to the next code: -, red; -1, blue; 0, green.

From a thermodynamic point of view, the 4 electrons/4 protons process is the less demanding one. This means that oxidation of water to oxygen (O<sub>2</sub>) is the most feasible reaction and nature uses it.

However, it exhibits a mechanistic complexity, because all the 4 e<sup>-</sup> and the 4 H<sup>+</sup> cannot be removed at the same time, 4 O-H bonds from two water molecules have to be broken and a double O-O bond has to be formed.

Water oxidation to oxygen can also be contemplated as an addition of hydrogen transferring<sup>22</sup> reactions (Scheme 3). Under this perspective, oxidizing water to O<sub>2</sub> requires a hydrogen atom abstracting reagent or the combination of an oxidant and a base with a higher homolytic bond dissociation free energy for the X-H bond (BDFE) than the calculated average BDFE for the O-H bonds of water (BDFE<sub>average</sub> = 86 kcal mol<sup>-1</sup>). In PSII, the oxidizing equivalents pass through a tyrosine/tyrosyl radical couple, which has BDFE = 87.8 kcal mol<sup>-1</sup> in aqueous solution. Although this BDFE could change inside the protein, it seems reasonable to assume that tyrosyl radical has just enough energy to oxidize water at low overpotential.



**Scheme 3.** H-transferring oxygen reduction.

### 1.2.1.2. Photosystem II (PSII).

PSII is the natural occurring assembly where water oxidation to oxygen takes place during photosynthesis. Several X-Ray structures have been resolved with a gradual increase of the atomic resolution: 3.5 Å by Barber<sup>23</sup> and coworkers, 3.0 Å and 2.9 Å by Saenger<sup>24,25</sup> and coworkers and recently 1.9 Å by Umena<sup>26</sup> and coworkers. PSII is located in the thylakoid membrane and contains 20 subunits. It performs a series of light induced processes<sup>27</sup> (Figure 5) leading to the oxidation of water. The first event after the absorption of a photon by the chlorophyll P<sub>680</sub> is a primary charge separation: an electron is transferred from the excited chlorophyll P<sub>680</sub>\* to a single electron acceptor pheophytin (process **a**, Figure 5), the electron transfer lasts a few ps. After that, the electron is transferred to secondary quinone acceptors (processes **b** and **c**, Figure 5). On the other hand, a tyrosine residue transfers an electron to the oxidized chlorophyll (process **d**, Figure 5) which came back to its initial state ready to absorb another photon. Then tyrosine will be able to oxidize once (process **e**, Figure 5) the oxygen evolving complex (OEC), responsible for the water oxidation reaction. Tyrosine is a good donor and regenerates quickly P<sub>680</sub> and shuttles efficiently the redox equivalents needed for water oxidation. The complete pathway has to be repeated four times to provide four redox equivalents to OEC. The mechanistic complexity of water oxidation by PSII lies in storing four redox equivalents in OEC avoiding back electron transfers or other quenching mechanism. The long distance between OEC and P<sub>680</sub> (approx. 13 Å) reduces the possibility of back electron transfer.

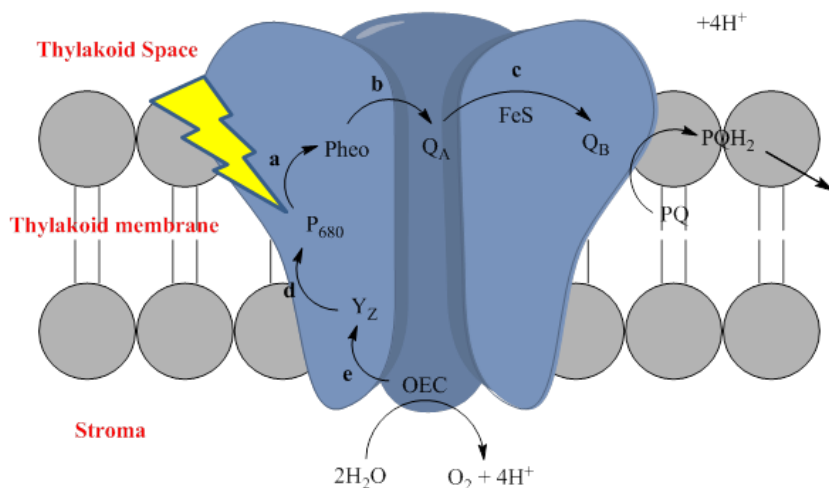


**Figure 5.** Schematic view of PSII and light induced water oxidation.

### 1.2.1.3. The Oxygen Evolving Complex (OEC).

The oxygen evolving complex is a  $Mn_4O_5Ca$  cluster. X-Ray crystallographic studies of PSII, indicated above, have revealed its structure. The cluster consist in a cubane-like structure (Figure 6) where there are three manganese and one calcium atoms linked by oxo bridge ligands. A forth manganese atom is connected with the cubane by a single oxo bridge, referred to as “dangler”. Several amino acid residues surround the  $Mn_4O_5Ca$  cluster and provide a coordination framework to the metal atoms or facilitate a hydrogen bonding network.

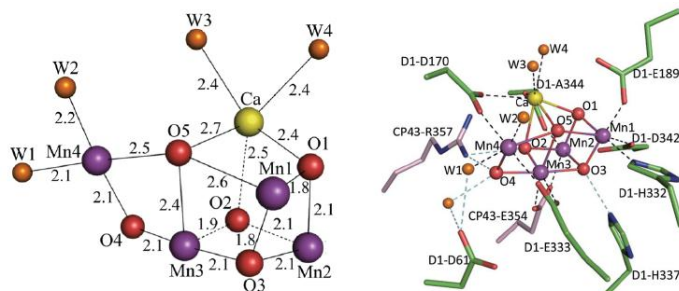


**Figure 6.** X-Ray structure of the  $\text{Mn}_4\text{O}_5\text{Ca}$  cluster taking from reference 25. (Left)  $\text{Mn}_4\text{O}_5\text{Ca}$  cubane (distance in Å), (right)  $\text{Mn}_4\text{O}_5\text{Ca}$  cubane and surrounding amino acid residues.

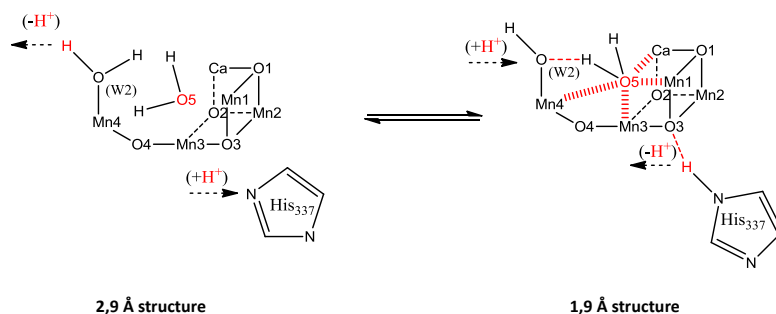
The high atomic resolution structure provided by Umena *et al.*<sup>26</sup> has controversial points, although it has been the only structure where the localization of the oxo bridge atoms within the  $\text{Mn}_4\text{O}_5\text{Ca}$  cluster has been observed.

Two main features<sup>28</sup> have attracted attention: 1) The identity of O5 and its placement, it could be assigned as a weak oxo bridge, a hydroxo or an aquo ligand; 2) Earlier high precision extended X-ray absorption fine structure (EXAF) results and previous X-Ray structures gave some key metal-metal distances different from the 1.9 Å resolution structure. The discussion has led to two proposals.

Firstly, it has been postulated that photoreduction of the manganese atoms occurs during data collection<sup>29-31</sup> due to exposure to X-Ray light. The XRD structure would not correspond to the resting state of PSII,  $S_1$ , but it would be a lower oxidation state.

Secondly, it has been proposed that the mean oxidation state of manganese in the resting state  $S_1$  is actually +3.0<sup>28,32</sup> and not +3.5 as several research groups<sup>33</sup> have claimed. In the 1.9 Å resolution structure the

distribution of oxidation states would correspond to III/III/III/III and in the 2.9 Å III/IV/III/II. Both structures would be one proton tautomers (Scheme 4) and exchanging would occur with a low activation barrier (40 kJ mol<sup>-1</sup>) that favors the 1.9 Å structure.

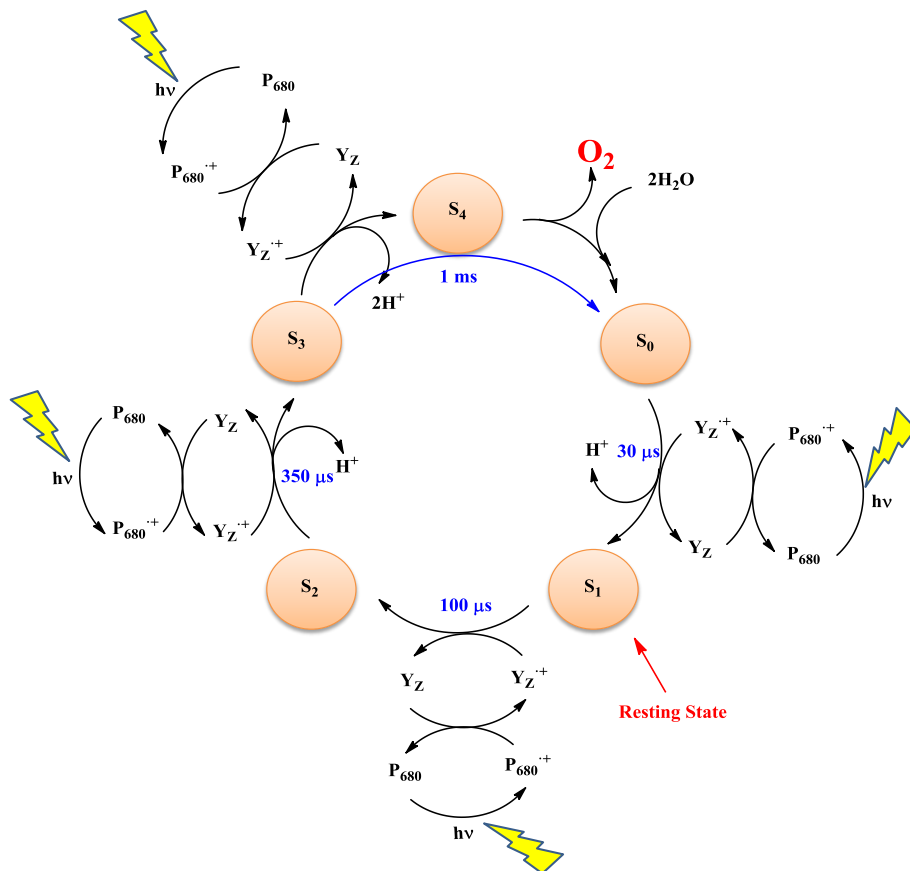


**Scheme 4.** Tautomers exchange in the  $S_1$  state of OEC.

### Water oxidation mechanism.

The oxygen evolution reaction is mediated by a nearby oxidized tyrosine molecule (residue 161 of the D1 protein) that oxidizes OEC four times. The amino acid works as an intermediate<sup>7</sup> electron carrier between the  $Mn_4O_5Ca$  cluster and  $P_{680}^{+}$ .

It is known that the oxidation of water by OEC involves at least five intermediate states, called S-states. The gradual change from the most reduced state  $S_0$  to the most oxidized one  $S_4$  is driven by each photochemical turnover of the PSII center (Scheme 5). The state  $S_4$  is achieved after the accumulation of four oxidizing equivalents. Then,  $S_4$  can oxidize two molecules of water and OEC comes back to the  $S_0$  state.

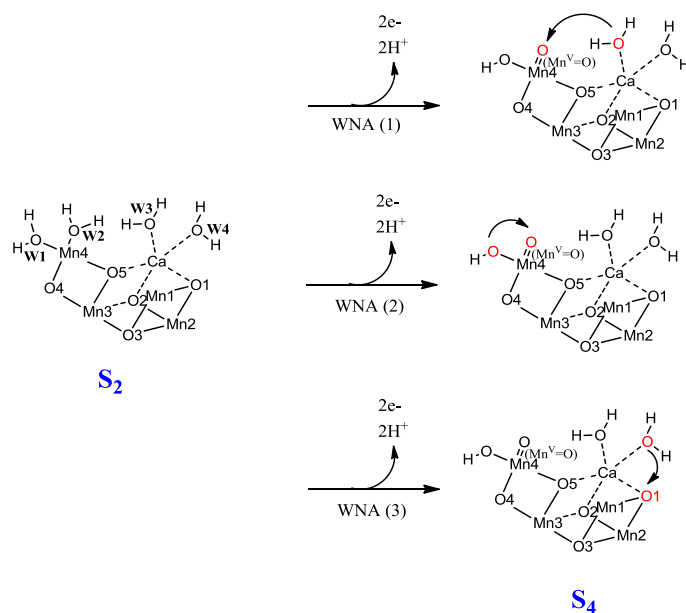


**Scheme 5.** S-state cycle for the photooxidation of two water molecules to oxygen by OEC mediated by a nearby tyrosine ( $Y_z$ ) residue. The time scale for the conversion of each S-state is marked in blue.

The  $S_1$  state is thermodynamically stable<sup>34</sup> and samples in the dark evolve to this state after some hours. The state  $S_2$  can be obtained after flash illumination at room temperature or via low temperature illumination at 200 K. The transition  $S_1 \rightarrow S_2$  occurs without protein rearrangement. The state  $S_3$  quickly decays to the  $S_0$  state with the concomitant release of triplet oxygen<sup>35</sup> and the rebinding of at least one water molecule. The state  $S_4$  has never been spectroscopically identified.

The pathway that OEC employs to form an O-O bond is unknown at present, although there are two main proposals based on computational and spectroscopic experiments:

➤ Mechanisms where water nucleophilic attack occurs between two substrate oxygen atoms. There are several proposed pathways of this kind, although three of them are more consistent with crystallographic and spectroscopic data: **a)** A  $\text{Ca}^{2+}$ -bound water/hydroxo<sup>36-38</sup> attacks to a  $\text{Mn}^{\text{IV}}$ -oxyl or a  $\text{Mn}^{\text{V}}$ -oxo moiety, probably W3 and W2 (Scheme 6, WNA(1)); **b)** the water nucleophilic attack involves two water/hydroxo (W1 and W2) ligands<sup>39</sup> on the “dangler” Mn (Mn4) atom (Scheme 6, WNA(2)); **c)** A  $\text{Ca}^{2+}$ -bound water/hydroxo attacks to a  $\mu$ -oxo/hydroxo bridge<sup>40</sup> (O1) between Mn2 and Mn1 (Scheme 6, WNA(3)).

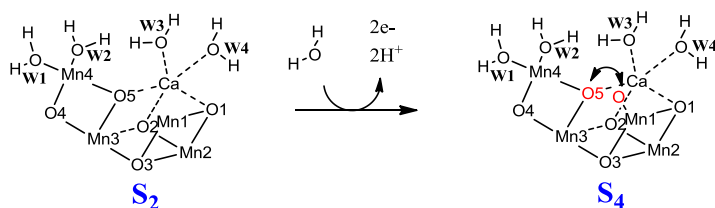


**Scheme 6.** Water nucleophilic attack pathways for the O-O bond formation by OEC.



➤ Oxo/oxyl radical coupling<sup>41</sup> of two Mn oxygen ligands.

An exchanging fast substrate binds to the open coordination side on the Mn1 as an aquo or hydroxo ligand in the states  $S_2$  or  $S_3$  and becomes an oxyl radical in  $S_4$ . Then, the radical coupling with O5 occurs and oxygen is produced (Scheme 7).



**Scheme 7.** Radical coupling pathway for the O-O formation by OEC.

### 1.2.2. Artificial Photosynthesis.

The concept of artificial photosynthesis is based on mimicking the light (photo collection) and dark (energy conversion and  $\text{CO}_2$  capture) processes of natural photosynthesis in order to produce energy (electricity and hydrogen) and biopolymers (including food) with high efficiency.

The simplest model of a photoelectrochemical cell<sup>42,43</sup> for water splitting consists of two compartments physically separated by a proton exchange membrane (Figure 7). One compartment corresponds to the anode and it is usually divided in 3 components: a photosensitizer, a photoanode semiconductor and a water oxidation catalysts. The other compartment is made only of a proton reduction catalyst.

Water splitting starts with irradiation of the photosensitizer which is excited and transfers an electron to the conduction band of a photoanode semiconductor, usually related to  $\text{TiO}_2$  (Scheme 8, eq. 1). Then, the electron moves to the cathode where there is a proton reduction catalyst that produces

the hydrogen (Scheme 8 eq. 2). On the other hand, the oxidized photosensitizer is reduced by a water oxidation catalyst that can oxidize water to oxygen when reaches a high oxidation state (Scheme 8 eq. 3). Water splitting requires exchanging 4 electrons, thus the absorption of 4 photons is needed to carry out the process. Furthermore, multielectronic and fast catalysts are indispensable since multielectron catalytic processes must proceed before back electron transfers.

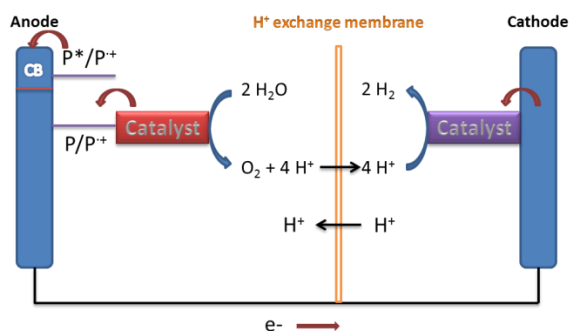
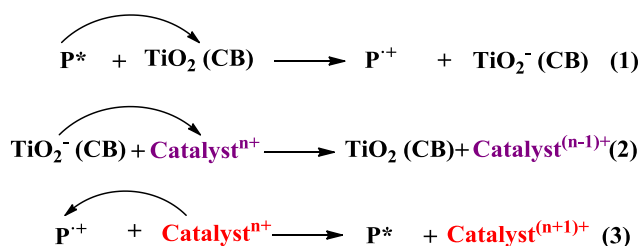


**Figure 7.** Model of a photoelectrochemical cell. The movement of electrons after irradiation has been indicated by red curve arrows.



**Scheme 8.** Electron transfer processes after irradiation of the photosensitizer. In purple, the proton reduction catalyst, in red, the water oxidation catalyst.

### 1.3. WATER OXIDATION CATALYSIS.

Water oxidation catalysis is currently recognized as a bottleneck<sup>44,45</sup> for the development of the described photoelectrochemical cells and is an active area<sup>46-51</sup> of research. Catalysts of different transition metals have been synthesized and tested. Molecular catalysts are usually mononuclear, dinuclear and multinuclear complexes of ruthenium, manganese, iridium, iron, cobalt and copper. In addition, polyoxometalates of ruthenium, cobalt or copper have been extensively used. There is even an example of a completely organic catalyst.

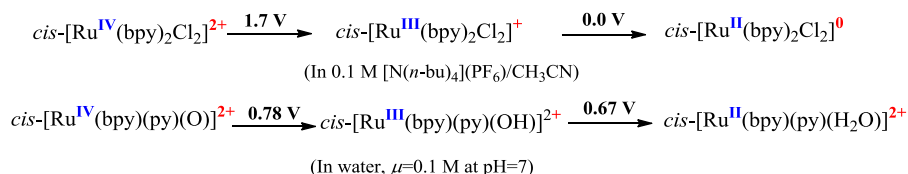
Heterogeneous catalysts have also been developed. Some of them correspond to anchored molecular catalysts, but there are more examples of metal oxides of manganese, cobalt and iridium working as water oxidation catalysts (WOCs).

In the next sections the aforementioned catalysts will be presented. We will specially focus in molecular catalysts made of polypyridyl ruthenium complexes since the compounds synthesized and studied in this work belong to this kind.

#### 1.3.1. Polypyridilic ruthenium catalysts.

At the end of the 70s, Thomas J. Meyer *et al.* found<sup>52,53</sup> the Ru-OH<sub>2</sub>/Ru=O system where aqua polypyridyl ruthenium(II) complexes can achieve the high oxidation state IV in a narrow potential window by means of simultaneous loss of protons and electrons. This is illustrated by the Latimer diagrams<sup>54</sup> of [Ru(bpy)<sub>2</sub>Cl<sub>2</sub>] and [Ru(bpy)(py)(H<sub>2</sub>O)]<sup>2+</sup> (Scheme 9). In the case of [Ru(bpy)<sub>2</sub>Cl<sub>2</sub>], the difference of Ru(IV/III) and Ru(III/II) standard potentials is 1.7 V, the large  $\Delta E^0$  is due to the increase in charge and oxidation state in the

Ru(IV/III) couple with regard to the Ru(III/II) one; in contrast, for  $[\text{Ru}(\text{bpy})(\text{py})(\text{H}_2\text{O})]^{2+}$  the difference is only 0.11 V. The small  $\Delta E^0$  can be explained considering two main features:

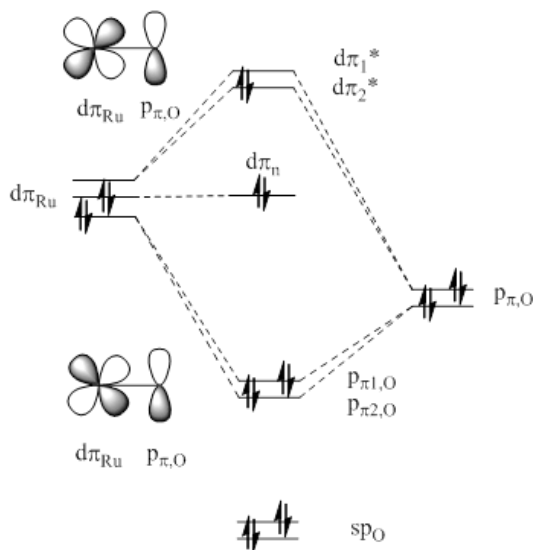


**Scheme 9.** Latimer diagrams of complexes  $[\text{Ru}(\text{bpy})_2\text{Cl}_2]$  and  $[\text{Ru}(\text{bpy})(\text{py})(\text{H}_2\text{O})]^{2+}$ .

❖ The net positive charge does not change in the Ru(IV/III) and Ru(III/II) couples, it is always +2. The release of protons while increasing the oxidation state maintains the net charge of the complex.

❖ A great stabilization of Ru(IV) because the formation of an oxo complex. A molecular orbital diagram (Scheme 10) of the Ru(IV)=O motif shows the multiple character of the Ru-O bond that stabilizes Ru(IV), the bond order is 2.

The HOMO and LUMO orbitals are  $d\pi^*$  antibonding and are widely mixed with the  $2p_{\text{O},\pi}$  orbitals, although they have a strong  $4d_{\text{Ru}}$  character. The LUMO orbital constitutes a suitable site for initial orbital interaction with electron donors. The bonding  $sp^2$  and  $p_{\pi\text{O}}$  orbitals have available electron pairs for donation or orbital interaction with electron acceptors. The  $d\pi_n$  orbital is nonbonding and has largely  $4d_{\text{Ru}}$  character.

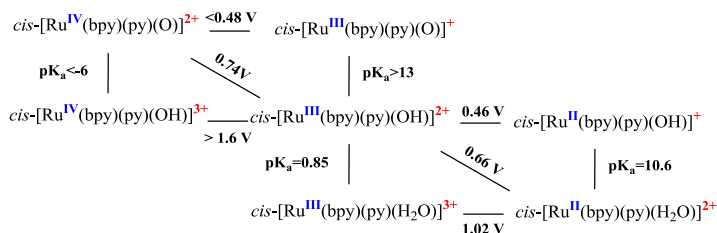


**Scheme 10.** Molecular Orbital diagram of the Ru(IV)=O moiety.

The Ru-OH<sub>2</sub>/Ru=O system is the base for the activity for the most of ruthenium water oxidation catalyst. In addition, analogous M-OH<sub>2</sub>/M=O systems have been invoked as a key element in the catalytic activity of the most of molecular catalysts, where M=Ir, Co or Cu.

The Ru-OH<sub>2</sub>/Ru=O system plays also an important role in the study of proton coupled electron transfer processes (PCET), a currently very active area<sup>22,55-59</sup> of research and related to water oxidation<sup>51,60</sup> among other oxidation<sup>54</sup> processes.

PCET is a mechanistic concept that describes the simultaneous transfer of an electron and a proton in an elementary step. This transfer avoids the formation of high energy intermediates. A redox potential diagram<sup>61</sup> of [Ru(bpy)(py)(H<sub>2</sub>O)]<sup>2+</sup> can illustrate it (Scheme 11).



**Scheme 11.** Potential diagram (square scheme) of  $[Ru(bpy)(py)(H_2O)]^{2+}$ . The horizontal lines represent redox processes and the vertical lines represent acid-base processes.

The oxidation of  $[Ru^{II}(bpy)(py)(H_2O)]^{2+}$  to  $[Ru^{III}(bpy)(py)(OH)]^{2+}$  could occur in three ways according to the diagram:

- An initial electron transfer to give a  $Ru^{III}-OH_2$  intermediate followed by proton transfer to achieve the final  $Ru^{III}-OH$ . The pathway is abbreviated as ET-PT (electron transfer-proton transfer).
- An initial proton transfer to give a  $Ru^{II}-OH$  intermediate followed by electron transfer to get  $Ru^{III}-OH$ . The pathway is abbreviated as PT-ET (proton transfer-electron transfer).
- The simultaneous loss of a proton and an electron, that is, proton couple electron transfer or PCET.

At pH=7 the ET-PT and PE-ET processes are high energy pathways compare to PCET. In the case of ET-PT the initial electron transfer has a larger standard potential (1.02 V) than PCET (0.66V), thus the process would be slower if we take into account that the Gibbs free energy of a redox process is related to its activation Gibbs energy according to Marcus theory<sup>62</sup> in outer sphere electron transfers. For PT-ET the initial deprotonation step is thermodynamically unfavorable with  $\Delta G^{0r} = +0.19$  eV. Therefore, ET-PT and PT-ET mechanisms present high energy intermediates that can decrease the rate. In contrast, PCET avoids the formation of such intermediates and the rate is

faster. The same energetic considerations can be argued for the oxidation of  $[\text{Ru}^{\text{III}}(\text{bpy})(\text{py})(\text{OH})]^{2+}$  to  $[\text{Ru}^{\text{IV}}(\text{bpy})(\text{py})(\text{O})]^{2+}$ .

Pourbaix diagrams, the plot of potential vs. pH, are a useful tool to collect the electrochemical properties of aquo complexes. In a typical Pourbaix diagram like the one from  $[\text{Ru}(\text{trpy})(\text{bpy})(\text{H}_2\text{O})]^{2+}$  (Figure 8) the horizontal and diagonal lines delimit the  $E^0$ -pH regions in which the different stable species predominate. The slope of the lines depends on the redox couple<sup>63-65</sup> according to eq. 1

$$E_{app}^0 \propto -\frac{0.059m}{n} pH \text{ at } 25^\circ\text{C} \quad (1)$$

where  $m$  is the number of protons and  $n$  of electrons involve in the couple. Thus the slope gives the stoichiometry of the considered redox process. The vertical lines represent the  $\text{pK}_a$  values of the specie to the left of the line.

Additionally, in the case of  $1\text{H}^+/1\text{e}^-$  couples the values of the horizontal and diagonal lines can be used to calculate the BDFEs<sup>22</sup> of the O-H bonds according to equation 2

$$\text{BDFE}(\text{XH}) = 23.06[E_{\text{pH}}^0(\text{X}^\bullet/\text{XH})] + 1.37(\text{pH}) + 57.6 \text{ kcal mol}^{-1} \quad (2)$$

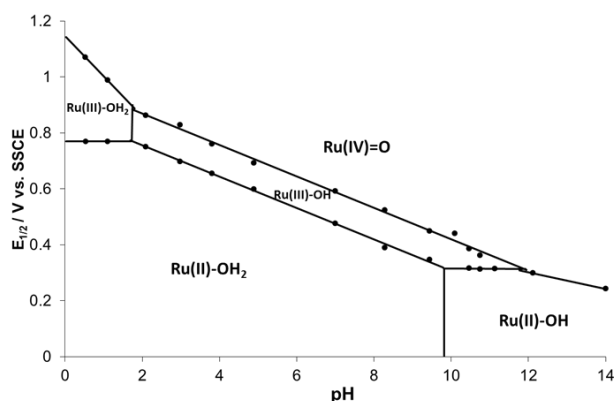


**Figure 8.** Pourbaix diagram of the aquo complex  $[\text{Ru}(\text{trpy})(\text{bpy})(\text{H}_2\text{O})]^{2+}$ .

### 1.3.1.1. Dinuclear polypyridilic ruthenium catalysts.

The oxidation of water to oxygen is a  $4e^-/4\text{H}^+$  process so it seems a reasonable strategy the combination of two  $\text{Ru}-\text{OH}_2/\text{Ru}=\text{O}$  systems linked by a ligand to achieve an effective catalyst. In 1982, Thomas J. Meyer *et al.*<sup>66,67</sup> reported that the dinuclear  $\mu$ -oxo bridge complex  $\text{cis},\text{cis}-\{[\text{Ru}(\text{bpy})(\text{H}_2\text{O})]_2(\mu\text{-O})\}^{4+}$ , known as “blue dimer”, can oxidize water to oxygen using  $\text{Ce}^{4+}$  or  $\text{Co}^{3+}$  as sacrificial oxidants. The catalytic mechanism remains to be established although a huge amount of UV-vis,<sup>60,68,69</sup> EPR,<sup>69-72</sup> rRAMAN,<sup>69-75</sup> X-Ray spectroscopic<sup>71</sup> and isotopic labeling experiments<sup>76,77</sup> have been carried out. Moreover, the medium has a strong influence<sup>60,76,78,79</sup> on the mechanism making more complex its analysis. For instance, differences have been observed<sup>60</sup> in 0.1 M  $\text{HNO}_3$  or 0.1 M  $\text{CF}_3\text{SO}_3\text{H}$ . In the most recent proposal<sup>71</sup> by Meyer *et al.* (Scheme 12) the blue dimer is oxidized to IV,V and then water nucleophilic attack occurs to generate a peroxidic intermediate in the oxidation state III,IV. After that, the intermediate is oxidized and oxygen is released.



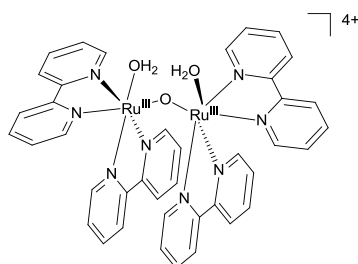
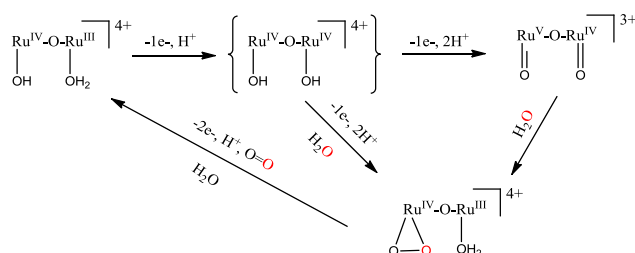
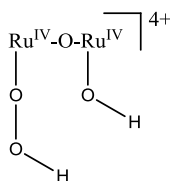


**Figure 9.** Structure of *cis,cis*-[[Ru(bpy)(H<sub>2</sub>O)<sub>2</sub>(μ-O)]<sub>2</sub>]<sup>4+</sup>, blue dimer.



**Scheme 12.** Proposed mechanism for water oxidation by the blue dimer in 0.1 M HNO<sub>3</sub>. The oxidation state III,IV was taken as initial complex.

However, this proposal is not exempt from controversy. Firstly, it suggests a peroxidic intermediate in the oxidation state III,IV, while previous works based on UV-vis spectroscopy<sup>60</sup> and DFT calculations<sup>80</sup> assigned a hydroperoxidic intermediate in the oxidation state IV,IV (Scheme 13).

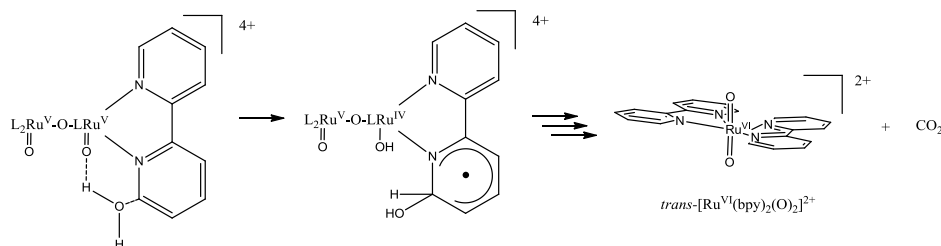


**Scheme 13.** Previously suggested hydroperoxidic intermediate by Meyer *et. al.* and Shaik *et. al.*

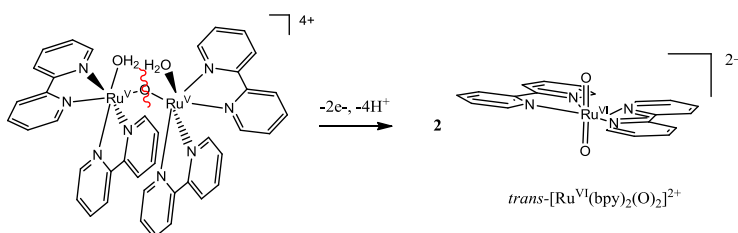
Secondly, Hurst *et al.* have recently questioned<sup>70</sup> the spectroscopic evidence for the proposed peroxidic intermediate. RR experiments discard the formation of a peroxidic complex, although they confirm the formation of an

intermediate. This intermediate appears only in the presence of  $\text{Ce}^{\text{IV}}$  and nitrate.

The blue dimer can be deactivated by several side reactions: polypyridyl ligand oxidation<sup>78</sup> in the higher oxidation states (Scheme 14), water oxidation induced anation<sup>60,68</sup> by the weak coordinating anions of the used acids ( $\text{NO}_3^-$ ,  $\text{CF}_3\text{SO}_3^-$  or  $\text{ClO}_4^-$ ) and *trans*-dioxide formation by overoxidation and subsequent  $\mu$ -oxo cleavage (Scheme 15).



**Scheme 14.** Blue dimer deactivation by polypyridyl ligand oxidation.



**Scheme 15.** Blue dimer deactivation by oxidative cleavage of the oxo bridge.

In 2004 Llobet *et al.* synthesized<sup>81</sup> a new dinuclear complex  $\{[\text{Ru}(\text{trpy})(\text{H}_2\text{O})_2(\mu\text{-bpp})]^{3+}$  (**1**) where the bridge is the tetradentate polypyridyl ligand bis(2-pyridyl)-3,5-pyrazolate (bpp) (Figure 10). The aromatic organic ligand provides a robust and rigid bridge that avoids the cleavage deactivation pathways of an oxo ligand. Moreover, from a mechanistic point of view bpp<sup>-</sup> places the two aquo groups in a closer proximity than blue dimer favoring an

intramolecular coupling of the oxo groups in the higher oxidation states versus a water nucleophilic attack.

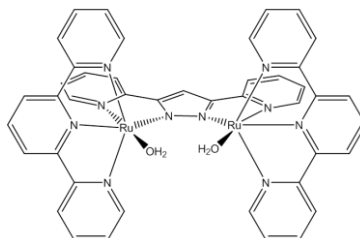
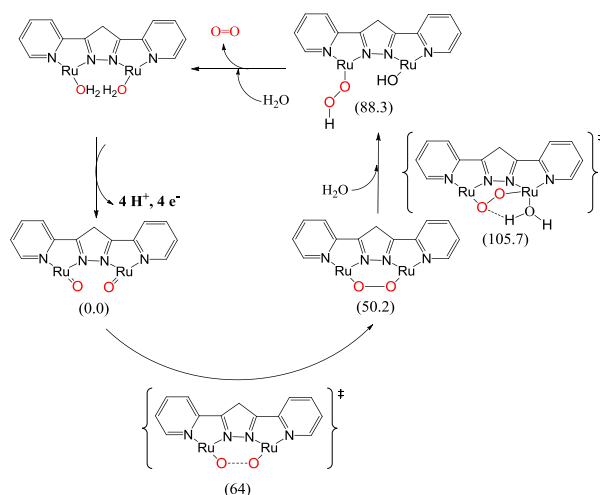


**Figure 10.** Structure of  $\{[\text{Ru}(\text{trpy})(\text{H}_2\text{O})]_2(\mu\text{-bpp})\}^{3+}$  (**1**)

**1** catalyzes the oxidation of water to oxygen using  $\text{Ce}^{4+}$  as sacrificial oxidant faster than blue dimer and with a higher efficiency. The mechanism of the reaction has been extensively studied<sup>82,83</sup> by UV-vis spectroscopy,  $\text{O}^{18}$ -labelling experiments and DFT calculations. When the oxidation state IV, IV is reached the two formed oxo group couple and generate an O-O bond (Scheme 16). The coupling can be explained if we take into account that the  $\text{Ru}=\text{O}$  moieties can have a certain radicaloid character, thus the complete description of this bond would be the combination of two extreme resonant forms:  $\text{Ru}^{\text{IV}}=\text{O} \leftrightarrow \text{Ru}^{\text{III}}-\text{O}^\bullet$



**Scheme 16.** Mechanism of water oxidation by **1**. The trpy ligands have been omitted for clarity. The values in parenthesis show relative energies in  $\text{KJ mol}^{-1}$  including an additional explicit molecule of water in the first solvation shell.

Other dinuclear complexes have been synthesized and evaluated as water oxidation catalysts, although they lack of a detailed mechanistic study.

Thummel *et al.* have reported<sup>84,85</sup> many dinuclear ruthenium catalysts (Figure 11) based on organic bridge ligands similar to  $\text{bpp}^-$ . Tanaka *et al.* have studied<sup>86</sup> a dinuclear complex (**5**) where each ruthenium is coordinated (Figure 12) to a bidentate non-innocent redox ligand, 3,5-di-*tert*-butyl-1,2-benzoquinone (3,5-Bu<sub>2</sub>SQ). The participation of the ancillary ligands in the redox processes adds a novelty to the catalytic mechanism that is a source of controversy<sup>87,88</sup> nowadays.

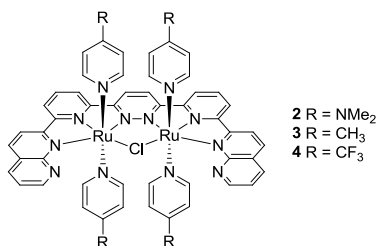


**Figure 11.** Some examples of the complexes reported by Thummel *et al.*

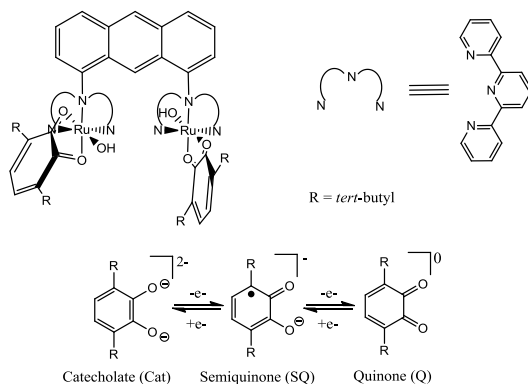


**Figure 12.** Structure of complex **5** and redox processes related to the ancillary ligand 3,5-Bu<sub>2</sub>SQ.

Other catalytic systems have been developed<sup>89,90</sup> in order to favor the radical coupling between two Ru<sup>IV</sup>=O moieties (Figure 13). However, DFT studies have shown that the distance between the two metal sites in these complexes could be as large as 7.4 Å when the two Ru<sup>IV</sup>=O are formed. The big separation is due to electrostatic repulsion between the two oxo groups. It would become even larger if Ru<sup>V</sup>=O moieties are invoked in the catalytic cycle. This distance precludes a radical coupling between the two oxo groups to generate an O-O bond.

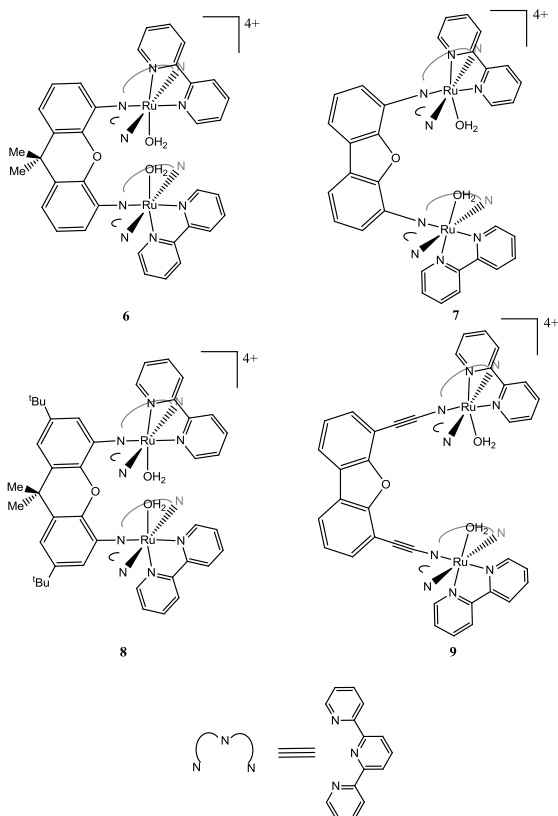


**Figure 13.** Structure of some complexes with cofacial metal sites

Sun *et al.* have also prepared and studied the interesting dinuclear complex **10** (Figure 14). The bridging ligand contains two carboxylate groups, which produce a decrease of the standard potentials. This catalyst is stable and has a high TOF value ( $1.2 \text{ s}^{-1}$ ) using  $\text{Ce}^{\text{IV}}$  as sacrificial oxidant. Moreover, photocatalysis is also observed using  $[\text{Ru}(\text{bpy})_3]^{2+}$  and  $\text{Na}_2\text{S}_2\text{O}_8$  as photosensitizer and sacrificial electron acceptor respectively (Scheme 17).

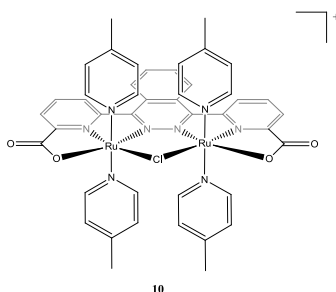
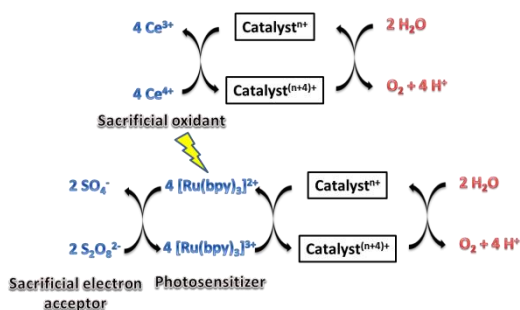


**Figure 14.** Structure of complex **10**.



The same group has synthesized the dinuclear complexes **11**, **12** and **13** (Figure 15). As it will be explained later, it has been demonstrated that mononuclear complexes can also oxidize water<sup>21,84,91,92</sup> to oxygen. In particular, Sun *et al.* have reported that complex **14** (Figure 15) oxidizes water with a TOF value comparable to the OEC one<sup>93</sup> under certain conditions by a bimolecular pathway. Therefore, they envisaged a dinuclear complex formed by two analogues of **14** linked by a bridging ligand. Flexible spacers were chosen instead of the usual rigid ones. The catalysts are better than their mononuclear compounds and the oxygen evolution rate is first order in complex. Nonetheless, it is well known<sup>54,94</sup> that Ru complexes in high oxidation states

oxidize easily  $sp^3$  C-H bonds. Therefore, it is unlikely that the used bridge ligands survive under the catalytic conditions.

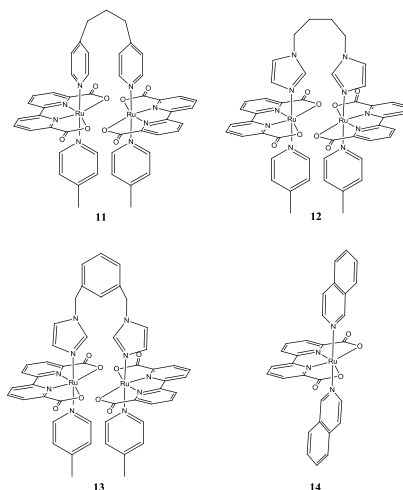


**Figure 15.** Structures of complexes **11**, **12**, **13** and **14**.

A complete different approach consists in dinuclear complexes where the two Ru-H<sub>2</sub>O groups are separated by a long distance, in a way that precludes an intramolecular reaction and leaving bimolecular interactions as the only possible pathways to form an O-O bond. This strategy results in catalysts, like **15** and **16** (Figure 16), that are usually less active and fast than complexes when an intramolecular process is feasible.

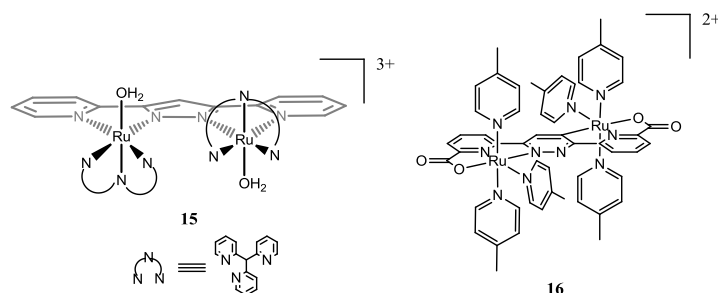
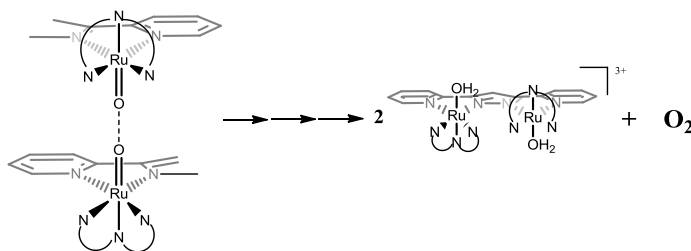


**Figure 16.** Structures of complexes **15** and **16**.



In the case of complex **15**, it has been demonstrated that generates oxygen by means of a bimolecular radical coupling (I2M, Scheme 18).



**Scheme 18.** I2M mechanism proposed for **15**.

### 1.3.1.2. Mononuclear polypyridilic ruthenium catalysts.

In 2005, Thummel *et al.* reported<sup>84</sup> that the presence of only one Ru-OH<sub>2</sub>/Ru=O system is enough to carry out water oxidation catalysis (Figure 17). Later, they synthesized and evaluated the catalytic activity of various mononuclear<sup>95</sup> complexes.

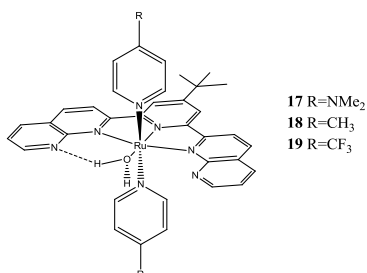


**Figure 17.** Structure of the first reported mononuclear ruthenium catalysts **17**, **18** and **19**.

On the other hand, Meyer *et al.* have also reported mononuclear catalysts (Figure 18) and have studied<sup>96-98</sup> thoroughly its mechanism. The proposed pathway (Scheme 19) is currently accepted and has been extended to different catalytic systems based on Ru,<sup>99</sup> Ir,<sup>100</sup> Co<sup>101</sup> or Cu<sup>102</sup>.

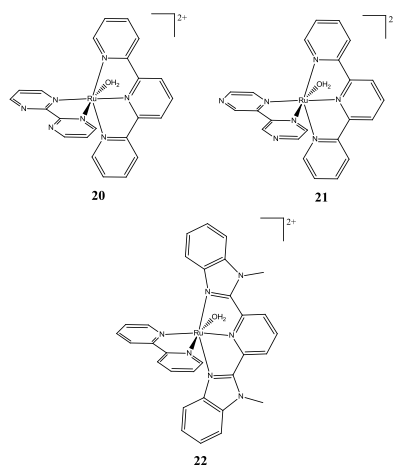
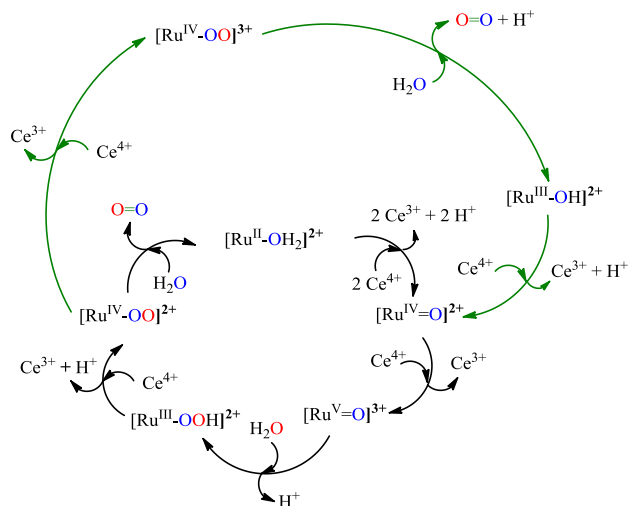


**Figure 18.** Structures of some of the complexes studied by Meyer *et al.*

The catalytic process starts with the oxidation of the initial Ru(II)-OH<sub>2</sub> complex to Ru(V)=O, where the first two redox processes are PCET. Then, water nucleophilic attack on Ru(V)=O occurs. This is the key O-O bond-forming step and results in the generation of the hydroperoxide intermediate Ru(III)-OOH. After that, a new oxidation step takes place and Ru(IV)-OO is formed. This is the dominant specie in the catalytic steady state. In 0.1 M HNO<sub>3</sub>, the peroxy complex evolves oxygen and the initial Ru(II)-OH<sub>2</sub> compound is recovered. In 1 M HNO<sub>3</sub>, Ru(IV)-OO is further oxidized to Ru(V)-OO and this intermediate evolves oxygen and re-enters in the cycle as Ru(III)-OH.



**Scheme 19.** Proposed mechanism for catalytic water oxidation by mononuclear Ru complexes. The black arrows indicate predominant pathways in 0.1 M HNO<sub>3</sub> and the green ones from Ru<sup>IV</sup>-OO in 1 M HNO<sub>3</sub>.

This mechanism has been extended with additional pathways,<sup>103,104</sup> although the main framework is maintained.

Mononuclear complexes with the Hbpp and H3p (2-(5-phenyl-1H-pyrazol-3-yl) pyridine) ligands (Figure 19) have been also synthesized and tested<sup>105</sup> as WOCs. The catalysts can evolve oxygen using Ce(IV) as sacrificial oxidant or photochemically using [Ru(bpy)<sub>3</sub>]<sup>2+</sup> as photosensitizer and [Co<sup>III</sup>(Cl)(NH<sub>3</sub>)<sub>5</sub>]<sup>2+</sup> as sacrificial electron acceptor. When Ce(IV) was employed, the *out* isomers demonstrated to be more active. However, the dinuclear analogue **1** is a better catalyst. They follow the mechanism proposed by Meyer *et al.*

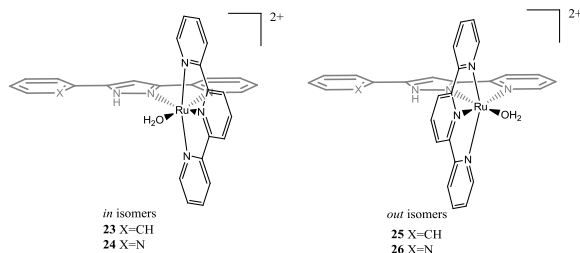
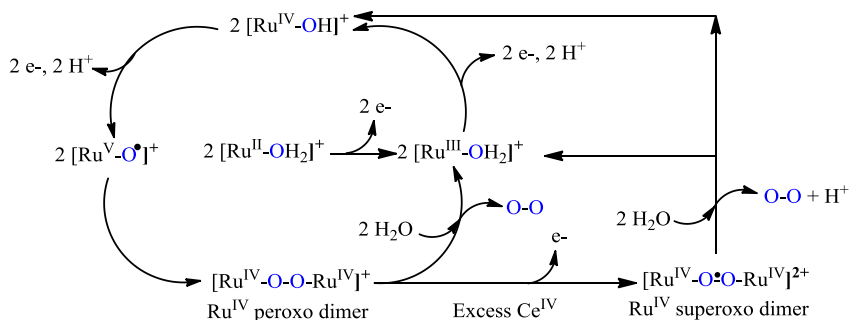


**Figure 19.** Structures of complexes **23**, **24**, **25** and **26**.

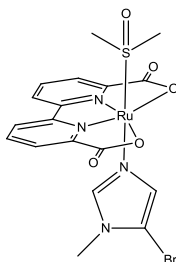
A different mechanism<sup>93</sup> has been suggested for complex **14** and structural analogues. Although these complexes apparently do not present a Ru-OH<sub>2</sub>/Ru=O system, it has been showed that a seven coordinated aquo complex<sup>106</sup> is generated after dissolution in acidic water. The main difference with the previous described mechanism is that the key O-O bond forming step is a radical coupling between the Ru(IV)-O<sup>•</sup> groups of two molecules of complex (Scheme 20).



**Scheme 20.** Proposed mechanism for water oxidation by **14** and analogues.

Catalyst **14** has reached currently the highest reported turnover frequency (TOF) which is 300 s<sup>-1</sup>, in the order of OEC (100-400 s<sup>-1</sup>). The structural analogue **27** attained also a high TOF value of 176.5 s<sup>-1</sup>. The striking feature of **27** is the presence of two different axial ligands, DMSO and 5-bromo-*N*-methylimidazol (Figure 20). Nevertheless it is highly probable that the DMSO ligand is oxidized under the catalytic conditions, forming an

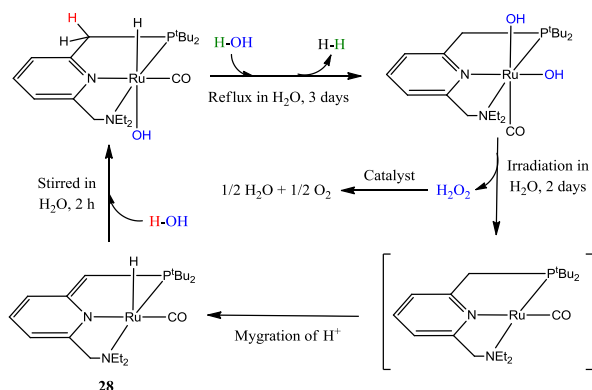
unknown complex that is the actual catalyst. The reported work lacks of a complete mechanistic study in order to know the evolution of the compound.



27

**Figure 20.** Structure of complex **27**.

A different approach for water oxidation is illustrated by the mononuclear PNN-ruthenium pincer-type complex **28**. This catalyst can evolve hydrogen and oxygen in consecutive steps driven by heating or irradiation<sup>107</sup> respectively (Scheme 21). In the beginning of the catalytic cycle **28** reacts with water to form a *trans* hydrido-hydroxo complex. Then, this intermediate reacts with water under refluxing conditions, producing hydrogen and creating a *cis* dihydroxo complex. The next step is irradiation to release hydrogen peroxide by reductive elimination and probably a Ru(0) intermediate is generated after that. This compound is converted to initial **28** by migration of a proton from the methylene group of the phosphorous side arm of the pincer ligand, thus a hydride ligand is formed and the heterocycle loses its aromaticity. The produced H<sub>2</sub>O<sub>2</sub> is catalytically decomposed into O<sub>2</sub> and H<sub>2</sub>O by **28**.



**Scheme 21.** Proposed mechanism for water splitting by **28**.

Although this approach has received a considerable attention and has been highlighted<sup>108,109</sup> because its novelty and great potential, it has several objections: the overall reaction is actually stoichiometric, it is very slow and the yields in hydrogen and oxygen are poor.

### 1.3.1.3. Anchored polypyridilic ruthenium catalysts.

Homogeneous catalysts have been considered so far, however the technology of water splitting will need a water oxidation catalyst absorbed or adsorbed on a photoanode next to a photosensitizer as explained in the section 1.2.2.

Therefore, the previous described ruthenium catalysts should be linked to a surface. There are several strategies for anchoring molecular catalysts to photoanodes:

- *Covalent bond.* The complex is attached to the surface by means of a covalent bond between a functional group of the molecule and a functional group in the surface of the photoanode. Phosphonate, carboxylate and sulfonate functionalities are usually the linking moiety

from the complex whereas the surface provides hydroxilic groups (Figure 21).

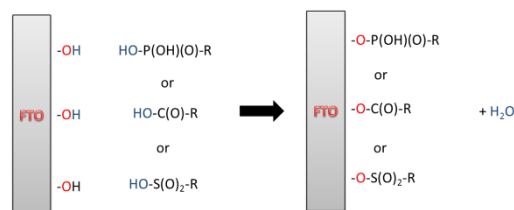
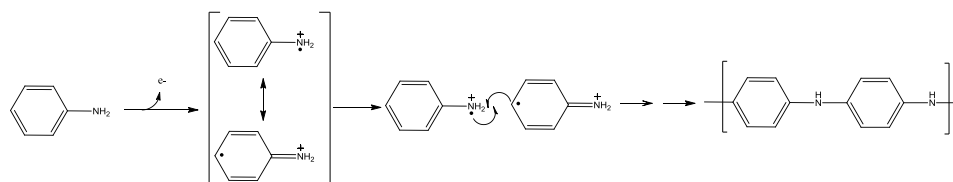


**Figure 21.** Example of covalent attaching in a fluorine doped tin oxide (FTO) anode.

- *Electrostatic interaction.* The complex is anchored because the electrostatic attraction between the positive charge of the molecule and the negative charge of the surface or *vice versa*.
- *Electropolymerization.* The molecular catalyst has a ligand that can electropolymerize and form a film on the surface. The polymerization process is initiated after oxidation or reduction of the aforementioned ligand, for this reason it is called electropolymerization. The electropolymerization of aniline into polyaniline (Scheme 22) is a very known and studied<sup>110,111</sup> example.



**Scheme 22.** Electropolymerization of aniline.

- *Intermolecular Forces.* The anchoring takes place by means of intermolecular interactions like H-bond or  $\pi$ - $\pi$  stacking.
- *Deposition.* The catalyst precipitates on the surface and remains as a solid during the catalysis. Deposition can be carried out by dropping a

solution of the complex on the electrode followed by evaporation of the solvent.

### Anchored dinuclear ruthenium polypyridyl catalysts.

In 2007, Meyer *et al.* synthesized and anchored<sup>112</sup> complex **29** in several supports: SnO<sub>2</sub> doped In<sub>2</sub>O<sub>3</sub> (ITO), TiO<sub>2</sub> and ZrO<sub>2</sub>. They carried out electrocatalytic water oxidation to evaluate the effectiveness of the attached catalyst. In electrocatalytic water oxidation a potential higher than E<sup>0</sup>(O<sub>2</sub>/H<sub>2</sub>O) is applied to the anode in order to evolve O<sub>2</sub> electrolytically, the difference between the applied potential and E<sup>0</sup>(O<sub>2</sub>/H<sub>2</sub>O) is called overpotential ( $\eta$ ) and it depends on pH since E<sup>0</sup>(O<sub>2</sub>/H<sub>2</sub>O) depends on it. The TON was 1.8 at pH = 1 and 1.5 V ( $\eta$  = 0.53 V) applied potential. It increases up to 3 at pH = 6 and 1.32 V ( $\eta$  = 0.64 V). In both cases, the activity is very low and the overpotentials are too high. An even lower TON had been previously observed<sup>113</sup> for the homogeneous analogue **30** using Ce(IV) as sacrificial oxidant at pH=1.

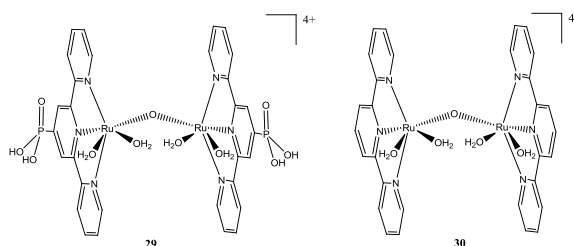


**Figure 22.** Structure of complexes **29** and **30**.

The previous presented complex **5** was deposited<sup>86</sup> on an ITO electrode. The electrocatalytic activity was evaluated at pH = 6 and 1.90 V ( $\eta$  = 0.90 V). The TON value reached 33500 after 40 hours and the decrease of activity with time was due to slowly exfoliation of the deposited complex. Although the TON is very high, the used overpotential is also too large.



Complex **31** has been attached to rutile  $\text{TiO}_2^{114}$  by means of the carboxylic group (Figure 23). This compound is analogous to **1**. The catalysis was tested chemically with Ce(IV) and yielded oxygen and  $\text{CO}_2$ . It has been suggested that the production of  $\text{CO}_2$  results from the partial degradation of the bridge ligand.

Another analogue of **1** has been electropolymerized on vitreous carbon sponges (VCS) and FTO electrodes. Complex **32** comprises pyrrole modified terpyridine ligands (Figure 23). The pyrrolic rings polymerize after oxidation and create a film deposited on the electrode. The deposited catalyst has been demonstrated to oxidize water electrochemically and chemically using Ce(IV). In this last case it could be reused until 3 times, although the activity was progressively decreasing. The complex enhanced its activity when it was copolymerized with a non-active and stable dicarbollide. Copolymerization diluted the active centers and avoided bimolecular deactivation pathways for the catalyst.

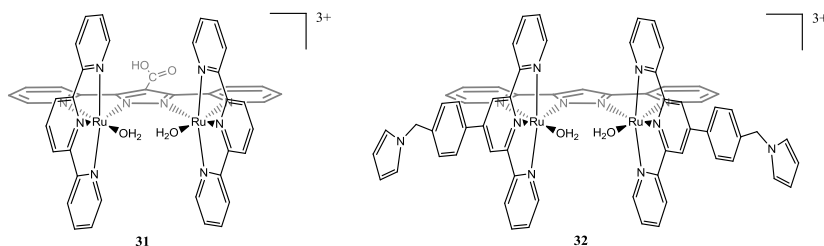


**Figure 23.** Structure of complexes **31** and **32**.

### **Anchored mononuclear ruthenium polypyridyl catalysts.**

Several mononuclear catalysts have been anchored to different surfaces. It is a common design that the mononuclear complex is firstly bound covalently to a photosensitizer and the complete assembly (catalyst-photosensitizer) is then linked to the electrode by the photosensitizer moiety (Figure 24).

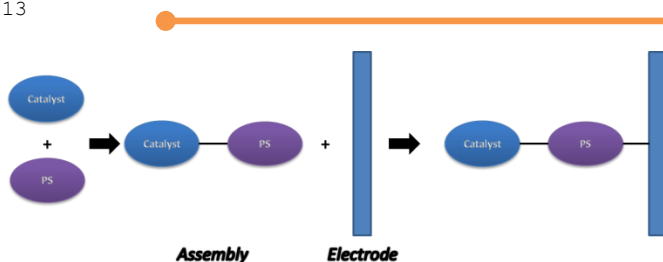


**Figure 24.** Anchoring of a catalyst-photosensitizer (PS) assembly on the surface of an electrode.

The assemblies **33** and **34** (Figure 25) were attached to ITO and FTO from acidic aqueous solutions. In this case the photosensitizer moiety works like a redox mediator; it means that it makes faster the electron transfer from the catalyst moiety to the electrode. The systems achieve impressive TONs of 8900 after 20 hours for **33** and 28000 after 13 hours for **34**. The electrocatalysis was carried out at pH = 0 and 1.8 V ( $\eta = 0.57$  V). Interestingly, no sign of reduction in activity was observed during the indicated time.

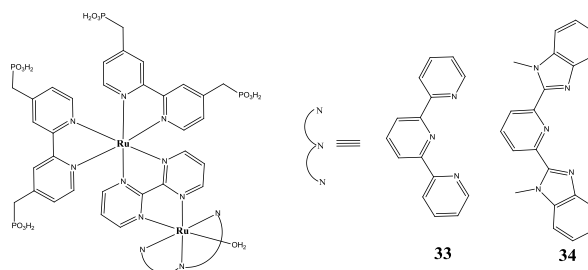


**Figure 25.** Structures of complexes **33** and **34**.

Sun *et al.* have exploited two different strategies<sup>115,116</sup> to anchor its complexes. On the one hand, they attached an azide group to the surface of a glassy carbon (GC) electrode<sup>115</sup> by means of electrografting of a diazonium aromatic compound that contained the azide group (Figure 26). Electrografting of diazonium salts by reduction is a well-known<sup>117</sup> and studied process. Then, the azide is subjected to a “click chemistry” reaction with a complex that

contains a terminal acetylene group. The process requires a copper(I) catalyst. The result is a catalyst linked to the GC surface by a triazole and a phenyl group. Electrochemical water oxidation at pH = 7 and  $\eta = 0.7$  V gave a TOF of  $1.6 \text{ s}^{-1}$  which decreases to  $0.073 \text{ s}^{-1}$  with  $\eta = 0.3$  V

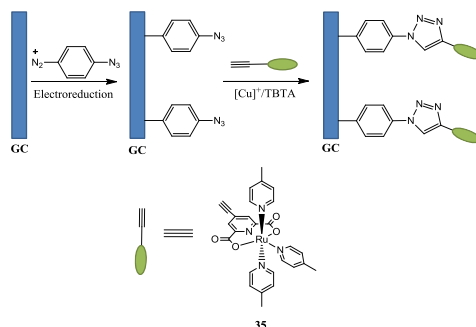


**Figure 26.** Electrografting of complex **35** in a GC electrode.

On the other hand, complex **36** was anchored to multiwalled carbon nanotubes (MWCNTs) previously coated on an ITO glass electrode.<sup>116</sup> The attaching is made by means of  $\pi$ - $\pi$  stacking interaction between the nanotubes and the pyrene moieties from the complex (Figure 27). The catalyst produced 11000 TONs in 10 hours in neutral aqueous 0.1 M  $\text{Na}_2\text{SO}_4$  solutions by setting 1.4 V ( $\eta = 0.58$ ). This means a TOF value of  $0.3 \text{ s}^{-1}$ . Interestingly, electrocatalysis can be carried out in a 0.1 M solution of NaCl without chlorine evolution, thus catalysis using sea water could be feasible. However, a slow desorption of CNTs from the ITO support has been reported, making long-term stability a problem.

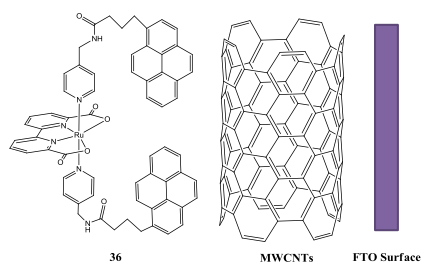


**Figure 27.** Assembly of complex **36** and MWCNTs on a FTO surface.

Meyer *et al.* have conceived a clever approach where the photosensitizer and the catalyst are arranged into two contiguous layers. The strategy is called self-assembled bilayers (SAB). The modified electrodes were prepared<sup>118</sup> in a two-steps sequence. Firstly, the photosensitizer **37** is attached and then the catalyst **38** (Figure 28). The inverse sequence does not work because it was shown that anchored **38** inhibits the subsequent attaching of **37**. In contrast, the length of the alkyl chains of **38** is enough to reach surface binding sites available between previous attached **37** molecules. In spite of CV experiments show electrocatalytic water oxidation, controlled potential electrolysis at 1.8 V ( $\eta = 0.63$  V) in 0.1 M HClO<sub>4</sub> over extended periods resulted in a fast decrease of the current to the background level. It is thought that **38** deactivates because the aquo ligand is replaced by a phosphonate group from the alkyl chain. The SAB structure is also released at higher pHs.

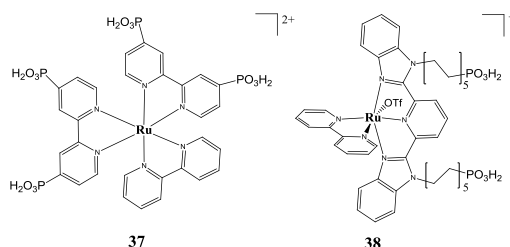


**Figure 28.** Structure of complexes **37** and **38**.

Any of the previous anchored catalysts have shown photoelectrochemical activity. However two assemblies developed by Sun *et al.* did it.

In 2010 they built a device<sup>119</sup> where a TiO<sub>2</sub> photoanode supported on glass FTO was covered by the photosensitizer **39**. A nafion film containing the catalyst **40** was later deposited after previous oxidation of **40** to **40<sup>+</sup>**. The electrostatic attraction between the positively charged complex and the negatively charged nafion membrane catches the catalyst into the polymeric and inert matrix. The anodic assembly was demonstrated to evolve oxygen after 60 minutes of irradiation with a visible light source and without a potential bias. The TON was 16 and the TOF was 27 h<sup>-1</sup>.

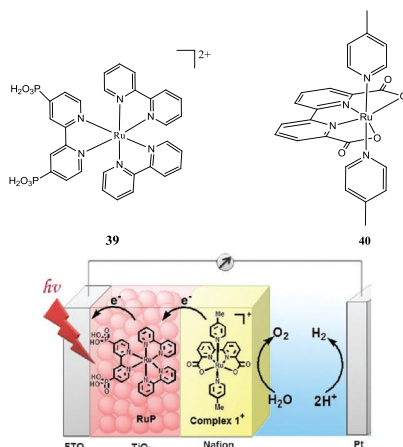


**Figure 29.** Structures of complexes **39** and **40** (upper) and assembly on a FTO anode taken from reference 117 (bottom).

Recently the same group has developed a photoelectrochemical device similar to the previous one. Instead of nafion and complex **40** they have attached<sup>120</sup> directly the modified catalysts **41** (Figure 30) to the surface of the

electrode. The photoelectrochemical cell achieves the highest photocurrent intensity reported until now with a low external bias of 0.2 V.

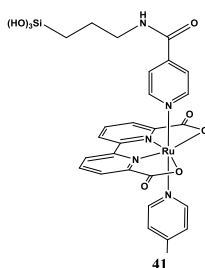


**Figure 30.** Structure of complex **41**.

### 1.3.2. Iridium catalysts.

It has been early known<sup>121-123</sup> that colloidal IrO<sub>2</sub> can oxidize water to oxygen chemically and photochemically. Recent modifications have improved its activity<sup>124</sup> for photo water splitting with visible light and a small bias.

In 2007, Bernhard *et al.* reported<sup>125</sup> the first molecular Ir catalysts using Ce(IV) as sacrificial oxidant (Figure 31).

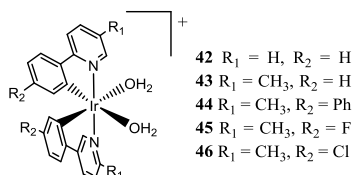


**Figure 31.** Structures of the first molecular Ir WOCs.

The complexes have been able to produce oxygen for hours; for instance, **45** can achieve 2760 TONs after one week. Thereafter a large number of Ir complexes that can oxidize water have been reported.<sup>92,100,126-130</sup> It is noteworthy the extensive mechanistic studies performance by Crabtree *et al.* using a wide set of Ir(III) complexes containing the

pentamethylcyclopentadienyl (Cp\*) ligand and different cyclometalated or *N,N*-bidentate ligands (Figure 32).

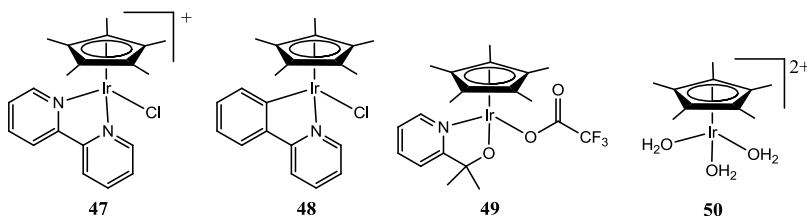


**Figure 32.** Some of the complexes synthesized and studied by Crabtree *et al.*

These compounds are currently questioned as true molecular catalysts, mainly when CAN is used as sacrificial oxidant. It was found<sup>131</sup> that Ir complexes solutions treated with a slight or a huge excess of CAN originate IrO<sub>x</sub> nanoparticles which are active catalysts. Furthermore, the electrochemical oxidation of complex **50** in 0.1 M KNO<sub>3</sub> results in the formation of an heterogeneous material onto the electrode,<sup>132,133</sup> which is irreversibly electrodeposited and work as a robust solid state WOC. The heterogeneous catalyst is called blue layer (BL) because it takes this colour. It is a robust catalyst that oxidizes water at low overpotential ( $\eta = 0.2$  V) during days without showing signs of degradation.

On the other hand, it is also known that the Cp\* ligand is oxidized under catalytic conditions as demonstrated by NMR and other spectroscopic techniques.<sup>134,135</sup> The resulting compounds could be catalytic active species, deactivation products or intermediates giving access to the formation of IrO<sub>x</sub> nanoparticles. A recent study carried out by Crabtree *et al.* showed that complex **51** evolves to the dinuclear bis- $\mu$ -oxo Ir(IV) coordination compound **52**<sup>136</sup> under catalytic conditions and using the mild sacrificial oxidant NaIO<sub>4</sub> (Figure 33). In contrast to the fate of the Cp\* ligand, the chelate ligand pyalc

(2-(2'-Pyridyl)-2-propanolate) does not suffer any decomposition pathway and is retained. The role of **52** in the catalysis must be still elucidated, although it is proposed as a metastable intermediate, i.e., a catalytic resting or deactivation state.

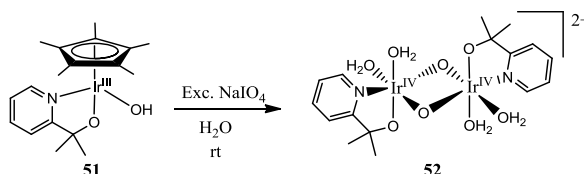


**Figure 33.** Conversion of **51** into **52** under catalytic conditions.

The same work established that the presence of an Ir<sup>III</sup>-OH<sub>2</sub> group is essential to induce catalytic activity, suggesting that sequential PCET oxidations enable to achieve reactive high oxidation states as in the case of the Ru<sup>II</sup>-OH<sub>2</sub>/Ru<sup>IV</sup>=O system.

### 1.3.3. Manganese catalysts.

The OEC consists in a tetranuclear Mn<sub>4</sub>O<sub>5</sub>Ca cluster, it is not surprising that oxo bridge polynuclear manganese complexes have been synthesized and evaluated as WOCs.

In 1999 Crabtree *et al.*<sup>137</sup> prepared the mixed-valence dinuclear compound [(trpy)(H<sub>2</sub>O)Mn<sup>III</sup>(μ-O)<sub>2</sub>Mn<sup>IV</sup>(H<sub>2</sub>O)(trpy)]<sup>3+</sup> (**53**) and claimed that it was able to oxidize water using oxone (KHSO<sub>5</sub>) or NaOCl as sacrificial oxidant. The actual capability of **53** to work as a WOC has been questioned because both oxidants are highly oxidizing oxygen-transfer reagents, so that the produced oxygen could proceed from these compounds instead from water. In 2005 a fundamental study<sup>138</sup> by Collomb *et al.* unambiguously demonstrated that the one electron oxidation of **53** produced the tetranuclear Mn complex {[(trpy)(H<sub>2</sub>O)Mn<sup>IV</sup>(μ-O)<sub>2</sub>Mn<sup>IV</sup>(trpy)]<sub>2</sub>(μ-O)}<sup>6+</sup> (**54**) (Figure 34). **54** cannot be



further oxidized and thus cannot work as a water oxidation catalyst. As a consequence, the dinuclear compound **53** cannot oxidize water without the intercession of an oxygen-donor reagent as oxone or NaOCl.

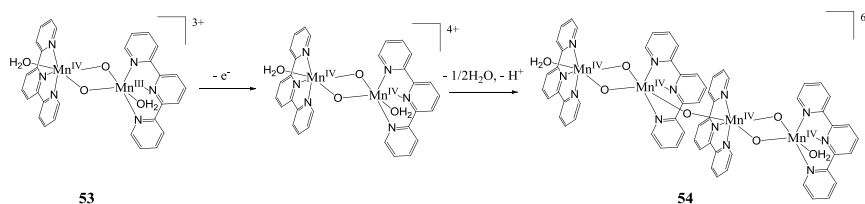


**Figure 34.** Conversion of **53** into **54** induced by oxidation.

However, a recent report by Crabtree *et al.*<sup>137</sup> showed that the tetranuclear complex **54** could oxidize electrochemically water, although the activity was very low. Additionally, it was found that the addition of **54** to a concentrated solution of CAN resulted in the formation of a low amount of oxygen and the disproportion of **54** into Mn(II) and MnO<sub>4</sub>.

In 2008, Dismukes *et al.* discovered that a structural mimic of the OEC was able to act as water oxidation catalyst in an efficient manner. The complex consists in a manganese oxo [Mn<sub>4</sub>O<sub>4</sub>L<sub>6</sub>] cubane (Figure 35) where L is bis(4-methoxyphenyl)phosphinate (**55**). The compound was embedded in a Nafion membrane deposited on a conducting electrode due to its insolubility in water and most organic solvents. The evolution of oxygen was driven electrochemically<sup>139</sup> or photochemically.<sup>140</sup> Later on, it was found that **55** dissociates into Mn(II) compounds after incorporation to the Nafion films. The low-valent Mn species are then reoxidized to create dispersed nanoparticles of a disordered Mn(III/IV)-oxide phase under catalytic conditions. This material constitutes the actual catalyst.

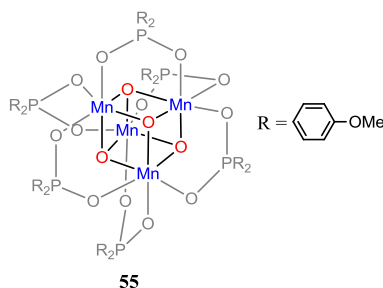


**Figure 35.** Structure of complex **55**. The [Mn<sub>4</sub>O<sub>4</sub>] core has been enhanced for clarity.

In spite of the rising development of single-site water oxidation catalysts based on Ru and Ir, there are a limited number of mononuclear Mn examples described in the literature. Sun *et al.* reported<sup>141</sup> a mononuclear Mn complex containing a ligand that comprised a xanthene and a corrole linked by an amide bond (complex **56** in Figure 36). The compound led to electrocatalytic oxygen evolution at low potential in a solution that consisted in a mixture of CH<sub>2</sub>Cl<sub>2</sub>, CH<sub>3</sub>CN, Bu<sub>4</sub>NOH and water as solvent. Brudvig *et al.* also published<sup>142</sup> the synthesis of three new candidates to work as single site WOCs (complexes **57**, **58** and **59** in Figure 36). The catalytic activity was evaluated using oxone or H<sub>2</sub>O<sub>2</sub> as sacrificial oxidant. **57** produced oxygen with both oxidants, **58** only when hydrogen peroxide was employed and **59** was totally inactive. However, the origin of the evolved oxygen must be questioned due to two main reasons: 1) oxone is a O-donor oxidant as previously discussed and 2) Mn compounds are known to catalyze the dismutation of H<sub>2</sub>O<sub>2</sub> into H<sub>2</sub>O and O<sub>2</sub>, the same reaction catalyzed by the enzyme manganese catalase,<sup>143</sup> thus the generation of O<sub>2</sub> when this sacrificial oxidant is used probably proceeds from this reaction.

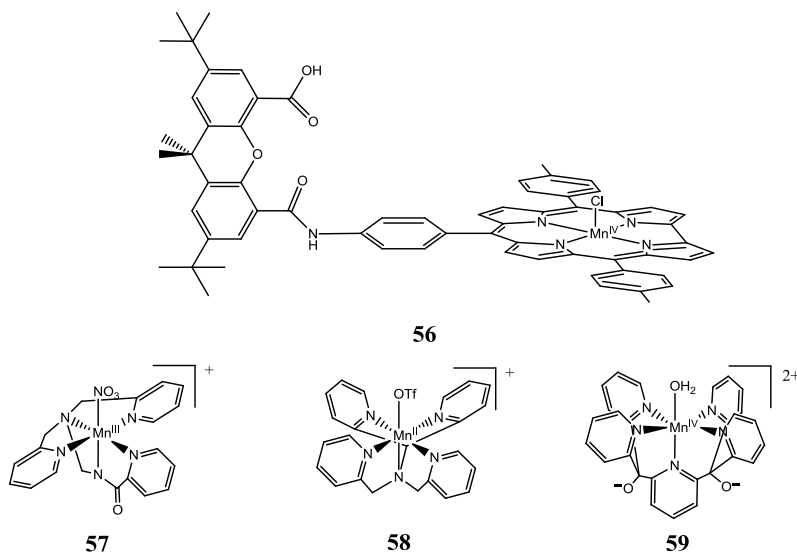
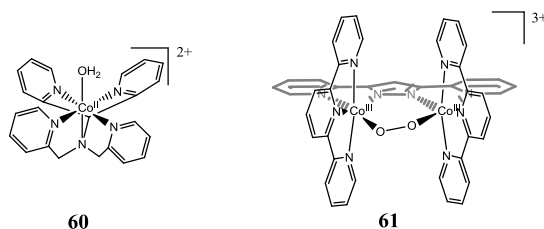


Figure 36. Structure of complexes **56**, **57**, **58** and **59**.

#### 1.3.4. Cobalt catalyst.

In 2011 Berlinguette *et al.* reported<sup>101</sup> the first cobalt single-site WOC. They used the pentadentate 2,6-(bis(bis-2-pyridil)methoxy-methane)-pyridine ligand (Py5) to prepare a mononuclear complex (**60**) where the sixth free coordination position is occupied by an aquo ligand (Figure 37). The activity of **60** was evaluated by cyclic voltammetry experiments, nevertheless it remains uncertain if **60** is the truly active species.<sup>144</sup> Later on, Llobet *et. al* synthesized<sup>145</sup> a new dinuclear Co(III) catalyst (**61**) based on the bridging ligand  $\text{bpp}^-$  (Figure 37). The complex is the cobalt analogue of **1**, though a peroxo bridge replaces the two aquo groups. Peroxo complexes are proposed to be key intermediates in the mechanism of water oxidation, as a consequence **61** represents an attractive compound to carry out electrochemical and kinetic studies. The catalyst could electrochemically oxidize water at pH = 2.1 at high overpotential ( $\eta = 0.89$  V), exhibiting only slight signs of degradation. However,

it could not be completely exclude the possibility that the actual catalyst proceeded from the decomposition of the complex.



**Figure 37.** Structure of complexes **60** and **61**.

Cobalt polyoxometalates constitute an important class of WOC, but they will be considered later.

It is worth noting in this section the development and study of the famous heterogeneous catalyst abbreviated as **CoP<sub>i</sub>**. In 2008, Nocera *et al.* found<sup>146</sup> that a cobalt oxide film formed by electrodeposition from a solution containing cobalt, potassium and phosphate ions was able to oxidize water. The central structure motif<sup>147,148</sup> of the material consists in a cluster of interconnected complete or incomplete Co<sup>III</sup>-oxo cubanes (Figure 38).

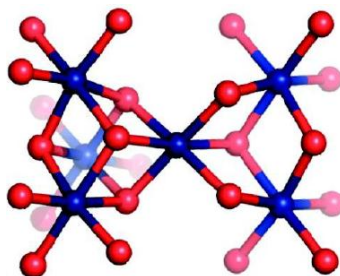


**Figure 38.** Structural motif of **CoP<sub>i</sub>** as deduced from X-Ray spectroscopy (XAS) data. The film can be composed of a mixture of complete and incomplete cubanes. Furthermore, the protonation states of the bridging oxo and terminal aquo ligands remain unknown. Taken from reference 145.

The heterogeneous catalyst has achieved a great media impact<sup>149</sup> and has been subjected to extensive mechanistic<sup>150-153</sup> studies. It was also successfully incorporated into a photoelectrochemical cell for the splitting of water<sup>154</sup> similar to the one depicted in Figure 7. The promissory results led Nocera to set up a spin-out company called Sun Catalytix in 2009. However, they failed in achieving a commercially viable water splitting device and now have abandoned the concept of “artificial leaf”<sup>155</sup> in order to return the venture capital initially invested by the Indian multinational Tata Group. This failure proves that the development of an effective photoelectrochemical cell is nowadays a very difficult task and it lacks active and robust WOCs.

### 1.3.5. Copper catalysts.

In 2012, *Mayer et al.* found<sup>156</sup> the first well characterized molecular copper WOC. The catalyst  $[\text{Cu}^{\text{II}}(\text{bpy})(\text{OH})_2]$  (**62**) is formed by self-assembling from copper salts and bipyridine at basic pH (Figure 39). It can electrochemically oxidize water at pH 11.8-13.3, although the overpotential is quite high ( $\eta = 0.75$  V). The TOF value of  $100 \text{ s}^{-1}$  is impressive and lies among the fastest homogeneous WOCs reported at the moment, but it has been obtained indirectly by means of CV experiments.

Afterwards, *Meyer et al.* demonstrated that simple Cu(II) salts could also electrochemically oxidize water in neutral or weakly basic solutions containing a  $\text{CO}_2/\text{HCO}_3^-/\text{CO}_3^{2-}$ , acetate or  $\text{HPO}_4^{2-}/\text{PO}_4^{3-}$  buffer. The same group reported a new single-site Cu(II) catalyst<sup>102</sup> constituted by a triglycylglycine macrocyclic ( $\text{TGG}^{4-}$ ) and an aquo ligands,  $[\text{Cu}^{\text{II}}(\text{TGG})(\text{H}_2\text{O})]^{2-}$  (**63** in Figure 39). The complex was able to electrochemically oxidize water at pH = 11 and at high overpotential ( $\eta = 0.72$  V) without showing any sign of degradation. The

calculated TOF of  $33 \text{ s}^{-1}$  is remarkable but it has been derived from CV experiments as in the case of **62**.

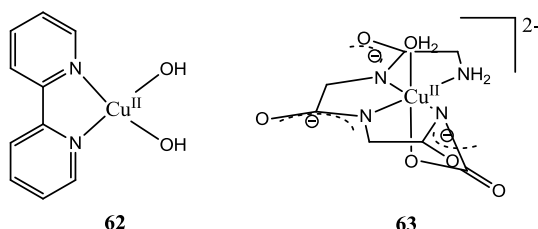


**Figure 39.** Structure of the copper complexes **62** and **63**.

### 1.3.6. Iron catalyst.

There are several Fe complexes that have been described<sup>157-160</sup> to work as WOCs using different sacrificial oxidants:  $[\text{Ru}^{\text{III}}(\text{bpy})_3]^{3+}$ , Ce(IV) and  $\text{NaIO}_4$ . This studies do not establish the truly nature of the active species in the catalytic cycle or preclude the formation of active nanoparticles. Lau *et. al.* have demonstrated<sup>161</sup> that various molecular Fe complexes, among them *cis*- $[\text{Fe}^{\text{II}}(\text{mcp})\text{Cl}_2]$  (**64** in Figure 40), produce  $\text{Fe}_2\text{O}_3$  nanoparticles at basic pH when photochemical catalytic water oxidation is evaluated using  $[\text{Ru}(\text{bpy})_3]^{2+}$  as photosensitizer and  $\text{S}_2\text{O}_8^{2-}$  as sacrificial electron acceptor. The solid is set up as the actual catalyst. Similar conclusions were achieved by Llobet *et. al.* recently<sup>162</sup> employing the Fe compounds  $[\text{Fe}^{\text{II}}(\text{BQEN})(\text{OTf})_2]$  and  $[\text{Fe}^{\text{II}}(\text{BQCN})(\text{OTf})_2]$  (**65** and **66** respectively in Figure 40) Furthermore, this group has proved that the same complexes operate as homogeneous catalyst in water oxidation using CAN as sacrificial oxidant, but the acidity of the media is a crucial factor. At  $\text{pH} = 1$ , dissociation of the BQEN and BQCN ligands occurs and the resulting complex is inactive. In contrast, if **65** and **66** are dissolved in an unbuffered solution and an excess of CAN is subsequently added, oxygen and a small amount of  $\text{CO}_2$  are released. Although it is known that the addition

of CAN decreases the pH and it could thus promote the dissociation of the ligands, the oxidation of the initial  $\text{Fe}^{\text{II}}\text{-OH}_2$  complex to  $\text{Fe}^{\text{IV}}\text{=O}$  is faster. Once the  $\text{Fe}^{\text{IV}}\text{=O}$  complex is formed, the dissociation of the ligands might be slowed down in this oxidation state. Therefore, this study shows that the current Fe catalysts are not efficient as WOCs, nevertheless it provides important mechanistic insights in order to develop more robust catalysts with this metal.

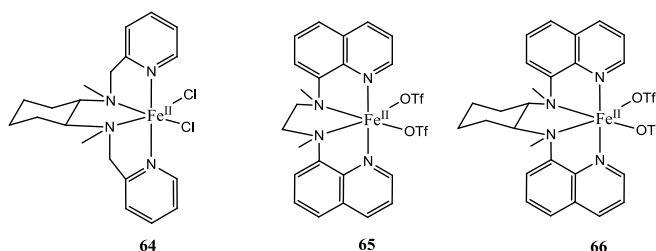


**Figure 40.** Structures of the Fe complexes **64**, **65** and **66**.

### 1.3.7. Polyoxometalates catalysts.

I have decided to consider WOCs based on polyoxometalates (POMs) as an independent section in spite of they can contain a variety of transition metals such as Ru, Co, Cu or Ir. Most of the described WOCs so far contain organic ligands which can be degraded<sup>163</sup> under the oxidatively harsh catalytic conditions. Inspired by this feature and the use of certain POM compounds in numerous catalytic organic oxidations,<sup>164</sup> Shannon *et al.* evaluated the performance<sup>165</sup> of the mono-Ru  $[\text{PW}_{11}\text{O}_{39}\text{Ru}^{\text{III}}(\text{H}_2\text{O})]^{4-}$  and di-Ru  $[\text{Ru}_2^{\text{III}}\text{Zn}_2(\text{H}_2\text{O})_2(\text{ZnW}_9\text{O}_{34})_2]^{14-}$  (**67** in Figure 41) POMs as water oxidation catalysts. The di-Ru POM was able to produce oxygen electrochemically whereas the mono-Ru was inactive. Later on, Bonchio *et al.* described<sup>166,167</sup> a tetranuclear Ru POM capable of oxidizing water using CAN as sacrificial oxidant. The compound with formula  $\{[\text{Ru}^{\text{IV}}_4\text{O}_4(\text{OH})_2(\text{H}_2\text{O})_4][\gamma\text{-SiW}_{10}\text{O}_{36}]_2\}^{10-}$  structurally consists in an electrophilic  $[\text{Ru}^{\text{IV}}_4(\mu\text{-O})_4(\mu\text{-OH})_2(\text{H}_2\text{O})_4]^{6+}$  central core

embedded in two divacant  $[\gamma\text{-SiW}_{10}\text{O}_{36}]^{8-}$  POMs (**68** in Figure 41). **68** has also been electrostatically anchored onto functionalized multiwalled carbon nanotubes. The assembly evolved electrochemically oxygen at overpotentials as low as 0.35 V when it was deposited on an ITO electrode. The TOFs achieved modest values (up to  $0.08\text{ s}^{-1}$ ) and were similar to those calculated in homogeneous catalysis. Furthermore, Hill *et al.* have reported<sup>168</sup> that **68** can photochemically oxidize water using  $[\text{Ru}(\text{bpy})_3]^{2+}$  as photosensitizer and  $\text{S}_2\text{O}_8^{2-}$  as sacrificial electron acceptor. The same group prepared and evaluated several POMs constituted by central cores based on Co as WOC, using  $[\text{Ru}(\text{bpy})_3]^{3+}$  as sacrificial oxidant. The cluster with formula  $\{[\text{Co}_4(\text{H}_2\text{O})_2][\text{PW}_9\text{O}_{34}]_2\}^{10-}$  (**69** in Figure 41) was the only active, attaining a TOF of  $5\text{ s}^{-1}$  and an efficiency of 64 % at pH = 8.0. The novelty of this work lied in the synthesis of the first POM catalyst with a central core made of an earth-abundant element. Nevertheless, a later work<sup>169</sup> by Stracke and Finke showed that the electrocatalytic oxidation of water by **69** at pH = 8.0 generates  $\text{CoO}_x$  nanoparticles onto the electrode which are the actual catalysts.

The single-site catalytic concept has also strongly influenced in the development of new polyoxometalates WOCs. Fukuzumi *et al.* have evaluated<sup>99</sup> the previously described POMs  $[\text{Ru}^{\text{III}}(\text{H}_2\text{O})\text{SiW}_{11}\text{O}_{39}]^{5-}$  and  $[\text{Ru}^{\text{III}}(\text{H}_2\text{O})\text{GeW}_{11}\text{O}_{39}]^{5-}$  (**70** and **71** respectively in Figure 41) as catalysts using CAN as sacrificial oxidant. The spectroscopic and kinetic studies revealed that the mechanism is similar to that proposed for complexes related to  $[\text{Ru}^{\text{II}}(\text{trpy})(\text{bpy})(\text{H}_2\text{O})]^{2+}$ , although the water nucleophilic attack on  $[\text{Ru}^{\text{V}}=\text{O}]$  was established as the rate determining step.



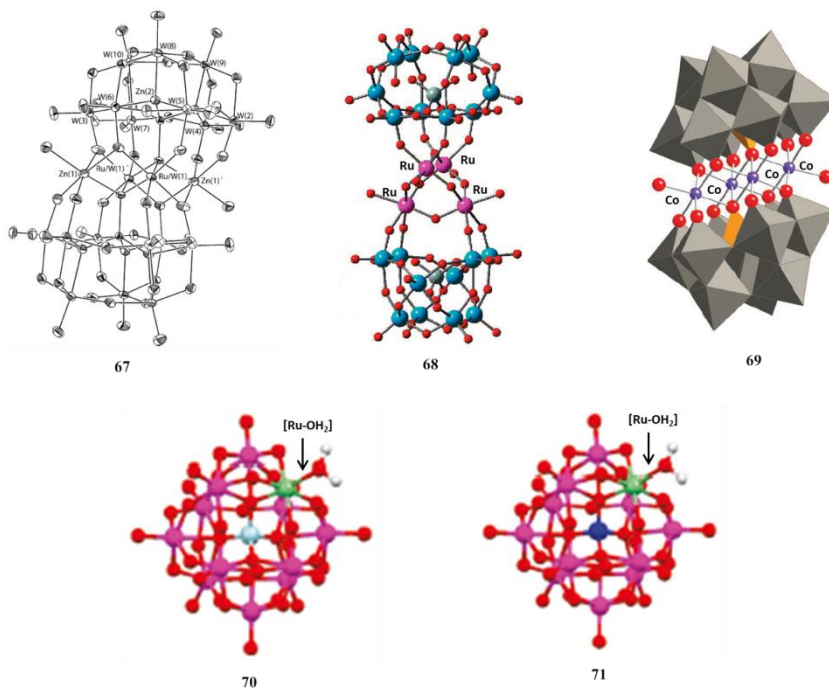


**Figure 41.** Structures of the most relevant WOCs based on POM scaffolds. The structures were taken directly from the original references.

### 1.3.8. Organic catalysts.

It has been recently demonstrated<sup>170</sup> that a fully organic compound can act as a WOC, what involves an exotic finding in the field. The N(5)-ethylflavinium ion (**72** in Figure 42) carries out electrode-assisted catalytic water oxidation at high overpotential ( $\eta > 0.79$  V). At the molecular level, it has been proposed that **72** is firstly oxidized to the flavinium radical dication Et-FI<sup>2+</sup>. Secondly this compound undergoes a water nucleophilic attack to form Et-FIOH<sup>+</sup>. The new specie is subsequently oxidized to the oxyl cationic radical Et-FIO<sup>+</sup>, which represents a key intermediate in the mechanism. The oxy radical from Et-FIO<sup>+</sup> enables an O-O coupling with an oxyl radical from the surface of the glassy carbon or Pt electrode leading to the release of oxygen (Figure 42).

On the basis of this work, new modified N-doped carbon electrodes could be assembled in order to find effective heterogeneous water oxidation catalysts.

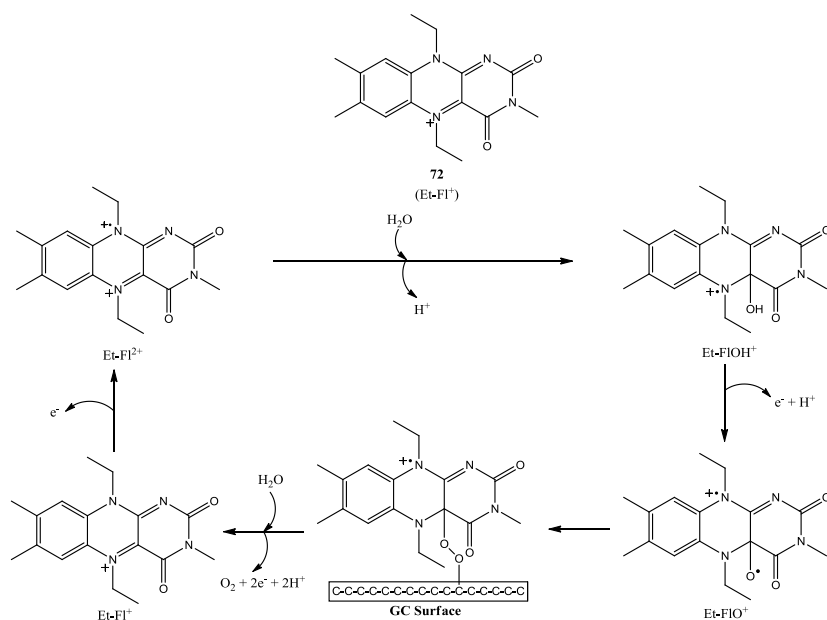


**Figure 42.** Structure of **71** and mechanism for electrocatalytic water oxidation mediated by a glassy carbon electrode.

#### 1.4. References.

- (1) Intergovernmental Panel on Climate Change (IPCC), [http://www.ipcc.ch/presentations and speeches/presentations and speeches.shtml](http://www.ipcc.ch/presentations_and_speeches/presentations_and_speeches.shtml)
- (2) Owen, N. A.; Inderwildi, O. R.; King, D. A. *Energy Policy* **2010**, *38*, 4743.
- (3) *Climate Change 2007: Synthesis Report* Core Writing Team; Pachauri, R. K.; Reisinger, A., Eds.; IPCC: Geneva, Switzerland, 2008.
- (4) Gordon, Z. J., Sunday Dialogue: Nuclear Energy, Pro and Con In *New York Times*, February 25, 2012.
- (5) Brook, B. W.; Lowe, I. *Why vs. Why: Nuclear Power* Pantera Press, 2010.
- (6) Lewis, N. S.; Nocera, D. G. *Proc. Natl. Acad. Sci. U.S.A.* **2006**, *103*, 15729.
- (7) *Energy...behind oil*; Armstrong, F.; Blundell, K., Eds. Oxford, UK, 2007.
- (8) Ballesteros, M., In *Investigación y Ciencia*, November 2006.

- (9) Carpintero, O., Biocombustibles y uso energético de la biomasa: un análisis crítico In *Ecologista*, September 2006.
- (10) Red Eléctrica de España *El sistema eléctrico español. Avance del informe de 2011*, 2012.
- (11) Energy Information Administration *International Energy Outlook*, 2006.
- (12) Milborrow, D., Is Wind Power reliable? In *New Power UK*, February 2009.
- (13) Jha, A., In *The Guardian*, May 26 2009.
- (14) World Nuclear Association *Renewable Energy and Electricity*, December 2012.
- (15) Moore, P., In *Theage.com.au*, December 10 2012.
- (16) Lovins, A., <http://www.calcars.org/calcars-news/570.html>
- (17) Nocera, D. G. *Inorg. Chem.* **2009**, *48*, 10001.
- (18) Brumfiel, G., Las piezas ausentes del Proyecto ITER In *Investigación y Ciencia*, January 2013.
- (19) Hammarström, L.; Hammes-Schiffer, S. *Acc. Chem. Res.* **2009**, *42*, 1859.
- (20) Chen, Z.; Concepcion, J. J.; Brennaman, M. K.; Kang, P.; Norris, M. R.; Hoertz, P. G.; Meyer, T. J. *Proc. Natl. Acad. Sci. U.S.A.* **2012**, *109*, 15606.
- (21) Romain, S.; Vigara, L.; Llobet, A. *Acc. Chem. Res.* **2009**, *42*, 1944.
- (22) Warren, J. J.; Tronic, T. A.; Mayer, J. M. *Chem. Rev. (Washington, DC, U. S.)* **2010**, *110*, 6961.
- (23) Ferreira, K. N.; Iverson, T. M.; Maghlaoui, K.; Barber, J.; Iwata, S. *Science* **2004**, *303*, 1831.
- (24) Guskov, A.; Kern, J.; Gabdulkhakov, A.; Broser, M.; Zouni, A.; Saenger, W. *Nat. Struct. Mol. Biol.* **2009**, *16*, 334.
- (25) Loll, B.; Kern, J.; Saenger, W.; Zouni, A.; Biesiadka, J. *Nature* **2005**, *438*, 1040.
- (26) Umena, Y.; Kawakami, K.; Shen, J.-R.; Kamiya, N. *Nature* **2011**, *473*, 55.
- (27) Karlsson, S.; Boixel, J.; Pellegrin, Y.; Blart, E.; Becker, H.-C.; Odobel, F.; Hammarstrom, L. *Faraday Discuss.* **2012**, *155*, 233.
- (28) Gatt, P.; Petrie, S.; Stranger, R.; Pace, R. J. *Angew. Chem. Int. Ed.* **2012**, *51*, 12025.
- (29) Luber, S.; Rivalta, I.; Umena, Y.; Kawakami, K.; Shen, J.-R.; Kamiya, N.; Brudvig, G. W.; Batista, V. S. *Biochemistry* **2011**, *50*, 6308.
- (30) Galstyan, A.; Robertazzi, A.; Knapp, E. W. *J. Am. Chem. Soc.* **2012**, *134*, 7442.
- (31) Grundmeier, A.; Dau, H. *Biochimica et Biophysica Acta (BBA) - Bioenergetics* **2012**, *1817*, 88.
- (32) Pace, R. J.; Jin, L.; Stranger, R. *Dalton Trans.* **2012**, *41*, 11145.

- (33) Gatt, P.; Stranger, R.; Pace, R. J. *Journal of Photochemistry and Photobiology B: Biology* **2011**, *104*, 80.
- (34) Rapatskiy, L.; Cox, N.; Savitsky, A.; Ames, W. M.; Sander, J.; Nowaczyk, M. M.; Rögnér, M.; Boussac, A.; Neese, F.; Messinger, J.; Lubitz, W. *J. Am. Chem. Soc.* **2012**, *134*, 16619.
- (35) Hillier, W.; Messinger, J. *Mechanism of Photosynthetic Oxygen Production*; Springer: The Netherlands, 2005; Vol. 1.
- (36) Barber, J.; Ferreira, K.; Maghlaoui, K.; Iwata, S. *Phys. Chem. Chem. Phys.* **2004**, *6*, 4737.
- (37) Messinger, J.; Badger, M.; Wydrzynski, T. *Proc. Natl. Acad. Sci. U.S.A.* **1995**, *92*, 3209.
- (38) Sproviero, E. M.; Gascón, J. A.; McEvoy, J. P.; Brudvig, G. W.; Batista, V. S. *J. Am. Chem. Soc.* **2008**, *130*, 3428.
- (39) Kusunoki, M. *Biochimica et Biophysica Acta (BBA) - Bioenergetics* **2007**, *1767*, 484.
- (40) Dau, H.; Haumann, M. *Biochimica et Biophysica Acta (BBA) - Bioenergetics* **2007**, *1767*, 472.
- (41) Siegbahn, P. E. M. *Acc. Chem. Res.* **2009**, *42*, 1871.
- (42) Sala, X.; Romero, I.; Rodríguez, M.; Escriche, L.; Llobet, A. *Angew. Chem. Int. Ed.* **2009**, *48*, 2842.
- (43) Herrero, C.; Lassalle-Kaiser, B.; Leibl, W.; Rutherford, A. W.; Aukauloo, A. *Coord. Chem. Rev.* **2008**, *252*, 456.
- (44) Sanderson, K. *Nature* **2008**, *452*, 400.
- (45) Nocera, D. G. *Acc. Chem. Res.* **2012**, *45*, 767.
- (46) Eisenberg, R.; Gray, H. B. *Inorg. Chem.* **2008**, *47*, 1697.
- (47) Hurst, J. K. *Science* **2010**, *328*, 315.
- (48) Hammarstrom, L.; Styring, S. *Nat Chem* **2009**, *1*, 185.
- (49) Llobet, A. *Nat Chem* **2010**, *2*, 804.
- (50) Gust, D.; Moore, T. A.; Moore, A. L. *Faraday Discuss.* **2012**, *155*, 9.
- (51) Gagliardi, C. J.; Vannucci, A. K.; Concepcion, J. J.; Chen, Z.; Meyer, T. J. *Energy Environ. Sci* **2012**, *5*, 7704.
- (52) Moyer, B. A.; Meyer, T. J. *J. Am. Chem. Soc.* **1978**, *100*, 3601.
- (53) Moyer, B. A.; Meyer, T. J. *Inorg. Chem.* **1981**, *20*, 436.
- (54) Meyer, T. J.; Huynh, M. H. V. *Inorg. Chem.* **2003**, *42*, 8140.
- (55) Mayer, J. M. *Acc. Chem. Res.* **2011**, *44*, 36.
- (56) Chen, Z.; Vannucci, A. K.; Concepcion, J. J.; Jurss, J. W.; Meyer, T. J. *Proc. Natl. Acad. Sci. U.S.A.* **2011**, *108*, E1461.
- (57) Weinberg, D. R.; Gagliardi, C. J.; Hull, J. F.; Murphy, C. F.; Kent, C. A.; Westlake, B. C.; Paul, A.; Ess, D. H.; McCafferty, D. G.; Meyer, T. J. *Chem. Rev. (Washington, DC, U. S.)* **2012**, *112*, 4016.

- (58) Anxolabehere-Mallart, E.; Costentin, C.; Policar, C.; Robert, M.; Saveant, J.-M.; Teillout, A.-L. *Faraday Discuss.* **2011**, *148*, 83.
- (59) Hammes-Schiffer, S. *Chem. Rev. (Washington, DC, U. S.)* **2010**, *110*, 6937.
- (60) Liu, F.; Concepcion, J. J.; Jurss, J. W.; Cardolaccia, T.; Templeton, J. L.; Meyer, T. J. *Inorg. Chem.* **2008**, *47*, 1727.
- (61) Huynh, M. H. V.; Meyer, T. J. *Chem. Rev. (Washington, DC, U. S.)* **2007**, *107*, 5004.
- (62) Marcus, R. A. *The Journal of Chemical Physics* **1956**, *24*, 966.
- (63) Laviron, E. *Journal of Electroanalytical Chemistry and Interfacial Electrochemistry* **1981**, *124*, 1.
- (64) Laviron, E. *Journal of Electroanalytical Chemistry and Interfacial Electrochemistry* **1983**, *146*, 1.
- (65) Laviron, E. *Journal of Electroanalytical Chemistry and Interfacial Electrochemistry* **1983**, *146*, 15.
- (66) Gilbert, J. A.; Eggleston, D. S.; Murphy, W. R.; Geselowitz, D. A.; Gersten, S. W.; Hodgson, D. J.; Meyer, T. J. *J. Am. Chem. Soc.* **1985**, *107*, 3855.
- (67) Gersten, S. W.; Samuels, G. J.; Meyer, T. J. *J. Am. Chem. Soc.* **1982**, *104*, 4029.
- (68) Binstead, R. A.; Chronister, C. W.; Ni, J.; Hartshorn, C. M.; Meyer, T. J. *J. Am. Chem. Soc.* **2000**, *122*, 8464.
- (69) Yamada, H.; Hurst, J. K. *J. Am. Chem. Soc.* **2000**, *122*, 5303.
- (70) Stull, J. A.; Britt, R. D.; McHale, J. L.; Knorr, F. J.; Lymar, S. V.; Hurst, J. K. *J. Am. Chem. Soc.* **2012**, *132*, 19973.
- (71) Moonshiram, D.; Jurss, J. W.; Concepcion, J. J.; Zakharova, T.; Alperovich, I.; Meyer, T. J.; Pushkar, Y. *J. Am. Chem. Soc.* **2012**, *134*, 4625.
- (72) Lei, Y.; Hurst, J. K. *Inorg. Chem.* **1994**, *33*, 4460.
- (73) Hurst, J. K.; Zhou, J.; Lei, Y. *Inorg. Chem.* **1992**, *31*, 1010.
- (74) Cape, J. L.; Lymar, S. V.; Lightbody, T.; Hurst, J. K. *Inorg. Chem.* **2009**, *48*, 4400.
- (75) Schoonover, J. R.; Ni, J.; Roecker, L.; White, P. S.; Meyer, T. J. *Inorg. Chem.* **1996**, *35*, 5885.
- (76) Yamada, H.; Siems, W. F.; Koike, T.; Hurst, J. K. *J. Am. Chem. Soc.* **2004**, *126*, 9786.
- (77) Cape, J. L.; Siems, W. F.; Hurst, J. K. *Inorg. Chem.* **2009**, *48*, 8729.
- (78) Hurst, J. K. *Coord. Chem. Rev.* **2005**, *249*, 313.
- (79) Yamada, H.; Koike, T.; Hurst, J. K. *J. Am. Chem. Soc.* **2001**, *123*, 12775.
- (80) Yang, X.; Baik, M.-H. *J. Am. Chem. Soc.* **2006**, *128*, 7476.
- (81) Sens, C.; Romero, I.; Rodríguez, M.; Llobet, A.; Parella, T.; Benet-Buchholz, J. *J. Am. Chem. Soc.* **2004**, *126*, 7798.

- (82) Bozoglian, F.; Romain, S.; Ertem, M. Z.; Todorova, T. K.; Sens, C.; Mola, J.; Rodri•guez, M.; Romero, I.; Benet-Buchholz, J.; Fontrodona, X.; Cramer, C. J.; Gagliardi, L.; Llobet, A. *J. Am. Chem. Soc.* **2009**, *131*, 15176.
- (83) Romain, S.; Bozoglian, F.; Sala, X.; Llobet, A. *J. Am. Chem. Soc.* **2009**, *131*, 2768.
- (84) Zong, R.; Thummel, R. P. *J. Am. Chem. Soc.* **2005**, *127*, 12802.
- (85) Deng, Z.; Tseng, H.-W.; Zong, R.; Wang, D.; Thummel, R. *Inorg. Chem.* **2008**, *47*, 1835.
- (86) Wada, T.; Tsuge, K.; Tanaka, K. *Inorg. Chem.* **2000**, *40*, 329.
- (87) Muckerman, J. T.; Polyansky, D. E.; Wada, T.; Tanaka, K.; Fujita, E. *Inorg. Chem.* **2008**, *47*, 1787.
- (88) Ghosh, S.; Baik, M.-H. *Inorg. Chem.* **2011**, *50*, 5946.
- (89) Betley, T. A.; Wu, Q.; Van Voorhis, T.; Nocera, D. G. *Inorg. Chem.* **2008**, *47*, 1849.
- (90) Wasylenko, D. J.; Ganesamoorthy, C.; Koivisto, B. D.; Berlinguette, C. P. *Eur. J. Inorg. Chem.* **2010**, *2010*, 3135.
- (91) Concepcion, J. J.; Jurss, J. W.; Brennaman, M. K.; Hoertz, P. G.; Patrocinio, A. O. v. T.; Murakami Iha, N. Y.; Templeton, J. L.; Meyer, T. J. *Acc. Chem. Res.* **2009**, *42*, 1954.
- (92) Hetterscheld, D. G. H.; Reek, J. N. H. *Angew. Chem. Int. Ed.* **2012**, *51*, 9740.
- (93) Duan, L.; Bozoglian, F.; Mandal, S.; Stewart, B.; Privalov, T.; Llobet, A.; Sun, L. *Nat Chem* **2012**, *4*, 418.
- (94) Bryant, J. R.; Matsuo, T.; Mayer, J. M. *Inorg. Chem.* **2004**, *43*, 1587.
- (95) Tseng, H.-W.; Zong, R.; Muckerman, J. T.; Thummel, R. *Inorg. Chem.* **2008**, *47*, 11763.
- (96) Concepcion, J. J.; Jurss, J. W.; Templeton, J. L.; Meyer, T. J. *J. Am. Chem. Soc.* **2008**, *130*, 16462.
- (97) Concepcion, J. J.; Tsai, M.-K.; Muckerman, J. T.; Meyer, T. J. *J. Am. Chem. Soc.* **2010**, *132*, 1545.
- (98) Chen, Z.; Concepcion, J. J.; Luo, H.; Hull, J. F.; Paul, A.; Meyer, T. J. *J. Am. Chem. Soc.* **2010**, *132*, 17670.
- (99) Murakami, M.; Hong, D.; Suenobu, T.; Yamaguchi, S.; Ogura, T.; Fukuzumi, S. *J. Am. Chem. Soc.* **2011**, *133*, 11605.
- (100) Blakemore, J. D.; Schley, N. D.; Balcells, D.; Hull, J. F.; Olack, G. W.; Incarvito, C. D.; Eisenstein, O.; Brudvig, G. W.; Crabtree, R. H. *J. Am. Chem. Soc.* **2010**, *132*, 16017.
- (101) Wasylenko, D. J.; Ganesamoorthy, C.; Borau-Garcia, J.; Berlinguette, C. P. *Chem. Commun. (Cambridge, U. K.)* **2011**, *47*, 4249.

- (102) Zhang, M.-T.; Chen, Z.; Kang, P.; Meyer, T. J. *J. Am. Chem. Soc.* **2013**, *135*, 2048.
- (103) Wasylenko, D. J.; Ganesamoorthy, C.; Henderson, M. A.; Koivisto, B. D.; Osthoff, H. D.; Berlinguette, C. P. *J. Am. Chem. Soc.* **2010**, *132*, 16094.
- (104) Polyansky, D. E.; Muckerman, J. T.; Rochford, J.; Zong, R.; Thummel, R. P.; Fujita, E. *J. Am. Chem. Soc.* **2011**, *133*, 14649.
- (105) Roeser, S.; Farràs, P.; Bozoglian, F.; Martínez-Belmonte, M.; Benet-Buchholz, J.; Llobet, A. *ChemSusChem* **2011**, *4*, 197.
- (106) Duan, L.; Fischer, A.; Xu, Y.; Sun, L. *J. Am. Chem. Soc.* **2009**, *131*, 10397.
- (107) Kohl, S. W.; Weiner, L.; Schwartsburd, L.; Konstantinovski, L.; Shimon, L. J. W.; Ben-David, Y.; Iron, M. A.; Milstein, D. *Science* **2009**, *324*, 74.
- (108) Eisenberg, R. *Science* **2009**, *324*, 44.
- (109) Hetterscheid, D. G. H.; van der Vlugt, J. I.; de Bruin, B.; Reek, J. N. H. *Angew. Chem. Int. Ed.* **2009**, *48*, 8178.
- (110) Cosnier, S.; Karyakin, A. *Electropolymerization. Concepts, materials and applications.*, 2010.
- (111) *Electropolymerization*; Schab-Balcerzak, E., Ed.; INTECHWEB.ORG: Rijeka, Croatia, 2011.
- (112) Liu, F.; Cardolaccia, T.; Hornstein, B. J.; Schoonover, J. R.; Meyer, T. J. *J. Am. Chem. Soc.* **2007**, *129*, 2446.
- (113) Lebeau, E. L.; Adeyemi, S. A.; Meyer, T. J. *Inorg. Chem.* **1998**, *37*, 6476.
- (114) Francàs, L.; Sala, X.; Benet-Buchholz, J.; Escriche, L.; Llobet, A. *ChemSusChem* **2009**, *2*, 321.
- (115) Tong, L.; Gothelid, M.; Sun, L. *Chem. Commun. (Cambridge, U. K.)* **2012**, *48*, 10025.
- (116) Li, F.; Zhang, B.; Li, X.; Jiang, Y.; Chen, L.; Li, Y.; Sun, L. *Angew. Chem. Int. Ed.* **2011**, *50*, 12276.
- (117) Belanger, D.; Pinson, J. *Chem. Soc. Rev.* **2011**, *40*, 3995.
- (118) Glasson, C. R. K.; Song, W.; Ashford, D. L.; Vannucci, A.; Chen, Z.; Concepcion, J. J.; Holland, P. L.; Meyer, T. J. *Inorg. Chem.* **2012**, *51*, 8637.
- (119) Li, L.; Duan, L.; Xu, Y.; Gorlov, M.; Hagfeldt, A.; Sun, L. *Chem. Commun. (Cambridge, U. K.)* **2010**, *46*, 7307.
- (120) Gao, Y.; Ding, X.; Liu, J.; Wang, L.; Lu, Z.; Li, L.; Sun, L. *J. Am. Chem. Soc.* **2013**, *135*, 4219.
- (121) Kiwi, J.; Grätzel, M. *Angew. Chem., Int. Ed. Engl.* **1978**, *17*, 860.
- (122) Kiwi, J.; Grätzel, M. *Angew. Chem., Int. Ed. Engl.* **1979**, *18*, 624.
- (123) Harriman, A.; Pickering, I. J.; Thomas, J. M.; Christensen, P. A. *J. Chem. Soc., Faraday Trans. 1* **1988**, *84*, 2795.

- (124) Youngblood, W. J.; Lee, S.-H. A.; Kobayashi, Y.; Hernandez-Pagan, E. A.; Hoertz, P. G.; Moore, T. A.; Moore, A. L.; Gust, D.; Mallouk, T. E. *J. Am. Chem. Soc.* **2009**, *131*, 926.
- (125) McDaniel, N. D.; Coughlin, F. J.; Tinker, L. L.; Bernhard, S. *J. Am. Chem. Soc.* **2007**, *130*, 210.
- (126) Bucci, A.; Savini, A.; Rocchigiani, L.; Zuccaccia, C.; Rizzato, S.; Albinati, A.; Llobet, A.; Macchioni, A. *Organometallics* **2012**, *31*, 8071.
- (127) Junge, H.; Marquet, N.; Kammer, A.; Denurra, S.; Bauer, M.; Wohlrab, S.; Gärtner, F.; Pohl, M.-M.; Spannenberg, A.; Gladiali, S.; Beller, M. *Chemistry – A European Journal* **2012**, *18*, 12749.
- (128) Joya, K. S.; Subbaiyan, N. K.; D'Souza, F.; de Groot, H. J. M. *Angew. Chem. Int. Ed.* **2012**, *51*, 9601.
- (129) Petronilho, A.; Rahman, M.; Woods, J. A.; Al-Sayyed, H.; Muller-Bunz, H.; Don MacElroy, J. M.; Bernhard, S.; Albrecht, M. *Dalton Trans.* **2012**, *41*, 13074.
- (130) DePasquale, J.; Nieto, I.; Reuther, L. E.; Herbst-Gervasoni, C. J.; Paul, J. J.; Mochalin, V.; Zeller, M.; Thomas, C. M.; Addison, A. W.; Papish, E. T. *Inorg. Chem.* **2013**, *52*, 9175.
- (131) Grotjahn, D. B.; Brown, D. B.; Martin, J. K.; Marelius, D. C.; Abadjian, M.-C.; Tran, H. N.; Kalyuzhny, G.; Vecchio, K. S.; Specht, Z. G.; Cortes-Llamas, S. A.; Miranda-Soto, V.; van Niekerk, C.; Moore, C. E.; Rheingold, A. L. *J. Am. Chem. Soc.* **2011**, *133*, 19024.
- (132) Schley, N. D.; Blakemore, J. D.; Subbaiyan, N. K.; Incarvito, C. D.; Dâ€™Souza, F.; Crabtree, R. H.; Brudvig, G. W. *J. Am. Chem. Soc.* **2011**, *133*, 10473.
- (133) Blakemore, J. D.; Mara, M. W.; Kushner-Lenhoff, M. N.; Schley, N. D.; Konezny, S. J.; Rivalta, I.; Negre, C. F. A.; Snoeberger, R. C.; Kokhan, O.; Huang, J.; Stickrath, A.; Tran, L. A.; Parr, M. L.; Chen, L. X.; Tiede, D. M.; Batista, V. S.; Crabtree, R. H.; Brudvig, G. W. *Inorg. Chem.* **2013**, *52*, 1860.
- (134) Savini, A.; Belanzoni, P.; Bellachioma, G.; Zuccaccia, C.; Zuccaccia, D.; Macchioni, A. *Green Chem.* **2011**, *13*, 3360.
- (135) Wang, C.; Wang, J.-L.; Lin, W. *J. Am. Chem. Soc.* **2012**, *134*, 19895.
- (136) Hintermair, U.; Sheehan, S. W.; Parent, A. R.; Ess, D. H.; Richens, D. T.; Vaccaro, P. H.; Brudvig, G. W.; Crabtree, R. H. *J. Am. Chem. Soc.* **2013**, *135*, 10837.
- (137) Gao, Y.; Crabtree, R. H.; Brudvig, G. W. *Inorg. Chem.* **2012**, *51*, 4043.
- (138) Baffert, C.; Romain, S.; Richardot, A.; Leprêtre, J.-C.; Lefebvre, B.; Deronzier, A.; Collomb, M.-N. *J. Am. Chem. Soc.* **2005**, *127*, 13694.
- (139) Brimblecombe, R.; Swiegers, G. F.; Dismukes, G. C.; Spiccia, L. *Angew. Chem. Int. Ed.* **2008**, *47*, 7335.



- (140) Brimblecombe, R.; Koo, A.; Dismukes, G. C.; Swiegers, G. F.; Spiccia, L. J. *Am. Chem. Soc.* **2010**, *132*, 2892.
- (141) Gao, Y.; Liu, J.; Wang, M.; Na, Y.; Åkermark, B.; Sun, L. *Tetrahedron* **2007**, *63*, 1987.
- (142) Young, K. J.; Takase, M. K.; Brudvig, G. W. *Inorg. Chem.* **2013**, *52*, 7615.
- (143) Pecoraro, V. L.; Baldwin, M. J.; Gelasco, A. *Chem. Rev. (Washington, DC, U. S.)* **1994**, *94*, 807.
- (144) Wasylenko, D. J.; Palmer, R. D.; Schott, E.; Berlinguette, C. P. *Chem. Commun. (Cambridge, U. K.)* **2012**, *48*, 2107.
- (145) Rigsby, M. L.; Mandal, S.; Nam, W.; Spencer, L. C.; Llobet, A.; Stahl, S. S. *Chem. Sci.* **2012**, *3*, 3058.
- (146) Kanan, M. W.; Nocera, D. G. *Science* **2008**, *321*, 1072.
- (147) Risch, M.; Khare, V.; Zaharieva, I.; Gerencser, L.; Chernev, P.; Dau, H. J. *Am. Chem. Soc.* **2009**, *131*, 6936.
- (148) Kanan, M. W.; Yano, J.; Surendranath, Y.; Dincă, M.; Yachandra, V. K.; Nocera, D. G. *J. Am. Chem. Soc.* **2010**, *132*, 13692.
- (149) Eisenberg, A., The Answer Is (Artificially) Blowing in the Wind In *The New York Times*, 2011.
- (150) Surendranath, Y.; Kanan, M. W.; Nocera, D. G. *J. Am. Chem. Soc.* **2010**, *132*, 16501.
- (151) Lutterman, D. A.; Surendranath, Y.; Nocera, D. G. *J. Am. Chem. Soc.* **2009**, *131*, 3838.
- (152) Surendranath, Y.; Lutterman, D. A.; Liu, Y.; Nocera, D. G. *J. Am. Chem. Soc.* **2012**, *134*, 6326.
- (153) McAlpin, J. G.; Surendranath, Y.; Dincă, M.; Stich, T. A.; Stoian, S. A.; Casey, W. H.; Nocera, D. G.; Britt, R. D. *J. Am. Chem. Soc.* **2010**, *132*, 6882.
- (154) Reece, S. Y.; Hamel, J. A.; Sung, K.; Jarvi, T. D.; Esswein, A. J.; Pijpers, J. J. H.; Nocera, D. G. *Science* **2011**, *334*, 645.
- (155) Howes, L. Artificial leaf in the shade but still growing. *chemistryworld* [Online Early Access]. Published Online: 25 July 2013. <http://www.rsc.org/chemistryworld/2013/07/artificial-leaf-synthetic-photosynthesis>.
- (156) Barnett, S. M.; Goldberg, K. I.; Mayer, J. M. *Nat Chem* **2012**, *4*, 498.
- (157) Elizarova, G. L.; Matvienko, L. G.; Lozhkina, N. V.; Parmon, V. N.; Zamaraev, K. I. *React. Kinet. Catal. Lett.* **1981**, *16*, 191.
- (158) Elizarova, G. L.; Matvienko, L. G.; Lozhkina, N. V.; Maizlish, V. E.; Parmon, V. N. *React. Kinet. Catal. Lett.* **1981**, *16*, 285.
- (159) Ellis, W. C.; McDaniel, N. D.; Bernhard, S.; Collins, T. J. *J. Am. Chem. Soc.* **2010**, *132*, 10990.

- (160) Fillol, J. L.; Codolà, Z.; Garcia-Bosch, I.; Gómez, L.; Pla, J. J.; Costas, M. *Nat Chem* **2011**, *3*, 807.
- (161) Chen, G.; Chen, L.; Ng, S.-M.; Man, W.-L.; Lau, T.-C. *Angew. Chem. Int. Ed.* **2013**, *52*, 1789.
- (162) Hong, D.; Mandal, S.; Yamada, Y.; Lee, Y.-M.; Nam, W.; Llobet, A.; Fukuzumi, S. *Inorg. Chem.* **2013**, *52*, 9522.
- (163) Francàs, L.; Sala, X.; Escudero-Adán, E.; Benet-Buchholz, J.; Escriche, L. s.; Llobet, A. *Inorg. Chem.* **2011**, *50*, 2771.
- (164) Neumann, R.; Khenkin, A. M. *Inorg. Chem.* **1995**, *34*, 5753.
- (165) Howells, A. R.; Sankarraj, A.; Shannon, C. J. *Am. Chem. Soc.* **2004**, *126*, 12258.
- (166) Sartorel, A.; Carraro, M.; Scorrano, G.; Zorzi, R. D.; Geremia, S.; McDaniel, N. D.; Bernhard, S.; Bonchio, M. *J. Am. Chem. Soc.* **2008**, *130*, 5006.
- (167) Sartorel, A.; Miroli, P.; Salvadori, E.; Romain, S.; Carraro, M.; Scorrano, G.; Valentin, M. D.; Llobet, A.; Bo, C.; Bonchio, M. *J. Am. Chem. Soc.* **2009**, *131*, 16051.
- (168) Geletii, Y. V.; Huang, Z.; Hou, Y.; Musaev, D. G.; Lian, T.; Hill, C. L. *J. Am. Chem. Soc.* **2009**, *131*, 7522.
- (169) Stracke, J. J.; Finke, R. G. *J. Am. Chem. Soc.* **2011**, *133*, 14872.
- (170) Mirzakulova, E.; Khatmullin, R.; Walpita, J.; Corrigan, T.; Vargas-Barbosa, N. M.; Vyas, S.; Oottikkal, S.; Manzer, S. F.; Hadad, C. M.; Glusac, K. D. *Nat Chem* **2012**, *4*, 794.

UNIVERSITAT ROVIRA I VIRGILI

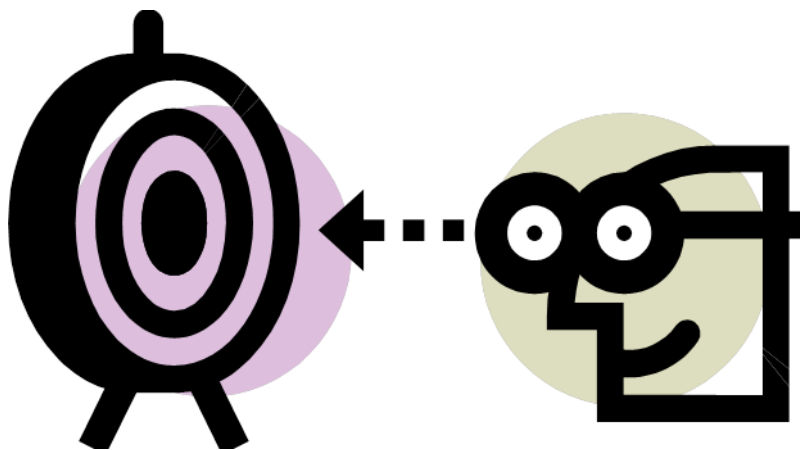
WATER OXIDATION WITH MONONUCLEAR RU COMPLEXES. BELOW THE TIP OF THE

ICEBERG: THE OXO-BRIDGE SCENARIO

Isidoro López Marin

Dipòsit Legal: T. 1505-2013

## Chapter 2. Objectives.



---

“We would never discover anything if we were to consider satisfied with things discovered”.

*Lucio Anneo Séneca, Roman Philosopher.*

---

UNIVERSITAT ROVIRA I VIRGILI

WATER OXIDATION WITH MONONUCLEAR RU COMPLEXES. BELOW THE TIP OF THE

ICEBERG: THE OXO-BRIDGE SCENARIO

Isidoro López Marin

Dipòsit Legal: T. 1505-2013

The driving force of this Thesis has been generating a meaningful knowledge about one of the current “hot topic” in chemistry: the catalytic oxidation of water to oxygen by single-site transition metal complexes. Our interest has been especially focused on revealing the molecular pathways taking place during the catalytic process. We have addressed this goal by means of the next points:

- i. The synthesis of new carefully designed mononuclear Ru complexes that can work as water oxidation catalysts (WOCs). The relationship between the electronic and steric properties of the complexes with the catalytic activity enables to gain an insight of the processes governing the catalysis.
- ii. The spectroscopic study of the mechanism of the reaction.
- iii. The synthesis and thorough study of the intermediates and side products. This research involves the spectroscopic, structural and electrochemical characterization of these compounds, its ability as WOCs and its interconnection.

UNIVERSITAT ROVIRA I VIRGILI

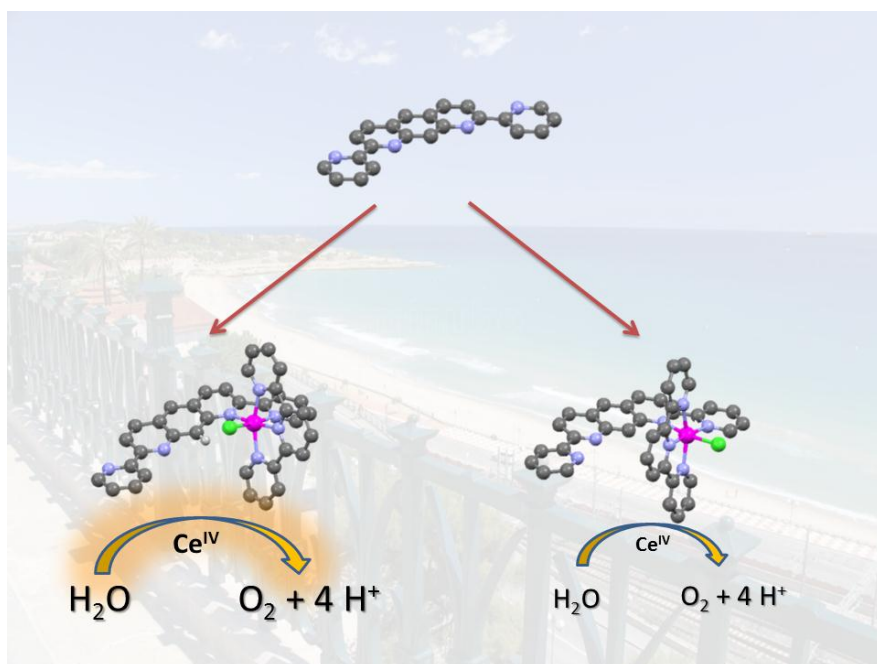
WATER OXIDATION WITH MONONUCLEAR RU COMPLEXES. BELOW THE TIP OF THE

ICEBERG: THE OXO-BRIDGE SCENARIO

Isidoro López Marin

Dipòsit Legal: T. 1505-2013

## **Chapter 3. New mononuclear Ru complexes containing the bipan ligand and their activity toward catalytic water oxidation.**



The six-step synthesis of the tetradentate bipan ligand has been successfully accomplished. The coordination of bipan in a bidentate fashion allowed the preparation of the isomeric mononuclear complexes *in-*, *out-* [Ru(trpy)(bipan)(Cl)]<sup>+</sup> (**1-in**<sup>+</sup> and **1-out**<sup>+</sup>) which were fully characterized by spectroscopic and electrochemical techniques. The different arrangement of the ligands in the two isomers has a slight, but perceptible, influence upon the standard potentials of the Ru<sup>III</sup>-Cl/Ru<sup>II</sup>-Cl couple that can be rationalized in terms of the nature of the aromatic ring placed in the *trans* position with regard to the Cl ligand. **1-in**<sup>+</sup> is an active catalyst for water oxidation while **1-out**<sup>+</sup> presents a low activity due to its insolubility under catalytic conditions.



UNIVERSITAT ROVIRA I VIRGILI

WATER OXIDATION WITH MONONUCLEAR RU COMPLEXES. BELOW THE TIP OF THE

ICEBERG: THE OXO-BRIDGE SCENARIO

Isidoro López Marin

Dipòsit Legal: T. 1505-2013

## Table of Contents.

### **Chapter 3. New mononuclear Ru complexes containing the bipan ligand and their activity toward catalytic water oxidation.**

<i>3.1. Introduction.</i>	81
<i>3.2. Experimental Section.</i>	83
<i>3.3. Results and discussion.</i>	87
<i>Synthesis of bipan.</i>	87
<i>Synthesis of the mononuclear complexes.</i>	89
<i>Characterization of the complexes.</i>	91
<i>Catalytic water oxidation.</i>	95
<i>3.4. Conclusions.</i>	98
<i>3.5. Acknowledgements.</i>	99
<i>3.6. References.</i>	99
<i>3.7. Supporting Information.</i>	103

UNIVERSITAT ROVIRA I VIRGILI

WATER OXIDATION WITH MONONUCLEAR RU COMPLEXES. BELOW THE TIP OF THE

ICEBERG: THE OXO-BRIDGE SCENARIO

Isidoro López Marin

Dipòsit Legal: T. 1505-2013

# New mononuclear Ru complexes containing the bipan ligand and their activity toward catalytic water oxidation

Isidoro López,<sup>a</sup> Chiara Dinoi,<sup>b</sup> Xavier Fontrodona,<sup>c</sup> J. Benet-Buchholz,<sup>a</sup> Carles Bo<sup>a</sup> and Antoni Llobet<sup>a,d</sup>

<sup>a</sup> Institute of Chemical Research of Catalonia (ICIQ), Av. Països Catalans, 16, 43007 Tarragona, Spain.

<sup>b</sup> Laboratoire de Chimie de Coordination, CNRS UPR 8241 Université de Toulouse UPS-INP-LCC 205, Route de Narbonne, 31077 Cedex 04, France.

<sup>c</sup> Departament de Química i Serveis Tècnics de Recerca, Universitat de Girona, Campus de Montilivi, E-17071 Girona, Spain.

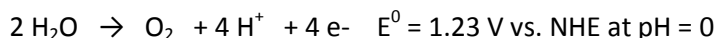
<sup>d</sup> Departament de Química, Universitat Autònoma de Barcelona, Cerdanyola del Vallès, 08193 Barcelona, Spain.

## 3.1. Introduction.

The depletion of fossil fuels reserves<sup>1</sup> and its recognized pollutant and global warming effects<sup>2</sup> has awakened a large interest in pursuing clean and environmentally friendly energy resources<sup>3</sup>. The conversion of sunlight into the so called solar fuels like H<sub>2</sub> or MeOH is one of the most promissory candidates because the solar energy is stored into powerful chemical bonds avoiding problems as intermittency of the resource. Furthermore, the energy could be stored at the individual level in the personalized energy (PE) framework<sup>4</sup> which would improve its efficiency because transport is not required and losses are diminished.

Water Oxidation to molecular oxygen represents one of the major bottlenecks in the development of commercial light harvesting devices for the photoproduction of H<sub>2</sub> from water.<sup>5</sup> In nature, this reaction takes place in the dark at the oxygen-evolving complex (OEC) in photosystem II. The core of OEC

consists in a  $\text{CaMn}_4\text{O}_5$  cubane that can oxidize water quickly and close to the thermodynamic limit<sup>6,7</sup> by effective accumulation of the four necessary redox equivalents.



The multielectronic character, the high thermodynamic energy barrier and the kinetic complexity of the process makes difficult to find good mimics of OEC. The dinuclear Ru complex  $[(\text{bpy})_2(\text{H}_2\text{O})\text{Ru}^{\text{III}}-\text{O}-\text{Ru}^{\text{III}}(\text{H}_2\text{O})(\text{bpy})_2]^{4+}$ , also known as blue dimer, was the first well characterized reported<sup>8</sup> molecular water oxidation catalyst (WOC). The complex contains two  $[\text{Ru}^{\text{III}}-\text{OH}_2]$  moieties than can be oxidized until  $[\text{Ru}^{\text{V}}=\text{O}]$  by PCET processes achieving the four redox equivalents necessary for the catalysis. This architecture was exploited later in improved dinuclear Ru catalysts<sup>9-12</sup> where the oxidatively unstable oxo bridge was replaced by rigid and robust aromatic organic bridging ligands. In 2005, it was shown that mononuclear Ru complexes containing a single  $[\text{Ru}^{\text{II}}-\text{OH}_2]$  group could work as WOCs. The discovery has favored an increase of the number of reported single-site WOCs in the recent years.<sup>13-20</sup> The synthetic simplicity and easy purification of mononuclear systems are attractive advantages of these catalysts.

Herein, we present the synthesis and characterization of the tetradentate 2,7-bipyridil-1,8-diazaanthracene (**bipan**) ligand and its two new isomeric mononuclear complexes *in*- $[\text{Ru}(\text{trpy})(\text{bipan})(\text{Cl})]^+$  (**1-in<sup>+</sup>**) and *out*- $[\text{Ru}(\text{trpy})(\text{bipan})(\text{Cl})]^+$  (**1-out<sup>+</sup>**) (where trpy is 2,2':6',2''-terpyridine). The activity of the complexes as WOCs was tested in order to gain insight of the influence exerted by a nearby and oxidatively accessible C-H bond on the catalysis.

### 3.2. Experimental section.

**Materials.** All reagents used in the present work were obtained from Aldrich Chemical Co. and were used without further purification.  $\text{RuCl}_3 \cdot 3\text{H}_2\text{O}$  was supplied by Alfa Aesar and was used as received. Trifluoromethanesulfonic acid (HOTf) was purchased from CYMIT. Reagent-grade organic solvents were obtained from SDS and high-purity deionized water was obtained by passing distilled water through a nanopure Milli-Q water purification system.

**Preparations.**  $[\text{Ru}(\text{trpy})\text{Cl}_3]$ , **3**, **5**, **6** and **bipan** were prepared as described in the literature.<sup>21,22</sup> The synthesis of **2** and **4** was carried out following a modified procedure to that reported.

*1,5-dimethyl-2,4-dinitrobenzene (2).* *m*-xylene (46 mL, 0.37 mols) was added dropwise over stirring fumaric nitric acid (110 mL, 2.36 mols) previously cooled at 0 °C by means of an ice-water bath. The addition lasted 2 hours. Then, the orange resulting solution was stirred for 30 min. at RT and was subsequently refluxed for 6 h. (aprox. at 90 °C). Finally, the reaction crude was kept in the fridge overnight. A pale yellow amorphous solid precipitated and was filtered and washed with cold water. The solid was comprised a mixture of the desired compound and 1,3-dimethyl-2,4-dinitrobenzene. Consecutive fractioned recrystallizations in EtOH/H<sub>2</sub>O 95:5 allowed us to separate **2**. The needle shape crystalline solid obtained 30 min. after cooling each crystallization solution was gradually enriched in the desired compound. The <sup>1</sup>H-NMR spectrum matched with the one reported.

*4,6-dinitro1,3-di[N,N'-bis(p-dimethylaminophenyl)iminomethylbenzol-N,N'-dioxide] (4).* All the operations, less filtration, were carried under Ar. 7.6 g of product crude (4.89 g of **3**, 8.07 mmols) were dissolved in deoxygenated EtOH (50 mL) and the mixture was cooled at -10 °C by means of a cryostat. Then,

*N,N*-dimethyl-4-Nitrosoaniline (2.42 g, 16.14 mmols) was added under stirring. After some minutes, deoxygenated 10% NaOH<sub>aq</sub>. (12 mL, 29.23 mmols) was added dropwise. When the addition finished, the solution was maintained under stirring at 2-3 °C for 7 h. using an ice-water bath. Then, it was left in the fridge overnight (aprox. 14 h.). A dark solid precipitated which was filtered, washed with cold water (3 x 30 mL), EtOH/Et<sub>2</sub>O 1:1 (10 mL), Et<sub>2</sub>O (5 mL) and dried under vacuum (4.12 g, 100 %). The <sup>1</sup>H-NMR spectrum matched with the one reported.

*In*-[Ru(*trpy*)(*bipan*)Cl]Cl (**1-in(Cl)**). All the operations, less filtration, were carried under Ar. Ru(*trpy*)Cl<sub>3</sub> (132.21 mg, 0.300 mmols) and LiCl (15 mg, 0.353 mmoles) were dissolved in deoxygenated EtOH (15 mL) and then NEt<sub>3</sub> was added (85 μL, 0.611 mmols). The suspension was stirred for 20 min. Then, *bipan* (50 mg, 0.150 mmols) was added and the solution was refluxed for 5 hours. A dark purple solid precipitated and the suspension was left to cool at RT. The solid was collected by filtration, washed with cold EtOH and dried under vacuum (93.8 mg, 85 % yield). Anal. Calcd for C<sub>37</sub>H<sub>25</sub>Cl<sub>2</sub>N<sub>7</sub>Ru: C, 60.08; H, 3.41; N, 13.26. Found: C, 59.94; H, 3.20; N, 13.17. <sup>1</sup>H-NMR (MeOD, 400 MHz) δ(ppm): 7.08 (t, 1H, H-b or b', <sup>3</sup>J=7.42 Hz), 7.23 (t, 1H, H-c or c', <sup>3</sup>J=5.77), 7.37 (t, 1H, H-b or b', <sup>3</sup>J=7.42 Hz), 7.45 (t, 2H, H-3, <sup>3</sup>J=6.59 Hz), 7.50 (d, 1H, H-a or a', <sup>3</sup>J=5.77 Hz), 7.73 (t, 1H, H-c or c', <sup>3</sup>J=7.42 Hz), 7.82 (m, 4H, H-1, H-2), 8.21 (d, 1H, Ha or a', <sup>3</sup>J=7.42 Hz), 8.26 (t, 1H, H-6, <sup>3</sup>J=8.24 Hz), 8.45 (d, 1H, Hd or d', <sup>3</sup>J=7.42 Hz), 8.51 (d, 2H, H-4, <sup>3</sup>J=8.24 Hz), 8.56 (d, 1H, H-f or f', <sup>3</sup>J=7.42 Hz), 8.68 (m, 5H, H-5, H-d or d', H-e or e', H-f or f'), 8.76 (s, 1H, H-g), 8.86 (d, 1H, H-e or e', <sup>3</sup>J=8.24 Hz), 10.82 (s, 1H, H-h). ESI-MS (MeOH): *m/z* = 704.1 ([M-Cl]<sup>+</sup>).

*Out*-[Ru(*trpy*)(*bipan*)Cl]PF<sub>6</sub> (**1-out(PF<sub>6</sub>)**). A saturated aqueous NH<sub>4</sub>PF<sub>6</sub> solution (1 mL) was added to the filtrate obtained from the preparation of **1-**

**in(Cl)**. A dark purple solid precipitated, which was filtered, washed with cold EtOH and Et<sub>2</sub>O (46.5 mg). This solid contained **1-out(PF<sub>6</sub>)**, [Ru(trpy)<sub>2</sub>](PF<sub>6</sub>)<sub>2</sub> and another unidentified products. **1-out(PF<sub>6</sub>)** was isolated after column chromatography in alumina using CH<sub>2</sub>Cl<sub>2</sub>/MeOH 20:1 as eluent. The first fraction resulted be the desired compound. After evaporation of the eluent a dark blue amorphous solid was obtained and was dried under high vacuum (6.1 mg, 6%). Anal. Calcd for C<sub>37</sub>H<sub>25</sub>ClF<sub>6</sub>N<sub>7</sub>PRu: C, 52.34; H, 2.97; N, 11.55. Found: C, 52.15; H, 3.01; N, 11.43. <sup>1</sup>H-NMR (CD<sub>3</sub>CN, 400 MHz) δ(ppm): 7.21 (t, 2H, H-2, <sup>3</sup>J=5.91 Hz), 7.57 (t, 1H, H-b', <sup>3</sup>J=5.91 Hz), 7.63 (d, 2H, H-1, <sup>3</sup>J=5.91 Hz), 7.81 (t, 2H, H-3, <sup>3</sup>J=5.91 Hz), 8.01 (t, 1H, H-b, <sup>3</sup>J=5.91 Hz), 8.04 (s, 1H, H-g), 8.20 (t, 1H, H-c', <sup>3</sup>J=5.91 Hz), 8.42 (m, 8H, H-h, H-c, H-4, H-6, H-e, H-f, H-e' or f'), 8.58 (d, 1H, H-e' or f', <sup>3</sup>J=9.03 Hz), 8.61 (d, 1H, H-d', <sup>3</sup>J=7.99 Hz), .8.72 (d, 2H, H-5, <sup>3</sup>J=8.34 Hz), 8.75 (d, 1H, H-a', <sup>3</sup>J=4.86 Hz), 8.96 (d, 1H, H-d, <sup>3</sup>J=7.99 Hz), 10.51 (d, 1H, H-a, <sup>3</sup>J=5.56 Hz).ESI-MS (MeOH): *m/z* = 704.1 ([M-Cl]<sup>+</sup>).

**Equipment and measurements.** Cyclic voltammetry (CV) experiments were performed on an IJ-Cambria CHI-660 or a Bio-Logic SP-150 potentiostat using a three-electrode cell. Typical CV experiments were carried out at a scan rate of 100 mVs<sup>-1</sup>. The complexes were dissolved in MeCN or CH<sub>2</sub>Cl<sub>2</sub> containing the necessary amount of (*n*-Bu<sub>4</sub>N)(PF<sub>6</sub>) (TBAH), used as the supporting electrolyte, to yield a 0.1 M ionic strength solution. A glassy carbon electrode (2 mm diameter) was used as working electrode, platinum wire as auxiliary electrode, and SSCE as a reference electrode. Working electrodes were polished with 0.05 micron alumina paste, and rinsed with distilled water and acetone followed by blow-drying before each measurement. All cyclic voltammograms presented in this work were recorded in the absence of light and inside a Faradaic cage. E<sub>1/2</sub> values reported in this work were estimated



from CV experiments as the average of the oxidative and reductive peak potentials ( $E_{pa} + E_{pc}$ )/2.

A 400 MHz Bruker Avance II spectrometer and a Bruker Avance 500 MHz were used to carry out NMR spectroscopy at room temperature. Samples were run in CD<sub>3</sub>CN or MeOD with internal references (residual protons). Elemental analysis was performed using an EA-1108, CHNS-O elemental analyzer from Fisons Instruments.

On-line manometric O<sub>2</sub> measurements were carried out on a Testo 521 differential pressure manometer with an operating range of 1-100 hPa and accuracy within 0.5 % of the measurement. The manometer was coupled to thermostated reaction vessels for dynamic monitoring of the headspace pressure above each reaction. The manometer's secondary ports were connected to thermostated reaction vessels containing the same solvents and headspace volumes as the sample vials. . Composition of the gaseous phase was determined by online mass-spectrometry with an OmniStar GSD 301 C (Pfeiffer) quadrupole mass-spectrometer.

**Single-Crystal X-Ray Structure Determination.** Single crystals for **bipan** and **1-out**<sup>+</sup> were grown by slow evaporation of acetone or ethanol solutions of the compounds. All measured crystals were prepared under inert conditions immersed in perfluoropolyether as the protecting oil for manipulation.

*Data collection.* Crystal structure determination for **1-out**<sup>+</sup> was carried out on a *BRUKER SMART APEX CCD* diffractometer using graphite-monochromated Mo K $\alpha$  radiation ( $\lambda = 0.71073 \text{ \AA}$ ) from an x-Ray Tube. The measurements were made in the range 1.87 to 28.21° for  $\theta$ . Full-sphere data collection was carried out with  $\omega$  and  $\phi$  scans. A total of 28043 reflections were collected of which 8623 [R(int) = 0.0946] were unique. Programs used:

data collection, Smart version 5.631 (Bruker AXS 1997-02); data reduction, Saint + version 6.36A (Bruker AXS 2001); absorption correction, SADABS version 2.10 (Bruker AXS 2001).

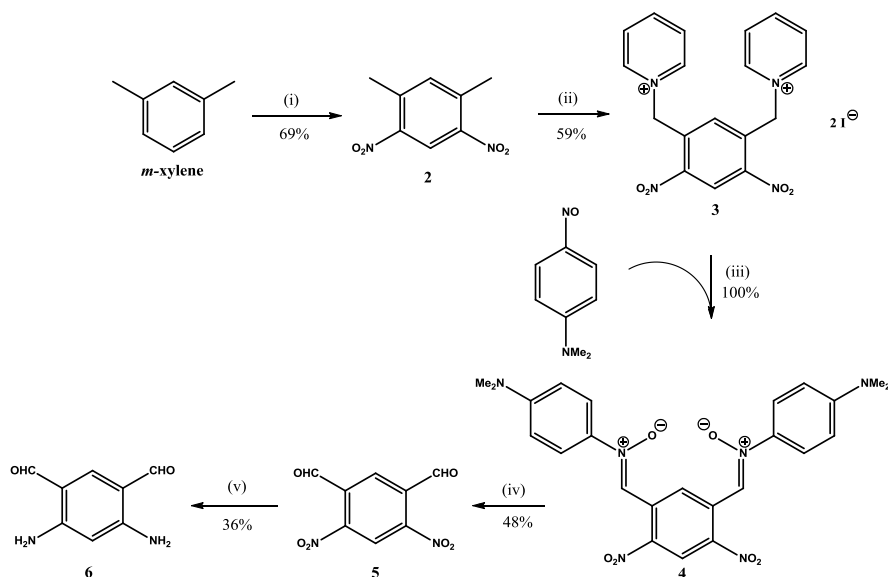
*Structure solution and refinement.* Crystal structure solution was achieved using direct methods as implemented in SHELXTL Version 6.14 (Bruker AXS 2000-2003) and refined by full-matrix least-squares methods on  $F^2$ . The non-hydrogen atoms were refined anisotropically. The H-atoms were placed in geometrically optimized positions and forced to ride on the atom to which they are attached. Spurious electron density peaks non attributable to any solvent molecule was removed using the SQUEEZE option in PLATON. (Spek, A. L. (2005). PLATON, A Multipurpose Crystallographic Tool, Utrecht University, Utrecht, The Netherlands.).

**Computational details.** All calculations were carried out with the ADF program system, version 2013.01, developed by Baerends, Ziegler and coworkers.<sup>23-25</sup> We used a density functional theory (DFT) based method, which included the local VWN exchange-correlation potential<sup>26</sup> with GGA Becke's exchange correction<sup>27</sup> and Perdew's correlation correction<sup>28,29</sup> (BP86). A triple- $\zeta$  plus one polarization function basis set was used on all atoms, treating the core electrons with a relativistic frozen-core potential. Relativistic corrections were introduced by scalar-relativistic zero-order regular approximation (ZORA).<sup>30,31</sup>

### 3.3. Results and discussion.

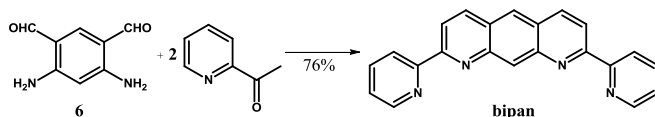
**Synthesis of bipan.** The preparation of **bipan** consists in a six steps synthesis that starts with *m*-xylene. The first part (Scheme 1) lies in the synthesis of the key intermediate 1,3-diamino-4,6-benzenedicarboxaldehyde (**6**) and it was carried out according to the literature<sup>21,22</sup> procedures, although

in our hands the conversion of **2** into **3** yielded a mixture of the latter and pyridinium cation in a 1:1.47 ratio in the collected solid (Figures S1 and S2). The finding allows us to improve the yield of the next step, because the exact amount of 10 % aqueous NaOH for double deprotonation of **3** and neutralization of the pyridinium cation could be controlled more precisely.



**Scheme 1.** Synthetic route for 1,3-diamino-4,6-benzenedicarboxaldehyde (**6**). Reagents and conditions: (i) HNO<sub>3</sub> conc., 0 °C to RT, (ii) pyridine-I<sub>2</sub>, 95 °C; (iii) EtOH/ NaOH 10%; (iv) H<sub>2</sub>SO<sub>4</sub> 3 M, toluene, 65 °C; (v) FeSO<sub>4</sub>·7H<sub>2</sub>O, EtOH-H<sub>2</sub>O-NH<sub>4</sub>OH, 80 °C.

Once the dialdehyde compound **6** was obtained, it was subjected to a double Friedländer condensation reaction with an excess of 2-acetylpyridine to give the final compound **bipan** (Scheme 2).



**Scheme 2.** Synthesis of **bipan**. Reagents and conditions: KOH 10 %, EtOH, 100 °C.

All the prepared organic compounds were characterized by  $^1\text{H-NMR}$  and the spectra fit with the reported ones. Furthermore, single crystals for suitable X-ray determination of bipan were successfully grown. The structure consists in an aromatic planar system that comprises a central azaanthracene ligand bound to two pyridilic rings in the 1 and 8 positions (Figure 1). The nitrogen atoms of the pyridilic and the central azaanthracene ring point in opposite directions because this conformation avoids the sterical hindrance between the protons bound to C14 and C4 or alternatively C19 and C10.

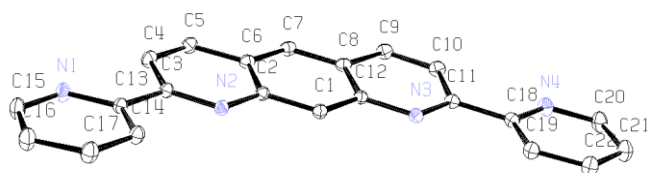
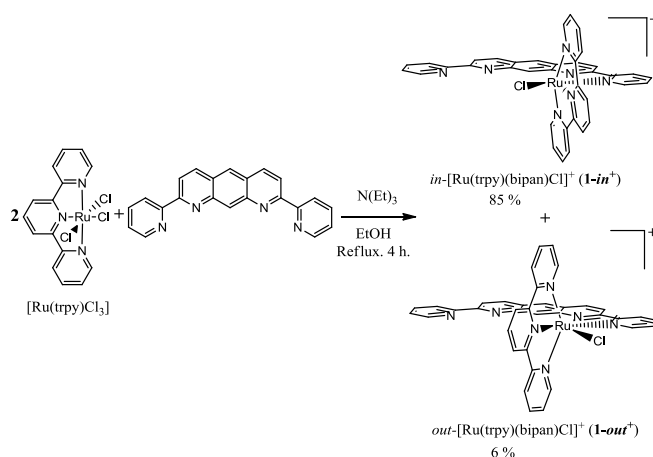


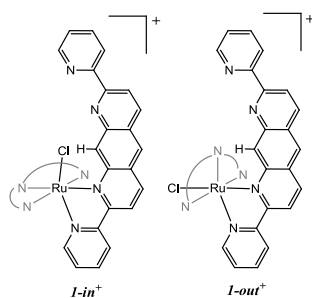
**Figure 1.** Ortep plot (40 % at probability) of the X-ray structure of **bipan**. Color codes: N, navy blue; C, grey. H atoms were omitted for clarity.

**Synthesis of the mononuclear complexes.** The initial approach was using the tetradentate bipan ligand as a dinucleating bridge similarly to Hbpp.<sup>9</sup> For this reason one equivalent of bipan was reacted with 2 equivalents of the starting material  $[\text{Ru}(\text{trpy})(\text{Cl})_3]$  in EtOH under refluxing conditions (Scheme 3) for 4 hours. However, the mononuclear complex **1-in<sup>+</sup>** precipitated directly from the crude of the reaction as the main product and it was easily purified by successive EtOH washings. DFT calculations show that the *in*- isomer is more stable than the *out*- by  $6.2 \text{ kcal mol}^{-1}$ , thus the favored formation and precipitation of **1-in<sup>+</sup>** probably prevents the generation of the dinuclear complex. The isomeric annotation *in/out* has already been employed in similar complexes<sup>16,32</sup> and indicates whether the monodentate Cl ligand is oriented toward or away, respectively, from the inner H atom of bipan (Scheme 4). The

out isomer **1-out**<sup>+</sup> was isolated with a poor yield after column chromatography in alumina of the solid precipitated after the addition of a sat. aq. solution of NH<sub>4</sub>PF<sub>6</sub> to the filtered crude of the reaction. One of the side products of the reaction was also separated and identified as [Ru(trpy)<sub>2</sub>]<sup>2+</sup> according to NMR spectroscopy and cyclic voltammetry (CV) (Figures S3, S4 and S5). **1-in**<sup>+</sup> and **1-out**<sup>+</sup> were characterized by the usual spectroscopic and electrochemical techniques as well as by single crystal X-ray diffraction in the case of **1-out**<sup>+</sup>.



**Scheme 3.** Synthesis of the mononuclear complexes **1-in**<sup>+</sup> and **1-out**<sup>+</sup>.



**Scheme 4.** Schematic drawing of the mononuclear complexes indicating the relative position of the Cl ligand and the inner proton of bipan in each isomer. The coordinating N atoms of the trpy ligand are shown in grey.

**Characterization of the complexes.** The structure of the isomer **1-out<sup>+</sup>** was corroborated by single crystal X-ray diffraction analysis. The Ortep plot of the molecule (Figure 2) shows that the Ru atom adopts a distorted octahedral geometry where the trpy is coordinated as a meridional ligand, bipan acts in a bidentate fashion and the Cl ligand occupies the remaining sixth coordination position pointing away from the inner H atom of bipan (H27).

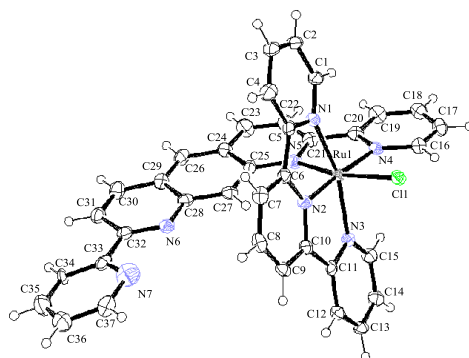


**Figure 2.** Ortep plot (ellipsoids at 40 %probability) of the X-ray structure of **1-out<sup>+</sup>**. Color codes: N, navy blue; Ru, black; C, grey; H, white.

The bond distances and angles are comparable to related complexes.<sup>16,32</sup> The small bite angle of bipan (77.89°) and the steric hindrance between H27 and the trpy ligand elongate the N5Ru1N2 angle (106.52°). The unit cell of **1-out<sup>+</sup>** contains two molecules of the complex, one PF<sub>6</sub><sup>-</sup> counterion and one molecule of ethanol. The presence of a single counterion discards protonation in the non-coordinated pyridil ring. Selected bond distances and angles are collected in Table 1. Single crystals of good quality for X-ray determination of **1-in<sup>+</sup>** could not be obtained.

**Table 1.** Selected bond distances and angles for **1-out<sup>+</sup>**.

Bond Lengths (Å)			
Ru1-N1	2.065(4)	Ru1-N2	1.956(4)
Ru1-N3	2.071(4)	Ru1-N4	2.066(4)
Ru1-N5	2.099(4)	Ru1-Cl	2.4054(13)
Bond Angles (degrees)			
N4-Ru1-N5	77.89(17)	N4-Ru1-Cl1	92.93(12)
N1-Ru1-N3	158.47(16)	N5-Ru1-Cl1	168.79(12)

The number of signals and the integration of the <sup>1</sup>H-NMR spectrum of **1-in<sup>+</sup>** is consistent with a mononuclear bipan Ru complex with C<sub>5</sub> symmetry (Figure 3). The singlet of the inner proton of the azaanthracene ligand is held in a strongly deshielded environment (10.81 ppm) because the effect of the nearby Cl ligand. The large influence exerted by the near proximity of a chloro ligand has already been evidenced<sup>11,16,32</sup> in structurally related complexes. The described feature confirms unambiguously that **1-in<sup>+</sup>** is the *in* isomer. Further 2D NMR spectroscopic experiments (Figures S6 and S7) provided the assignment of the resonances, although we could not differentiate the two halves of the bipan ligand.

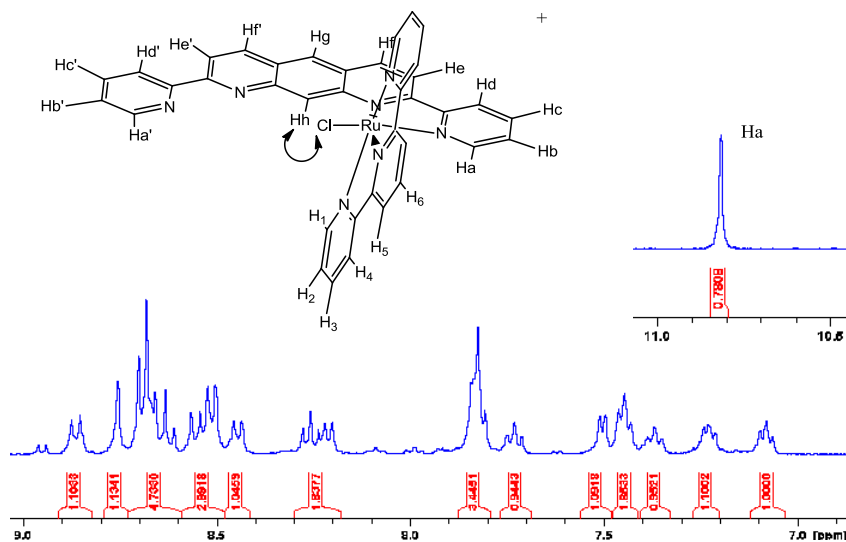


**Figure 3.**  $^1\text{H-NMR}$  spectrum ( $\text{CD}_3\text{OD}$ , 400 MHz) of  $\mathbf{1-in}^+$ . The inset shows the deshielded resonance for Hh.

A strongly deshielded doublet (10.51 ppm) is observed in the  $^1\text{H-NMR}$  spectrum of  $\mathbf{1-out}^+$  (Figure S8). The resonance corresponds to the proton next to the coordinating N atom of one of the pyridil ring of the anthracene ligand. It is downfield shifted due to the proximity of the Cl ligand as it was considered in  $\mathbf{1-in}^+$ . The experiment also corroborates that the arrangement of the ligands found in the X-ray structure is preserved in solution. The complete assignment of all the resonances was provided by 2D NMR experiments (Figure S11).

The electrospray mass spectra (ESI-MS) of  $\mathbf{1-in}^+$  and  $\mathbf{1-out}^+$  in MeOH exhibit two main peaks at  $m/z = 704.1$  which correspond to  $[\text{M}]^+$ . The simulated isotopic patterns fit pretty well with the experimental one (Figures S10 and S11).



Cyclic Voltammetries (CV) of **1-*in***<sup>+</sup> and **1-*out***<sup>+</sup> present a single chemically reversible and electrochemically quasireversible wave which is attributed to the Ru<sup>III</sup>-Cl/Ru<sup>II</sup>-Cl couple according to related systems.<sup>16,32</sup>

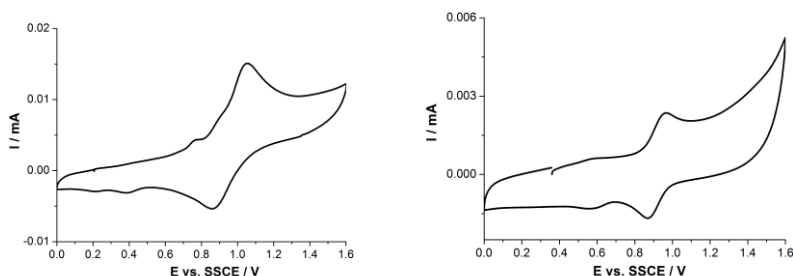


**Figure 4** CVs of **1-*in***<sup>+</sup> in CH<sub>3</sub>CN (left) and **1-*out***<sup>+</sup> in CH<sub>2</sub>Cl<sub>2</sub> (right) both solvents with 0.1 M TBAH as supporting electrolyte. Glassy carbon was used as working electrode, a Pt wire as counter electrode and SSCE as reference electrode. Scan rate = 100 mV s<sup>-1</sup>.

The *out* isomer has a lower standard potential than the *in* complex (Table 2). This feature has already been observed and it is interpreted considering the electro donation capability of the group placed in the *trans* position of the Cl ligand. The difference in standard potential for the isomers from complexes [Ru(Hbpp)(trpy)(Cl)]<sup>+</sup> and [Ru(H3p)(trpy)(Cl)]<sup>+</sup> is 230 and 120 respectively (Table 2) with the *out* isomer having the lower potential. The more basic imidazole ring is situated *trans* with regard to the Cl ligand in the *out* isomer. This arrangement facilitates the transmission of sigma bonding electron density to the metal center, what stabilizes the Ru<sup>III</sup> oxidation state. In the case of the isomeric bipan mononuclear complexes the difference is markedly smaller (Table 2) suggesting that the electro donation abilities of the central azaanthracene and the outer pyridil rings are similar and it is less relevant which ring is the *trans* to the Ru-Cl bond.

**Table 2.** Electrochemical data for related mononuclear complexes.

Complex <sup>a</sup>	E <sup>0</sup> / V	ΔE / mV <sup>b</sup>	Reference
<b>1-in<sup>+</sup></b>	0.96		Tw. <sup>c</sup>
<b>1-out<sup>+</sup></b>	0.92	40	Tw.
<i>in</i> -[Ru(Hbpp)(trpy)(Cl)] <sup>+</sup>	0.86		32
<i>out</i> -[Ru(Hbpp)(trpy)(Cl)] <sup>+</sup>	0.63	230	32
<i>in</i> -[Ru(H3p)(trpy)(Cl)] <sup>+</sup>	0.81		16
<i>out</i> -[Ru(H3p)(trpy)(Cl)] <sup>+</sup>	0.69	120	16

<sup>a</sup> Ligand abbreviation: Hbpp = 3,5-bis(2-pyridyl)pyrazole; H3p = 2-(5-phenyl-1H-pyrazol-3-yl)pyridine. <sup>b</sup> ΔE = E<sup>0</sup><sub>in</sub> - E<sup>0</sup><sub>out</sub>. <sup>c</sup> Tw. means this work.

**Catalytic water oxidation.** Because we were unable to remove the chloro ligand and it has been reported<sup>15</sup> that mononuclear chloro complexes convert into the aquo compounds in water, **1-in<sup>+</sup>** and **1-out<sup>+</sup>** were tested directly as WOCs using an excess (100 equivalents) of (NH<sub>4</sub>)<sub>2</sub>Ce(NO<sub>3</sub>)<sub>6</sub> as sacrificial oxidant. The manometric monitoring of the evolved gas indicated that **1-in<sup>+</sup>** is a much better catalyst than **1-out<sup>+</sup>** (Figure 5 and Figure S12) achieving 13 TONs in 20 minutes, however **1-out<sup>+</sup>** was poorly soluble under catalytic conditions, what precludes a reliable comparison of the catalytic activities. Furthermore, on-line MS monitoring of the reaction with **1-in<sup>+</sup>** confirmed that O<sub>2</sub> was the only produced gas (Figure S13).

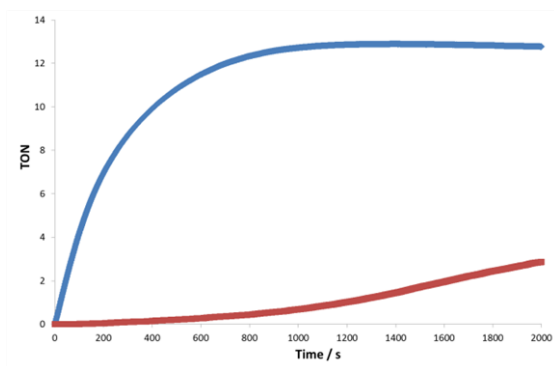


**Figure 5.** Dioxygen evolution versus time manometric profiles for catalysts **1-*in*<sup>+</sup>** (blue) and **1-*out*<sup>+</sup>** (red) under 1:100 Cat/Ce<sup>IV</sup> ratios in 0.1 M triflic acid solutions (pH = 1.0) at 25°C.

The activity of **1-*in*<sup>+</sup>** is slightly lower than the observed for the previous reported complex *out*-[Ru(Hbpp)(trpy)(Cl)]<sup>+</sup>, but it is higher with regard to the *in* isomer, *in*-[Ru(Hbpp)(trpy)(Cl)]<sup>+</sup> (Figure 6).

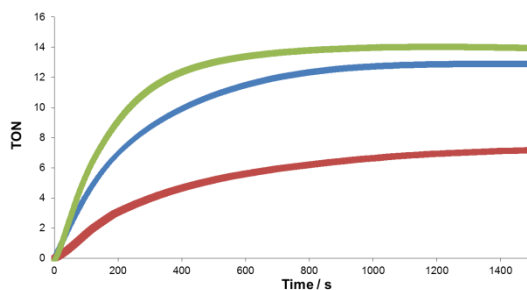


**Figure 6.** Dioxygen evolution versus time manometric profiles for catalysts **1-*in*<sup>+</sup>** (blue) *in*- (red) and *out*-[Ru(Hbpp)(trpy)(H<sub>2</sub>O)]<sup>+</sup> (green) under 1:100 Cat/Ce<sup>IV</sup> ratios in 0.1 M triflic acid solutions (pH = 1.0) at 25°C.

Figure 7 illustrates the arrangement of the active site in the four considered catalysts. The structures were obtained by means of DFT

calculations, except for  $out-[Ru(Hbpp)(trpy)(H_2O)]^+$  which is a reported<sup>32</sup> XRD structure.

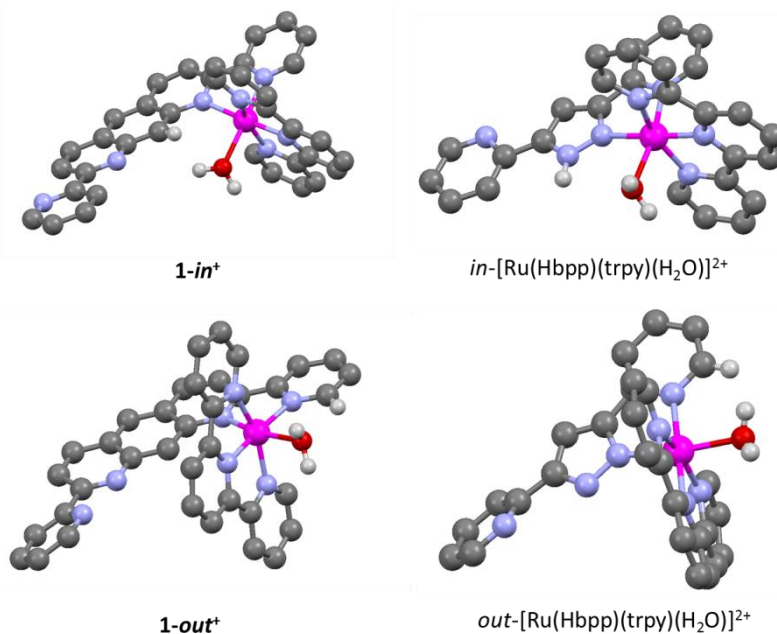
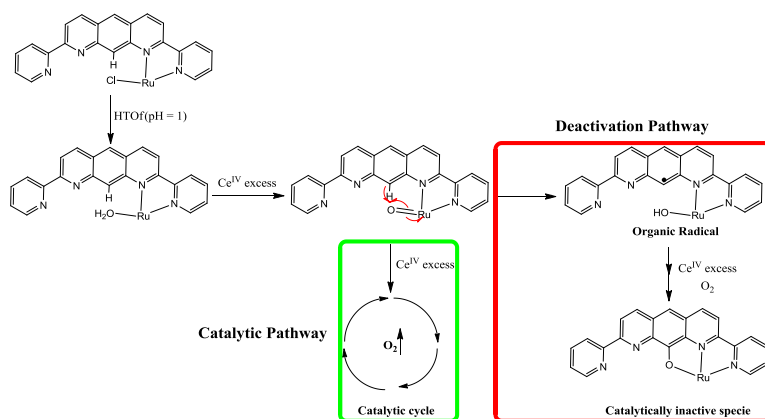


**Figure 7.** Comparison of the structure of the considered catalyst. Color code: Ru, pink; O, Red; N, Blue, C, grey. Hydrogen atoms are omitted for clarity, except for the aquo ligand and the H atom from the ligand nearer to it that are represented as white circles.

The remarkable dioxygen production by **1-*in*<sup>+</sup>** suggests that the H atom placed close to the active site of the catalyst (Figure 7) does not have a detrimental effect upon the catalysis in spite of the known high reactivity of  $Ru^{IV}=O$  groups to carry out H-atom abstraction processes<sup>33-36</sup> and the relative low potential found for the first oxidation of the free ligand in acetonitrile (Figure S14). The current accepted mechanistic proposal for mononuclear Ru water oxidation catalysts sets up the formation of high electrophilic intermediates,<sup>37</sup> like  $Ru^{IV}=O$  and  $Ru^V=O$  systems. These complexes are good

oxidants and could abstract the nearby inner proton of the azaanthracene ring by an intramolecular PCET process. The formed organic radical could be quickly trapped by oxygen or another intermediate and evolve to give a non-catalytic mononuclear complex where the active site is now coordinated to bipan through an additional oxygen atom (Scheme 5). Further kinetic studies must be done in order to confirm this reactivity. The high activity for water oxidation of **1-in**<sup>+</sup> suggests that the catalytic pathway is faster than the aforementioned deactivation reactions.



**Scheme 5.** Feasible pathways after the addition of an excess of Ce<sup>IV</sup> to **1-in**<sup>+</sup> in 0.1 M HOTf (pH = 1).

### 3.4. Conclusions.

In this work, we have accomplished successfully the six-step synthesis of the tetradentate ligand bipan after improving some of the described preparations of the intermediates. The ligand was later employed for the synthesis of the two new chloro isomeric complexes **1-in**<sup>+</sup> and **1-out**<sup>+</sup>, where bipan is coordinated in a bidentate fashion. Both compounds were fully characterized by the usual analytic and spectroscopic techniques. From an electrochemical point of view the different arrangement of the ligands in the

two isomers has a slight influence on the standard potentials, in contrast to previous reported related complexes where the effect is more pronounced. This feature suggests similar electrodonation ability for the outer pyridil and the central rings of bipan. **1-out<sup>+</sup>** is a poor catalyst for water oxidation probably due to its insolubility under catalytic conditions while **1-in<sup>+</sup>** presents a high activity in the order or even higher than the reported for previous structurally related mononuclear complexes. The good catalytic performance of **1-in<sup>+</sup>** suggests that processes leading to oxygen are faster than feasible deactivation pathways where the active site of the catalyst is trapped by a C-H bond that has been previously activated by the Ru<sup>IV</sup>=O group.

### 3.5 Acknowledgements.

Support from MINECO (CTQ2010-21497 and PRI-PIBIN-2011-1278) is gratefully acknowledged. IL thanks MINECO for a FPU grant.

I have carried out this work supervised by Dr. Chiara Dinoi.

### 3.6 References.

- (1) Owen, N. A.; Inderwildi, O. R.; King, D. A. *Energy Policy* **2010**, *38*, 4743.
- (2) *Climate Change 2007: Synthesis Report* Core Writing Team; Pachauri, R. K.; Reisinger, A., Eds.; IPCC: Geneva, Switzerland, 2008.
- (3) *Energy...behind oil*; Armstrong, F.; Blundell, K., Eds. Oxford, UK, 2007.
- (4) Nocera, D. G. *Inorg. Chem.* **2009**, *48*, 10001.
- (5) Dau, H.; Limberg, C.; Reier, T.; Risch, M.; Roggan, S.; Strasser, P. *ChemCatChem* **2010**, *2*, 724.
- (6) Ferreira, K. N.; Iverson, T. M.; Maghlaoui, K.; Barber, J.; Iwata, S. *Science* **2004**, *303*, 1831.
- (7) McEvoy, J. P.; Brudvig, G. W. *Chem. Rev. (Washington, DC, U. S.)* **2006**, *106*, 4455.
- (8) Gersten, S. W.; Samuels, G. J.; Meyer, T. J. *J. Am. Chem. Soc.* **1982**, *104*, 4029.

- (9) Sens, C.; Romero, I.; Rodríguez, M.; Llobet, A.; Parella, T.; Benet-Buchholz, J. J. *Am. Chem. Soc.* **2004**, *126*, 7798.
- (10) Zong, R.; Thummel, R. P. *J. Am. Chem. Soc.* **2005**, *127*, 12802.
- (11) Deng, Z.; Tseng, H.-W.; Zong, R.; Wang, D.; Thummel, R. *Inorg. Chem.* **2008**, *47*, 1835.
- (12) Xu, Y.; Åkermark, T. r.; Gyollai, V.; Zou, D.; Eriksson, L.; Duan, L.; Zhang, R.; Åkermark, B. r.; Sun, L. *Inorg. Chem.* **2009**, *48*, 2717.
- (13) Concepcion, J. J.; Jurss, J. W.; Templeton, J. L.; Meyer, T. J. *J. Am. Chem. Soc.* **2008**, *130*, 16462.
- (14) Tseng, H.-W.; Zong, R.; Muckerman, J. T.; Thummel, R. *Inorg. Chem.* **2008**, *47*, 11763.
- (15) Wasylenko, D. J.; Ganesamoorthy, C.; Koivisto, B. D.; Henderson, M. A.; Berlinguette, C. P. *Inorg. Chem.* **2010**, *49*, 2202.
- (16) Roeser, S.; Farràs, P.; Bozoglian, F.; Martínez-Belmonte, M.; Benet-Buchholz, J.; Llobet, A. *ChemSusChem* **2011**, *4*, 197.
- (17) Duan, L.; Fischer, A.; Xu, Y.; Sun, L. *J. Am. Chem. Soc.* **2009**, *131*, 10397.
- (18) Duan, L.; Bozoglian, F.; Mandal, S.; Stewart, B.; Privalov, T.; Llobet, A.; Sun, L. *Nat Chem* **2012**, *4*, 418.
- (19) Yoshida, M.; Masaoka, S.; Abe, J.; Sakai, K. *Chem. Asian J.* **2010**, *5*, 2369.
- (20) Maji, S.; López, I.; Bozoglian, F.; Benet-Buchholz, J.; Llobet, A. *Inorg. Chem.* **2013**, *52*, 3591.
- (21) Quast, H.; Schön, N. *Liebigs Ann. Chem* **1984**, 133.
- (22) Jain, R.; Caldwell, S. L.; Louie, A. S.; Hicks, R. G. *Can. J. Chem.* **2006**, *84*, 1263.
- (23) te Velde, G.; Bickelhaupt, F. M.; Baerends, E. J.; Fonseca Guerra, C.; van Gisbergen, S. J. A.; Snijders, J. G.; Ziegler, T. *J. Comput. Chem.* **2001**, *22*, 931.
- (24) Fonseca Guerra, C.; Snijders, J. G.; te Velde, G.; Baerends, E. J. *Theor. Chem. Acc.* **1998**, *99*, 391.
- (25) ADF2013, SCM, Theoretical Chemistry, Vrije Universiteit, Amsterdam, The Netherlands, <http://www.scm.com>
- (26) Vosko, S. H.; Wilk, L.; Nusair, M. *Can. J. Phys.* **1980**, *58*, 1200.
- (27) Becke, A. D. *Phys. Rev. A* **1988**, *38*, 3098.
- (28) Perdew, J. P. *Phys. Rev. B* **1986**, *33*, 8822.
- (29) Perdew, J. P. *Phys. Rev. B* **1986**, *34*, 7406.
- (30) Lenthe, E. v.; Baerends, E. J.; Snijders, J. G. *J. Chem. Phys.* **1994**, *101*, 9783.
- (31) van Lenthe, E.; Baerends, E. J.; Snijders, J. G. *J. Chem. Phys.* **1993**, *99*, 4597.

- (32) Sens, C.; Rodríguez, M.; Romero, I.; Llobet, A.; Parella, T.; Benet-Buchholz, J. *Inorg. Chem.* **2003**, *42*, 8385.
- (33) Meyer, T. J.; Huynh, M. H. V. *Inorg. Chem.* **2003**, *42*, 8140.
- (34) Matsuo, T.; Mayer, J. M. *Inorg. Chem.* **2005**, *44*, 2150.
- (35) Hirai, Y.; Kojima, T.; Mizutani, Y.; Shiota, Y.; Yoshizawa, K.; Fukuzumi, S. *Angew. Chem. Int. Ed.* **2008**, *47*, 5772.
- (36) Kojima, T.; Nakayama, K.; Ikemura, K.; Ogura, T.; Fukuzumi, S. *J. Am. Chem. Soc.* **2011**, *133*, 11692.
- (37) Concepcion, J. J.; Tsai, M.-K.; Muckerman, J. T.; Meyer, T. J. *J. Am. Chem. Soc.* **2010**, *132*, 1545.



UNIVERSITAT ROVIRA I VIRGILI

WATER OXIDATION WITH MONONUCLEAR RU COMPLEXES. BELOW THE TIP OF THE

ICEBERG: THE OXO-BRIDGE SCENARIO

Isidoro López Marin

Dipòsit Legal: T. 1505-2013

## Supporting Information for,

# New mononuclear Ru complexes containing the bipan ligand and their activity toward catalytic water oxidation

III

Isidoro López,<sup>a</sup> Chiara Dinoi,<sup>b</sup> Xavier Fontrodona,<sup>c</sup> J. Benet-Buchholz,<sup>a</sup> Carles Bo<sup>a</sup> and Antoni Llobet<sup>a,d</sup>

<sup>a</sup> Institute of Chemical Research of Catalonia (ICIQ), Av. Països Catalans, 16, 43007 Tarragona, Spain.

<sup>b</sup> Laboratoire de Chimie de Coordination, CNRS UPR 8241 Université de Toulouse UPS-INP-LCC 205, Route de Narbonne, 31077 Cedex 04, France.

<sup>c</sup> Departament de Química i Serveis Tècnics de Recerca, Universitat de Girona, Campus de Montilivi, E-17071 Girona, Spain.

<sup>d</sup> Departament de Química, Universitat Autònoma de Barcelona, Cerdanyola del Vallès, 08193 Barcelona, Spain.

**Table S 1.** Crystal data for bipan.

Empirical formula	C22 H14 N4
Formula weight	334.37
Temperature	100(2) K
Wavelength	0.71073 Å
Crystal system	Monoclinic
Space group	P2(1)/c
Unit cell dimensions	a = 6.3462(5) Å $\alpha$ = 90.00 °. b = 33.381(2) Å $\beta$ = 90.810(2) °. c = 7.4749(6) Å $\gamma$ = 90.00 °.
Volume	1802.8(5) Å <sup>3</sup>
Z	1583.3(2) Å <sup>3</sup>
Density (calculated)	4
Absorption coefficient	1.403 Mg/m <sup>3</sup>
F(000)	0.086 mm <sup>-1</sup>
Crystal size	696
Theta range for data collection	0.40 x 0.20 x 0.10 mm <sup>3</sup>
Index ranges	2.99 to 36.60 °.
Reflections collected	-10 <=h<=10 , -47 <=k<=55 , -7 <=l<=12
Independent reflections	7111
Completeness to theta =36.60 °	6325 [R(int) = 0.0162 ]
Absorption correction	0.906 %
Max. and min. transmission	Empirical
Refinement method	0.9915 and 0.9664
Data / restraints / parameters	Full-matrix least-squares on F <sup>2</sup>
Goodness-of-fit on F <sup>2</sup>	7111 / 0 / 235
Final R indices [I>2sigma(I)]	1.740
R indices (all data)	R1 = 0.0485 , wR2 = 0.1709
Largest diff. peak and hole	R1 = 0.0535 , wR2 = 0.1749

**Table S 2.** Crystal data for **1-out<sup>†</sup>**.

Empirical formula	C <sub>39</sub> H <sub>31</sub> Cl F <sub>6</sub> N <sub>7</sub> O P Ru
Formula weight	895.20
Temperature	T100(2)K
Wavelength	0.71073 Å
Crystal system	Triclinic
Space group	P-1
Unit cell dimensions	a = 8.6274(15) Å α = 79.921(3) °. b = 14.107(2) Å β = 79.688(3) °. c = 15.818(3) Å γ = 73.800(3) °.
Volume	1802.8(5) Å <sup>3</sup>
Z	2
Density (calculated)	1.647 Mg/m <sup>3</sup>
Absorption coefficient	0.630 mm <sup>-1</sup>
F(000)	904
Crystal size	0.2 x 0.2 x 0.1 mm <sup>3</sup>
Theta range for data collection	1.87 to 28.21 °.
Index ranges	-11<=h<=11, -18<=k<=18, -20<=l<=20
Reflections collected	28043
Independent reflections	8623 [R(int) = 0.0946]
Completeness to theta =28.21 °	0.968 %
Absorption correction	Empirical
Max. and min. transmission	1.0 and 0.675795
Refinement method	Full-matrix least-squares on F <sup>2</sup>
Data / restraints / parameters	8623 / 0 / 507
Goodness-of-fit on F <sup>2</sup>	0.923
Final R indices [I>2sigma(I)]	R1 = 0.0636, wR2 = 0.1387
R indices (all data)	R1 = 0.1297, wR2 = 0.1599
Largest diff. peak and hole	1.101 and -1.024 e.Å <sup>-3</sup>

III

**Figure S 1.**  $^1\text{H-NMR}$  spectra of (top) *p*-toluensulfonate of pyridinium and (bottom) Crude solid that contains compound **3**.

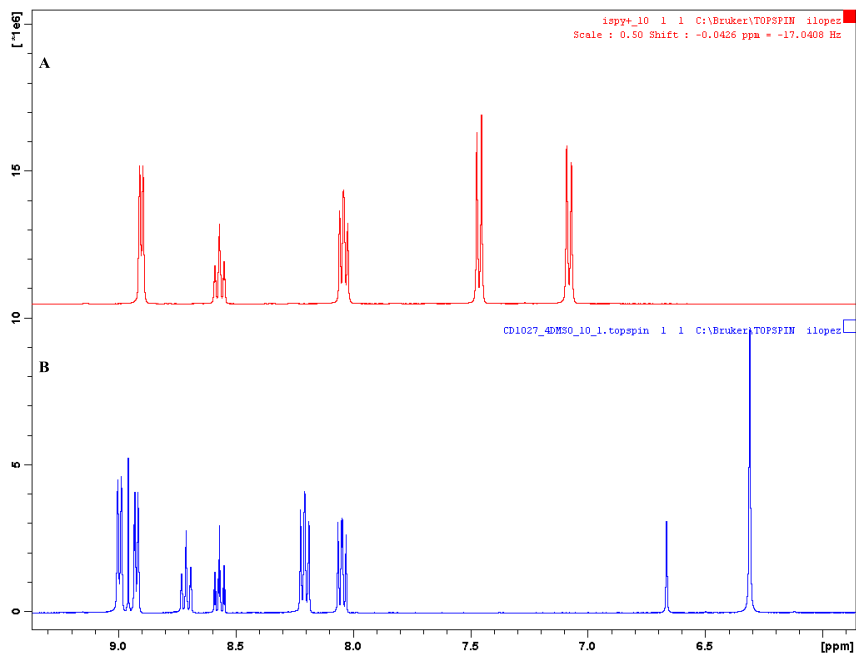
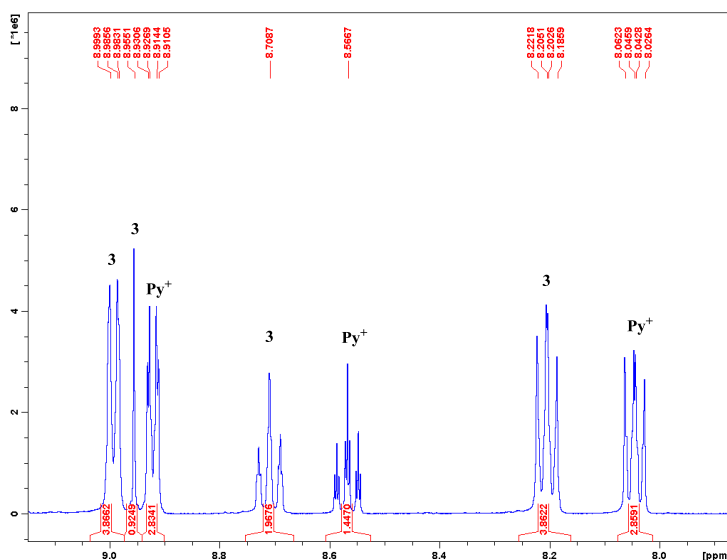


**Figure S 2.** Calculation of the ratio **3**/Py<sup>+</sup>.



From the integrals of the triplets at 8.57 and 8.71 ppm it's known that:

$$\frac{1.9676}{2 \text{ protons}} : \frac{1.4470}{1 \text{ proton}} = 0.9838 \text{ mols } \mathbf{3} : 1.4470 \text{ mols } \text{py}^+$$

$$1 \text{ mol } \mathbf{3} : 1.47 \text{ mols } \text{py}^+$$

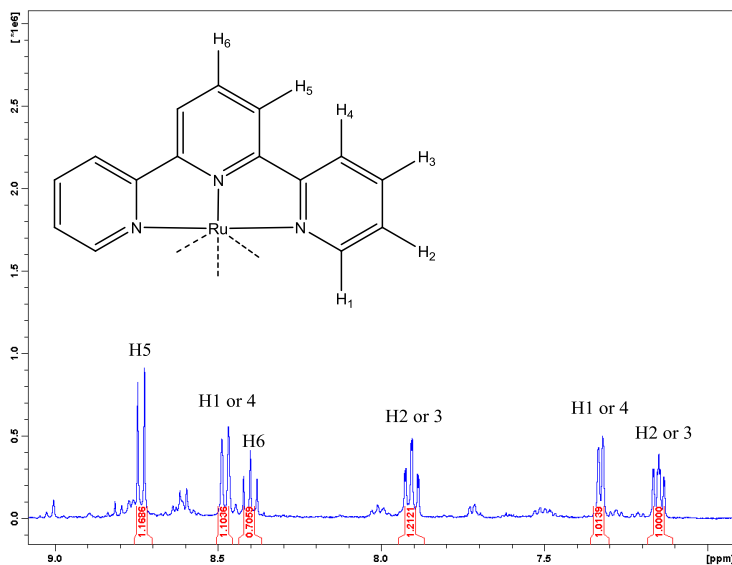
This molar relationship is converted to a weight relationship:

$$606.15 \text{ g mol}^{-1} * 1 \text{ mol } \mathbf{3} : 207.08 \text{ g mol}^{-1} * 1.47 \text{ mols } \text{py}^+$$

$$606.15 \text{ g } \mathbf{3} : 304.41 \text{ g } \text{py}^+$$

This ratio allows us to estimate the amount of each compound in the final solid.

**Figure S 3.**  $^1\text{H-NMR}$  of the isolated  $[\text{Ru}(\text{trpy})_2]^{2+}$ .



$^1\text{H-NMR}$  ( $\text{CD}_3\text{CN}$ , 400 MHz)  $\delta$  (ppm): 7.15 (t, 2H, H-2 or 3,  $^3J=6.29$  Hz), 7.33 (d, 2H, H-1 or 4,  $^3J=6.29$  Hz), 7.97 Hz (t, 2H, H-2 or 3,  $^3J=7.97$  Hz), 8.40 (t, 1H, H-5,  $^3J=8.39$  Hz), 8.48 (d, 2H, H-6,  $^3J=8.39$  Hz), 8.74 (d, 2H, H-1 or H-4,  $^3J=7.97$  Hz).

**Figure S 4.** COSY experiment of the isolated  $[\text{Ru}(\text{trpy})_2]^{2+}$ .

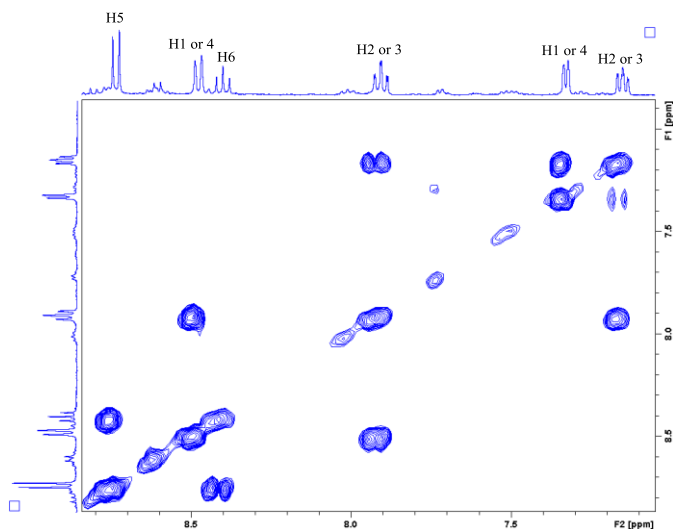
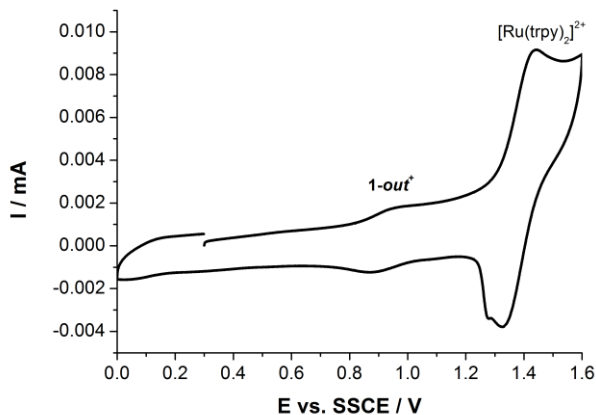


**Figure S 5.** CV of the isolated  $[\text{Ru}(\text{trpy})_2]^{2+}$  in dichloromethane (0.1 M TBAH). GC was used as working electrode, a Pt wire as counter electrode and SSCE as reference electrode. Scan rate =  $100 \text{ mV s}^{-1}$ .



Two waves can be observed. The smallest one at  $E^0 = 0.90 \text{ V}$  corresponds to  $\text{out-}[\text{Ru}(\text{trpy})(\text{bipan})\text{Cl}]^+$  which is presented as an impurity, the biggest one at  $E^0 = 1.35 \text{ V}$  corresponds to  $[\text{Ru}(\text{trpy})_2]^{2+}$ .



**Figure S 6.** Overlapped NOESY (green and blue) and COSY (red) NMR experiments of **1-*in*<sup>+</sup>**.

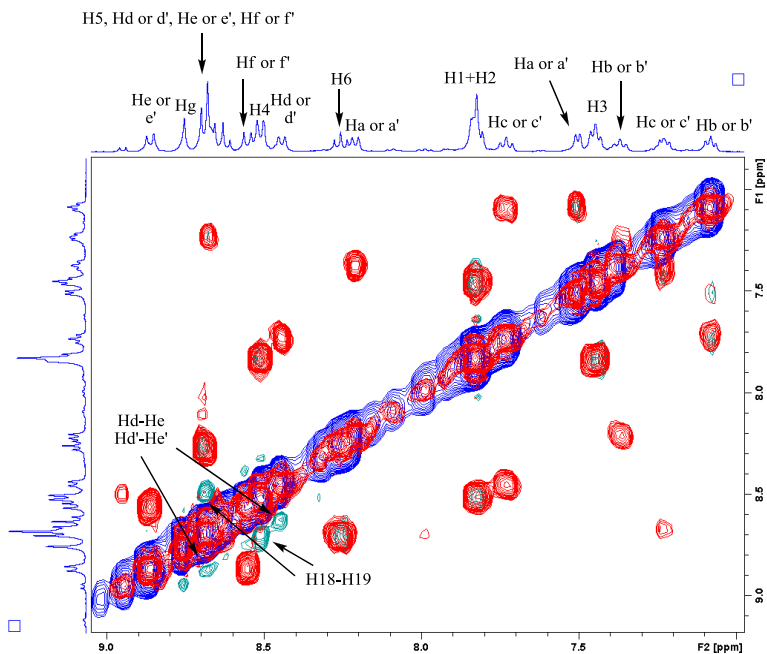


**Figure S 7.** Same experiment that previous focusing on the H1-Hh NOE interaction.

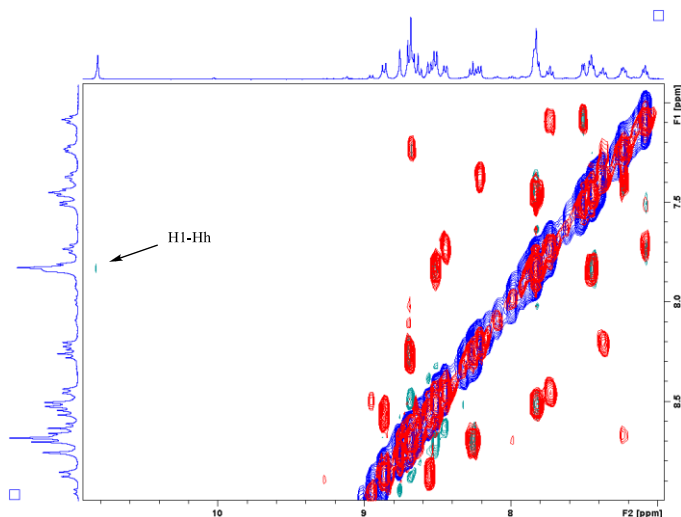


**Figure S 8.**  $^1\text{H-NMR}$  spectrum ( $\text{CD}_3\text{CN}$ ) spectrum of **1-out**<sup>+</sup>. The inset shows the deshielded resonance for Ha.

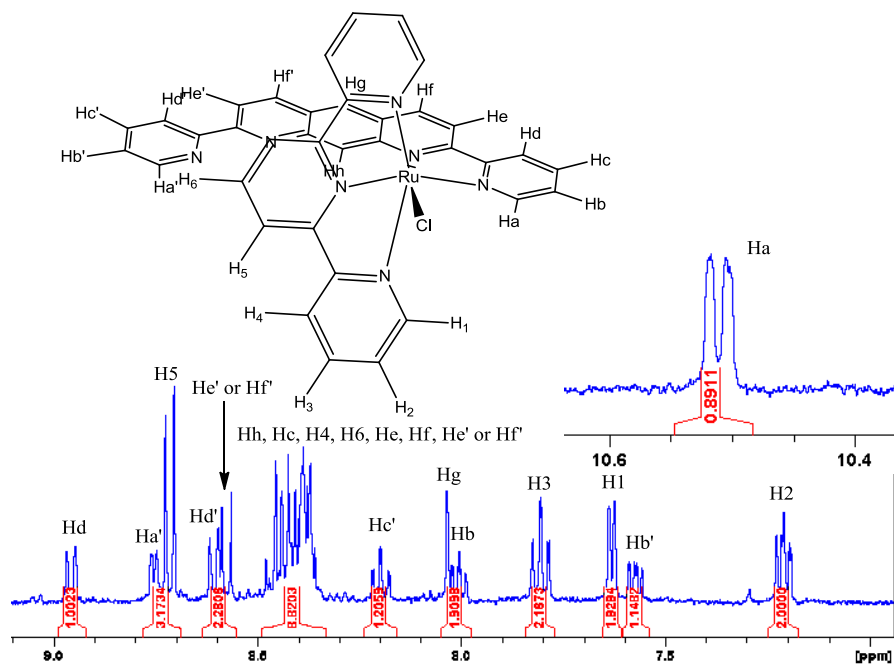


**Figure S 9.** Overlapped NOESY (green and blue) and COSY (red) NMR experiments of **1-out<sup>+</sup>**.

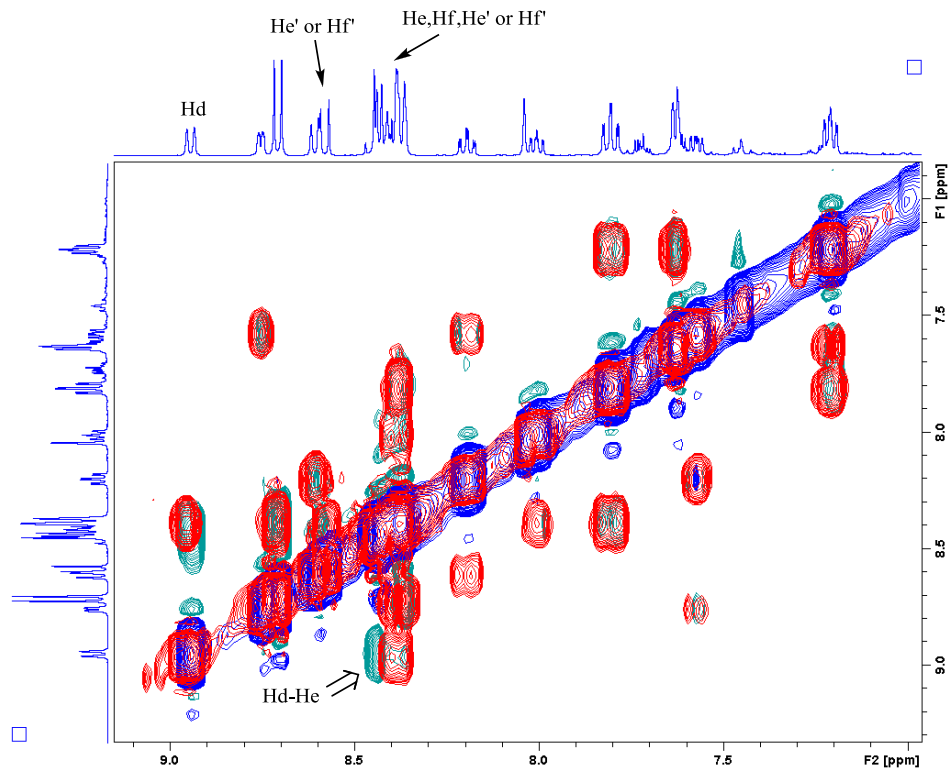


**Figure S 10.** ESI-MS of **1-in<sup>+</sup>** in MeOH. (Top) Extended spectrum. (Bottom) Comparison of observed isotopic pattern for the main peak (left) and simulated (right).

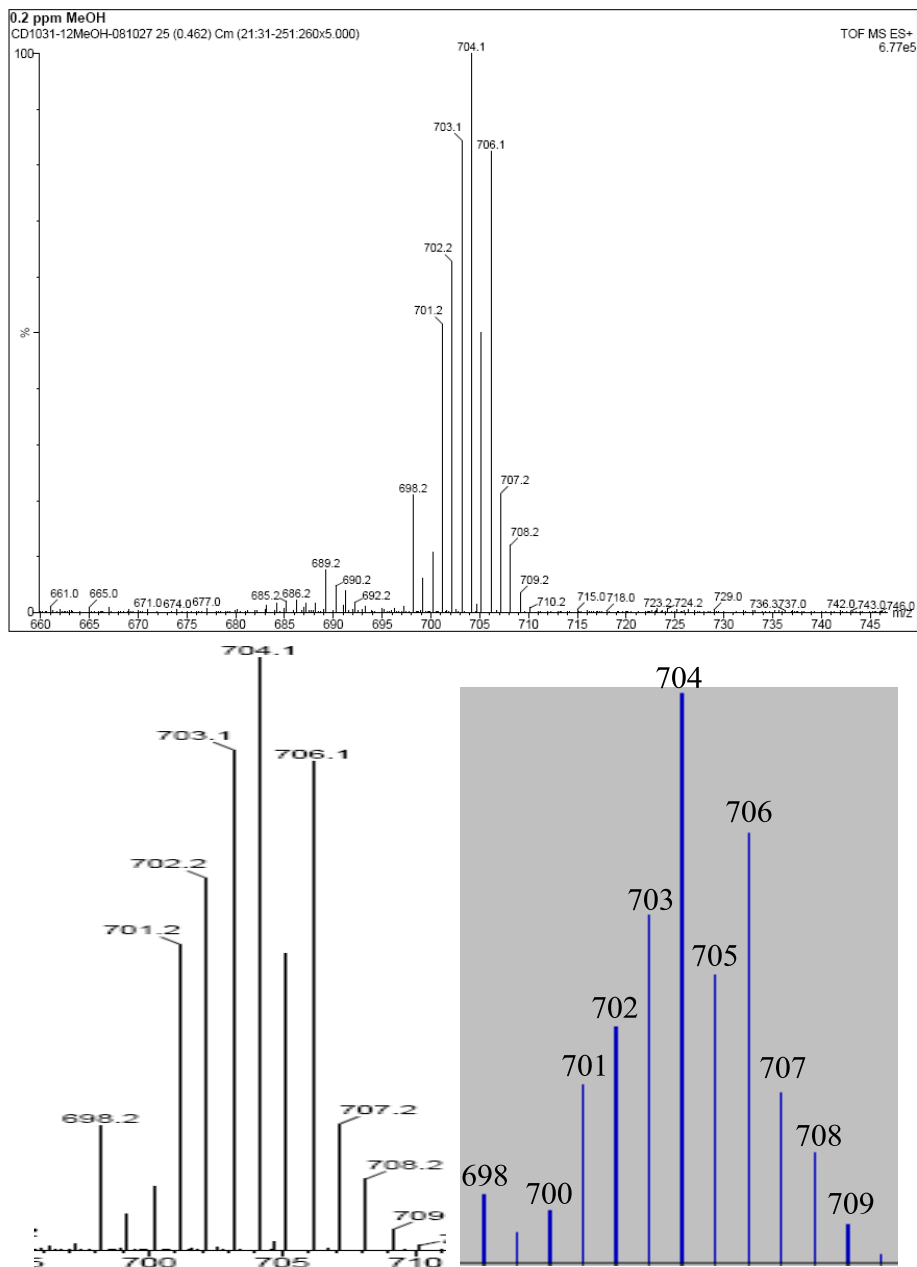


**Figure S 11.** ESI-MS of **1-out<sup>+</sup>** in MeOH. Comparison of observed isotopic pattern for the main peak and simulated (inset).

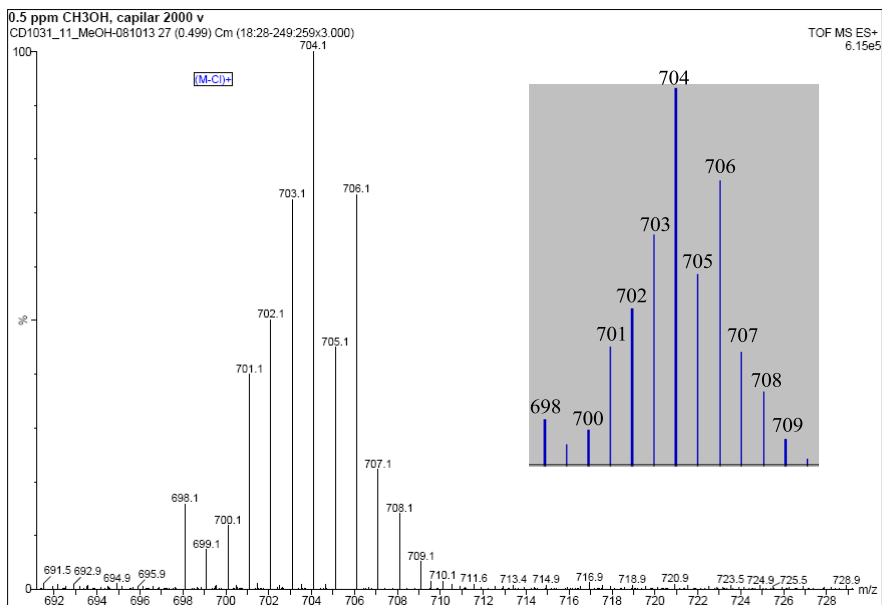


**Figure S 12.** Complete dioxygen evolution versus time manometric profile for **1-out<sup>+</sup>** under 1:100 Cat/Ce<sup>IV</sup> ratio in 0.1 M triflic acid solutions (pH = 1.0) at 25°C.

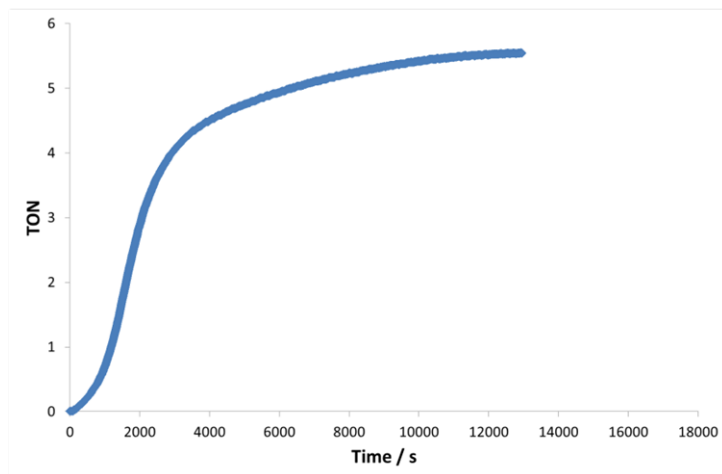


**Figure S 13.** On-line MS monitoring of the evolved O<sub>2</sub>(red) and CO<sub>2</sub> (black) after the addition of 100 equivalents of Ce<sup>IV</sup> to a 1 mM solution of **1-in<sup>+</sup>** in 0.1 M triflic acid (pH = 1) at RT

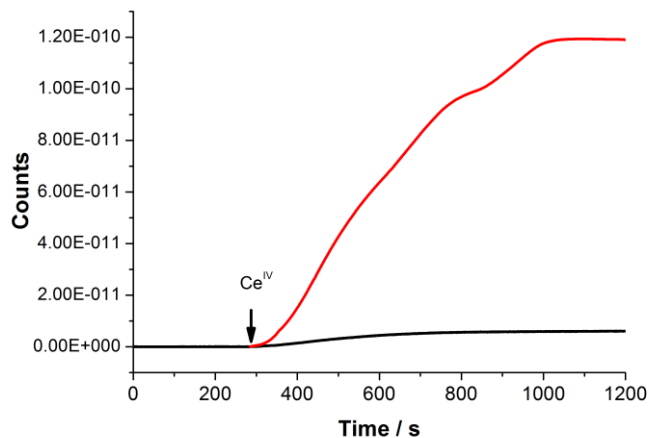
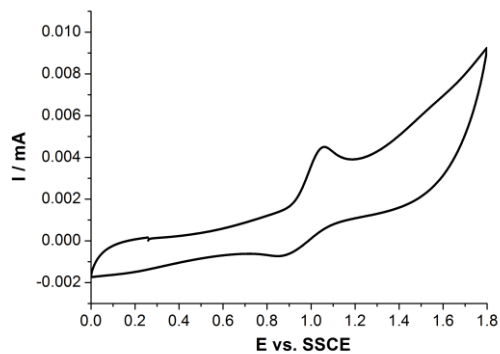
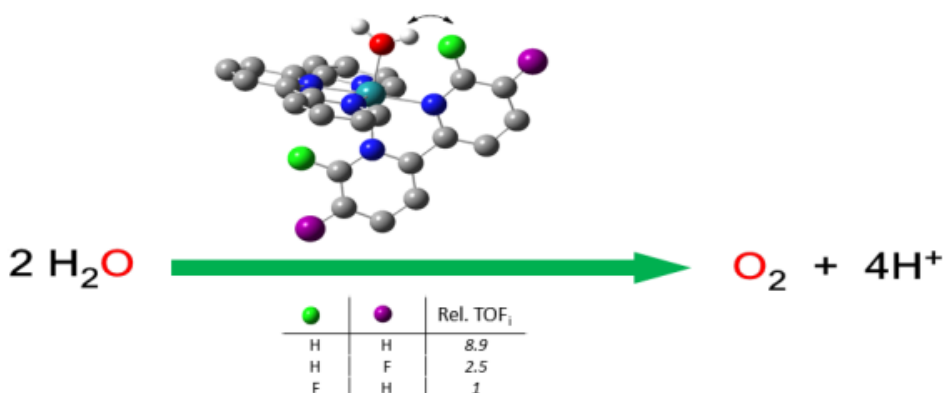


**Figure S 14.** CV of the free ligand **bipan** in MeCN (0.1 M TBAH). GC was used as working electrode, a Pt wire as counter electrode and SSCE as reference electrode. Scan rate = 100 mV s<sup>-1</sup>.



## **Chapter 4. Mononuclear Ru water oxidation catalysts: Discerning between electronic and hydrogen bonding effects.**



IV

New mononuclear complexes of general formula  $[\text{Ru}(\text{trpy})(n,n'\text{-F}_2\text{-bpy})\text{X}]^{m+}$ , ( $n = n' = 5$ :  $\text{X} = \text{Cl}$ ,  $3^+$  and  $\text{X} = \text{H}_2\text{O}$ ,  $5^{2+}$ ;  $n = n' = 6$ :  $\text{X} = \text{Cl}$ ,  $4^+$  and  $\text{X} = \text{H}_2\text{O}$ ,  $6^{2+}$ ; trpy is 2,2':6',2''-terpyridine) have been prepared and thoroughly characterized. The 5,5'- and 6,6'-F<sub>2</sub>-bpy ligands allow exerting a remote electronic perturbation to the Ru metal center that affects at the combination of species involved in the catalytic cycle. Additionally the 6,6'-F<sub>2</sub>-bpy also allows to interact through space with the Ru-O moiety of the complex via hydrogen bonding that also affects the stability of the different species involved in the catalytic cycle. The combination of both effects has strong impact into the kinetics of the catalytic process as observed through manometric monitoring.



UNIVERSITAT ROVIRA I VIRGILI

WATER OXIDATION WITH MONONUCLEAR RU COMPLEXES. BELOW THE TIP OF THE

ICEBERG: THE OXO-BRIDGE SCENARIO

Isidoro López Marin

Dipòsit Legal: T. 1505-2013

## Table of Contents.

### **Chapter 4. *Mononuclear Ru water oxidation catalysts: Discerning between electronic and hydrogen bonding effects.***

<i>4.1. Introduction.</i>	121
<i>4.2. Results and discussion.</i>	122
<i>4.3. Conclusions</i>	128
<i>4.4. Acknowledgements.</i>	128
<i>4.5. References.</i>	129
<i>4.6. Supporting Information.</i>	131

UNIVERSITAT ROVIRA I VIRGILI

WATER OXIDATION WITH MONONUCLEAR RU COMPLEXES. BELOW THE TIP OF THE

ICEBERG: THE OXO-BRIDGE SCENARIO

Isidoro López Marin

Dipòsit Legal: T. 1505-2013

## Mononuclear Ru water oxidation catalysts: Discerning between electronic and hydrogen bonding effects

*Inorg. Chem.* **2013**, *52*, 3591.

Somnath Maji,<sup>a</sup> Isidoro López,<sup>a</sup> Fernando Bozoglian,<sup>a</sup> J. Benet-Buchholz<sup>a</sup> and Antoni Llobet<sup>a,b,\*</sup>

<sup>a</sup> Institute of Chemical Research of Catalonia (ICIQ), Av. Països Catalans, 16, 43007 Tarragona, Spain.

<sup>b</sup> Departament de Química, Universitat Autònoma de Barcelona, Cerdanyola del Vallès, 08193 Barcelona, Spain.

### 4.1. Introduction.

Since the discovery by Thummel *et al.*<sup>1</sup> that mononuclear Ru complexes were also active as water oxidation catalysts, there has been a large development of the field based on this type of complexes. In 2008 Meyer *et al.*<sup>2</sup> offered a mechanistic description, of how the water oxidation occurred at a molecular level, where the O-O bond formation is proposed to occur based on the water nucleophilic attack pathway (WNA). This description has now been adopted to many mononuclear Ru complexes but also to those of Ir and other first row transition metals, where the water oxidation catalysis is claimed to proceed in a molecular manner.<sup>3-7</sup> Later on Berlinguette and coworkers studied the strong influence that electronic perturbation of the metal center exerted through remote positions of the ligands over the whole water oxidation catalysis process.<sup>8</sup> Recent reports by Yagi and Fujita have shown how the presence of a N-lone pair can influence reactivity in isomeric 2-(2-pyridyl)-1,8-naphthyridine complexes.<sup>9,10</sup> In order to evaluate electronic and hydrogen

bonding effects individually we have designed complexes containing ligands that allow to have a trough space interaction with the active Ru-OH<sub>2</sub> entourage in mononuclear complexes, in combination with others that only exert a remote electronic perturbation. In the present paper we report a new family of complexes of general formula [Ru(trpy)(n,n'-F<sub>2</sub>-bpy)X]<sup>m+</sup>, (n = n' = 5: X = Cl, **3**<sup>+</sup> and X = H<sub>2</sub>O, **5**<sup>2+</sup>; n = n' = 6: X = Cl, **4**<sup>+</sup> and X = H<sub>2</sub>O, **6**<sup>2+</sup>) that allow us to discern and quantify the electronic and hydrogen bonding effects. Additionally we report their activity as water oxidation catalysts and compare them with the reference complex [Ru(tpry)(bpy)OH<sub>2</sub>]<sup>2+</sup>, **2**<sup>2+</sup>.<sup>11-14</sup>

## 4.2. Results and discussion.

The synthetic strategy followed for the synthesis of complexes **3-6** uses [RuCl<sub>3</sub>(tpry)], **1**, as a starting material and is similar to the one used for the preparation of **2**<sup>2+</sup>. Synthetic details together with a complete structural and spectroscopic characterization is presented as Sup. Inf. An Ortep plot of the X-ray structure of **6**<sup>2+</sup> is exhibited in Figure 1 whereas that of **5**<sup>2+</sup> is presented as Sup. Inf. In both cases the Ru center presents an octahedrally distorted geometry around the metal center and bond distances and angles are unremarkable except for the hydrogen bonding interaction of the F atom with the aqua group in **6**<sup>2+</sup>. This interaction is also responsible for the rotation of one of the pyridyl groups of bpy generating a dihedral angle of 11.6°, needed to be able to accommodate the F atom of the bpy so close to the aqua group. In turn this close and rigid interaction will ensure that all the potential species that can be generated along the catalytic cycle will have an interaction with this group.

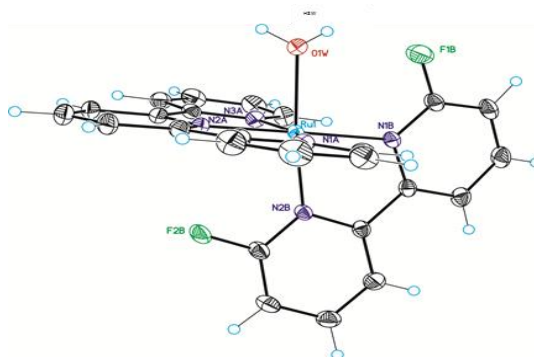


**Figure 1.** Ortep plot (50 % probability) of the crystal structure of the complex  $6^{2+}$ . Color codes: Ru, cyan; N, navy blue; F, green; O, red; H, blue empty circles. Interesting metric parameters:  $d_{(H2W-F1B)}=2.316 \text{ \AA}$ ;  $d_{(F1B-O1W)}=2.630 \text{ \AA}$ ;  $\angle_{(O1W-H2W-F1B)}=100.71^\circ$ ; the dihedral angle between the pyridyl moieties of 6,6'-F<sub>2</sub>-bpy is  $11.6^\circ$ .

The redox properties of complexes  $5^{2+}$  and  $6^{2+}$  were investigated from CV and DPV experiments in water at different pHs and are reported in Table 1, Figure 2 and in the Supp. Inf. The presence of the F substituent at the bpy ligand produces a dramatic influence into the electronic structure of the metal center in the sense that for this complexes their oxidation state III, is unstable with regard to disproportionation and thus a two electron wave is found,

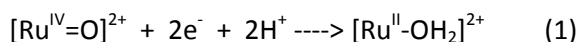


**Table 1.** Thermodynamic and catalytic data for  $5^{2+}$  and  $6^{2+}$  and for related Ru-aqua complexes described in the literature at pH = 7.

Entry	Complex <sup>a</sup>	$E_{1/2}(V)$ vs. SSCE				$\Delta E_{1/2}$ <sup>b</sup>	$pK_{a,II}$ <sup>c</sup>	$pK_{a,III}$ <sup>c</sup>	TOF <sub>T</sub> ·10 <sup>3e</sup>	Ref
		IV/III	III/II	IV/II	V/IV					
1	[Ru(trpy)(bpy)(H <sub>2</sub> O)] <sup>2+</sup>	0.59	0.48	0.54	1.62	110	9.8	1.7	15.1 (18.3)	Tw <sup>f</sup>
2	[Ru(trpy)(6,6'-F <sub>2</sub> -bpy)(H <sub>2</sub> O)] <sup>2+</sup>	--	--	0.56 <sup>d</sup>	1.69	--	10.4	--	1.7 (7.8)	Tw
3	[Ru(trpy)(5,5'-F <sub>2</sub> -bpy)(H <sub>2</sub> O)] <sup>2+</sup>	--	--	0.54 <sup>d</sup>	1.68	--	9.0	--	4.3 (13.0)	Tw
5	[Ru(CNC)(bpy)(H <sub>2</sub> O)] <sup>2+</sup>	0.50	0.45	0.48		50	10.9	2.3		15
6	[Ru(trpy)(bpm)(H <sub>2</sub> O)] <sup>2+</sup>	--	--	0.62 <sup>d</sup>	--		9.7			2
7	[Ru(damp)(bpy)(H <sub>2</sub> O)] <sup>2+</sup>	0.44	0.30	0.37		140	11.5	--		16,17

<sup>a</sup> Ligand abbreviations: CNC is 2,6-bis(butylimidazol-2-ylidene)pyridine; bpm is 2,2'-bipyrimidine; damp is 2,6-bis((dimethylamino)methyl)pyridine. <sup>b</sup>  $\Delta E_{1/2} = E_{1/2}(IV/III) - E_{1/2}(III/II)$  in mV. <sup>c</sup>  $pK_{a,II}$  and  $pK_{a,III}$  represent the  $pK_a$  of the corresponding Ru<sup>II</sup>-OH<sub>2</sub> and Ru<sup>III</sup>-OH<sub>2</sub> species, respectively. <sup>d</sup> 2 electron process. <sup>e</sup> TOF<sub>T</sub> stands for initial Turn Over Frequencies in cycles per second and TN for Turn over Numbers. This values are extracted for the catalytic reactions involving 1.0 mM Cat/100 mM Ce(IV) in a 0.1 M triflic acid solution with a total volume of 2 mL. <sup>f</sup> Tw means this work.

$E^0 = 0.54$  V for  $5^{2+}$  and  $0.56$  V for  $6^{2+}$  at pH = 7.0 (trpy and bpy ligands are not drawn). This is in sharp contrast to complex  $2^{2+}$ ,<sup>6</sup> where the two one electron processes are separated by 110 mV. It is interesting to see here that the standard potential for the Ru(IV/II) couple for  $2^{2+}$  is practically identical to that of the F complexes  $5^{2+}$  and  $6^{2+}$ . This reveals that the presence of the F substituent in the bpy produces an increase of the Ru(III/II) couple as expected for the electron withdrawing properties of the F-group but surprisingly produces a dramatic decrease of the IV/III redox potential. It is also important to realize here that the IV/II standard potential for  $5^{2+}$  and  $6^{2+}$  differ merely by 20 mV and thus indicates that the direct contact of the F with the aqua group, distorting slightly its geometry, practically does not affect the electronic structure of the metal center. A similar phenomenon is observed for the next redox couple corresponding to the oxidation of Ru(IV) to Ru(V), where in this case the potentials for  $5^{2+}$  and  $6^{2+}$  differ now by only 10 mV (1.68 V for  $5^{2+}$  and 1.69 V for  $6^{2+}$ ). However, while for the two electron transfer process Ru(IV/II)

there is not much influence because of the opposite trend of the individual redox potentials just described, for the Ru(V/IV) standard potential the F-substituent produces an anodic shift of 60 to 70 mV for  $5^{2+}$  and  $6^{2+}$  respectively with regard to the unsubstituted bpy complex  $2^{2+}$ . As it can be observed in Figure 2 this wave is accompanied with a large electrocatalytic current intensity associated with the oxidation of water to dioxygen.

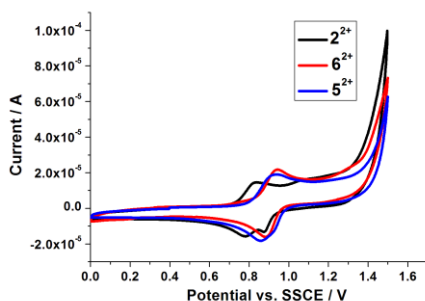
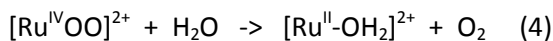
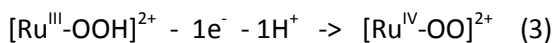
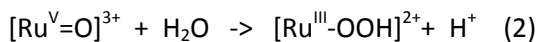


**Figure 2.** Cyclic Voltammetry of 1 mM solutions in 0.1 M  $\text{CF}_3\text{SO}_3\text{H}$  (pH=1.0) for complexes  $2^{2+}$  (black),  $5^{2+}$  (blue) and  $6^{2+}$  (red). Scan rate  $100 \text{ mVs}^{-1}$  using a glassy carbon working electrode, Pt wire as an auxiliary electrode and the SSCE reference electrode.

For the  $2^{2+}$  case it is proposed that right at this high oxidation state the O-O bond formation occurs, followed by a sequence of reactions that lead to the formation of  $\text{O}_2$ , as exemplified below (again trpy and bpy ligands are not shown),



and where the rate determining step (rds) is proposed to be the last reaction (equation 4) where the release of oxygen is produced.<sup>6b,6c</sup> The perturbation

IV



Chapter 4

exerted by the presence of the F group in  $5^{2+}$  and  $6^{2+}$  is nicely perceived in their acidities at oxidation state II. Whereas  $5^{2+}$  decreases the  $pK_{a,II}$  by 0.8 log units compared to  $2^{2+}$ , as expected from the electron withdrawing effect of the F substituent,  $6^{2+}$  causes the opposite effect increasing the  $pK_a$  by 0.6 log units (see Table 1). The latter is attributed to hydrogen bonding in  $6^{2+}$ , that stabilizes the  $Ru^{II}-OH_2$  species as seen in the Figure 1 (X-ray structure) and in Figure 4. Taking into account that both  $5^{2+}$  and  $6^{2+}$  isomers, according to the electrochemical data, have practically the same electronic effect over the metal center, it implies then that the hydrogen bonding effect is responsible for the 1.4 log units increase of the  $pK_a$ , that is  $6^{2+}$  is roughly 25 times more basic than  $5^{2+}$ .

The catalytic activity of complex  $5^{2+}$  and  $6^{2+}$  towards the oxidation of water to dioxygen was also evaluated and compared to the unsubstituted by complex  $2^{2+}$ . Figure 3 presents the oxygen evolution profile obtained when 1 mM catalysts are treated with 100 mM Ce(IV) oxidant at pH = 1.0 in a triflic acid aqueous solution with a total volume of 2 mL. The oxygen generation was monitored manometrically and the nature of the gases was also followed on line by Mass Spectroscopy (MS) indicating that no other gases were formed in the reaction. As can be observed in the graph both the  $O_2$  generation initial rate ( $TOF_i$ ) and the overall Turn Over Number (TN) (See Table 1) are strongly affected by the substituted F-bpys compared to the unsubstituted. In the purely electronic scenario, that is comparing  $2^{2+}$  with  $5^{2+}$ , the initial rates decreases by a factor near to 4 (15.1 vs. 4.3). On the other hand the purely H-bonding scenario, that is comparing  $5^{2+}$  and  $6^{2+}$ , the initial rate decrease by a factor bigger than 2 (4.3 vs. 1.7). Thus since both factors operate in the same

direction when comparing  $2^{2+}$  with  $6^{2+}$  the initial rate decreases by a factor of 9.

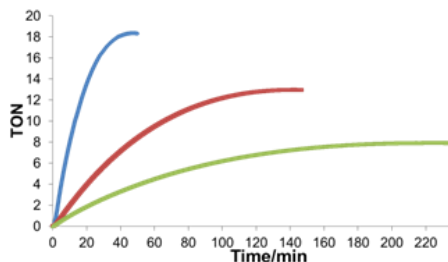
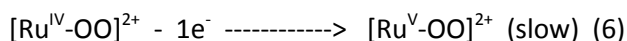
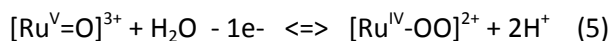
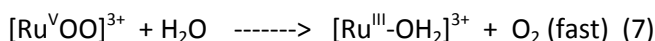


**Figure 3.** O<sub>2</sub> evolution vs. time manometric profiles for catalysts  $2^{2+}$  (blue),  $5^{2+}$  (red) and  $6^{2+}$  (green) under 1:100 Cat:Ce(IV) ratios in 0.1 M triflic acid solutions (pH = 1.0).

The 4 times decrease in the TOF<sub>i</sub> for the purely electronic effect exerted by  $5^{2+}$  with regard to  $2^{2+}$  indicates that equation 4 is not any more the rds since this is formally an intramolecular Electron Transfer (ET) step where Ru(IV) oxidizes the peroxide to dioxygen concomitant with its release, therefore an increase in the standard potentials would suppose an increase in rate. Indeed a kinetic study based on initial oxygen evolution velocities shows that the rate of the reaction is first order in Ru and second order in Ce (see sup inf.). This is consistent with a rds where the  $[Ru^{IV}OO]^{2+}$  species is further oxidized to Ru(V) (equation 6) preceded by a fast equilibrium step as shown in equations 5, below,



followed by a fast release of dioxygen.



IV

Finally, the fact that all the standard potentials for  $5^{2+}$  and  $6^{2+}$  are practically identical contrasts with the 2 times decrease on  $\text{TOF}_i$  for  $6^{2+}$  with regard to that of  $5^{2+}$ . This clearly points towards a potential stabilization of the  $[\text{Ru}^{\text{III}}\text{-OOH}]^{2+}$ , **7**, intermediate through H-bonding as shown in the Figure 4. This stabilization produces a severe slowing down in the process, in line with the basicity increase described above for the  $\text{pK}_{\text{a,II}}$  for  $6^{2+}$ , given the Proton Coupled Electron Transfer (PCET) nature of the process.

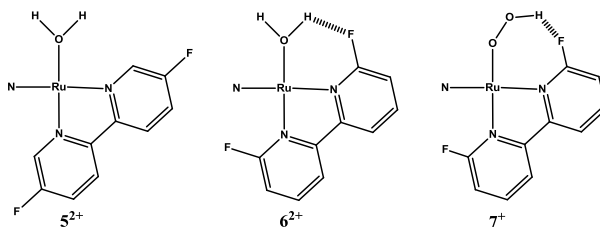


**Figure 4.** Drawings of  $5^{2+}$ ,  $6^{2+}$  and  $7^+$  (trpy ligands are omitted except for the central N atom) showing the Hydrogen interactions between the aqua and peroxo ligands with the F-group of the bpy ligand, where appropriate.

### 4.3. Conclusions.

In conclusion, careful ligand design of mononuclear tpy-bpy-Ru-aqua type of complexes allows understanding how electronic perturbations and hydrogen bonding interactions influence their water oxidation activity.

### 4.4. Acknowledgements.

Support from MINECO (CTQ2010-21497 and PRI-PIBIN-2011-1278) is gratefully acknowledged. SM thanks MINECO for a Torres Quevedo contract and IL for a FPU grant.

I have carried out the electrochemical and catalytic studies of this work.

#### 4.5. References.

- (1) Zong, R.; Thummel, R. P. *J. Am. Chem. Soc.* **2005**, *127*, 12802.
- (2) Concepcion, J. J.; Jurss, J. W.; Templeton, J. L.; Meyer, T. J. *J. Am. Chem. Soc.* **2008**, *130*, 16462.
- (3) Ellis, W. C.; McDaniel, N. D.; Bernhard, S.; Collins, T. J. *J. Am. Chem. Soc.* **2010**, *132*, 10990.
- (4) Wasylenko, D. J.; Palmer, R. D.; Schott, E.; Berlinguette, C. P. *Chem. Commun. (Cambridge, U. K.)* **2012**, *48*, 2107.
- (5) Chen, Z.; Concepcion, J. J.; Luo, H.; Hull, J. F.; Paul, A.; Meyer, T. J. *J. Am. Chem. Soc.* **2010**, *132*, 17670.
- (6) Roeser, S.; Farràs, P.; Bozoglian, F.; Martínez-Belmonte, M.; Benet-Buchholz, J.; Llobet, A. *ChemSusChem* **2011**, *4*, 197.
- (7) Blakemore, J. D.; Schley, N. D.; Balcells, D.; Hull, J. F.; Olack, G. W.; Incarvito, C. D.; Eisenstein, O.; Brudvig, G. W.; Crabtree, R. H. *J. Am. Chem. Soc.* **2010**, *132*, 16017.
- (8) Wasylenko, D. J.; Ganesamoorthy, C.; Henderson, M. A.; Koivisto, B. D.; Osthoff, H. D.; Berlinguette, C. P. *J. Am. Chem. Soc.* **2010**, *132*, 16094.
- (9) Yamazaki, H.; Hakamata, T.; Komi, M.; Yagi, M. *J. Am. Chem. Soc.* **2011**, *133*, 8846.
- (10) Boyer, J. L.; Polyansky, D. E.; Szalda, D. J.; Zong, R.; Thummel, R. P.; Fujita, E. *Angew. Chem. Int. Ed.* **2011**, *50*, 12600.
- (11) Yoshida, M.; Masaoka, S.; Abe, J.; Sakai, K. *Chem. Asian J.* **2010**, *5*, 2369.
- (12) Concepcion, J. J.; Jurss, J. W.; Norris, M. R.; Chen, Z.; Templeton, J. L.; Meyer, T. J. *Inorg. Chem.* **2010**, *49*, 1277.
- (13) Wasylenko, D. J.; Ganesamoorthy, C.; Koivisto, B. D.; Henderson, M. A.; Berlinguette, C. P. *Inorg. Chem.* **2010**, *49*, 2202.
- (14) Angeles-Boza, A. M.; Roth, J. P. *Inorg. Chem.* **2012**, *51*, 4722.
- (15) Masllorens, E.; Rodríguez, M.; Romero, I.; Roglans, A.; Parella, T.; Benet-Buchholz, J.; Poyatos, M.; Llobet, A. *J. Am. Chem. Soc.* **2006**, *128*, 5306.
- (16) Welch, T. W.; Ciftan, S. A.; White, P. S.; Thorp, H. H. *Inorg. Chem.* **1997**, *36*, 4812.
- (17) Vigara, L.; Ertem, M. Z.; Planas, N.; Bozoglian, F.; Leidel, N.; Dau, H.; Haumann, M.; Gagliardi, L.; Cramer, C. J.; Llobet, A. *Chem. Sci.* **2012**, *3*, 2576.

UNIVERSITAT ROVIRA I VIRGILI

WATER OXIDATION WITH MONONUCLEAR RU COMPLEXES. BELOW THE TIP OF THE

ICEBERG: THE OXO-BRIDGE SCENARIO

Isidoro López Marin

Dipòsit Legal: T. 1505-2013

## Supporting Information for,

# Mononuclear Ru water oxidation catalysts: discerning between electronic and hydrogen bonding effects

Somnath Maji,<sup>a</sup> Isidoro López,<sup>a</sup> Fernando Bozoglian,<sup>a</sup> J. Benet-Buchholz<sup>a</sup> and  
Antoni Llobet<sup>a,b,\*</sup>

<sup>a</sup>Institute of Chemical Research of Catalonia (ICIQ) Av. Països Catalans, 16, 43007 Tarragona, Catalonia, Spain. E-mail: allobet@iciq.cat

<sup>b</sup>Departament de Química, Universitat Autònoma de Barcelona, Cerdanyola del Vallès, 08193 Barcelona, Catalonia, Spain.

IV

## Experimental Section.

### Materials:

All reagents used in the present work were obtained from Aldrich Chemical Co. and were used without further purification. Reagent-grade organic solvents were obtained from SDS.  $\text{RuCl}_3 \cdot 3\text{H}_2\text{O}$  was supplied by Alfa Aesar and was used as received.  $\text{Ru}(\text{trpy})\text{Cl}_3^1$  and  $(n, n' \text{-F}_2\text{-bpy})$  where  $[n = n' = 5^2$  (5,5'-difluoro-2,2'-bipyridine) and  $n = n' = 6^3$  (6,6'-difluoro-2,2'-bipyridine)] were prepared according to literature procedures.

(1) Sullivan, B. P.; Calvert, J. M.; Meyer, T. J. *Inorg. Chem.* **1980**, *19*, 1404.

(2) Jenkins, D. M.; Bernhard, S. *Inorg. Chem.* **2010**, *49*, 11297-11308.

(3) Singh, R. P.; Eggers, G. V.; Shreeve, J. M. *Synthesis* **2003**, *7*, 1009-1011.

### Synthesis of Chloro (5,5'-difluoro-2,2'-bipyridine) (2,2':6',2''-terpyridine) ruthenium(II) hexafluorophosphate: $[\text{Ru}(\text{trpy})(n, n' \text{-F}_2\text{-bpy})\text{X}]^+$ , ( $n = n' = 5$ : X=Cl, 3<sup>+</sup>).

A mixture of  $\text{Ru}(\text{trpy})\text{Cl}_3$  (0.572 g, 1.302 mmol), the ligand 5,5'-difluoro-2,2'-bipyridine (0.250 g, 1.302 mmol) in ethylene glycol (3 mL) was refluxed for 4 h. After cooling to room temperature 5 mL ethanol was added and the mixture was filtered to remove the excess ligand and starting metal complex. The filtrate was concentrated by rotary evaporation and added dropwise excess saturated aqueous  $\text{NH}_4\text{PF}_6$ . The resulting precipitate was separated from the solution by vacuum filtration, washed with little portions of chilled water and 50 mL of diethyl ether, and dried under vacuum. This crude product was then purified by alumina chromatography using a 100:1 (v/v) dichloromethane/methanol solvent mixture as the eluent. The desired product eluted first as a purple band, which was then concentrated by rotary

evaporation, dissolved in a minimal amount of dichloromethane, and precipitated by addition of to 200 mL of diethyl ether. The precipitate was again isolated by vacuum filtration and washed with diethyl ether. This procedure produced 0.430 g of a purple solid. Yield: 47%. Anal. Calcd (%) for  $C_{25}H_{17}ClF_8N_5PRu \cdot H_2O$ : C, 41.42; H, 2.64; N, 9.66. Found: C, 41.69; H, 2.63; N, 9.68.  $\lambda$ [nm] ( $\epsilon$  [ $M^{-1}cm^{-1}$ ]) in acetonitrile: 630 (2290), 489 (18020), 363 (12755), 315 (55765), 300 (65205), 277 (40755), 259 (39215), 239 (54370). ESI-MS ( $m/z$ ): 562.1  $[M-PF_6]^+$ .  $^1H$  NMR in  $CD_2Cl_2$  [ $\delta$ /ppm ( $J$ /Hz)]: 10.19 (d, 2.5, H16), 9.53 (d, 9.2, H19), 9.31 (d, 9.2, H22), 8.46 (d, 7.8, H7 and H9), 8.34 (d, 7.8, H4 and H12), 8.15 (t, 7.8, H8), 8.11 (d, 9.28, H18), 7.92 (t, 7.0, H3 and H13), 7.68 (d, 5.3, H1 and H15), 7.61 (d, 6.8, H23), 7.33 (t, 7.0, H2 and H14), 7.09 (d, 2.5, H25).  $^{13}C\{^1H\}$  NMR (400 MHz,  $CD_3CN$ ):  $\delta$  =160.72, 159.47, 158.71, 155.70, 153.37, 142.00, 141.75, 138.97, 138.27, 138.04, 135.38, 128.12, 125.98, 125.91, 125.38, 125.32, 124.81, 124.64, 124.12, 123.96, 123.63. Single X-ray crystal structure was obtained by slow evaporation from a mixture of  $CH_2Cl_2$  and diethyl ether (1:2).

**Synthesis of Chloro (6,6'-difluoro-2,2'-bipyridine) (2,2':6',2''-terpyridine) ruthenium(II) hexafluorophosphate :  $[Ru(trpy)(n,n'-F_2-bpy)X]^+$ , ( $n = n' = 6$ :  $X = Cl, 4^+$ ).**

A mixture of  $Ru(trpy)Cl_3$  (0.572 g, 1.302 mmol), the ligand 6,6'-difluoro-2,2'-bipyridine (0.250 g, 1.302 mmol) in ethylene glycol (3 mL) was refluxed for 4 h. After cooling to room temperature 5 mL ethanol was added and the mixture was filtered to remove the excess ligand and starting metal complex. The filtrate was concentrated by rotary evaporation and added dropwise excess saturated aqueous  $NH_4PF_6$ . The resulting precipitate was separated from the solution by vacuum filtration, washed with little portions of chilled water and



50 mL of diethyl ether, and dried under vacuum. This crude product was then purified by alumina chromatography using a 100:1 (v/v) dichloromethane/methanol solvent mixture as the eluent. The desired product eluted first as a purple band, which was then concentrated by rotary evaporation, dissolved in a minimal amount of dichloromethane, and precipitated by addition of to 200 mL of diethyl ether. The precipitate was again isolated by vacuum filtration and washed with diethyl ether. This procedure produced 0.247 g of a purple solid. Yield: 27%. Anal. Calcd (%) for  $C_{25}H_{17}ClF_8N_5PRu$ : C, 42.48; H, 2.42; N, 9.91. Found: C, 42.69; H, 2.63; N, 9.88.  $\lambda$ [nm]( $\epsilon$ [ $M^{-1}cm^{-1}$ ]) in acetonitrile: 632 (1765), 508 (13165), 373 (8030), 315 (54945), 304 (55600), 280 (35390), 240 (41360). ESI-MS ( $m/z$ ): 562.0 [M-PF<sub>6</sub>]<sup>+</sup>. <sup>1</sup>H NMR in CD<sub>3</sub>CN [ $\delta$ /ppm( $J$ /Hz)]: 8.55 (d, 7.0, H19), 8.43 (t, 8.0, H18), 8.42(d, 8.0, H7 and H9), 8.36 (d, 7.8, H4 and H12), 8.26 (d, 7.8, H22), 8.06 (t, 8.0, H8), 7.94 (t, 4.9, H2 and H14), 7.92 (d, 7.8, H1 and H15), 7.83 (t, 8.0, H23), 7.69 (d, 8.2, H17), 7.34 (t, 7.0, H3 and H13), 6.75 (d, 8.2, H24). <sup>13</sup>C{<sup>1</sup>H} NMR (400 MHz, CD<sub>3</sub>CN):  $\delta$  = 170.36, 170.04, 168.27, 168.01, 159.35, 159.16, 157.53, 155.19, 153.27, 142.29, 142.21, 140.86, 140.78, 137.24, 134.24, 127.09, 123.27, 121.75, 121.09, 121.07, 121.05, 117.33, 113.85, 113.62, 111.62, 111.38. Single X-ray crystal structure was obtained by slow vapour diffusion from a mixture of CH<sub>2</sub>Cl<sub>2</sub> and diethyl ether(1:4).

**Synthesis of Aqua (5,5'-difluoro-2,2'-bipyridine) (2,2':6',2''-terpyridine) ruthenium(II) hexafluorophosphate [Ru(trpy)(n,n'-F<sub>2</sub>-bpy)X]<sup>2+</sup>, (n = n' = 5: X= H<sub>2</sub>O, 5<sup>2+</sup>).**

A (0.100 g, 0.141 mmol) amount of **3**<sup>+</sup> and (0.035 g, 0.168 mmol) of AgClO<sub>4</sub> were heated together at reflux for 2 h in 40 mL of 75% acetone/25% water. AgCl was filtered off, the solution volume reduced to 5 mL on a rotary

evaporator and added dropwise excess saturated aqueous  $\text{NH}_4\text{PF}_6$ . The resulting dark red precipitate was separated from the solution by vacuum filtration, washed with little portions of chilled water and 50 mL of diethyl ether, and dried under vacuum. This procedure produced 0.092 g of a dark red solid. Yield: 77.8 %. Anal. Calcd (%) for  $\text{C}_{25}\text{H}_{19}\text{F}_{14}\text{N}_5\text{OP}_2\text{Ru}\cdot\text{H}_2\text{O}$ : C, 35.22; H, 2.48; N, 8.22. Found: C, 35.48; H, 2.37; N, 8.30. ESI-MS ( $m/z$ ): 713.9  $[\text{M-PF}_6 + \text{Na}]^+$ .  $^1\text{H}$  NMR in  $\text{D}_2\text{O}$  [ $\delta/\text{ppm}$  ( $J/\text{Hz}$ )]: 9.37 (d, 2.3, 1H), 8.60 (d, 9.3, 1H), 8.53 (d, 8.0, 2H), 8.40 (d, 8.0, 2H), 8.24 (d, 9.0, 1H), 8.19 (t, 8.0, 1H), 8.08 (d, 9.3, 1H), 7.93 (t, 7.8, 2H), 7.72 (t, 5.3, 2H), 7.44 (d, 9.3, 1H), 7.28 (t, 6.7, 1H), 7.22 (d, 2.3, 1H). The crystal was grown by slow evaporation in mixture of acetone and water (1:1).

**Synthesis of Aqua (6,6'-difluoro-2,2'-bipyridine) (2,2':6',2''-terpyridine) ruthenium(II) hexafluorophosphate  $[\text{Ru}(\text{trpy})(\text{n},\text{n}'\text{-F}_2\text{-bpy})\text{X}]^{2+}$ , ( $\text{n} = \text{n}' = 6$ :  $\text{X} = \text{H}_2\text{O}$ ,  $6^{2+}$ ).**

A (0.100 g, 0.141 mmol) amount of  $4^+$  and (0.035 g, 0.168 mmol) of  $\text{AgClO}_4$  were heated together at reflux for 2 h in 40 mL of 75% acetone/25% water.  $\text{AgCl}$  was filtered off, the solution volume reduced to 5 mL on a rotary evaporator and added dropwise excess saturated aqueous  $\text{NH}_4\text{PF}_6$ . The resulting dark red precipitate was separated from the solution by vacuum filtration, washed with little portions of chilled water and 50 mL of diethyl ether, and dried under vacuum. This procedure produced 0.086 g of a dark red solid. Yield: 72.8 %. Anal. Calcd (%) for  $\text{C}_{25}\text{H}_{19}\text{F}_{14}\text{N}_5\text{OP}_2\text{Ru}$ : C, 35.98; H, 2.30; N, 8.39. Found: C, 36.28; H, 2.47; N, 8.28. ESI-MS ( $m/z$ ): 714.1  $[\text{M-PF}_6 + \text{Na}]^+$ .  $^1\text{H}$  NMR in  $\text{D}_2\text{O}$  [ $\delta/\text{ppm}$  ( $J/\text{Hz}$ )]: 8.56 (d, 8.5, 1H), 8.47 (d, 8.0, 2H), 8.43 (d, 8.3, 1H), 8.38 (d, 8.0, 2H), 8.23 (d, 7.8, 1H), 8.15 (t, 8.1, 1H), 7.95 (d, 7.8, 2H), 7.91 (d, 5.3, 2H), 7.77 (t, 8.0, 1H), 7.72 (d, 8.0, 1H), 7.31 (d, 6.8, 2H), 6.67 (d, 8.3, 1H).

The crystal was grown by slow evaporation in mixture of acetone and water (1:1).

### Instrumentation

UV/Vis spectroscopy was performed on a Cary 50 (Varian) UV/Vis spectrophotometer in 1 cm quartz cuvettes. Cyclic voltammetry (CV), differential pulse voltammetry (DPV) and square wave voltammetry (SWV) experiments were performed on an IJ-Cambria CHI-660 potentiostat or a Bio-Logic SP-150 potentiostat using a three-electrode cell. Typical CV experiments were carried out at a scan rate of  $100 \text{ mV s}^{-1}$ . DPV experiments were carried out with the parameters: Pulses Height = 50 mV, Pulses Width = 50 ms, Step Height = 4 mV and Step Time = 200 ms; A glassy carbon electrode (3 mm diameter) was used as working electrode, platinum wire as auxiliary electrode, and a SSCE as a reference electrode. Working electrodes were polished with 0.05 micron alumina paste, and rinsed with distilled water and acetone followed by blow-drying before each measurement. All cyclic voltammograms presented in this work were recorded in the absence of light and inside a Faradaic cage. Glassy carbon electrodes were activated following the protocol: a polished GC electrode was immersed in a non-degassed 0.1 M  $\text{H}_2\text{SO}_4$  solution and four cycles of 30 s at 1.8 V (vs. SSCE) immediately followed by 15 s at -0.2 V (vs. SSCE). After the last reductive potential, the electrode was removed from the solution rinsed with distilled water and acetone and dried. The complexes were dissolved either in  $\text{CH}_2\text{Cl}_2$  (DCM) containing the necessary amount of  $(n\text{-Bu})_4\text{NPF}_6$  (TBAH) as supporting electrolyte to yield a 0.1 M ionic strength solution. In aqueous solution the electrochemical experiments were carried out in 0.1 M  $\text{CF}_3\text{SO}_3\text{H}$  (pH 1.0).

For construction of the Pourbaix diagrams, the following buffers were used: dihydrogen phosphate/phosphoric acid up to pH = 4 ( $pK_a = 2.12$ ), hydrogen phosphate/dihydrogen phosphate up to pH = 9 ( $pK_a = 7.67$ ), hydrogen phosphate/sodium phosphate up to pH = 13 ( $pK_a = 12.12$ ) and sodium hydroxide for pH = 14. The concentration of the species was approximately 1 mM.  $E_{1/2}$  values reported in this work were estimated from CV experiments as the average of the oxidative and reductive peak potentials ( $E_{p,a} + E_{p,c}$ )/2 or taken as  $E(I_{max})$  from SWV or DPV measurements. The NMR spectroscopy experiments were performed on a Bruker Avance 400 Ultrashield NMR spectrometer. Samples were run in dichloromethane- $d_2$ , acetonitrile- $d_3$  or  $D_2O$  with internal references (residual protons). Elemental analysis was performed using an EA-1108, CHNS-O elemental analyzer from Fisons Instruments.

### **O<sub>2</sub> Measurements.**

On-line manometric measurements were carried out on a Testo 521 differential pressure manometer with an operating range of 1-100 hPa and accuracy within 0.5 % of the measurement. The manometer was coupled to thermostated reaction vessels for dynamic monitoring of the headspace pressure above each reaction. The manometer's secondary ports were connected to thermostated reaction vessels containing the same solvents and headspace volumes as the sample vials. Composition of the gaseous phase was determined by online mass-spectrometry with an OmniStar GSD 301 C (Pfeiffer) quadrupole mass-spectrometer.

Reaction order in catalyst has been obtained from initial rates method applied to manometric oxygen evolution plots. No more than 5% of total reaction time has been used for linear least square regression. One advantage of this method is that it avoids any complications arising from product inhibition or

from subsequent reactions. All experiments have been done at least by duplicate.

### **Kinetics.**

For determining the order of catalyst (Ru) we recorded manometric data oxygen evolution vs. time obtained at the initial stages of the reaction adding 100 mM Ce(IV) oxidant to catalysts solutions containing 0.34 to 1.0 mM of catalyst. Reaction order in catalyst was determined by plotting initial rates ( $v_i$ ) vs. [Ru]. All experiments were carried out in 0.1 M aqueous triflic acid solution at 298 K with a total volume of 2 mL.

For determining the order of Ce<sup>IV</sup> we followed the previously described procedure adding Ce<sup>IV</sup> solutions in the range 25 to 100 mM to a 1mM Catalyst solution. Reaction order in Cerium was determined by plotting initial rates ( $v_i$ ) vs. [Ce<sup>IV</sup>]<sup>2</sup>. All experiments were carried out in 0.1 M aqueous triflic acid solution at 298 K with a total volume of 2 mL.

### **X-Ray Crystal Structure Determination.**

Crystals of **5**<sup>2+</sup> and **6**<sup>2+</sup> were grown by slow evaporation in mixture of acetone and water (1:1). The measured crystal was prepared under inert conditions immersed in perfluoropolyether as protecting oil for manipulation.

**Data collection:** Crystal structure determination was carried out using a Apex DUO Kappa 4-axis goniometer equipped with an APPEX 2 4K CCD area detector, a Microfocus Source E025 IuS using MoK<sub>α</sub> radiation, Quazar MX multilayer Optics as monochromator and an Oxford Cryosystems low temperature device Cryostream 700 plus ( $T = -173$  °C). Full-sphere data collection was used with  $\omega$  and  $\varphi$  scans. *Programs used:* Data collection APEX-2<sup>4</sup>, data reduction Bruker Saint<sup>5</sup> V/.60A.

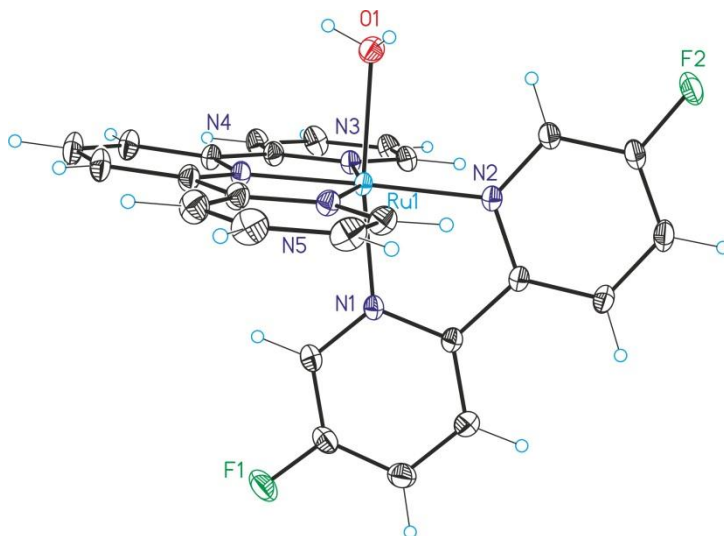
**Structure Solution and Refinement:** Crystal structure solution was achieved using direct methods as implemented in SHELXTL<sup>6</sup> and visualized using the program XP. Missing atoms were subsequently located from difference Fourier synthesis and added to the atom list. Least-squares refinement on  $F^2$  using all measured intensities was carried out using the program SHELXTL. All non hydrogen atoms were refined including anisotropic displacement parameters.

(4) Data collection with APEX II version v2009.1-02. Bruker **2007**. Bruker AXS Inc., Madison, Wisconsin, USA.

(5) Data reduction with Bruker SAINT version V7.60A. Bruker **2007**. Bruker AXS Inc., Madison, Wisconsin, USA.

(6) Sheldrick, G.M. *Acta Cryst.* **2008** A64, 112-122. SHELXTL version V6.14.

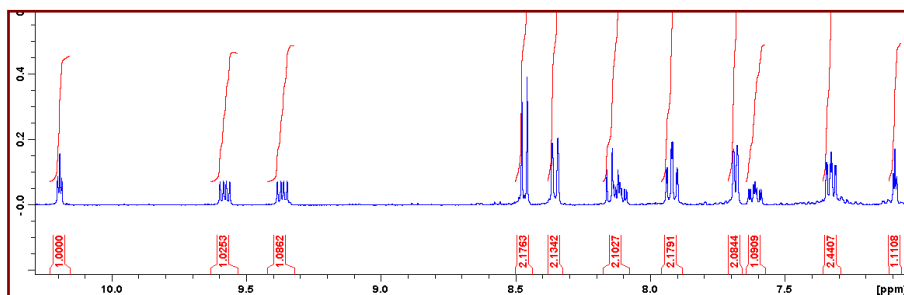
**Figure S 1.** Ortep plot (50 % probability) of the crystal structure of the complex  $5^{2+}$ .  
Color codes: Ru, cyan; N, navy blue; F, green; O, red; H, blue empty circles.



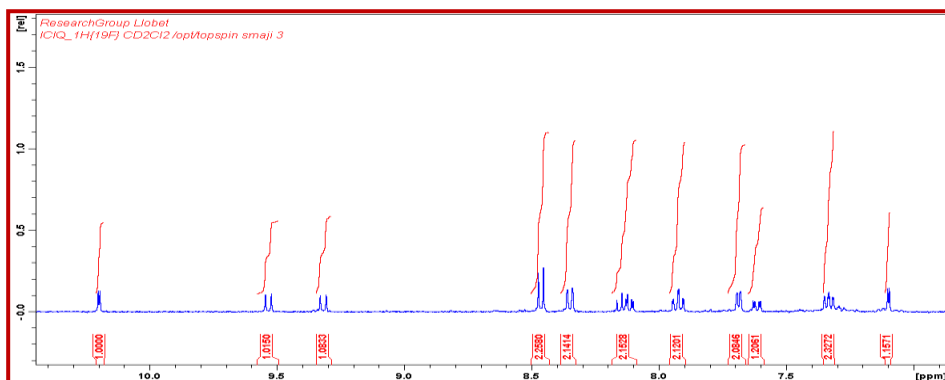
## NMR Characterization.

**Figure S 2.** 1D and 2D NMR spectra (400 MHz, 298 K, in dichloromethane- $d_2$ ) for complex  $3^+$ : (a)  $^1\text{H}$ -NMR, (b)  $\{^1\text{H}-^{19}\text{F}\}$ -NMR, (c) COSY, (d) NOESY, (e) HSQC, (f) HMQC, (g)  $\{^{19}\text{F}-^1\text{H}\}$  (h) DEPT, (i)  $\{^{13}\text{C}-^1\text{H}\}$ .

(a)  $^1\text{H}$ NMR in  $\text{CD}_2\text{Cl}_2$ :

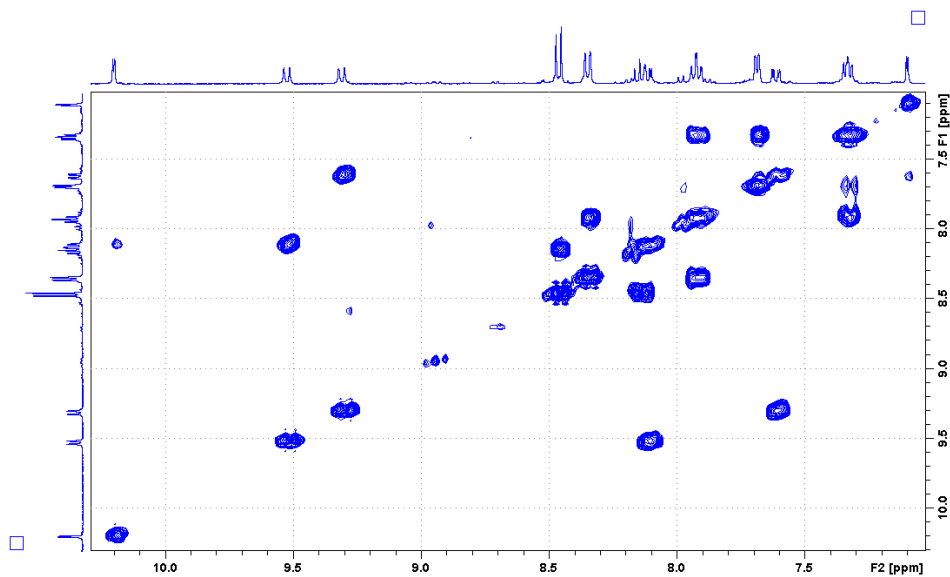


(b)  $\{^1\text{H}-^{19}\text{F}\}$  NMR in  $\text{CD}_2\text{Cl}_2$ :

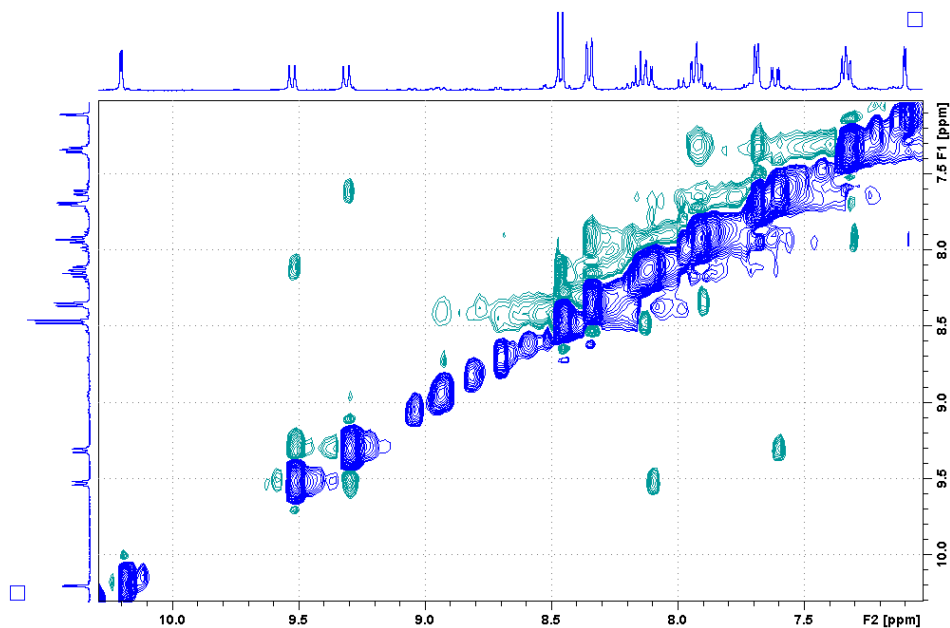




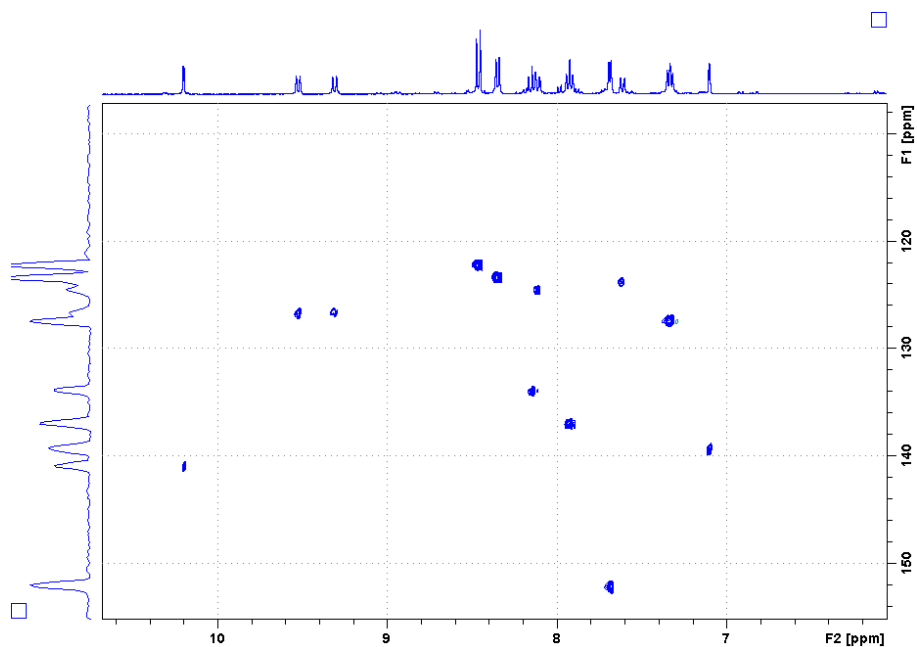
(c) COSY



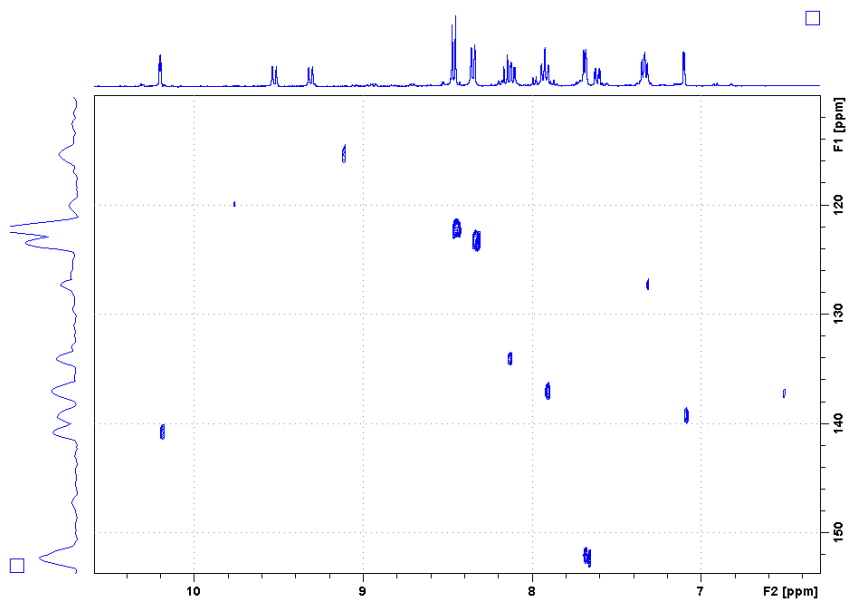
(d) NOESY



(e) HSQC

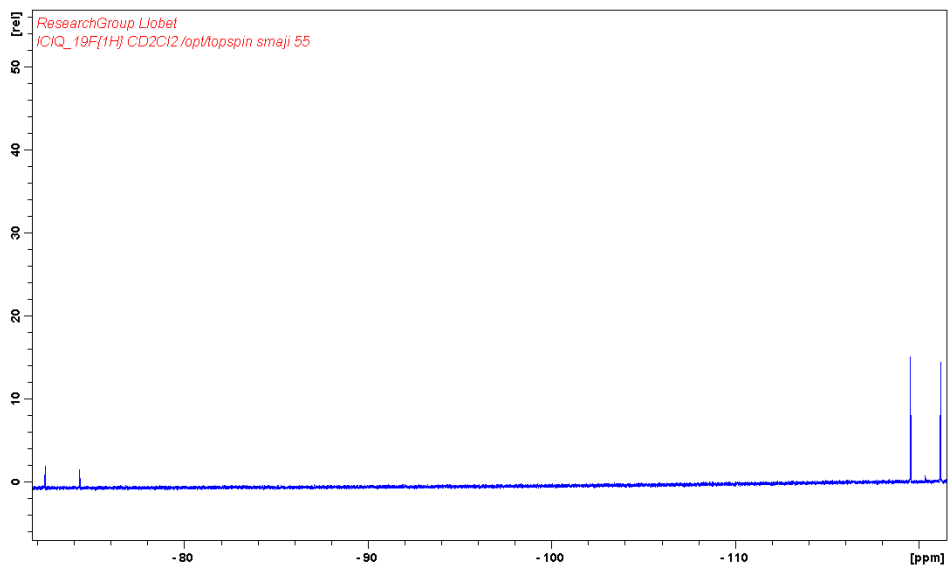


(f) HMQC

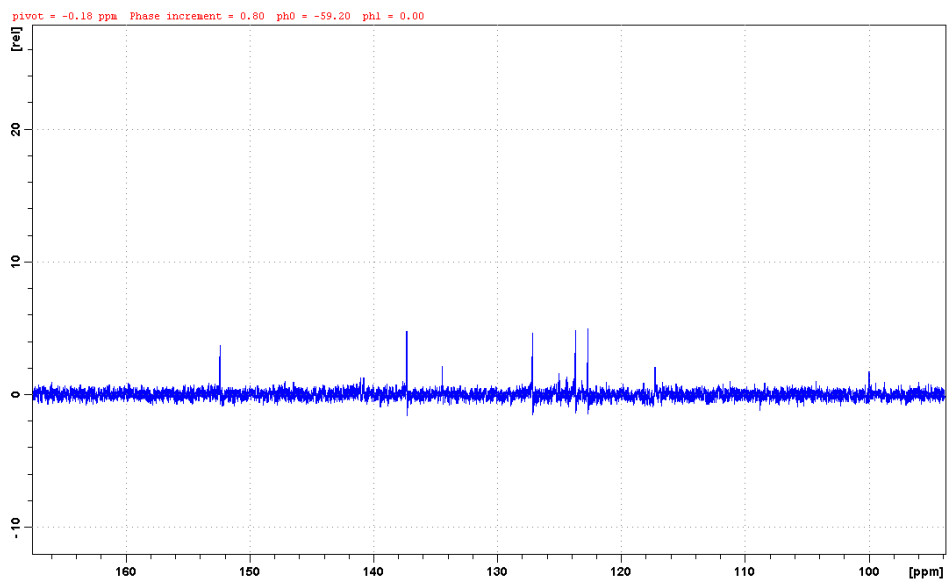


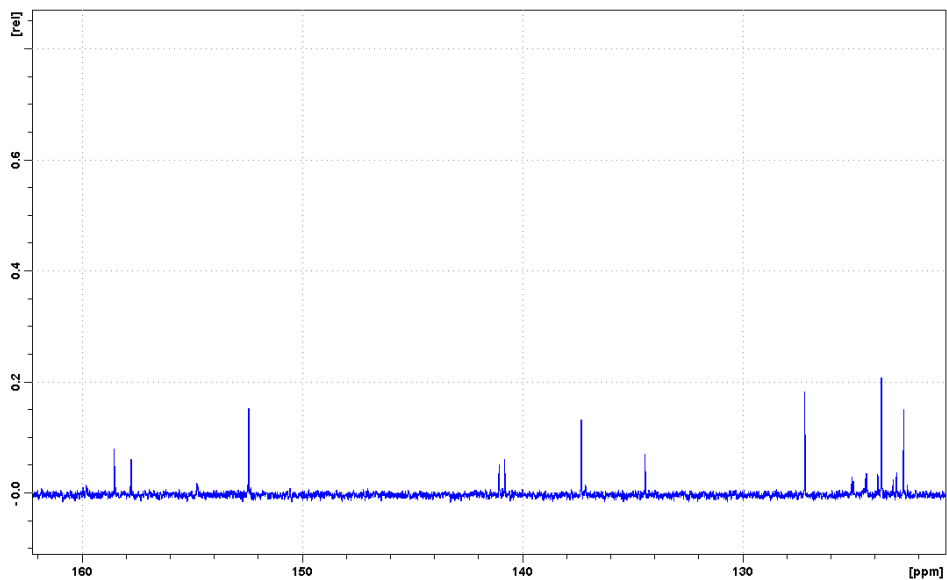
IV

(g)  $\{^{19}\text{F}-^1\text{H}\}$



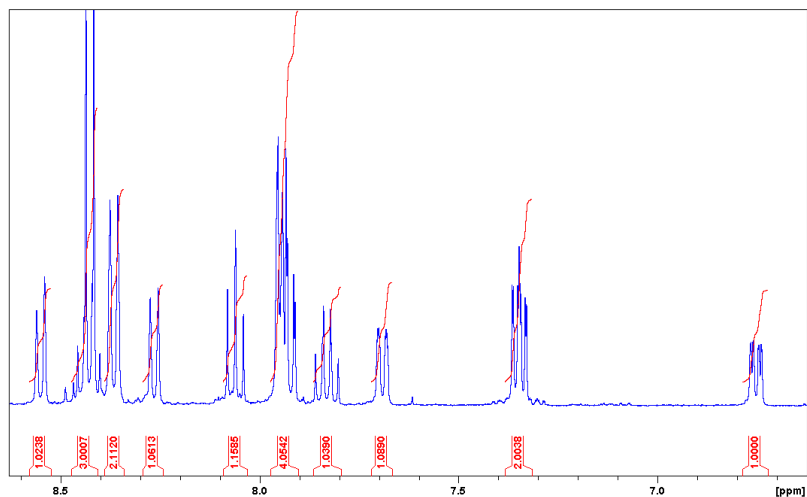
(h) DEPT



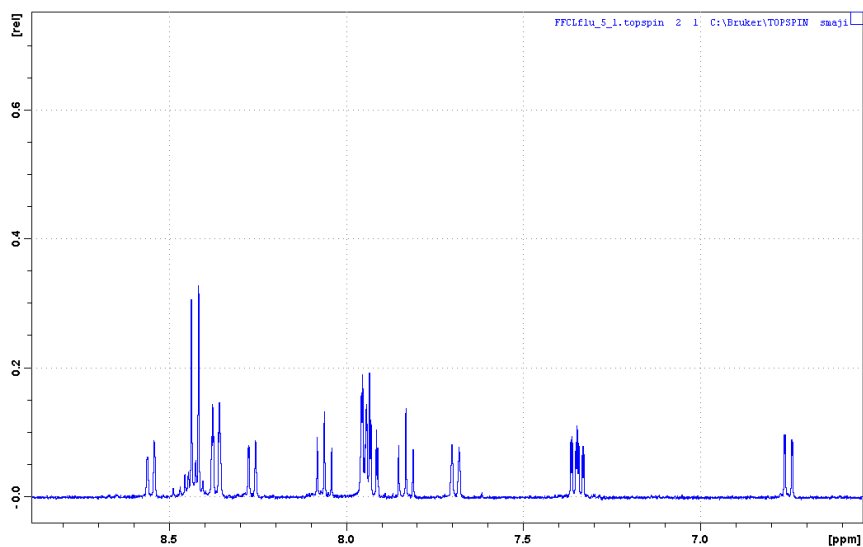
(i)  $\{^{13}\text{C}-^1\text{H}\}$ 

**Figure S 3.** 1D and 2D NMR spectra (400 MHz, 298 K, in  $\text{CD}_3\text{CN}$ ) for complex  $4^+$ : (a)  $^1\text{H}$ -NMR, (b)  $\{^1\text{H}-^{19}\text{F}\}$ -NMR, (c) COSY, (d) NOESY, (e) HMBC, (f) HSQC, (g)  $\{^{19}\text{F}-^1\text{H}\}$  (h) DEPT, (i)  $\{^{13}\text{C}-^1\text{H}\}$ , (j)  $\{^{19}\text{F}-^1\text{H}\}$  HOESY.

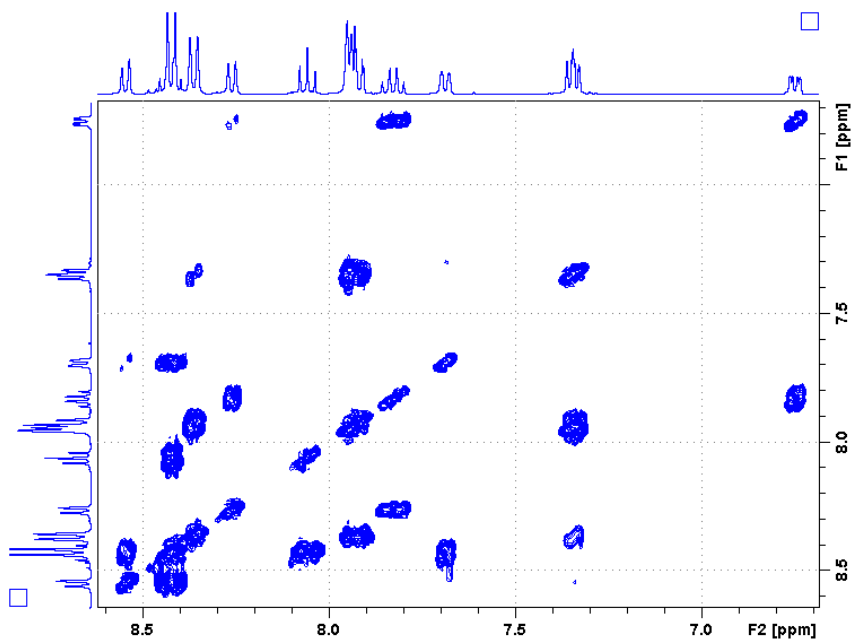
(a)  $^1\text{H}$ -NMR in  $\text{CD}_3\text{CN}$ :



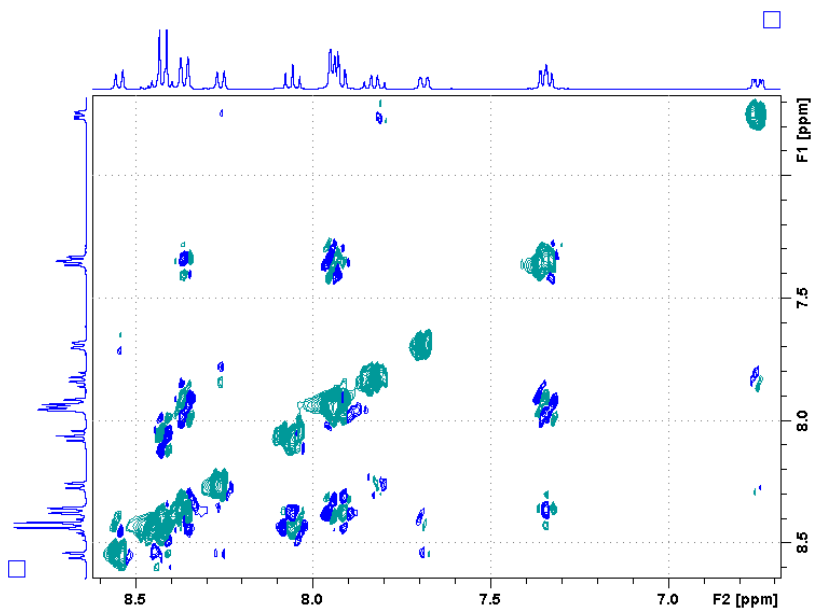
(b)  $\{^1\text{H}-^{19}\text{F}\}$ -NMR



(c) COSY

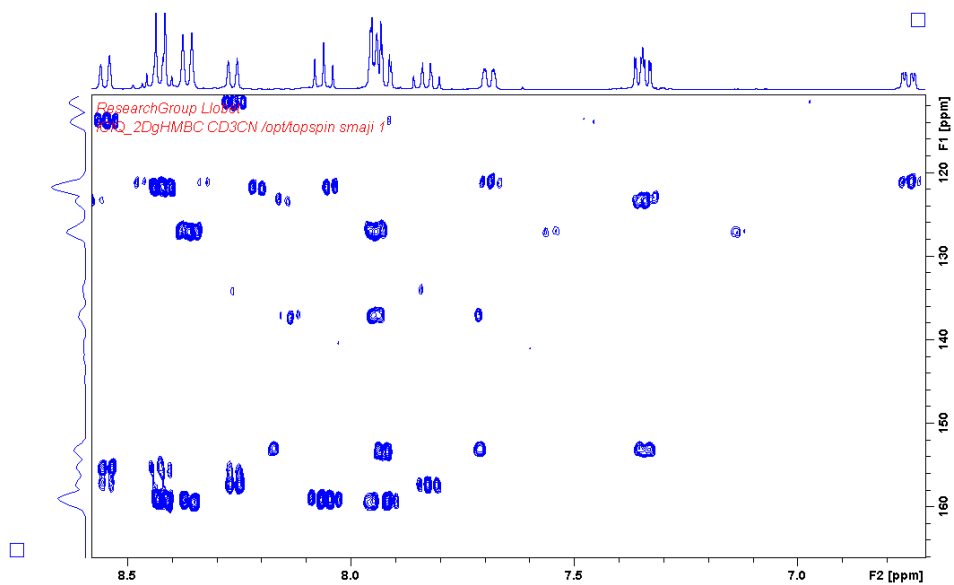


(d) NOESY

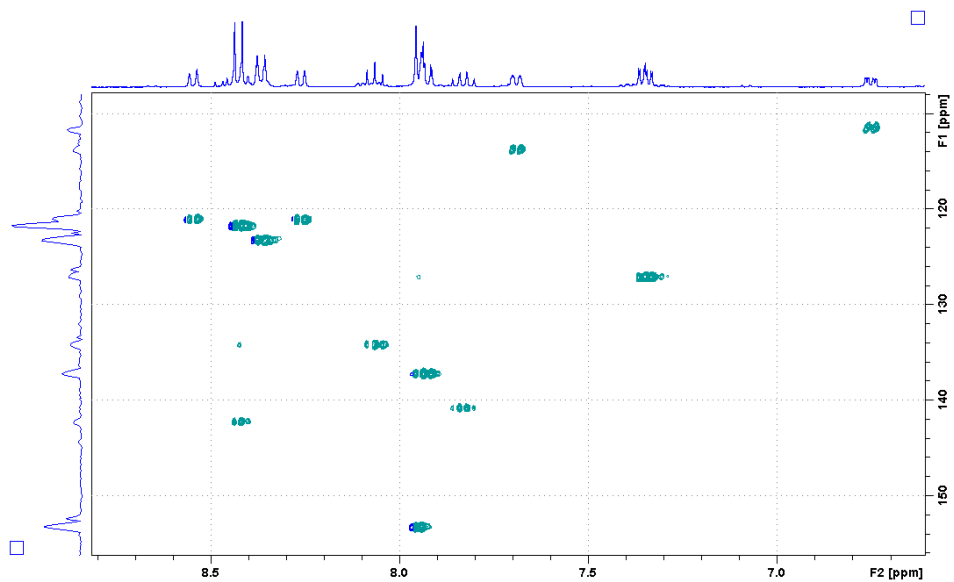


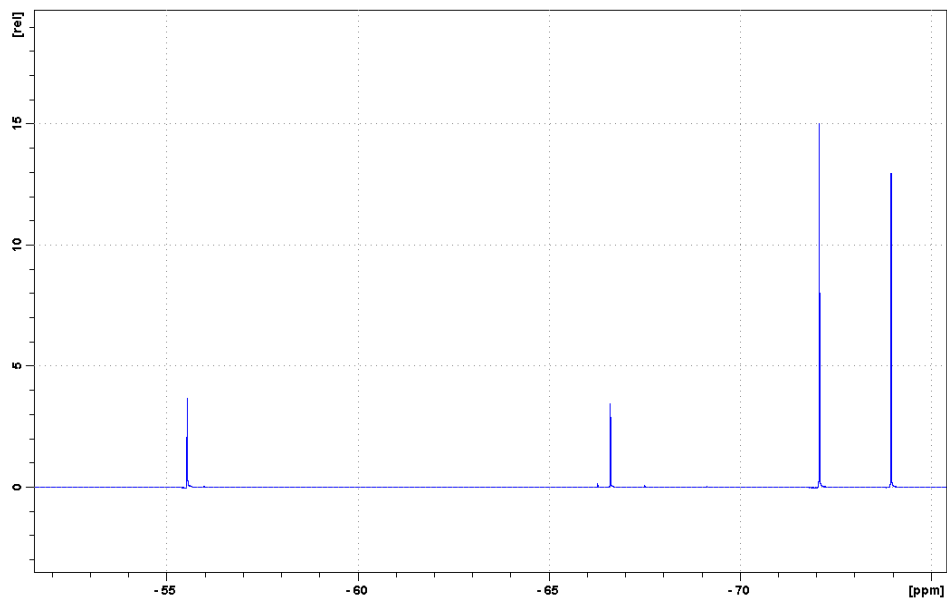
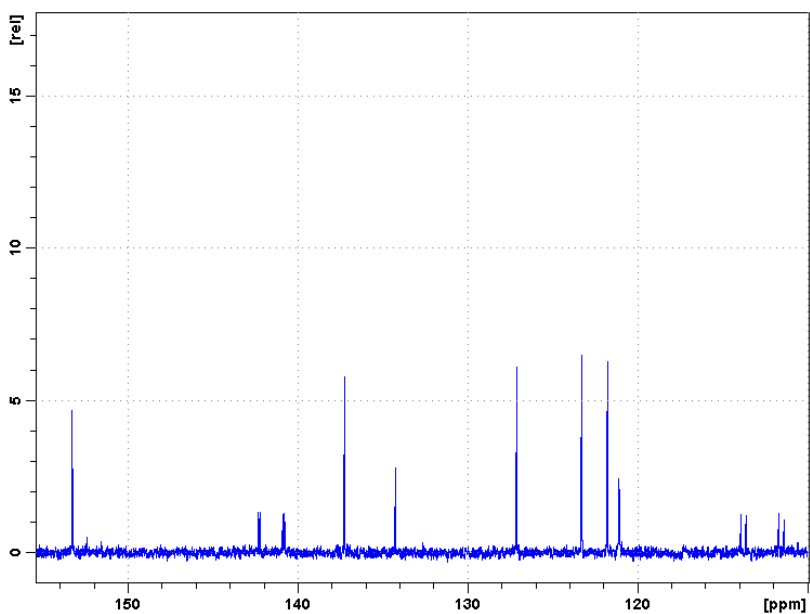
IV

(e) HMBC



(f) HSQC

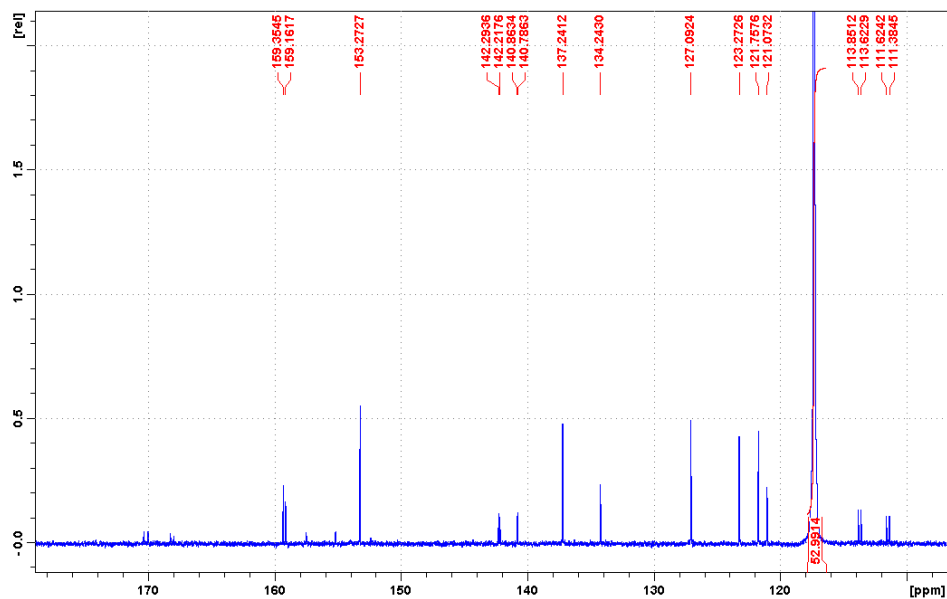


**(g)**  $\{^{19}\text{F}-^1\text{H}\}$ **(h)** DEPT

IV



(i)  $\{^{13}\text{C}-^1\text{H}\}$



(j)  $\{^{19}\text{F}-^1\text{H}\}$  HOESY

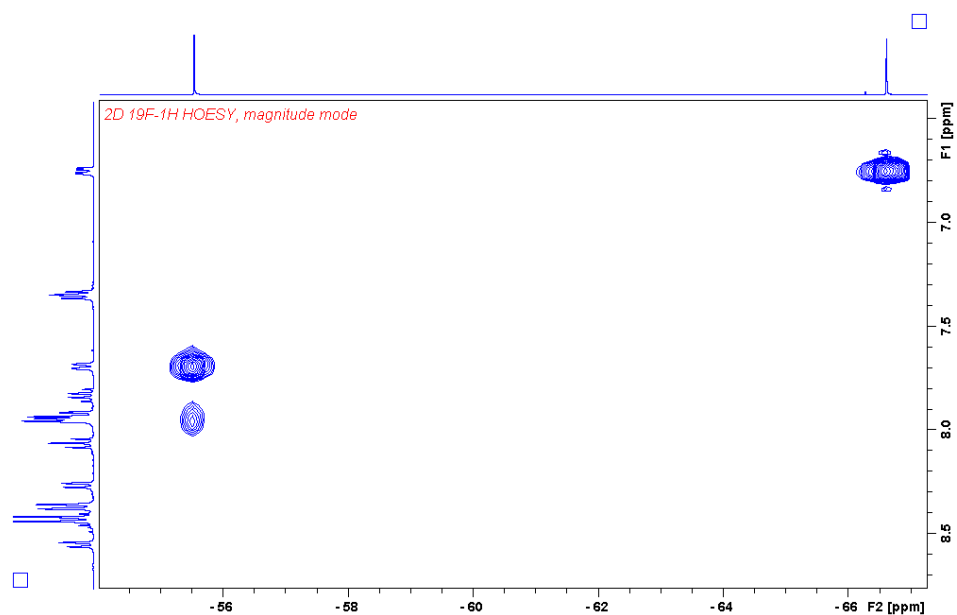
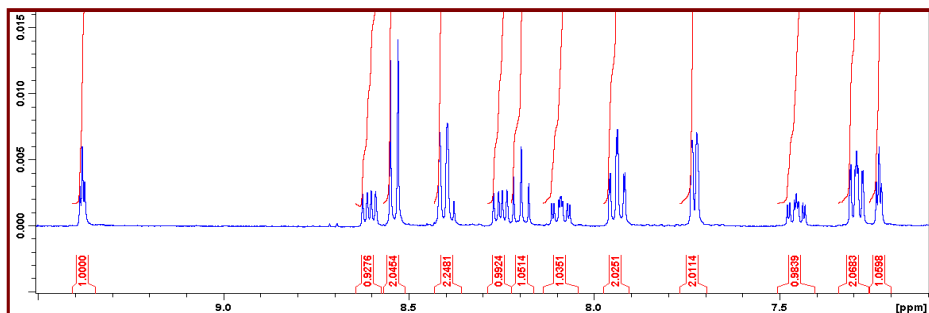
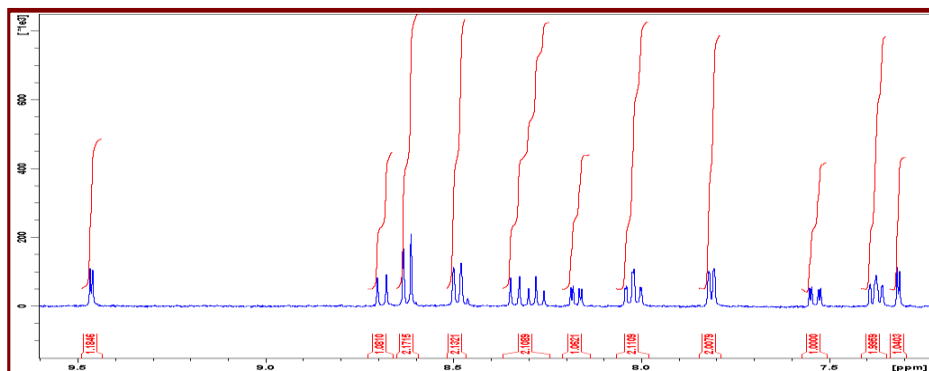


**Figure S 4.** 1D NMR spectra (400 MHz, 298 K, in D<sub>2</sub>O) for complex **5**<sup>2+</sup>: (a) <sup>1</sup>H-NMR, (b) {<sup>1</sup>H-<sup>19</sup>F}-NMR.

(a) <sup>1</sup>H-NMR in D<sub>2</sub>O



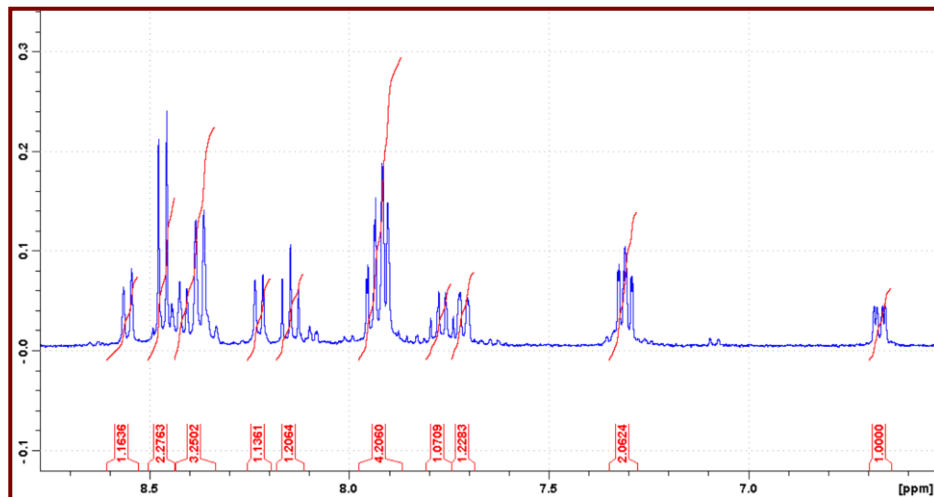
(b) {<sup>1</sup>H-<sup>19</sup>F}-NMR in D<sub>2</sub>O



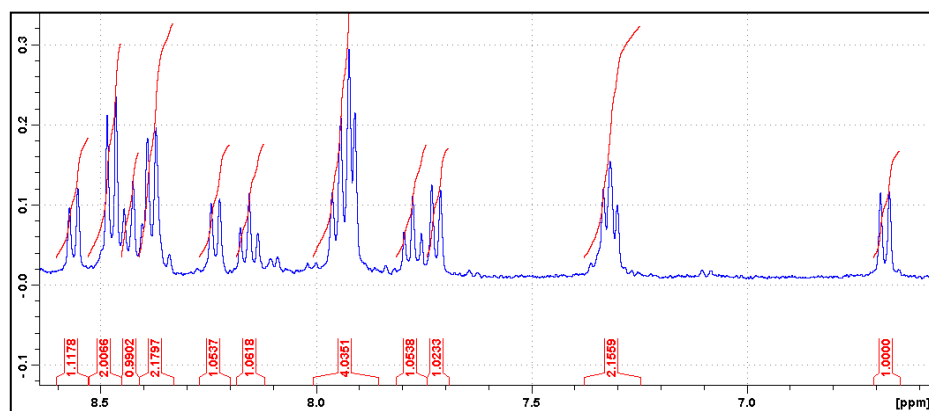
IV

**Figure S 5.** 1D NMR spectra (400 MHz, 298 K, in D<sub>2</sub>O) for complex **6<sup>2+</sup>**: (a) <sup>1</sup>H-NMR, (b) {<sup>1</sup>H-<sup>19</sup>F}-NMR.

(a) <sup>1</sup>H-NMR in D<sub>2</sub>O

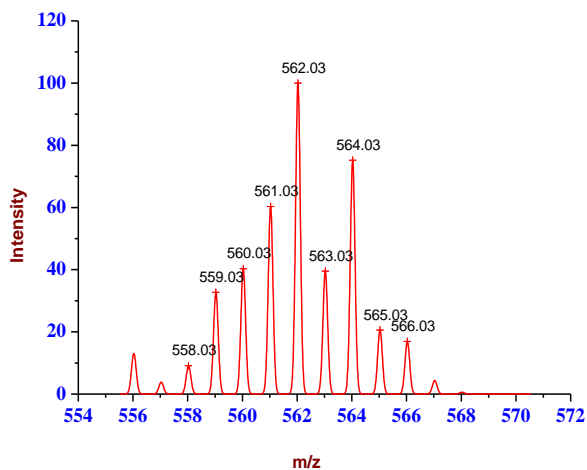
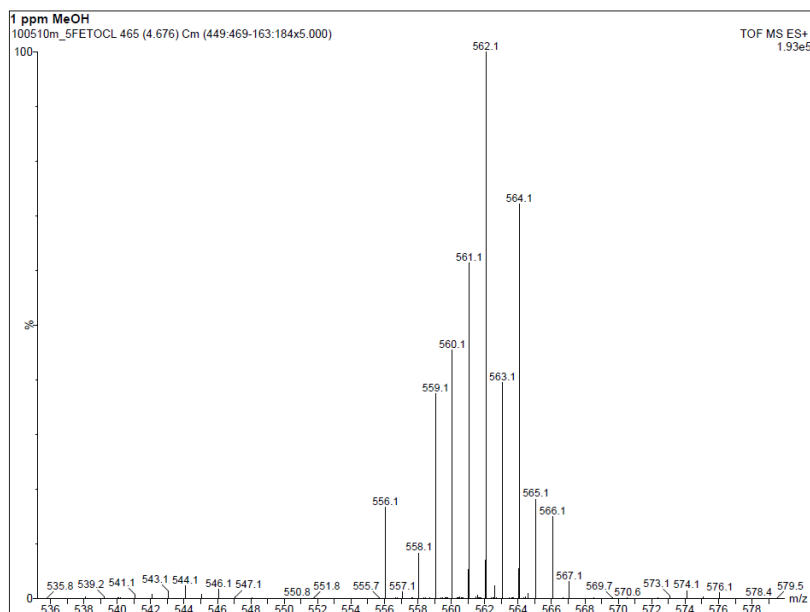


(b) {<sup>1</sup>H-<sup>19</sup>F}-NMR in D<sub>2</sub>O



## 1. MS Characterization.

**Figure S 6.** Experimental (top) and simulated (bottom) Mass Spectrum for complex **3<sup>+</sup>** in methanol.



IV

**Figure S 7.** Experimental (top) and simulated (bottom) Mass Spectrum for complex  $4^+$  in acetonitrile.

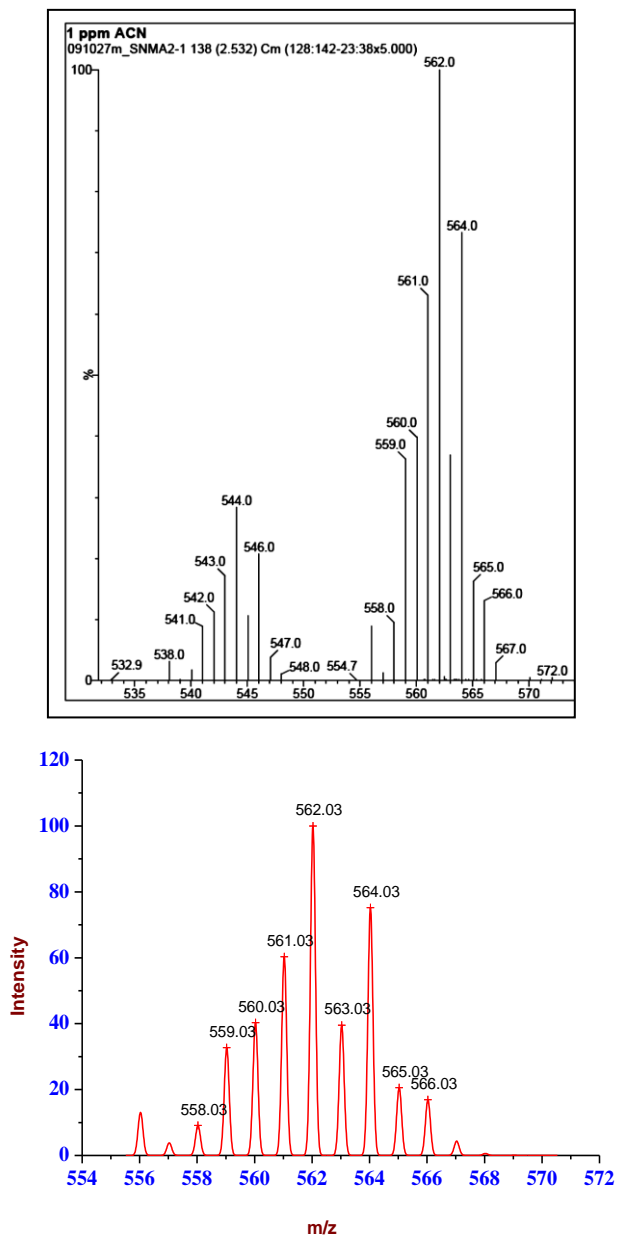
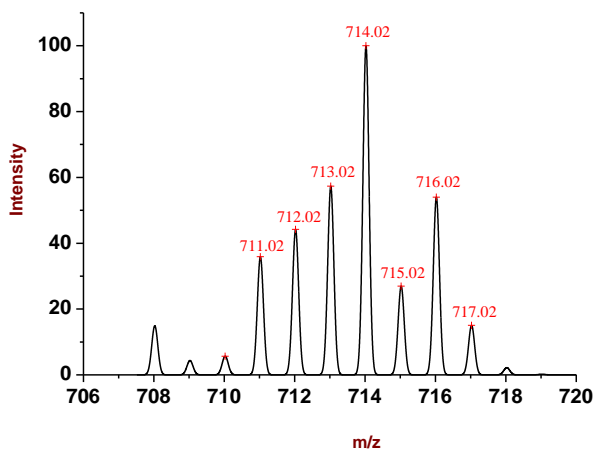
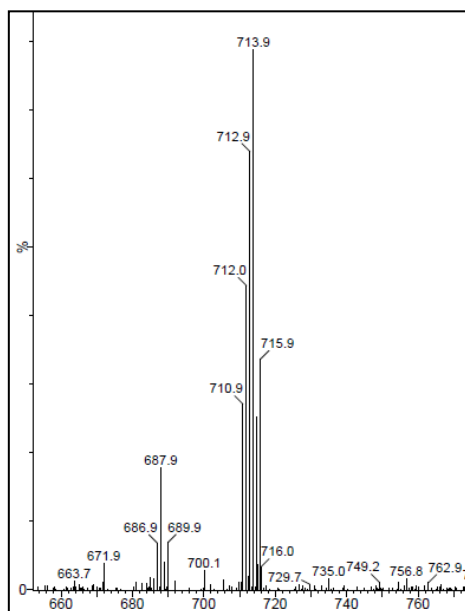
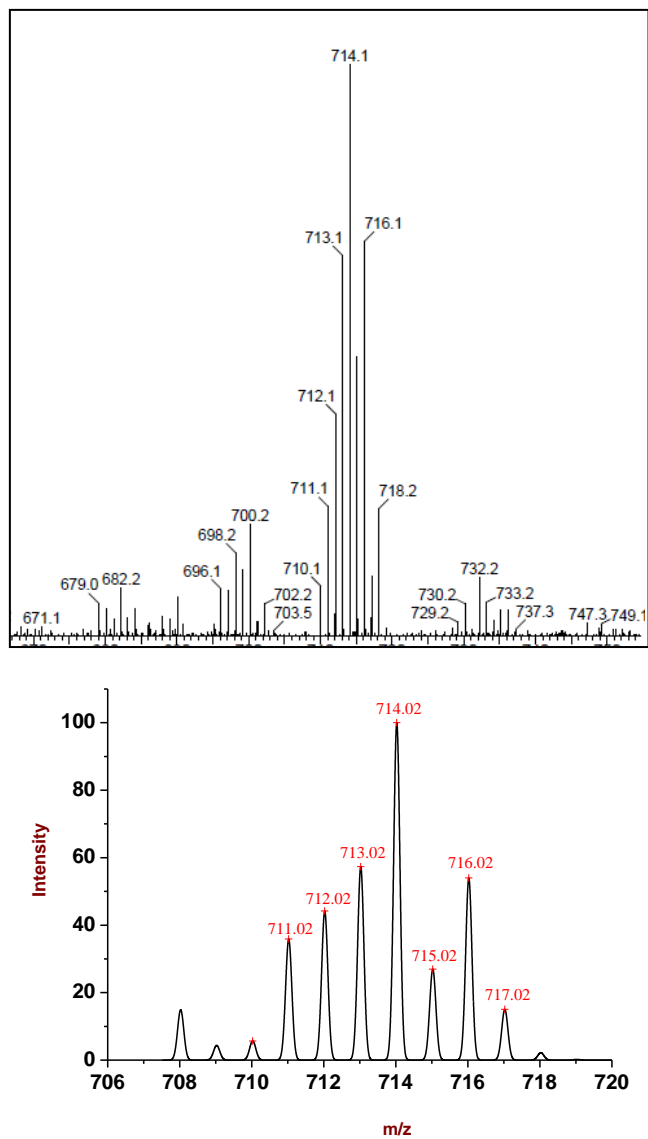


**Figure S 8.** Experimental (top) and simulated (bottom) Mass Spectrum for complex  $5^{2+}$  in water.



IV

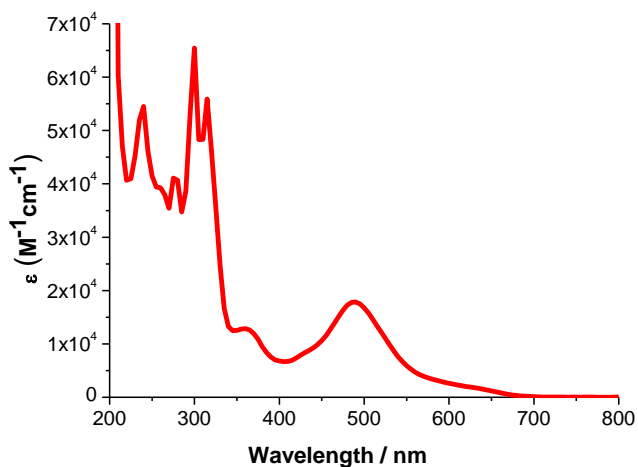
**Figure S 9.** Experimental (top) and simulated (bottom) Mass Spectrum for complex  $5^{2+}$  in water.



## UV-vis Characterization.

**Figure S 10.** UV-vis Spectra in  $\text{CH}_3\text{CN}$  (a)  $3^+$ , (b)  $4^+$ .

(a)



(b)

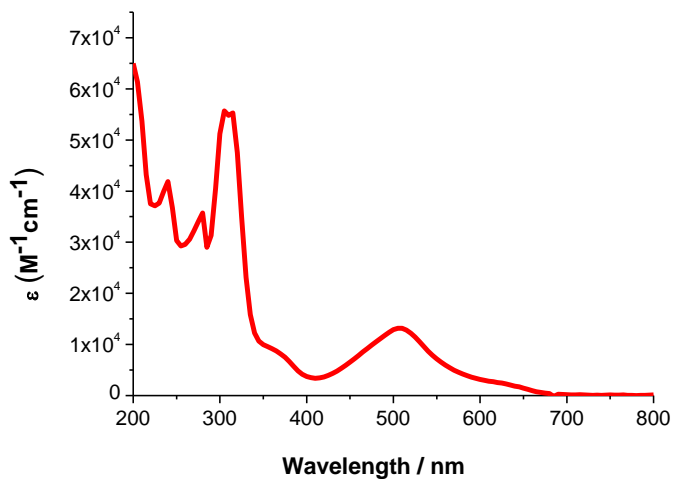
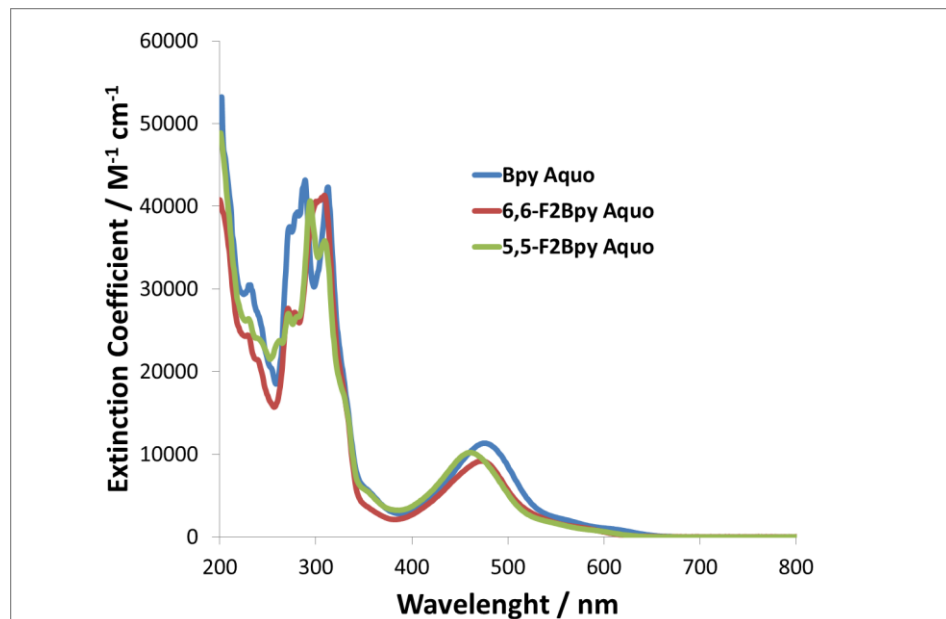




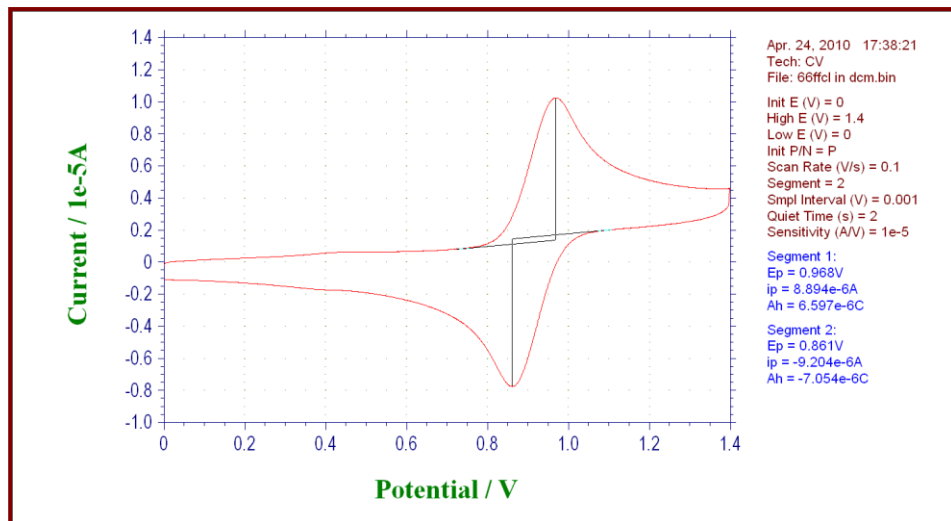
**Figure S 11.** UV-vis spectra of complexes  $2^{2+}$  (blue),  $5^{2+}$  (green) and  $6^{2+}$  (red) in 0.1 M triflic acid.



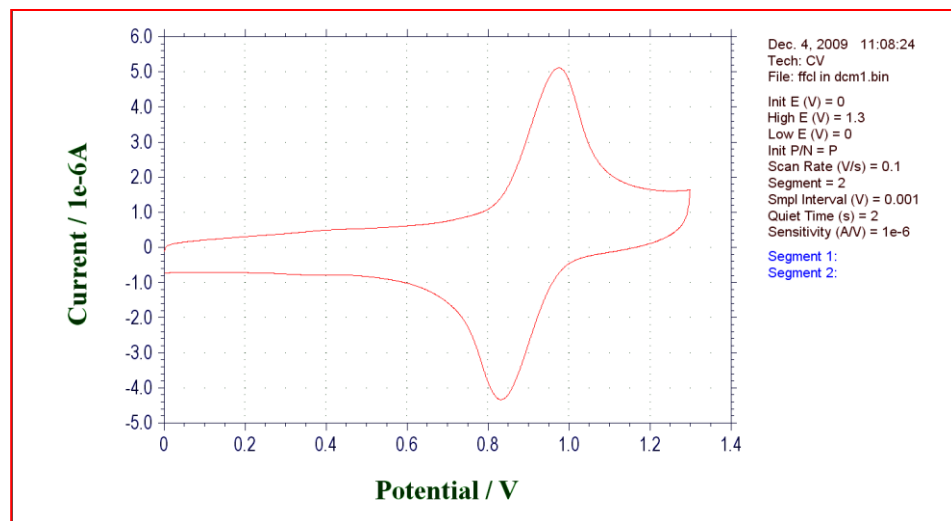
## Electrochemistry.

**Figure S 12.** Cyclic voltammogram in DCM (0.1 M TBAH) (a)  $3^+$ , (b)  $4^+$ .

(a)

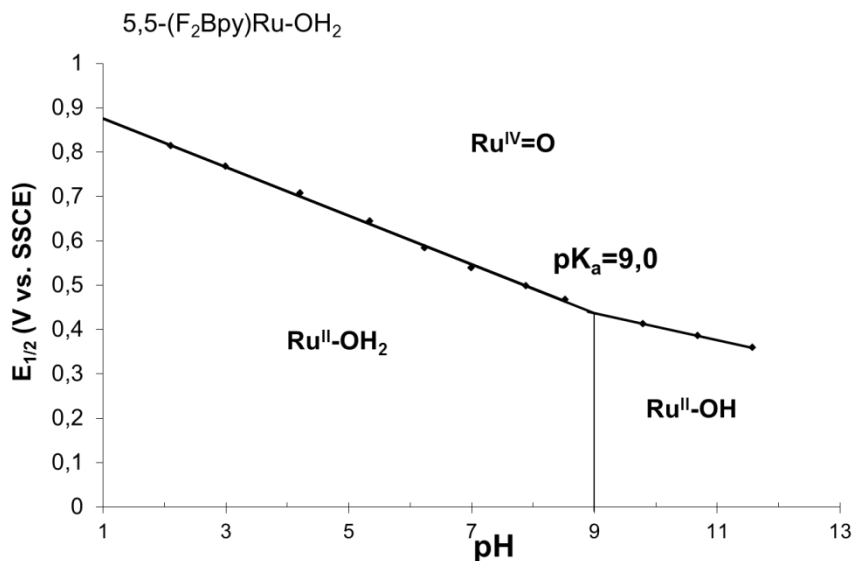


(b)



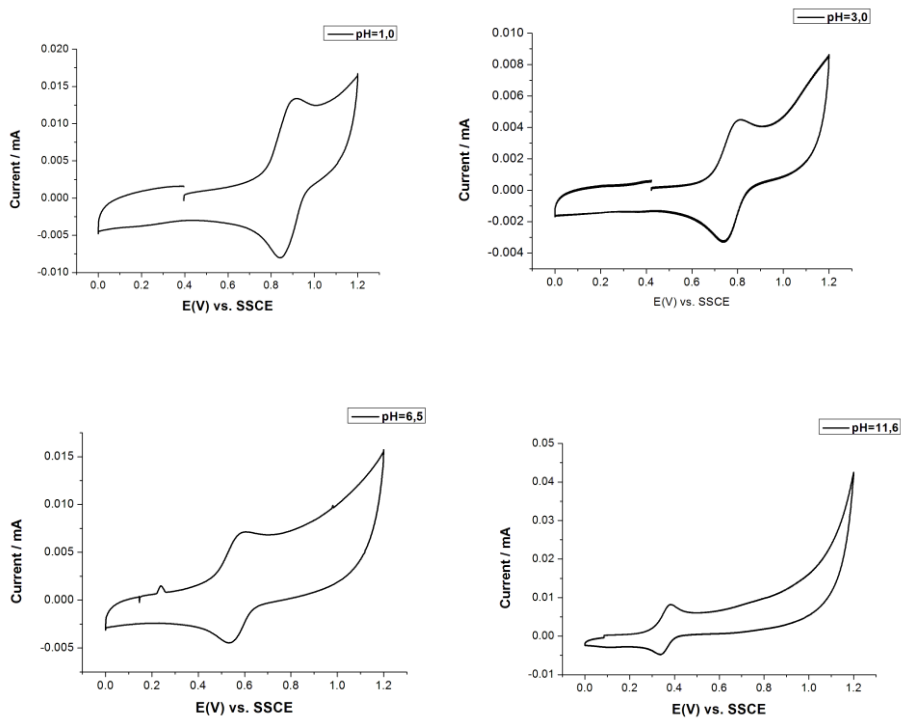
IV

**Figure S 13.** Pourbaix Diagram for complex  $5^{2+}$ . The diagram was built by CV experiments in aqueous solution at different pH ( $I = 0.1$  M, glassy carbon working electrode, standard potentials vs. SSCE reference).



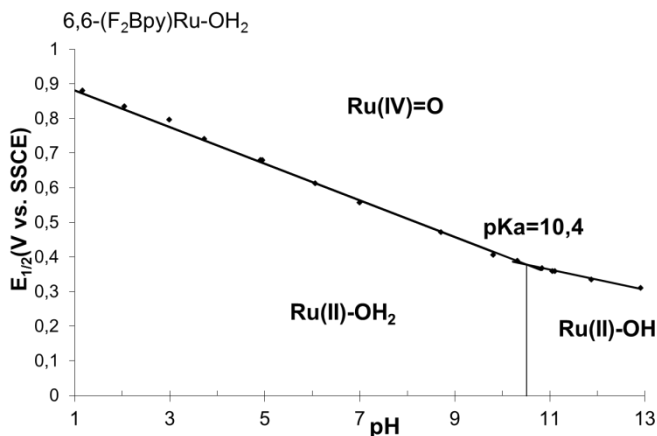
From pH=1.0 to  $pK_a$  the slope is 55 mV per pH unit very close to the expected value (59 mV per pH) for a  $2H^+/2e^-$  process. After  $Ru^{II}-OH_2$  deprotonation at pH=9.0 the slope changes to 30 mV per pH unit which is approximately the expected value for a  $1H^+/2e^-$  process.

**Figure S 14.** CVs of complex  $5^{2+}$  at different pHs. 0.2 mM complex concentration. Glassy carbon working electrode, Pt wire counter electrode and SSCE reference electrode. Scan rate=100  $\text{mV s}^{-1}$ .



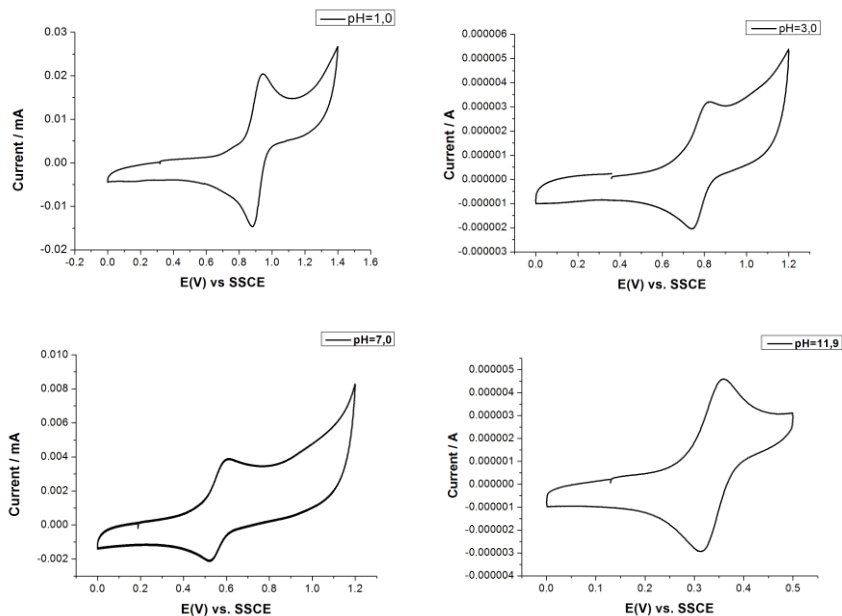
IV

**Figure S 15.** Pourbaix Diagram for complex  $6^{2+}$ . The diagram was built by CV experiments in aqueous solution at different pH ( $I = 0.1$  M, glassy carbon working electrode, standard potentials vs. SSCE reference).



From pH=1.0 to  $pK_a$  the slope is 53 mV per pH unit very close to the expected value (59 mV per pH) for a  $2H^+/2e^-$  process. After  $Ru^{II}-OH_2$  deprotonation at pH=10.4 the slope changes to 29mV per pH unit indicating a  $1H^+/2e^-$  process.

**Figure S 16.** Cyclic Voltammograms of complex  $6^{2+}$  at different pHs. 0.2 mM complex concentration. Glassy carbon working electrode, Pt wire counter electrode and SSCE reference electrode. Scan rate=100 mV s<sup>-1</sup>.



IV

**Figure S 17.** Differential Pulse Voltammograms of 0.5 mM solutions in 0.1 M  $\text{CF}_3\text{SO}_3\text{H}$  ( $\text{pH} = 1.0$ ) for complexes  $2^{2+}$  (black),  $5^{2+}$  (blue) and  $6^{2+}$  (red). Glassy carbon working electrode, Pt wire counter electrode and SSCE reference electrode. Scan rate =  $20 \text{ mV s}^{-1}$  (Pulses Height = 50 mV, Pulses Width = 50 ms, Step Height = 4 mV and Step Time = 200 ms).

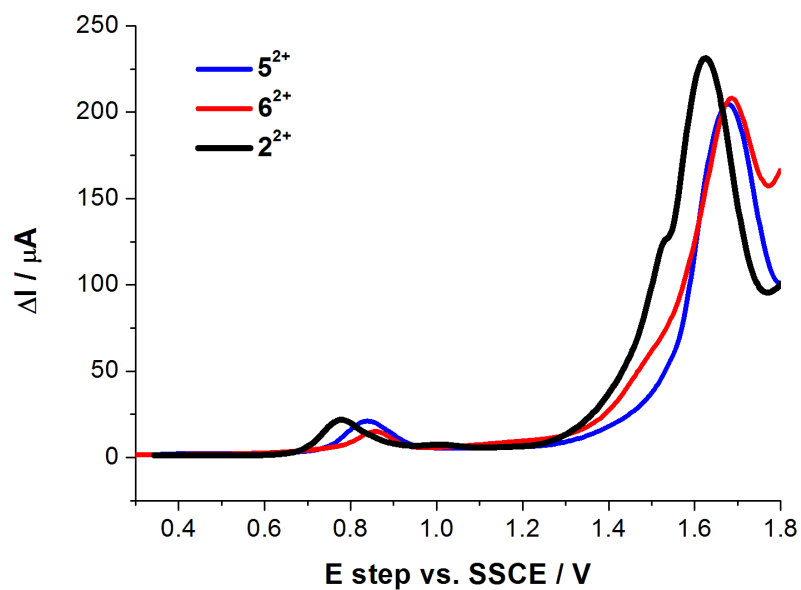
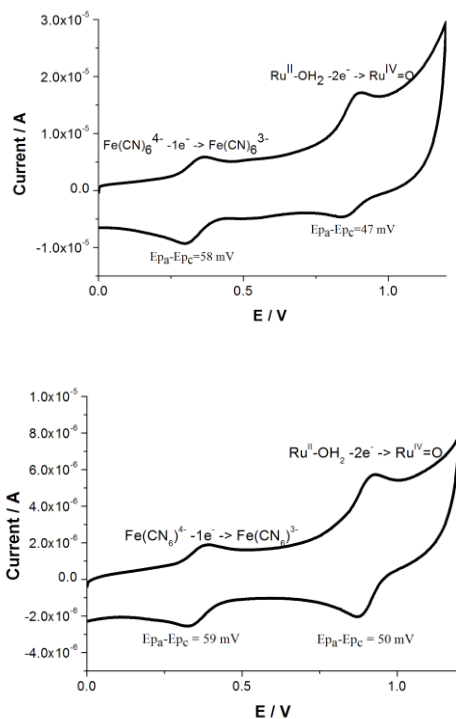


**Figure S 18.** Upper, CV of 0.2 mM  $\text{K}_4\text{Fe}(\text{CN})_6 \cdot 3\text{H}_2\text{O}$  and 0.2 mM  $5^{2+}$  (scan rate = 500 mV  $\text{s}^{-1}$ ). Bottom, CV of 0.2 mM  $6^{2+}$  (scan rate = 100 mV  $\text{s}^{-1}$ ). Both at pH = 1.0 (0.1 M  $\text{CF}_3\text{SO}_3\text{H}$ ) using a glassy carbon working electrode, Pt counter electrode and SSCE as reference electrode. The comparison of the areas under the anodic waves gives a 1:2 ratio which is indicative of 2  $e^-$  process for  $5^{2+}$  and  $6^{2+}$ .



IV



**Figure S 19.** CV of a 0.5 mM solution of  $5^{2+}$  at pH = 1.0 (0.1 M HOTf) using an activated glassy carbon electrode, Pt counter electrode and SSCE reference electrode. Scan rate =  $100 \text{ mV s}^{-1}$ . The peak to peak separation is 40 mV which is a further indication of a  $2e^-$  process.

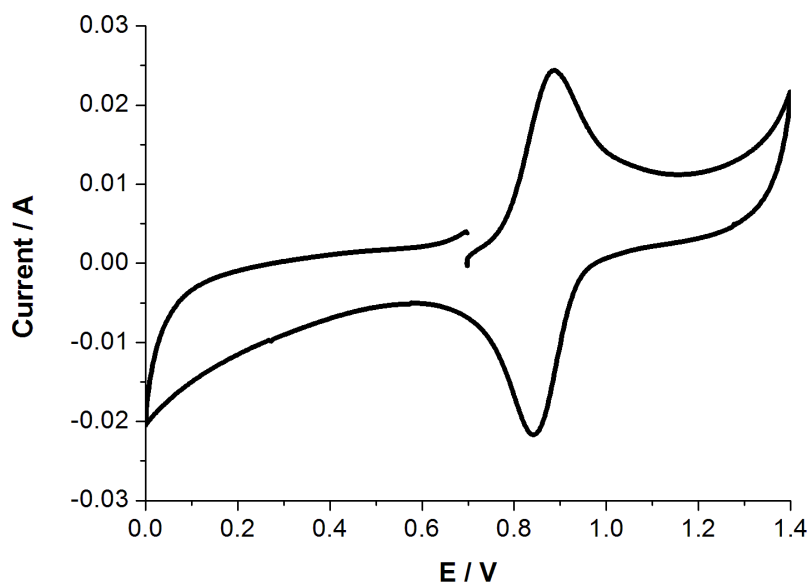
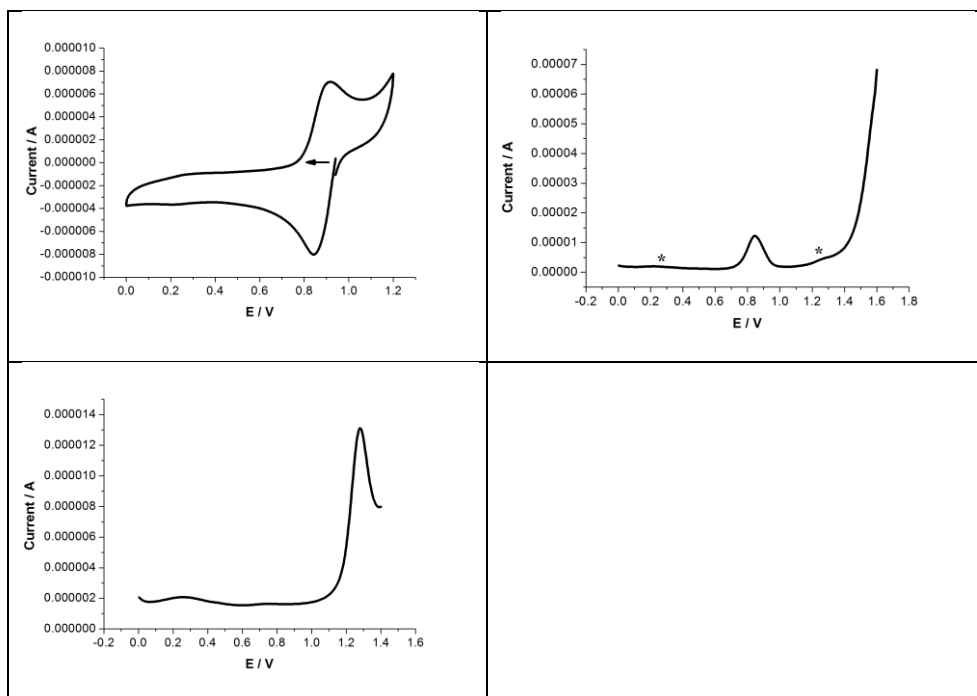


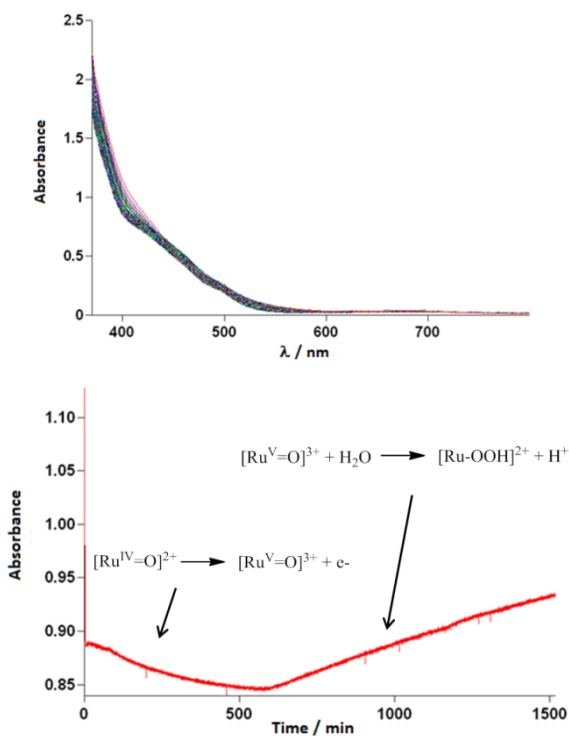
**Figure S 20.** Top left, CV and DPV (20 mV s<sup>-1</sup> scan rate), top right, of the reaction of 3 equivalents of (NH<sub>4</sub>)<sub>2</sub>Ce(NO<sub>3</sub>)<sub>6</sub> with a 0.5 mM solution of 5<sup>2+</sup> in 0.1 M HOTf after 4 days. Polished glassy carbon working electrode, Pt counter electrode and SSCE reference electrode. Scan rate = 100 mV s<sup>-1</sup>. The asterisks correspond to Ce. Bottom, DPV of a 30 mM solution of Ce(IV).



IV

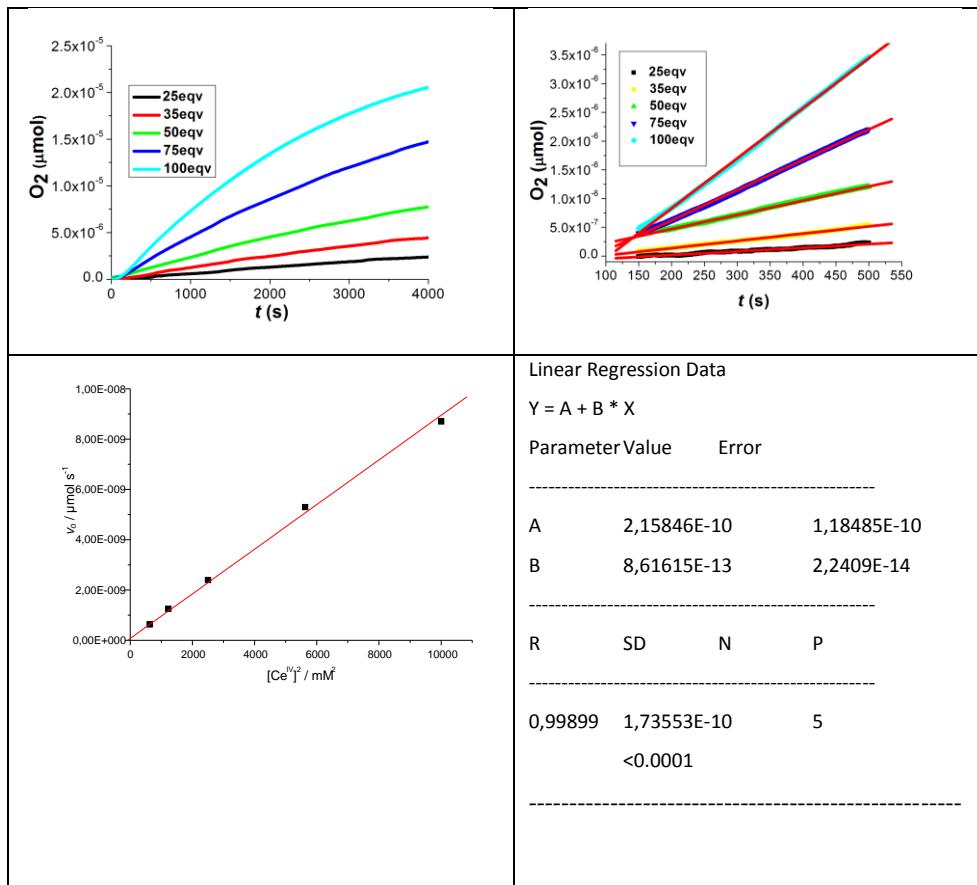
**Figure S 21.** Upper, UV-vis monitoring of the reaction of 3 equivalents of  $(\text{NH}_4)_2\text{Ce}(\text{NO}_3)_6$  with a 0.5 mM solution of  $5^{2+}$  in 0.1 M HOTf at 20 °C. A cuvette with an optical path length of 2 mm was used. Bottom, plot of absorbance vs. time at 403 nm.

The UV-vis monitoring of the reaction of 3 equivalents of CAN with  $5^{2+}$  shows a slow formation of a  $[\text{Ru}-\text{OOH}]^{2+}$  intermediate as in previously reported cases (*J. Am. Chem. Soc.* **2010**, *132*, 1545 and *J. Am. Chem. Soc.* **2010**, *132*, 16094). However in our case we could not see it neither by CV nor by DPV, as shown in Figure S 20.



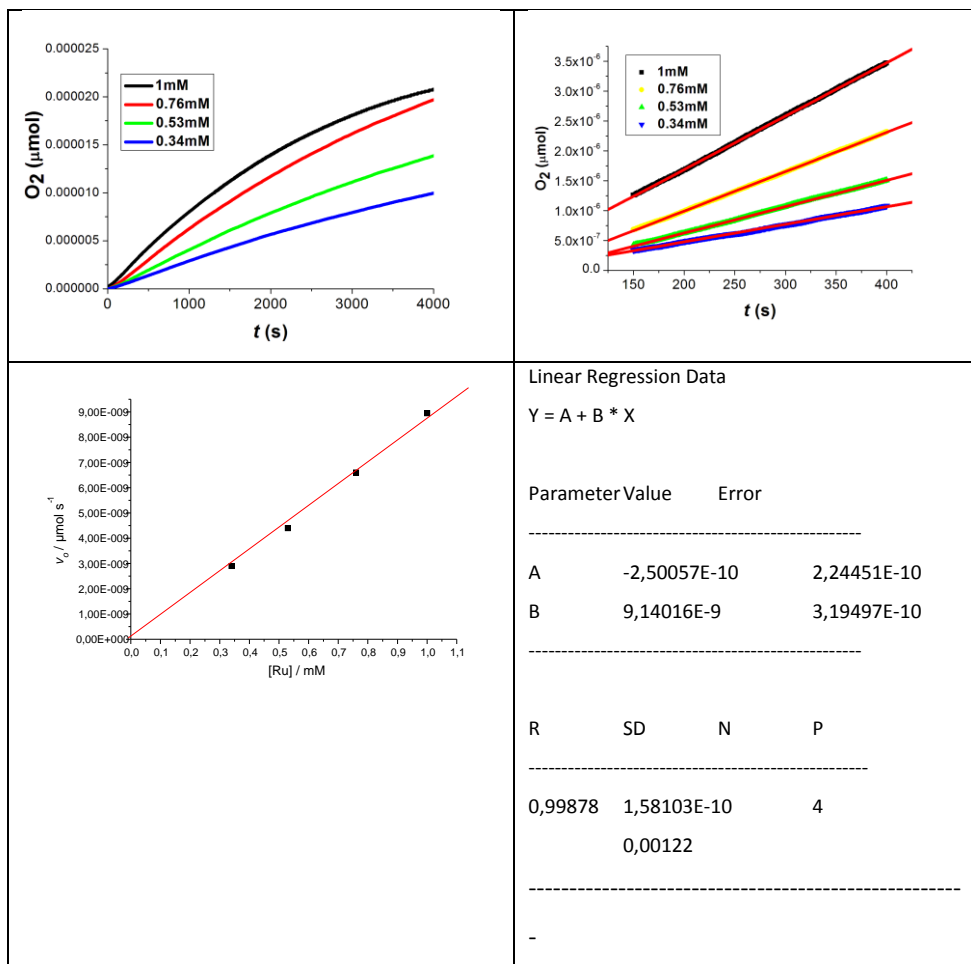
### Kinetics.

**Figure S 22.** Top left, O<sub>2</sub> evolution vs. time manometric profiles for catalyst 5<sup>2+</sup> 1 mM with Ce(IV) (25-100 mM; see graph) in 0.1 M triflic acid solutions (pH = 1.0). Top right, initial stages of the oxygen evolution profile, together with linear fitting. Bottom left, plot of initial rates vs. Ce(IV) concentration. Bottom right, linear regression data from previous plot.



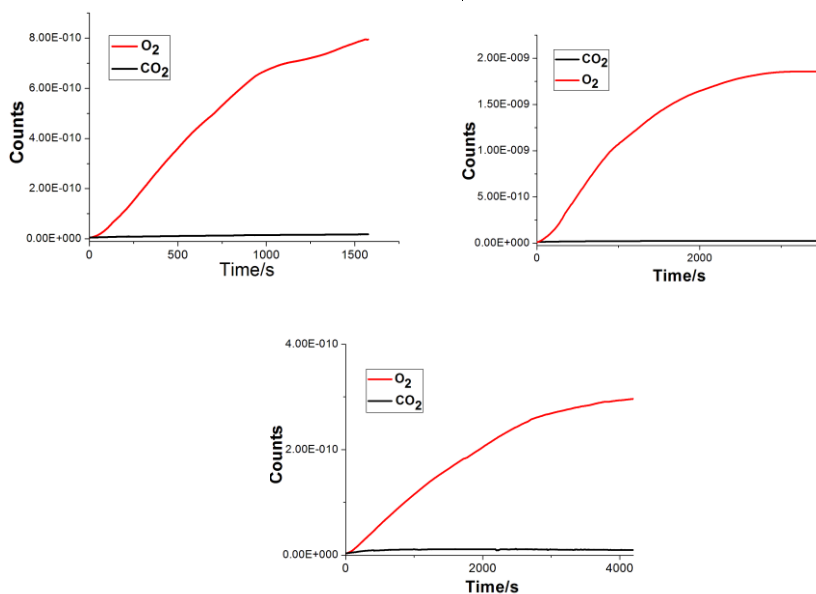
IV

**Figure S 23.** Top left, O<sub>2</sub> evolution vs. time manometric profiles for catalyst 5<sup>2+</sup> (0.34 mM to 1 mM; see graph) with 100 equivalents of Ce(IV) in 0.1 M triflic acid solutions (pH = 1.0). Top right, initial stages of the oxygen evolution profile, together with linear fitting. Bottom left, plot of initial rates vs. catalyst concentration. Bottom right, linear regression data from previous plot.



## Catalysis.

**Figure S 24.** Online MS monitoring of the evolved gas after the addition of 100 equivalents of CAN to a 1 mM solution of complex  $2^{2+}$  (upper left),  $5^{2+}$  (upper right) or  $6^{2+}$  (bottom) in 0.1 M HOTf at RT.



IV

UNIVERSITAT ROVIRA I VIRGILI

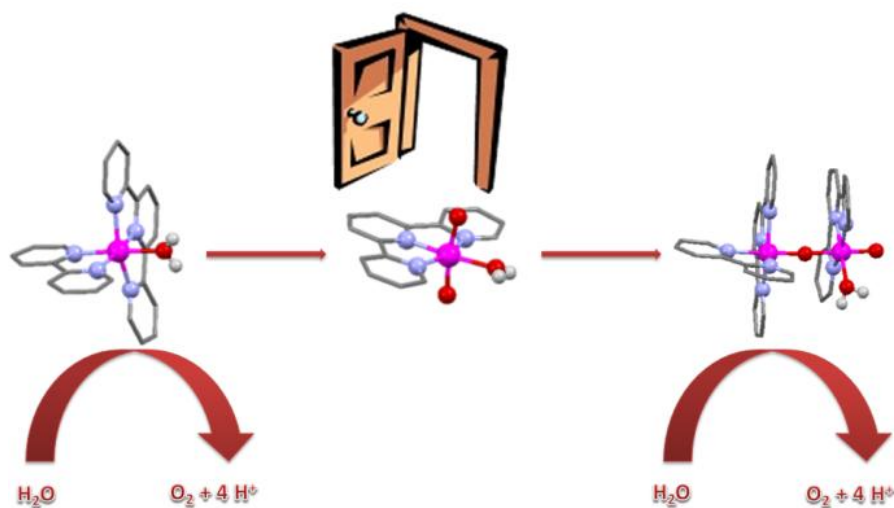
WATER OXIDATION WITH MONONUCLEAR RU COMPLEXES. BELOW THE TIP OF THE

ICEBERG: THE OXO-BRIDGE SCENARIO

Isidoro López Marin

Dipòsit Legal: T. 1505-2013

## **Chapter 5. A Self Improved Water Oxidation Catalyst, Is One Site Really Enough?**



We show for the first time that highly active mononuclear Ru-aqua water oxidation catalysts are transformed into dinuclear complexes during oxygen evolution catalysis, even from the very beginning of the catalytic process. The new dinuclear species are much more robust than their mononuclear counterparts and remain active catalyst for the water oxidation, establishing the coexistence of two different catalytic cycles in solution.



UNIVERSITAT ROVIRA I VIRGILI

WATER OXIDATION WITH MONONUCLEAR RU COMPLEXES. BELOW THE TIP OF THE

ICEBERG: THE OXO-BRIDGE SCENARIO

Isidoro López Marin

Dipòsit Legal: T. 1505-2013

## Table of Contents.

### Chapter 5. A Self Improved Water Oxidation Catalyst, Is One Site Really Enough?

<i>5.1. Introduction.</i>	177
<i>5.2. Results and discussion.</i>	179
<i>Synthesis and spectroscopic characterization of new dinuclear     Ru WOCs.</i>	179
<i>Electrochemistry and catalytic activity of the new dinuclear Ru     WOCs.</i>	181
<i>5.3. Conclusions.</i>	187
<i>5.4. Acknowledgment.</i>	187
<i>5.5. References.</i>	188
<i>5.6. Supporting information.</i>	191

UNIVERSITAT ROVIRA I VIRGILI

WATER OXIDATION WITH MONONUCLEAR RU COMPLEXES. BELOW THE TIP OF THE

ICEBERG: THE OXO-BRIDGE SCENARIO

Isidoro López Marin

Dipòsit Legal: T. 1505-2013

# A Self Improved Water Oxidation Catalyst; Is One Site Really Enough?

*Angew. Chem. Int. Ed.* **2013**, submitted.

Isidoro López,<sup>a</sup> Mehmed Z. Ertem,<sup>b,c</sup> Somnath Maji,<sup>a</sup> Jordi Benet-Buchholz,<sup>a</sup> Anke Keidel,<sup>d</sup> Uwe Kuhlmann,<sup>d</sup> Peter Hildebrandt,<sup>d</sup> Victor S. Batista<sup>c</sup> and Antoni Llobet.<sup>a,e</sup>

<sup>a</sup> Institute of Chemical Research of Catalonia (ICIQ), Av. Països Catalans, 16, 43007 Tarragona, Spain.

<sup>b</sup> Department of Chemistry, Brookhaven National Laboratory, Building 555A, Upton, NY 11973, USA.

<sup>c</sup> Department of Chemistry, Yale University, P.O. Box 208107, New Haven, CT 06520-8107, USA.

<sup>d</sup> Technische Universität Berlin, Institut für Chemie, Sekr. PC14, Straße des 17. Juni 135, D-10623 Berlin, Germany.

<sup>e</sup> Departament de Química, Universitat Autònoma de Barcelona, Cerdanyola del Vallès, 08193 Barcelona, Spain.

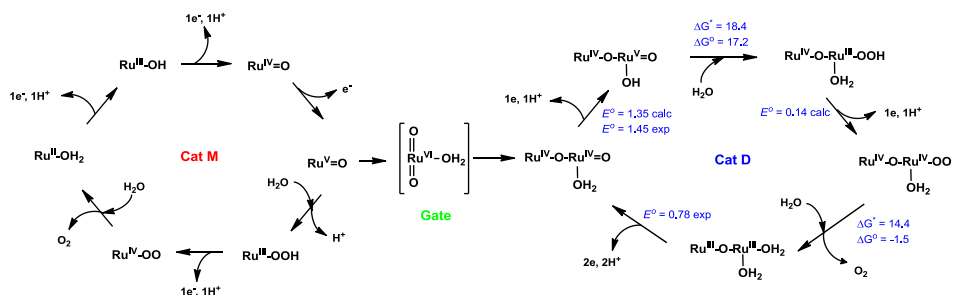
## 5.1. Introduction.

The replacement of fossil fuels by green and renewable solar energy carriers is one of the most important challenges our society is facing today. Intense research is currently being devoted to this topic, with emphasis on the development and characterization of new catalysts for water splitting such as the dinuclear Ru complexes introduced in this paper.<sup>1</sup>

Nature has been using sunlight to oxidize water and generate carbohydrates (solar fuels) in photosynthesis for over 2.5 billion years.<sup>2</sup> Artificial systems inspired by Nature have been designed to capture solar light and extract reducing equivalents (protons and electrons) from water to

generate useful chemical fuels. Therefore, mastering and understanding water oxidation catalysis is one of the key elements needed for this strategy to succeed. While the research field is becoming extremely active,<sup>3</sup> significant advances are still needed to develop a sufficiently rugged and efficient water oxidation catalyst that could be useful in large scale practical applications.

Since the discovery by Thummel *et al.*<sup>4</sup> that even mononuclear Ru complexes were active as water oxidation catalysts (WOCs), there has been a vivid development of several studies on this type of complexes.<sup>5-8</sup> Several catalysts have been developed and considerable knowledge on this type of catalysts has been advanced.<sup>9-13</sup> From a mechanistic perspective, Meyer *et al.*<sup>14</sup> offered a description of water oxidation at a molecular level. It was proposed that the O-O bond formation would take place through a water nucleophilic attack (WNA) pathway, as shown in a simplified manner on the left side of Scheme 1. Catalysts such as  $[\text{Ru}(\text{trpy})(\text{bpym})(\text{H}_2\text{O})]^{2+}$  (trpy: 2,2':6',2''-terpyridine; bpym: 2,2'-bipyrimidine),<sup>15</sup> have been reported to have impressive turn over numbers (TNs) larger than 28.000. However, practical applications require catalysts with TNs that are at least a few orders of magnitude higher. In order to design such highly efficient water oxidation catalysts, it is of paramount importance to understand the pathways that lead oxygen evolution from water and also the different reactions coupled to the catalytic cycle that might drive the intervening species towards unproductive pathways and decomposition. In addition, understanding pathways that derail from the initial catalytic cycle and generate new catalytic species with superior performance would be particularly valuable.

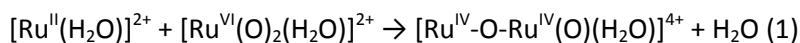


**Scheme 1.** Proposed interconnection of catalytic schemes (polypyridyl ligands are not shown). Energies are reported in kcal/mol and redox potentials are reported in V vs. the SSCE reference electrode. DFT calculations at M06-L level of theory (*calc*) are compared to experiments (*exp*).

Here we report the synthesis and characterization of new dinuclear Ru complexes of general formula  $[(trpy)(5,5'-X_2-bpy)Ru^{IV}(\mu-O)Ru^{IV}(trpy)(O)(H_2O)]^{4+}$  (bpy is 2,2'-bipyridine; X = H for  $\mathbf{1}^{4+}$  and X = F for  $\mathbf{2}^{4+}$ ) that are highly efficient and very robust WOCs. We find that these complexes are generated in the catalytic cycle of their related mononuclear counterparts  $[Ru(trpy)(5,5'-X_2-bpy)(H_2O)]^{2+}$ .<sup>16</sup>

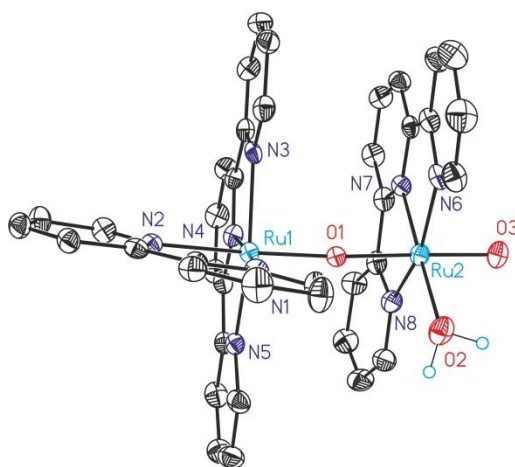
## 5.2. Results and discussion.

**Synthesis and spectroscopic characterization of new dinuclear Ru WOCs.** Addition of  $[Ru^{VI}(trpy)(O)_2(H_2O)]^{2+}$ ,  $\mathbf{3}^{2+}$ , to  $[Ru^{II}(trpy)(bpy)(H_2O)]^{2+}$ ,  $\mathbf{4}^{2+}$ , in the presence of Ce(IV) in acidic conditions generates complex  $\mathbf{1}^{4+}$  (polypyridilic ligands not shown),



Similarly addition of  $\mathbf{3}^{2+}$  to  $[(trpy)(5,5'-F_2-bpy)Ru^{II}(H_2O)]^{2+}$ ,  $\mathbf{5}^{2+}$ , forms the related dinuclear fluoro complex  $\mathbf{2}^{4+}$ . Complexes  $\mathbf{1}^{4+}$  and  $\mathbf{2}^{4+}$  were thoroughly characterized by analytic, spectroscopic and electrochemical techniques. The X-ray crystal structures of  $\mathbf{1}^{4+}$  and  $\mathbf{2}^{4+}$  were solved by means of single crystal

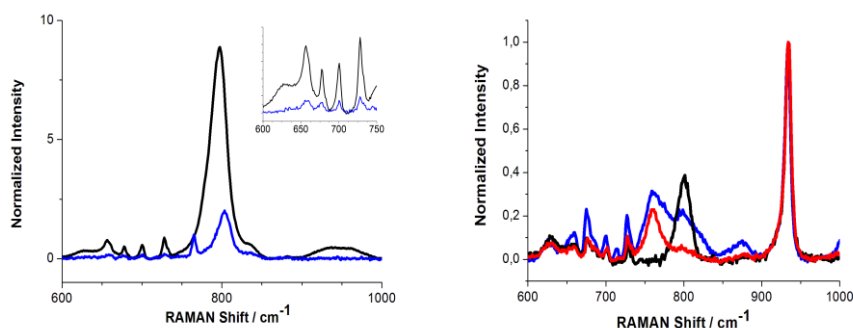
XRD and their Ortep views are shown in Figure 1 and in the Supplementary Information, respectively. It is interesting to point out here the short Ru-O distance (1.747 Å) presented by  $\mathbf{1}^{4+}$  that falls in the lower range of values reported for Ru<sup>IV</sup>=O groups.<sup>17-22</sup> In sharp contrast, the Ru-O distance for the Ru<sup>IV</sup>-OH<sub>2</sub> group is 2.120 Å. Additionally; also the nearly linear Ru-O-Ru angle (176.1°) is worth noting. Complexes  $\mathbf{1}^{4+}$  and  $\mathbf{2}^{4+}$  are diamagnetic as expected for high field  $\mu$ -oxo dinuclear d<sup>4</sup> Ru complexes<sup>23-26</sup> and their NMR spectra are presented in the SI.



**Figure 1.** Ortep plot (ellipsoids drawn at 50 % probability) of the X-ray structure of  $\mathbf{1}^{4+}$ . Color codes: Ru, cyan; O, Red; N, Blue; C, black. H atoms are not shown except for the aqua ligands that are represented as small light blue circles.

Complex  $\mathbf{2}^{4+}$  has a very strong vibrational band at 801 cm<sup>-1</sup> as shown in the resonance Raman (rR) spectrum (Figure 2), that we assign to the Ru=O stretching mode. Labeling experiments with H<sub>2</sub><sup>18</sup>O lead to a downshift of this mode to 760 cm<sup>-1</sup> corresponding to an isotopic shift of 41 cm<sup>-1</sup>. Mixed labeling achieved with a 1:1 H<sub>2</sub><sup>16</sup>O:H<sub>2</sub><sup>18</sup>O mixture do not generate any new modes in the rR spectrum, consistently with a terminal Ru=O bond. The frequency of this

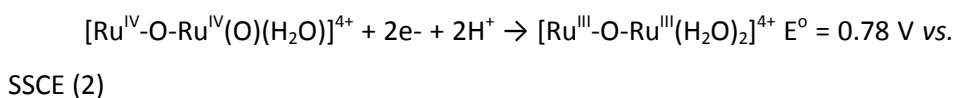
mode is in agreement with related Ru=O complexes reported in the literature.<sup>21,27-30</sup> A very interesting feature of the rR spectrum is the small bands at 727, 714, 700 and 675 cm<sup>-1</sup> that can be used as a fingerprint for the identification of this complex.



**Figure 2.** Left, overlay of rR spectra of  $2^{4+}$  (black) and the reaction product obtained after addition of 3 eq. of Ce(IV) to complex  $5^{2+}$  (blue), both measured in 0.1 M HOTf in  $H_2^{16}O$ . The inset shows an enlargement of the fingerprint region mentioned in the main text. Right, overlay of rR spectra obtained after reaction of 3 eq. of Ce(IV) with complex  $5^{2+}$  in 0.1 M  $HClO_4$  in  $H_2^{16}O$  (black),  $H_2^{18}O$  (red) and  $H_2^{16}O:H_2^{18}O$  (1:1) (blue). Further experimental details are given in SI.

### Electrochemistry and catalytic activity of the new dinuclear Ru WOCs.

The electrochemistry of complexes  $1^{4+}$  and  $2^{4+}$  was carried out in 0.1 M triflic acid, was explored by means of CV, DPV and Coulometry, and is reported in Figure 3 and the SI. Complex  $1^{4+}$  undergoes a 2-electron reduction, as confirmed by Coulometry, from the formal oxidation state IV,IV to III,III, associated with two proton transfer steps according to (polypyridyl ligands not shown),





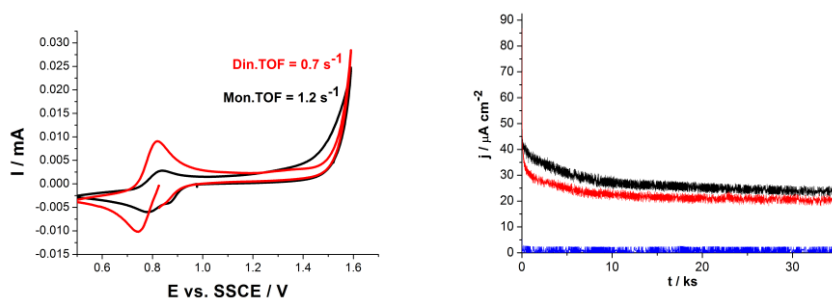
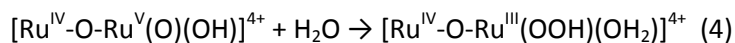
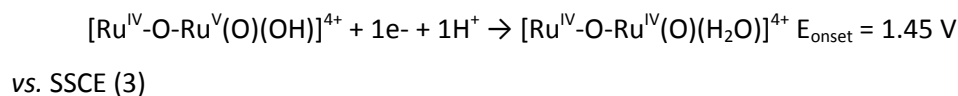


**Figure 3.** Left, CV of 0.5 mM solutions of  $1^{4+}$  (red) and  $4^{2+}$  (black) in 0.1 M HOTf (pH = 1.0) using a polished glassy carbon working electrode, a Pt wire counter electrode and a Hg/Hg<sub>2</sub>SO<sub>4</sub>, K<sub>2</sub>SO<sub>4</sub> (sat.) as reference electrode (potentials reported vs. SSCE). Right, controlled potential electrolysis at 1.6 V vs. SSCE of a 0.4 mM solution of  $4^{2+}$  (black) and  $1^{4+}$  (red) complexes in 0.1 M triflic acid and a blank experiment without catalyst (blue). An activated boron doped diamond disk (3 mm diameter) was used as a working electrode, Pt wire as a counter electrode and a Hg/Hg<sub>2</sub>SO<sub>4</sub>, K<sub>2</sub>SO<sub>4</sub> (sat) reference electrode (potentials are converted to SSCE).

On the anodic part, a further electron transfer process is observed together with a large current intensity, assigned to the electrocatalytic oxidation of water to dioxygen. A one-electron process that generates a very reactive species responsible for the O-O bond formation (eqs 3-4) is proposed, followed by a sequence of reactions leading to dioxygen formation (Scheme 1, right side),



Formal oxidation states are indicated to facilitate electron counting even though it is well known that the oxo-bridge promotes charge transfer interactions between the Ru metal centers.<sup>31</sup> DFT calculations at the M06-L<sup>32-34</sup>

level of theory (see SI for details) were carried out to characterize the reaction intermediates as well as the transition states, providing a complete catalytic cycle (Scheme 1, right). The O-O bond formation step through water nucleophilic attack to  $[\text{Ru}^{\text{IV}}\text{-O-Ru}^{\text{V}}(\text{O})(\text{OH})]^{4+}$  (equation 4) was found to be the rds of the catalytic cycle with a  $\Delta G^\ddagger$  of 18.4 kcal/mol. The optimized transition state structure features a water molecule which forms the O-O bond with concomitant transfer of a proton to the neighboring Ru-OH group (Figure 4, left), to generate the corresponding hydroperoxo complex,  $[\text{Ru}^{\text{IV}}\text{-O-Ru}^{\text{III}}(\text{OOH})(\text{OH}_2)]^{4+}$ .

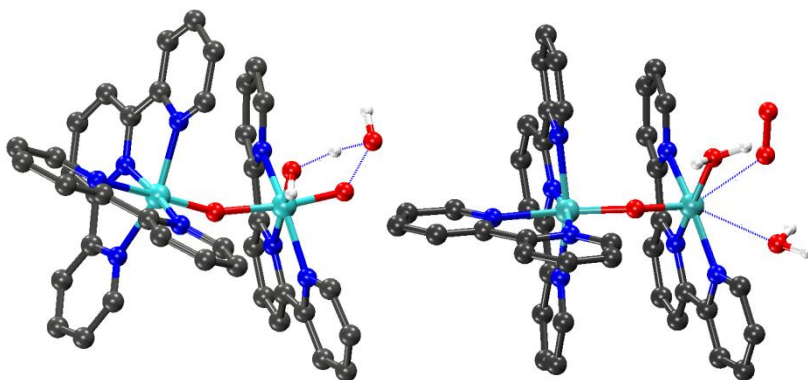
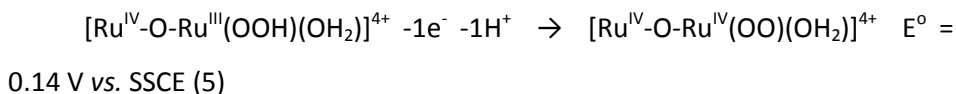
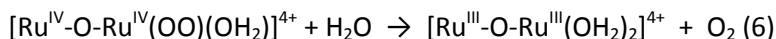


**Figure 4.** Ball and stick representation of the optimized transition state structures for the O-O bond formation (left) and  $\text{O}_2$  evolution steps (right). H atoms are only shown for the aqua and hydroxy ligands.

The next step corresponds to a proton coupled electron transfer with a very low redox potential leading to the formation of a superoxo intermediate,



which subsequently evolves  $\text{O}_2$  (Figure 4, right) and generates the initial complex,



closing the catalytic cycle.

From the electrochemical experiments shown in Figure 3, TOFs of 0.7 cycles per second for  $\mathbf{1}^{4+}$  and  $1.2 \text{ s}^{-1}$  for  $\mathbf{4}^{2+}$  were calculated<sup>35</sup> which are comparable to mononuclear complexes reported in the literature.<sup>15,16,36</sup> The capacity of  $\mathbf{1}^{4+}$  to act as a WOC was also tested electrochemically under a constant applied potential. A potentiometric experiment was performed for both  $\mathbf{1}^{4+}$  and  $\mathbf{4}^{2+}$  in order to evaluate their relative performance at longer time scales as shown in Figure 3. At an applied potential of 1.6 V vs. SSCE, initial current densities of approximately  $40 \mu\text{A}/\text{cm}^2$  are reached for  $\mathbf{1}^{4+}$  and  $\mathbf{4}^{2+}$ . For  $\mathbf{1}^{4+}$  the current density decreases to  $20 \mu\text{A}$  at about 10 ks and is maintained constant thereafter. On the other hand, for  $\mathbf{4}^{2+}$  the current slowly drops over time until it merges with that of  $\mathbf{1}^{4+}$  at approximately 30 ks. This phenomenon is attributed to the slow but progressive and irreversible conversion of the mononuclear complex  $\mathbf{4}^{2+}$  to the corresponding dinuclear  $\mathbf{1}^{4+}$  complex, as proposed in Scheme 1, and demonstrated by UV-vis and rR spectroscopy (vide infra). At 35 ks TONs of 14930 and 6683 were obtained for  $\mathbf{4}^{2+}$  and  $\mathbf{1}^{4+}$  respectively.

A bulk electrolysis experiment at 1.4 V applied potential was also followed spectrophotometrically by UV-vis absorption spectroscopy as indicated in Figure 5. Very interestingly it was found that the absorption bands of  $\mathbf{1}^{4+}$  at 457 and 690 nm start to emerge as the catalysis proceeds. After two days of applied constant potential, 23 % conversion of  $\mathbf{4}^{2+} \rightarrow \mathbf{1}^{4+}$  was observed. This mononuclear to dinuclear conversion can also be observed in the rR spectra at the very early stages of the water oxidation reaction when adding 3 equivalents of Ce(IV) to  $\mathbf{5}^{2+}$  (Figure 2). Indeed, shortly after Ce(IV) addition, the rR spectrum displays a highly intense band at  $801 \text{ cm}^{-1}$  and four weaker bands at 727, 714, 700 and  $675 \text{ cm}^{-1}$  characteristic of  $\mathbf{2}^{4+}$ . In sharp contrast, exposure

of  $1^{4+}$  or  $2^{4+}$  for long periods of time under the same conditions (35 ks at 1.6 V vs. SSCE), does not show any change in the UV-vis spectrum. This manifests the ruggedness of  $1^{4+}$  as a water oxidation catalyst that does not show any sign of fatigue even after 35 ks controlled potential electrolysis at 1.6 V vs. SSCE.

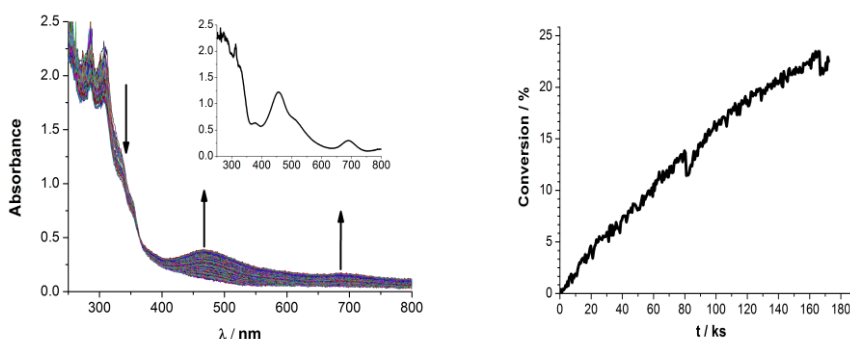
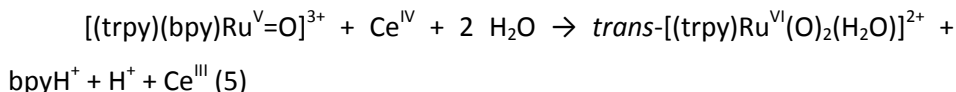


**Figure 5.** Left, UV-vis absorption spectra monitoring the controlled potential electrolysis of a 0.5 mM solution of  $4^{2+}$  in 0.1 M HOTf, for two days at 1.4 V vs. SSCE using a Pt mesh working electrode, a Pt wire counter electrode and a Ag/AgCl, NaCl (3M) reference electrode. Spectra were recorded every ten minutes. Inset, UV-vis spectra of  $1^{4+}$  in 0.1 M HOTf. Right, conversion of mononuclear  $4^{2+}$  to dinuclear  $1^{4+}$  over time, based on absorbance change at 460 nm.

These experiments manifest the interconnection of the two catalytic cycles for the mononuclear  $4^{2+}$  and dinuclear  $1^{4+}$  species. The link between the two catalytic cycles is essentially  $[\text{Ru}^{\text{VI}}(\text{trpy})(\text{O})_2(\text{H}_2\text{O})]^{2+}$ ,  $3^{2+}$ , that can be generated by bpy loss from the mononuclear complex, potentially at oxidation state V,



The strong *trans* effect generated by the  $\text{Ru}^{\text{V}}=\text{O}$  group produces a weakening of one of the Ru-N bpy bonds that eventually leads to the loss of

the bpy ligand. Furthermore the *trans*-Ru(O)<sub>2</sub> entity is known to generate very stable complexes<sup>37,38</sup> and thus is an additional driving force for the bpy loss. Once the bpy ligand is released, the reaction of **3**<sup>2+</sup> with **4**<sup>2+</sup> (equation 1), constitutes the entry to the dinuclear catalytic cycle. The free energy values obtained at DFT level of theory indicate that the proposed interconversion pathway is feasible (Scheme S2 in the supporting information) and further supports this hypothesis. This interconversion process also occurs between **5**<sup>2+</sup> and **2**<sup>4+</sup>, suggesting a general interconversion process of single site catalysts. These findings shine light on the *in-situ* generation of long lasting water oxidation catalysts based on dinuclear complexes.

The larger stability of the dinuclear complexes is due to a number of factors. First, the presence of two electronically coupled Ru centers through an oxo-bridge allows for fast intramolecular ET within the species generated in the catalytic cycle. Thus, due to the involvement of two metal-centers, the burden of multiple electron transfer at a single site is overcome. Second, the presence of spatially separated non-symmetrical Ru centers allows fine-tuning of each site, i.e. to optimize one site for electron relay and the other site for proton-coupled ET, responsible for the primary interaction with the water molecules. Third, the *trans*-dioxo geometry at higher oxidation states stabilizes the dinuclear complex as opposed to the mononuclear **3**<sup>2+</sup> that is not an active water oxidation catalyst. In addition the higher oxidation states of mononuclear mono-aqua Ru complexes suffer from ligand loss and subsequent decomposition. Fourth, the presence of the oxo-bridge and the terminal Ru=O group can act as anchors for hydrogen bonding if required, as nicely illustrated in the transition state structure depicted in Figure 4. This hydrogen bonding

has been previously shown to be crucial for reducing the energy of activation of transition states.<sup>39,40</sup>

### 5.3. Conclusions.

In summary, we have shown that WOCs based on mononuclear mono-aqua Ru complexes are slowly converted into active dinuclear catalysts through a self-assembly type of process. These dinuclear complexes are much more robust than the mononuclear precursors and exhibit similar activity as WOCs. Thus, we have shown for the first time that two interconnected catalytic cycles coexist where the mononuclear catalytic system is slowly and irreversibly converted to the more stable dinuclear catalytic system. We have further characterized the catalytic cycle based on DFT calculations, providing very good agreement with the available experimental observations.

**The mononuclear Ru complexes were prepared by Dr. Somnath Maji and the DFT calculations were carried by Dr. Mehmed Z. Ertem under the supervision of Prof. Víctor S. Batista.**

### 5.4. Acknowledgement.

Support from MINECO (CTQ2010–21497 and PRI-PIBIN-2011-1278) and FPU grant to IL and Torres Quevedo contract to SM are gratefully acknowledged. Support has also been received from the Cluster of Excellence (UniCat) and the U.S. Department of Energy (DOE) Grant DE-SC0001423 (V.S.B.), M.Z.E. was funded by a Computational Materials and Chemical Sciences (CMCSN) project at Brookhaven National Laboratory under contract DE-AC02-98CH10886 with the U.S. DOE and supported by its Division of Chemical Sciences, Geosciences & Biosciences, Office of Basic Energy Sciences.

## 5.5. References.

- (1) Melis, A. *Energy Environ. Sci* **2012**, *5*, 5531.
- (2) *Photosystem II - The Light-driven Water: Plastoquinone Oxidoreductase*; 1 ed.; Wydrzynski, T. J.; Satoh, K., Eds.; Springer: Dordrecht, 2005.
- (3) Bofill, R.; García-Antón, J.; Escriche, L.; Sala, X.; Llobet, A. In *Comprehensive Inorganic Chemistry II. Coordination and Organometallic Chemistry*; Vivian, W. W. Y., Ed.; Elsevier Limited: Oxford, 2012; Vol. 8.
- (4) Zong, R.; Thummel, R. P. *J. Am. Chem. Soc.* **2005**, *127*, 12802.
- (5) Concepcion, J. J.; Jurss, J. W.; Templeton, J. L.; Meyer, T. J. *J. Am. Chem. Soc.* **2008**, *130*, 16462.
- (6) Wasylenko, D. J.; Ganesamoorthy, C.; Koivisto, B. D.; Henderson, M. A.; Berlinguette, C. P. *Inorg. Chem.* **2010**, *49*, 2202.
- (7) Duan, L.; Fischer, A.; Xu, Y.; Sun, L. *J. Am. Chem. Soc.* **2009**, *131*, 10397.
- (8) Boyer, J. L.; Polyansky, D. E.; Szalda, D. J.; Zong, R.; Thummel, R. P.; Fujita, E. *Angew. Chem. Int. Ed.* **2011**, *50*, 12600.
- (9) Concepcion, J. J.; Jurss, J. W.; Brennaman, M. K.; Hoertz, P. G.; Patrocinio, A. O. v. T.; Murakami Iha, N. Y.; Templeton, J. L.; Meyer, T. J. *Acc. Chem. Res.* **2009**, *42*, 1954.
- (10) Wasylenko, D. J.; Ganesamoorthy, C.; Henderson, M. A.; Koivisto, B. D.; Osthoff, H. D.; Berlinguette, C. P. *J. Am. Chem. Soc.* **2010**, *132*, 16094.
- (11) Polyansky, D. E.; Muckerman, J. T.; Rochford, J.; Zong, R.; Thummel, R. P.; Fujita, E. *J. Am. Chem. Soc.* **2011**, *133*, 14649.
- (12) Hettterscheid, D. G. H.; Reek, J. N. H. *Angew. Chem. Int. Ed.* **2012**, *51*, 9740.
- (13) Wasylenko, D. J.; Palmer, R. D.; Berlinguette, C. P. *Chem. Commun. (Cambridge, U. K.)* **2013**, *49*, 218.
- (14) Concepcion, J. J.; Tsai, M.-K.; Muckerman, J. T.; Meyer, T. J. *J. Am. Chem. Soc.* **2010**, *132*, 1545.
- (15) Concepcion, J.; Jurss, J.; Hoertz, P.; Meyer, T. *Angew. Chem. Int. Ed.* **2009**, *48*, 9473.
- (16) Maji, S.; López, I.; Bozoglian, F.; Benet-Buchholz, J.; Llobet, A. *Inorg. Chem.* **2013**, *52*, 3591.
- (17) Welch, T. W.; Ciftan, S. A.; White, P. S.; Thorp, H. H. *Inorg. Chem.* **1997**, *36*, 4812.
- (18) Che, C. M.; Lai, T. F.; Wong, K. Y. *Inorg. Chem.* **1987**, *26*, 2289.
- (19) Cheng, W.-C.; Yu, W.-Y.; Cheung, K.-K.; Che, C.-M. *J. Chem. Soc., Dalton Trans.* **1994**, 57.

- (20) Che, C. M.; Tang, W. T.; Wong, W. T.; Lai, T. F. *J. Am. Chem. Soc.* **1989**, *111*, 9048.
- (21) Kojima, T.; Nakayama, K.; Ikemura, K.; Ogura, T.; Fukuzumi, S. *J. Am. Chem. Soc.* **2011**, *133*, 11692.
- (22) Cheng, W.-C.; Yu, W.-Y.; Zhu, J.; Cheung, K.-K.; Peng, S.-M.; Poon, C.-K.; Che, C.-M. *Inorg. Chim. Acta* **1996**, *242*, 105.
- (23) Aoyagi, K.; Yukawa, Y.; Shimizu, K.; Mukaida, M.; Takeuchi, T.; Kakihana, H. *Bull. Chem. Soc. Jpn.* **1986**, *59*, 1493.
- (24) Weaver, T. R.; Meyer, T. J.; Adeyemi, S. A.; Brown, G. M.; Eckberg, R. P.; Hatfield, W. E.; Johnson, E. C.; Murray, R. W.; Untereker, D. *J. Am. Chem. Soc.* **1975**, *97*, 3039.
- (25) Llobet, A.; Curry, M. E.; Evans, H. T.; Meyer, T. J. *Inorg. Chem.* **1989**, *28*, 3131.
- (26) Schneider, R.; Weyhermueller, T.; Wieghardt, K.; Nuber, B. *Inorg. Chem.* **1993**, *32*, 4925.
- (27) Moyer, B. A.; Meyer, T. J. *Inorg. Chem.* **1981**, *20*, 436.
- (28) Bailey, C. L.; Drago, R. S. *J. Chem. Soc., Chem. Commun.* **1987**, 179.
- (29) Chatterjee, D. *Inorg. Chim. Acta* **2008**, *361*, 2177.
- (30) *Ruthenium Oxidation Complexes: Their Uses as Homogeneous Organic Catalysts*; Griffith, W. P., Ed.; Springer, 2011; Vol. 34.
- (31) Jurss, J. W.; Concepcion, J. J.; Butler, J. M.; Omberg, K. M.; Baraldo, L. M.; Thompson, D. G.; Lebeau, E. L.; Hornstein, B.; Schoonover, J. R.; Jude, H.; Thompson, J. D.; Dattelbaum, D. M.; Rocha, R. C.; Templeton, J. L.; Meyer, T. J. *Inorg. Chem.* **2012**, *51*, 1345.
- (32) Zhao, Y.; Truhlar, D. G. *The Journal of Chemical Physics* **2006**, *125*, 194101.
- (33) Zhao, Y.; Truhlar, D. G. *Acc. Chem. Res.* **2008**, *41*, 157.
- (34) Zhao, Y.; Truhlar, D. *Theor. Chem. Acc.* **2008**, *120*, 215.
- (35) The TOFs were calculated transforming the current intensity at 1.6 V vs. SSCE in mols of produced oxygen per second:  $I/(4 \text{ electrons} \times 96485)$ , and dividing this value by the amount of catalyst next to the electrode surface, which was determined based on the area under the anodic wave of the IV,IV/III,III couple in the case of  $1^{4+}$  or the III/II couple in the case of  $4^{2+}$ .
- (36) Kärkäs, M. D.; Åkermark, T.; Chen, H.; Sun, J.; Åkermark, B. *Angew. Chem. Int. Ed.* **2013**, *52*, 4189.
- (37) Adeyemi, S. A.; Doveloglou, A.; Guadalupe, A. R.; Meyer, T. J. *Inorg. Chem.* **1992**, *31*, 1375.
- (38) Mayer, J. M. *Comments Inorg. Chem.* **1988**, *8*, 125.



- (39) Bozoglian, F.; Romain, S.; Ertem, M. Z.; Todorova, T. K.; Sens, C.; Mola, J.; Rodríguez, M.; Romero, I.; Benet-Buchholz, J.; Fontrodona, X.; Cramer, C. J.; Gagliardi, L.; Llobet, A. *J. Am. Chem. Soc.* **2009**, *131*, 15176.
- (40) Sala, X.; Ertem, M. Z.; Vígara, L.; Todorova, T. K.; Chen, W.; Rocha, R. C.; Aquilante, F.; Cramer, C. J.; Gagliardi, L.; Llobet, A. *Angew. Chem. Int. Ed.* **2010**, *49*, 7745.

## Supporting Information for,

# A Self Improved Water Oxidation, Is One Site Really Enough?

Isidoro López,<sup>a</sup> Mehmed Z. Ertem,<sup>b,c</sup> Somnath Maji,<sup>a</sup> Jordi Benet-Buchholz,<sup>a</sup>  
Anke Keidel,<sup>d</sup> Uwe Kuhlmann,<sup>d</sup> Peter Hildebrandt,<sup>d</sup> Victor S. Batista<sup>c</sup> and Antoni  
Llobet.<sup>a,e</sup>

<sup>a</sup> Institute of Chemical Research of Catalonia (ICIQ), Av. Països Catalans, 16, 43007 Tarragona,  
Spain.

<sup>b</sup> Department of Chemistry, Brookhaven National Laboratory, Building 555A, Upton, NY 11973,  
USA.

<sup>c</sup> Department of Chemistry, Yale University, P.O. Box 208107, New Haven, CT 06520-8107, USA.

<sup>d</sup> Technische Universität Berlin, Institut für Chemie, Sekr. PC14, Straße des 17. Juni 135, D-10623  
Berlin, Germany.

<sup>e</sup> Departament de Química, Universitat Autònoma de Barcelona, Cerdanyola del Vallès, 08193  
Barcelona, Spain.

V

## Experimental Section.

### Materials:

All reagents used in the present work were obtained from Aldrich Chemical Co. and Alfa Aesar and were used without further purification. Triflic Acid ( $\text{CF}_3\text{SO}_3\text{H}$ ) was purchased from CYMIT. Reagent-grade organic solvents were obtained from SDS and high purity deionized water was obtained by passing distilled water through a nanopore Milli-Q water purification system.

### Preparations.

$\text{Ru}(\text{trpy})\text{Cl}_3$ ,<sup>1</sup>  $[\text{Ru}(\text{trpy})(\text{bpy})(\text{H}_2\text{O})](\text{PF}_6)_2$  ( $\mathbf{4}^{2+}$ ),<sup>2</sup>  $[\text{Ru}(\text{trpy})(5,5'\text{-F}_2\text{-bpy})(\text{H}_2\text{O})](\text{PF}_6)_2$  ( $\mathbf{5}^{2+}$ )<sup>3</sup> and  $[\text{Ru}(\text{trpy})(\text{C}_2\text{O}_4)(\text{H}_2\text{O})]\cdot 2\text{H}_2\text{O}$ <sup>4</sup> were prepared according to literature procedures.  $[\text{Ru}(\text{trpy})(\text{O})_2(\text{H}_2\text{O})](\text{ClO}_4)_2\cdot\text{H}_2\text{O}$  was prepared following a procedure slightly modified to the reported one.<sup>4</sup>

- (1) Sullivan, B. P.; Calvert, J. M.; Meyer, T. J. *Inorg. Chem.* **1980**, *19*, 1404.
- (2) Takeuchi, K. J.; Thompson, M. S.; Pipes, D. W.; Meyer, T. J. *Inorg. Chem.* **1984**, *23*, 1845.
- (3) Maji, S.; López, I.; Bozoglian, F.; Benet-Buchholz, J.; Llobet, A. *Inorg. Chem.* **2013**, *52*, 3591.
- (4) Adeyemi, S. A.; Doveloglou, A.; Guadalupe, A. R.; Meyer, T. J. *Inorg. Chem.* **1992**, *31*, 1375.

$[\text{Ru}(\text{trpy})(\text{O})(\text{H}_2\text{O})](\text{ClO}_4)_2\cdot\text{H}_2\text{O}$  ( $\mathbf{3}^{2+}$ ).  $[\text{Ru}(\text{trpy})(\text{C}_2\text{O}_4)(\text{H}_2\text{O})]\cdot 2\text{H}_2\text{O}$  (50 mg, 0.079 mmols) was dissolved in deoxygenated 2 M  $\text{HClO}_4$  (8 mL) under Ar. The purple mixture was filtered with a Schlenck frit under Ar. If oxidation is thought to have occurred because the color of the solution changes from purple to blue, the filtered can be collected on a Zinc amalgam and stirred until the purple colour is recovered. The solution is added dropwise to a stirred solution of

$(\text{NH}_4)_2\text{Ce}(\text{NO}_3)_6$  (1.5 g, 2.68 mmols) dissolved in the minimum amount of 2 M  $\text{HClO}_4$ . A yellow solid starts to precipitate a few minutes after the addition of the complex is finished. The mixture is left stirred for 2 hours and then it is kept in the fridge overnight. The yellow solid is filtered, washed with some drops of a cold 0.1 M  $\text{HClO}_4$  solution and air-dried. Yield: 58 mg (93 %). rRAMAN (0.1 M HOTf,  $\text{cm}^{-1}$ ): 835 s ( $\nu_{\text{sym}}(\text{O}=\text{Ru}=\text{O})$ ).  $^1\text{H-NMR}$  (400 MHz, 0.1 M DOTf):  $\delta(\text{ppm}) = 9.31$  (dd,  $J = 5.7, 1.2$  Hz, 2H, H6-H6''), 8.91-8.82 (m, 5H, H3-H3''-H4'-H5'-H3'), 8.66 (ddd,  $J = 7.9, 7.9, 1.4$  Hz, 2H, H4-H4'') and 8.17 (ddd,  $J = 7.9, 5.7, 1.3$  Hz, 2H, H5'-H5'').

$\{[\text{Ru}(\text{trpy})(\text{bpy})][\text{Ru}(\text{O})(\text{trpy})(\text{H}_2\text{O})](\mu\text{-O})\}(\text{ClO}_4)_4 \cdot 4\text{H}_2\text{O}$  (**1<sup>4+</sup>**). A 0.75 mM solution of  $[\text{Ru}(\text{trpy})(\text{bpy})(\text{H}_2\text{O})](\text{PF}_6)_2$  (67.5 mg, 0.085 mmols) in 0.1 M  $\text{HClO}_4$  was prepared. An amount of 3 equivalents of  $(\text{NH}_4)_2\text{Ce}(\text{NO}_3)_6$  (139.0 mg, 0.254 mmols) dissolved in the minimum amount of 0.1 M  $\text{HClO}_4$  was added to the previous stirred solution. Then,  $[\text{Ru}(\text{trpy})(\text{O})(\text{H}_2\text{O})](\text{ClO}_4)_2$  (48.8 mg, 0.084 mmols) was added and the mixture was left stirred at room temperature for 3 days. A dark brown solid precipitated which was filtered and washed with drops of cold water. The solid was dried under vacuum for 5 hours. Yield: 54.6 mg (48%). Anal. Calcd for  $\text{C}_{40}\text{H}_{40}\text{Cl}_4\text{N}_8\text{O}_{23}\text{Ru}_2$ : C, 35.73; H, 3.00; N, 8.33. Found: C, 35.75; H, 2.50; N, 8.30.

$\{[\text{Ru}(\text{trpy})(5,5'\text{-F}_2\text{bpy})][\text{Ru}(\text{O})(\text{trpy})(\text{H}_2\text{O})](\mu\text{-O})\}(\text{ClO}_4)_4 \cdot 7\text{H}_2\text{O}$  (**2<sup>4+</sup>**). A procedure similar to **1<sup>4+</sup>** was followed. A 1.25 mM solution of  $[\text{Ru}(\text{trpy})(5,5'\text{-F}_2\text{bpy})(\text{H}_2\text{O})](\text{PF}_6)_2$  (57.7 mg, 0.069 mmols) in 0.1 M  $\text{HClO}_4$  was prepared and 3 equivalents of  $(\text{NH}_4)_2\text{Ce}(\text{NO}_3)_6$  (114.4 mg, 0.209 mmols) dissolved in the minimum amount of 0.1 M  $\text{HClO}_4$  were added to the stirred solution. Then,  $[\text{Ru}(\text{trpy})(\text{O})(\text{H}_2\text{O})](\text{ClO}_4)_2$  (40 mg, 0.069 mmols) was added and the mixture was left stirred at room temperature for 2 days. After that, it was kept in the

V

fridge at 8 °C for another 2 days. A dark brown solid precipitated which was filtered and washed with drops of cold water. The solid was dried at air. Yield: 55.5 mg (56 %). Anal. Calcd for.  $C_{40}H_{44}Cl_4F_2N_8O_{26}Ru_2$ : C, 33.48, H, 3.09, N, 7.81. Found: C, 33.33, H, 2.33, N, 7.64.

### Equipment and measurements.

UV/Vis spectroscopy was performed on a Cary 50 (Varian) UV/Vis spectrophotometer in 1 cm or 0.2 cm when indicated quartz cuvettes. Spectroelectrochemical experiments for  $\{[Ru(trpy)(bpy)][Ru(O)(trpy)(H_2O)](\mu-O)\}(ClO_4)_4 \cdot 4H_2O$  were carried out with an Agilent UV-vis Torlon probe with an optical path length of 2 mm in a two compartment electrochemical cell. A Pt mesh was used as working electrode, a Pt wire as counter electrode and an Ag/AgCl, NaCl(sat) as reference electrode.

Cyclic voltammetry (CV) and differential pulse voltammetry (DPV) experiments were performed on an IJ-Cambria CHI-660 potentiostat or a Bio-Logic SP-150 potentiostat using a three-electrode cell. Typical CV experiments were carried out at a scan rate of 100 mV s<sup>-1</sup>. DPV experiments were carried out with the parameters: Pulses Height = 50 mV, Pulses Width = 50 ms, Step Height = 4 mV and Step Time = 200 ms. A glassy carbon electrode (3 mm diameter) was used as working electrode, platinum wire as auxiliary electrode, and a SSCE as a reference electrode. Working electrodes were polished with 0.05 micron alumina paste, and rinsed with distilled water and acetone followed by blow-drying before each measurement. When glassy carbon electrodes were activated, a procedure described by Meyer *et al.* was used.<sup>5</sup> All cyclic voltammograms presented in this work were recorded in the absence of light and inside a Faradaic cage. The electrochemical experiments were carried out in 0.1 M CF<sub>3</sub>SO<sub>3</sub>H (pH 1.0). E<sub>1/2</sub> values reported in this work were estimated

from CV experiments as the average of the oxidative and reductive peak potentials ( $E_{p,a} + E_{p,c}$ )/2 or taken as  $E(I_{max})$  from DPV measurements. Controlled Potential Electrolysis (CPE) were carried out in a two compartment cell. The experiments at 1.6 V vs. SSCE were made with a 3 mm activated<sup>6</sup> boron doped diamond working electrode, a Pt wire counter electrode and a Hg/Hg<sub>2</sub>SO<sub>4</sub>, K<sub>2</sub>SO<sub>4</sub> (sat) reference electrode. For mononuclear complexes, the oxo compounds [Ru(trpy)(bpy)(O)]<sup>2+</sup> and [Ru(trpy)(5,5'-F<sub>2</sub>-bpy)(O)]<sup>2+</sup> were prepared electrochemically before oxidation at 1.6 V vs. SSCE by applying the suitable potentials (0.78 V and 0.70 V vs. SSCE) and using a Pt mesh as working electrode. The measured potentials referring to the Hg/Hg<sub>2</sub>SO<sub>4</sub>, K<sub>2</sub>SO<sub>4</sub> (sat) reference electrode were converted to SSCE according to literature values.<sup>7,8</sup>

A 400 MHz Bruker Avance II spectrometer and a Bruker Avance 500 MHz were used to carry out NMR spectroscopy at room temperature. Samples were run in 0.1 M DOTf or 0.1 M DNO<sub>3</sub> with internal references (residual protons). Elemental analysis was performed using an EA-1108, CHNS-O elemental analyzer from Fisons Instruments.

Samples for resonance Raman spectroscopy were prepared typically by mixing a 0.5 or 1 mM solution of the starting complex with the desired amount of (NH<sub>4</sub>)<sub>2</sub>Ce(NO<sub>3</sub>)<sub>6</sub> and transferring 100 μL of the reaction solution to a aluminium crucible and subsequently frozen at appropriate times in liquid N<sub>2</sub>. Then, the crucible was placed into a Linkam THMS 600 temperature controlled cryo stage to keep the temperature at -12°C. The rR spectrum was acquired using a Renishaw inVia Reflex RAMAN confocal microscope (Gloucestershire, UK), equipped with an Ar-ion laser at 514 nm and a Peltier-cooled CCD detector (-70°C) coupled to a Leica DM-2500 microscope. Calibration was carried out daily by recording the Raman spectrum of an internal Si standard. Rayleigh

scattered light was appropriately rejected by using edge-type filters. For wide spectral ranges (200-1500  $\text{cm}^{-1}$ ), the spectra were recorded in segments with the accumulation of 5 scans of 20 s each. For a short spectral range (600-1000  $\text{cm}^{-1}$ ), the spectra were recorded with the accumulation of 10 scans of 10 s scan each. A 10x working distance microscope objective was used to focus 50% of the laser power (25 mW) onto the sample.

- (5) Cabaniss, G. E.; Diamantis, A. A.; Murphy, W. R.; Linton, R. W.; Meyer, T. *J. J. Am. Chem. Soc.* **1985**, *107*, 1845.
- (6) Costentin, C.; Robert, M.; Savéant, J.-M.; Teillout, A.-L. *Proc. Natl. Acad. Sci. U.S.A.* **2009**, *106*, 11829.
- (7) Sawyer, D.T.; Sobkowiak, A. J.; Roberts, J. Jr. *Electrochemistry for Chemists*, 2nd ed., John Wiley & Sons: NY 1995.
- (8) Meites, L. *Handbook of Analytical Chemistry*, McGraw Hill: NY, 1963.

### Single-Crystal X-Ray Structure Determination.

Single crystals of **1**<sup>4+</sup> and **2**<sup>4+</sup> were obtained after the addition of some drops of an aqueous saturated NaClO<sub>4</sub> solution or an aqueous saturated NH<sub>4</sub>PF<sub>6</sub> solution to 0.1 M HOTf solutions of the complexes. Crystals were also obtained after the addition of some drops of an aqueous saturated NaClO<sub>4</sub> solution to catalytic solutions of the complexes, i. e., after the addition of 100 equivalents of CAN to 1 mM solutions of the complexes in 0.1 M HOTf. All measured crystals were prepared under inert conditions immersed in perfluoropolyether as the protecting oil for manipulation.

*Data collection.* Crystal structure determination for **1**<sup>4+</sup> and **2**<sup>4+</sup> was carried out using a Apex DUO Kappa 4-axis goniometer equipped with an APPEX 2 4K CCD area detector, a Microfocus Source E025 luS using MoK<sub>α</sub> radiation, Quazar MX multilayer Optics as monochromator and an Oxford Cryosystems low temperature device Cryostream 700 plus (*T* = -173 °C). Full-sphere data collection was used with  $\omega$  and  $\varphi$  scans. *Programs used:* Data collection APEX-2,<sup>7</sup> data reduction Bruker Saint<sup>5</sup> V/.60A.

*Structure solution and refinement.* Crystal structure solution was achieved using direct methods as implemented in SHELXTL<sup>8</sup> and visualized using the program XP. Missing atoms were subsequently located from difference Fourier synthesis and added to the atom list. Least-squares refinement on F<sup>2</sup> using all measured intensities was carried out using the program SHELXTL.<sup>9</sup> All non hydrogen atoms were refined including anisotropic displacement parameters.

(9) Data collection with APEX II version v2009.1-02. Bruker **2007**. Bruker AXS Inc., Madison, Wisconsin, USA.



- (10) Data reduction with Bruker SAINT versions V7.60A. Bruker **2007**.  
Bruker AXS Inc., Madison, Wisconsin, USA.
- (11) Sheldrick, G.M. *Acta Cryst.* **2008** A64, 112-122. SHELXTL version V6.14.

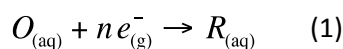
### Computational Methods.

*Density functional theory.* All geometries were fully optimized at the M06-L level<sup>12-14</sup> of density functional theory using the Stuttgart [8s7p6d2f | 6s5p3d2f] ECP28MWB contracted pseudopotential basis set<sup>15</sup> on Ru and the 6-31G(d) basis set<sup>16</sup> on all other atoms. Non-analytical integral evaluations made use of a pruned grid having 99 radial shells and 590 angular points per shell and an automatically generated density-fitting basis set was used within the resolution-of-the-identity approximation to speed the evaluation of Coulomb integrals as implemented in Gaussian 09 software package.<sup>17</sup> The nature of all stationary points was verified by analytic computation of vibrational frequencies, which were also used for the computation of zero-point vibrational energies, molecular partition functions (with all frequencies below 50 cm<sup>-1</sup> replaced by 50 cm<sup>-1</sup> when computing free energies), and for determining the reactants and products associated with each transition-state structure (by following the normal modes associated with imaginary frequencies). Partition functions were used in the computation of 298 K thermal contributions to free energy employing the usual ideal-gas, rigid-rotator, harmonic oscillator approximation.<sup>18</sup> Free energy contributions were added to single-point M06-L electronic energies computed with the SDD basis set on ruthenium and the 6-311+G(2df,p) basis set on all other atoms to arrive at final, composite free energies.

*Solvation and standard reduction potentials.* Solvation effects associated with water as solvent were accounted for using the SMD continuum solvation

model.<sup>19</sup> A 1 M standard state was used for all species in aqueous solution except for water itself, for which a 55.6 M standard state was employed. Thus, for all molecules but water, the free energy in aqueous solution is computed as the 1 atm gas-phase free energy, plus an adjustment for the 1 atm to 1 M standard-state concentration change of  $RT \ln (24.5)$ , or 1.9 kcal/mol, plus the 1 M to 1 M transfer (solvation) free energy computed from the SMD model. In the case of water, the 1 atm gas-phase free energy is adjusted by the sum of a 1 atm to 55.6 M standard-state concentration change, or 4.3 kcal/mol, and the experimental 1 M to 1 M solvation free energy,  $-6.3$  kcal/mol. The 1 M to 1 M solvation free energy of the proton was taken from experiment as  $-265.9$  kcal/mol.<sup>20-23</sup>

Standard reduction potentials were calculated for various possible redox couples to assess the energetic accessibility of different intermediates at various oxidation states. For a redox reaction of the form

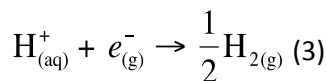


where  $O$  and  $R$  denote the oxidized and reduced states of the redox couple, respectively, and  $n$  is the number of electrons involved in redox reaction, the reduction potential  $E_{O|R}^{\circ}$  relative to NHE was computed as

$$E_{O|R}^{\circ} = -\frac{\Delta G_{O|R}^{\circ} - \Delta G_{\text{NHE}}^{\circ}}{nF} \quad (2)$$

where  $\Delta G_{O|R}^{\circ}$  is the free energy change associated with eq. 1 (using Boltzmann statistics for the electron),  $\Delta G_{\text{NHE}}^{\circ}$  is the free energy change associated with





which is  $-4.28$  eV with Boltzmann statistics for the electron,<sup>22,24,25</sup> and  $F$  is the Faraday constant. The calculated redox potentials were reported as E vs. SSCE by subtracting 0.244 V from E vs. NHE values.

*Non-single-determinantal state energies.* Several possible intermediates in the water oxidation mechanism have electronic structures that are not well described by a single determinant. In such instances, standard Kohn-Sham DFT is not directly applicable,<sup>18,26-28</sup> and we adopt the Yamaguchi broken-symmetry (BS) procedure<sup>29,30</sup> to compute the energy of the spin-purified low-spin (LS) state as

$${}^{\text{LS}}E = \frac{{}^{\text{BS}}E_{\dot{\epsilon}}^{\text{HS}} \langle S^2 \rangle_{\text{LS}} - {}^{\text{LS}}\langle S^2 \rangle_{\text{HS}} \dot{\epsilon} - {}^{\text{HS}}E_{\dot{\epsilon}}^{\text{BS}} \langle S^2 \rangle_{\text{LS}} - {}^{\text{LS}}\langle S^2 \rangle_{\text{HS}} \dot{\epsilon}}{{}^{\text{HS}}\langle S^2 \rangle_{\text{HS}} - {}^{\text{BS}}\langle S^2 \rangle_{\text{LS}}} \quad (4)$$

where HS refers to the single-determinantal high-spin coupled state that is related to the low-spin state by spin flip(s) and  $\langle S^2 \rangle$  is the expectation value of the total spin operator applied to the appropriate determinant. This broken-symmetry DFT approach has routinely proven effective for the prediction of state-energy splittings in metal coordination compounds.<sup>27,31-34</sup>

(12) Zhao, Y.; Truhlar, D. G. *J. Chem. Phys.* **2006**, *125*, 194101.

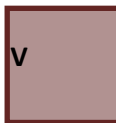
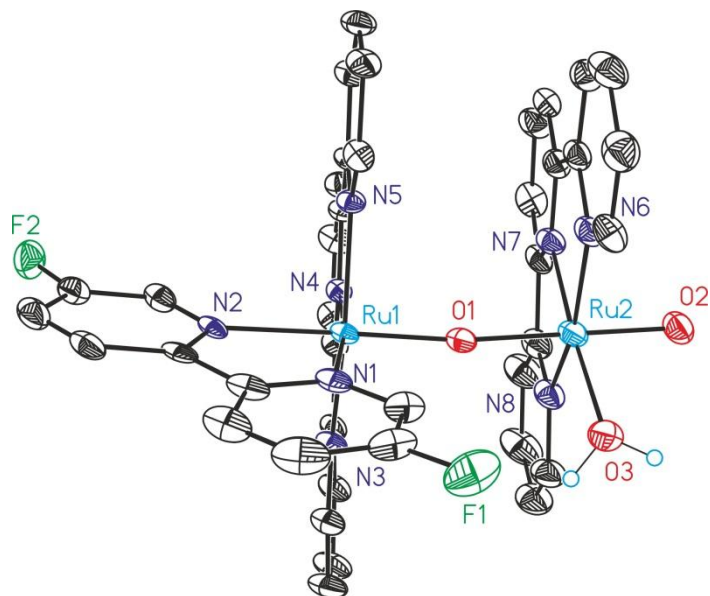
(13) Zhao, Y.; Truhlar, D. G. *Acc. Chem. Res.* **2008**, *41*, 157.

(14) Zhao, Y.; Truhlar, D. G. *Theor. Chem. Acc.* **2008**, *120*, 215.

- (15) Andrae, D.; Haussermann, U.; Dolg, M.; Stoll, H.; Preuss, H. *Theor. Chim. Acta* **1990**, *77*, 123.
- (16) Hehre, W. J.; Radom, L.; Schleyer, P. v. R.; Pople, J. A. *Ab Initio Molecular Orbital Theory*; Wiley: New York, 1986.
- (17) Frisch, M. J.; Trucks, G. W.; Schlegel, H. B.; Scuseria, G. E.; Robb, M. A.; Cheeseman, J. R.; Scalmani, G.; Barone, V.; Mennucci, B.; Petersson, G. A.; Nakatsuji, H.; Caricato, M.; Li, X.; Hratchian, H. P.; Izmaylov, A. F.; Bloino, J.; Zheng, G.; Sonnenberg, J. L.; Hada, M.; Ehara, M.; Toyota, K.; Fukuda, R.; Hasegawa, J.; Ishida, M.; Nakajima, T.; Honda, Y.; Kitao, O.; Nakai, H.; Vreven, T.; Montgomery, J. A.; Peralta, J. E.; Ogliaro, F.; Bearpark, M.; Heyd, J. J.; Brothers, E.; Kudin, K. N.; Staroverov, V. N.; Kobayashi, R.; Normand, J.; Raghavachari, K.; Rendell, A.; Burant, J. C.; Iyengar, S. S.; Tomasi, J.; Cossi, M.; Rega, N.; Millam, J. M.; Klene, M.; Knox, J. E.; Cross, J. B.; Bakken, V.; Adamo, C.; Jaramillo, J.; Gomperts, R.; Stratmann, R. E.; Yazyev, O.; Austin, A. J.; Cammi, R.; Pomelli, C.; Ochterski, J. W.; Martin, R. L.; Morokuma, K.; Zakrzewski, V. G.; Voth, G. A.; Salvador, P.; Dannenberg, J. J.; Dapprich, S.; Daniels, A. D.; Farkas, Ö.; Foresman, J. B.; Ortiz, J. V.; Cioslowski, J.; Fox, D. J. *Gaussian 09, Revision A.02*; Gaussian, Inc.: Wallingford, CT, 2010.
- (18) Cramer, C. J. *Essentials of Computational Chemistry: Theories and Models*; 2nd ed.; John Wiley & Sons: Chichester, 2004.
- (19) Marenich, A. V.; Cramer, C. J.; Truhlar, D. G. *J. Phys. Chem. B* **2009**, *113*, 6378.
- (20) Tissandier, M. D.; Cowen, K. A.; Feng, W. Y.; Gundlach, E.; Cohen, M. H.; Earhart, A. D.; Coe, J. V.; Tuttle, T. R. *J. Phys. Chem. A* **1998**, *102*, 7787.
- (21) Camaioni, D. M.; Schwerdtfeger, C. A. *J. Phys. Chem. A* **2005**, *109*, 10795.

- (22) Kelly, C. P.; Cramer, C. J.; Truhlar, D. G. *J. Phys. Chem. B* **2006**, *110*, 16066.
- (23) Bryantsev, V. S.; Diallo, M. S.; Goddard, W. A. *J. Phys. Chem. B* **2008**, *112*, 9709.
- (24) Lewis, A.; Bumpus, J. A.; Truhlar, D. G.; Cramer, C. J. *J. Chem. Educ.* **2004**, *81*, 596.
- (25) Winget, P.; Cramer, C. J.; Truhlar, D. G. *Theor. Chem. Acc.* **2004**, *112*, 217.
- (26) Ziegler, T.; Rauk, A.; Baerends, E. J. *Theor. Chim. Acta* **1977**, *43*, 261.
- (27) Noodleman, L. *J. Chem. Phys.* **1981**, *74*, 5737.
- (28) Cramer, C. J.; Truhlar, D. G. *Phys. Chem. Chem. Phys.* **2009**, *11*, 10757.
- (29) Yamaguchi, K.; Jensen, F.; Dorigo, A.; Houk, K. N. *Chem. Phys. Lett.* **1988**, *149*, 537.
- (30) Soda, T.; Kitagawa, Y.; Onishi, T.; Takano, Y.; Shigeta, Y.; Nagao, H.; Yoshioka, Y.; Yamaguchi, K. *Chem. Phys. Lett.* **2000**, *319*, 223.
- (31) Noodleman, L.; Peng, C. Y.; Case, D. A.; Mouesca, J.-M. *Coord. Chem. Rev.* **1995**, *144*, 199.
- (32) Ciofini, I.; Daul, C. A. *Coord. Chem. Rev.* **2003**, *238*, 187.
- (33) Harvey, J. N. *Struct. Bond.* **2004**, *112*, 151.
- (34) Neese, F. *Coord. Chem. Rev.* **2009**, *253*, 526.

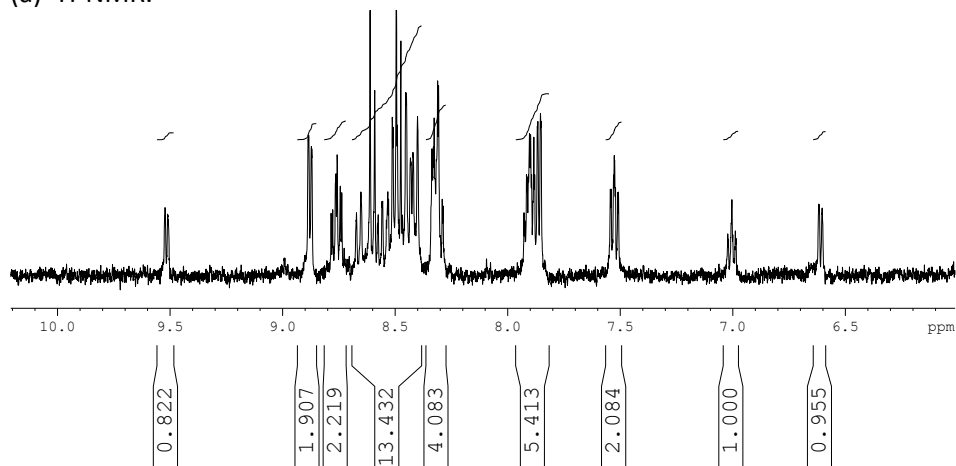
**Figure S 1.** Ortep plot (50 % probability) of the crystal structure of the complex  $5^{2+}$ . Color codes: Ru, cyan; N, navy blue; F, green; O, red. H atoms are not shown except for the aqua ligands that are represented as small light blue circles.



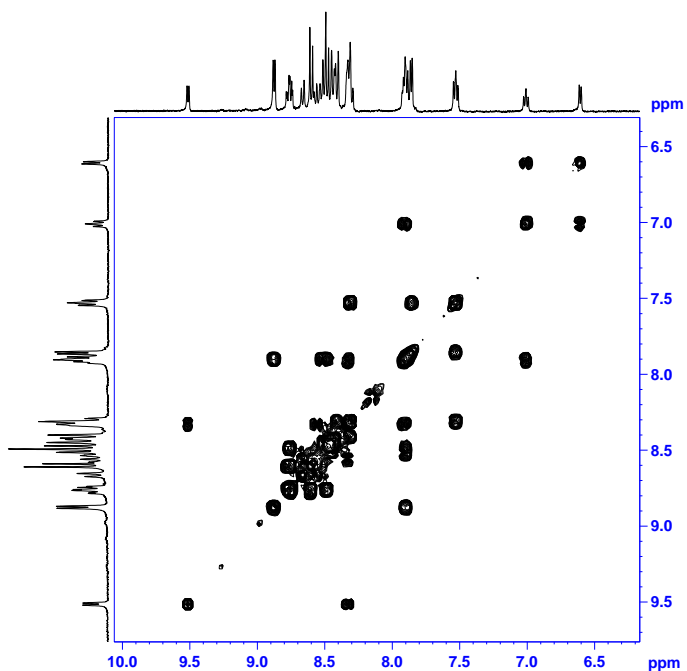
## NMR characterization.

**Figure S 2.** 1D and 2D NMR spectra (0.1 M DNO<sub>3</sub>) for complex **1**<sup>4+</sup>: (a) <sup>1</sup>H-NMR, (b) COSYD, (c) NOESY, (d) DOSY.

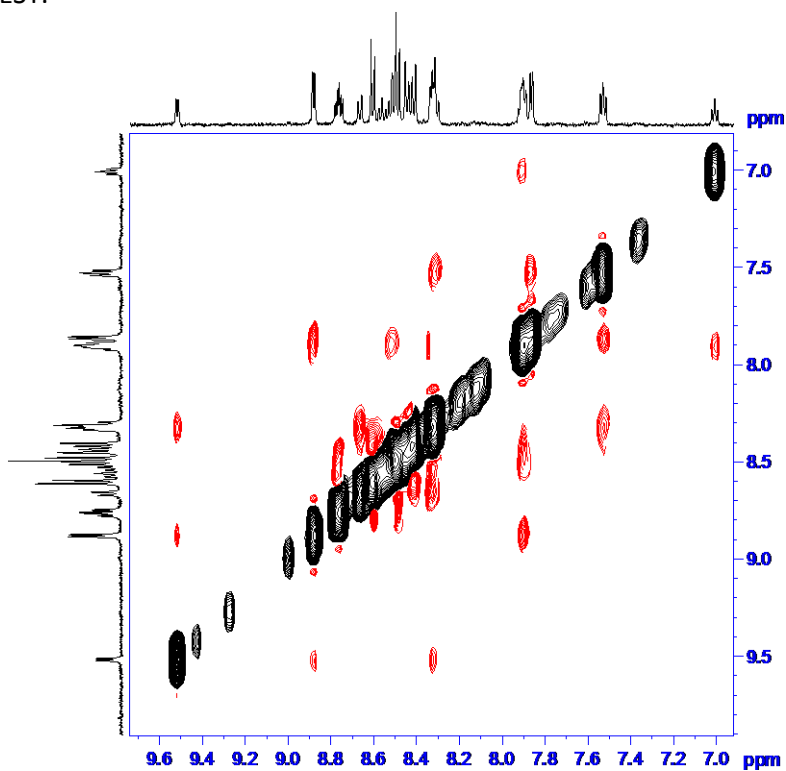
(a) <sup>1</sup>H-NMR.



(b) COSYD.



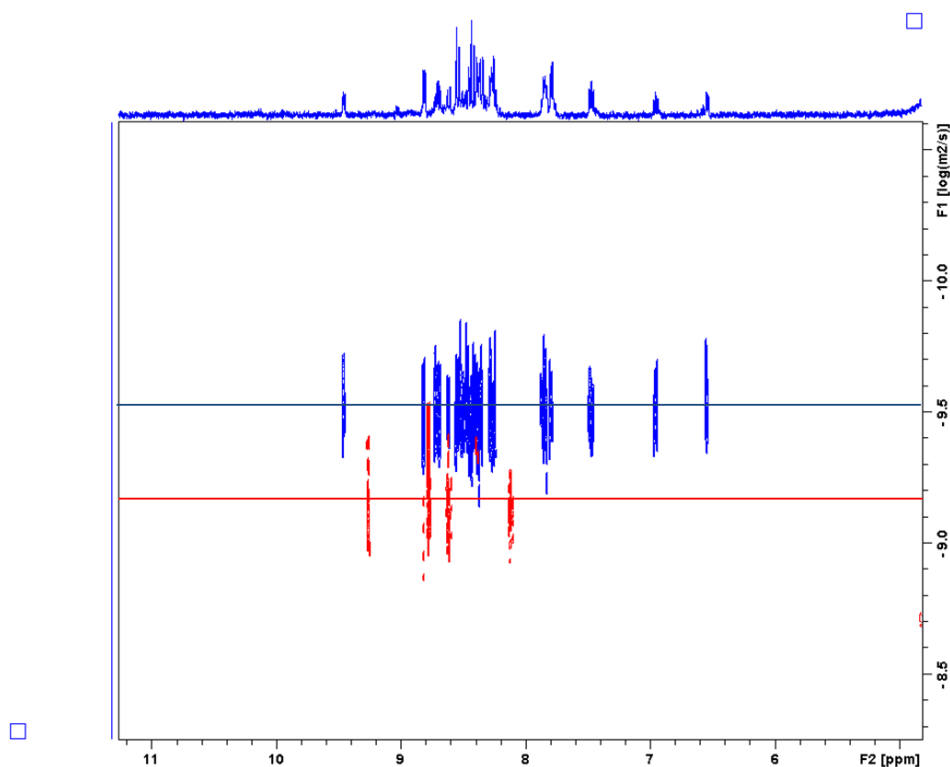
(c) NOESY.



V



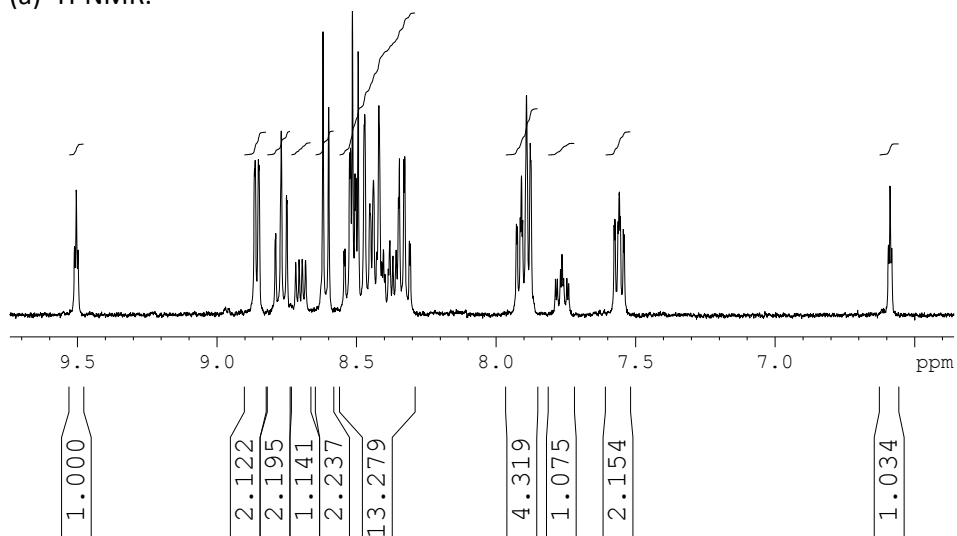
(d) DOSY experiments for 1 mM solutions of  $\mathbf{1}^{4+}$  (blue) and  $\mathbf{3}^{2+}$  (red) in  $\text{CF}_3\text{SO}_3\text{D}$  0.1 M. The  $^1\text{H}$ -NMR experiment of F2 axis corresponds to  $\mathbf{1}^{4+}$ .



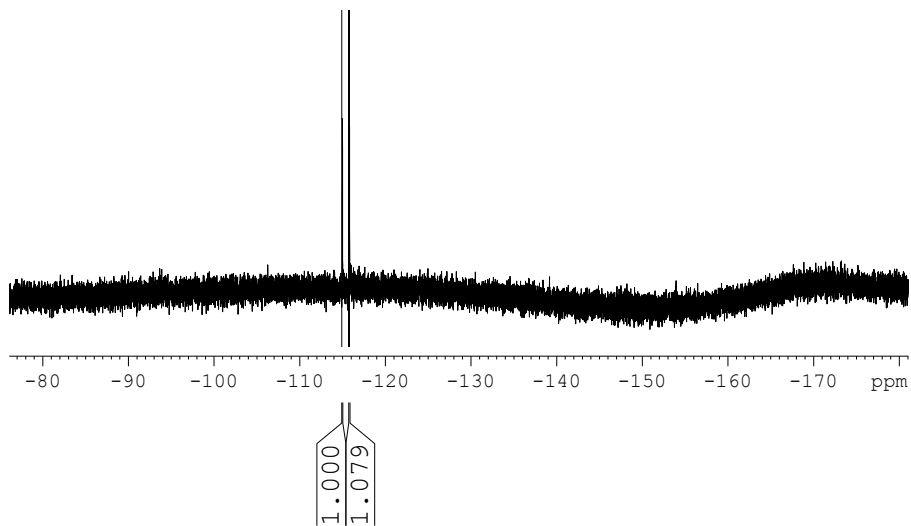
According to the relation between the diffusion coefficient ( $D$ ) and the hydrodynamic radius ( $r_s$ ) given by the Stokes-Einstein equation the ratio  $r_s(\text{dinuclear})/r_s(\text{mononuclear})$  can be calculated. The ratio is 2.29:1, it means that the dinuclear complex is 2.29 times larger than the mononuclear one. Additionally the DOSY experiment shows that the observed group of peaks for  $\mathbf{1}^{4+}$  belongs only to one compound.

**Figure S 3.** 1D and 2D NMR spectra (0.1 M DNO<sub>3</sub>) for complex **2<sup>4+</sup>**: (a) <sup>1</sup>H-NMR, (b) <sup>19</sup>F-NMR, (c) COSYD{<sup>19</sup>F}, (d) NOESY.

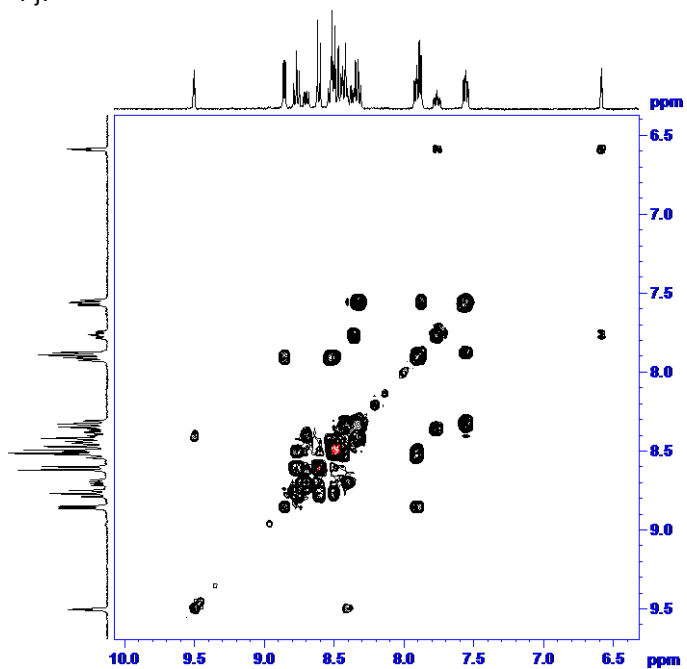
(a) <sup>1</sup>H-NMR.



(b) <sup>19</sup>F-NMR.



(c) COSYD{<sup>19</sup>F}.



(d) NOESY.

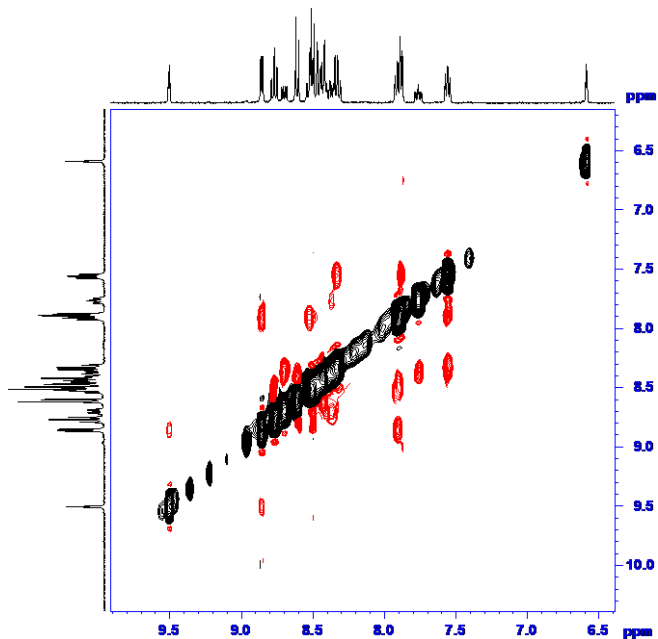
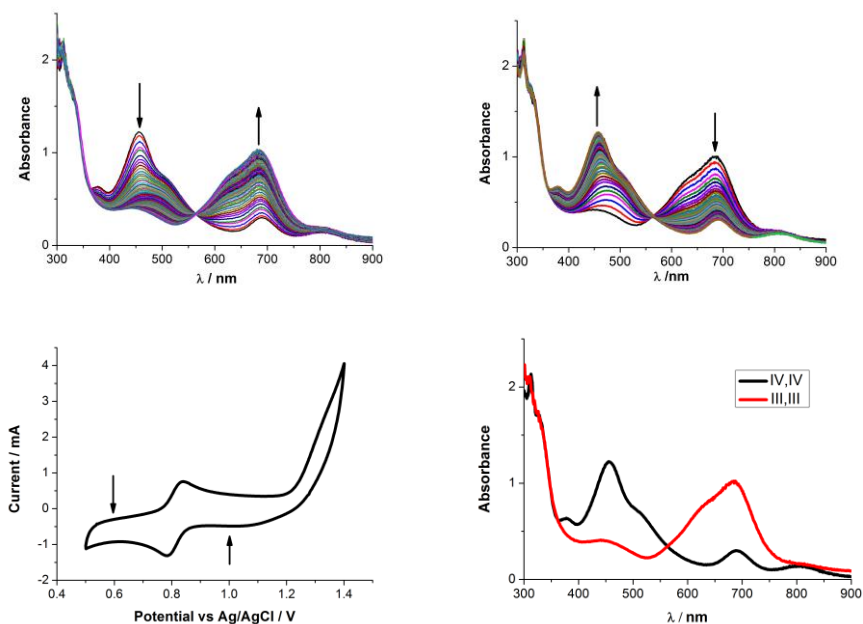


**Figure S 4.** Spectroelectrochemistry experiments of a 0.4 mM solution of  $\mathbf{1}^{4+}$  in 0.1 M HOTf. (Left upper)  $2e^-$  reduction at 0.6 V, (right upper)  $2e^-$  reoxidation at 1.0 V, (left bottom). CV experiment previous to electrolysis where the applied potentials are marked, (right bottom) UV-vis spectra of the oxidation states of the dinuclear complex. Pt mesh working electrode, Pt wire counter electrode and SSCE reference electrode.



V

**Figure S 5.** Differential Pulse Voltammetry (DPV) of 0.5 mM solutions of complexes **1**<sup>4+</sup> and **2**<sup>4+</sup> in 0.1 M HOTf. Activated boron-doped diamond working electrode, Pt wire counter electrode and Hg/Hg<sub>2</sub>SO<sub>4</sub>, K<sub>2</sub>SO<sub>4</sub> (sat) reference electrode.

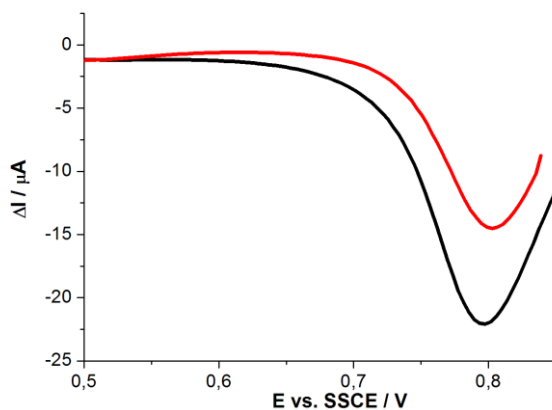


**Figure S 6.** Cyclic Voltammetry of 0.5 mM solutions of  $1^{4+}$  (black) and  $4^{2+}$  (red) in 0.1 M HOTf. Scan rate  $100 \text{ mV s}^{-1}$  using a polished glassy carbon working electrode, a Pt wire counter electrode and a Hg/Hg<sub>2</sub>SO<sub>4</sub>, K<sub>2</sub>SO<sub>4</sub> (sat) reference electrode.

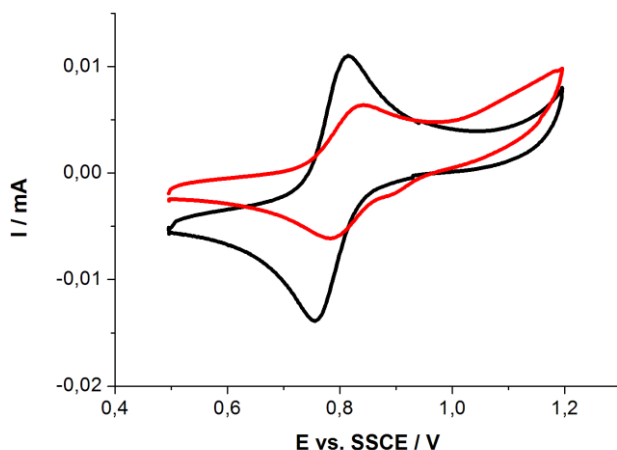


**Figure S 7.** Cyclic Voltammetry of 0.5 mM solutions of  $2^{4+}$  (black) and  $5^{2+}$  (red) in 0.1 M HOTf. Scan rate  $100 \text{ mV s}^{-1}$  using a polished glassy carbon working electrode, a Pt wire counter electrode and a Hg/Hg<sub>2</sub>SO<sub>4</sub>, K<sub>2</sub>SO<sub>4</sub> (sat) reference electrode.

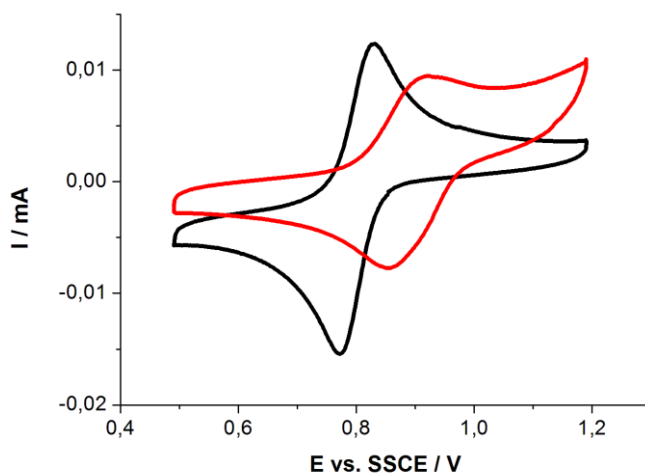


**Figure S 8.** Controlled potential electrolysis at 1.6 V vs. SSCE of a 0.4 mM solution of  $1^{4+}$  (black) and  $2^{4+}$  (red) complexes in 0.1 M HOTf and a blank experiment without catalyst (blue). Activated boron doped diamond as working electrode, Pt wire as counter electrode and Hg/Hg<sub>2</sub>SO<sub>4</sub>, K<sub>2</sub>SO<sub>4</sub> (sat) as reference electrode.

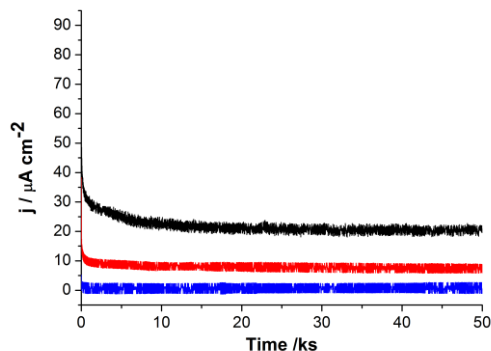


**Figure S 9.** Controlled potential electrolysis at 1.6 V vs. SSCE of a 0.4 mM solution of  $5^{2+}$  (black) and  $2^{4+}$  (red) complexes in 0.1 M HOTf and a blank experiment without catalyst (blue). Activated boron doped diamond as working electrode, Pt wire as counter electrode and Hg/Hg<sub>2</sub>SO<sub>4</sub>, K<sub>2</sub>SO<sub>4</sub> (sat) as reference electrode.

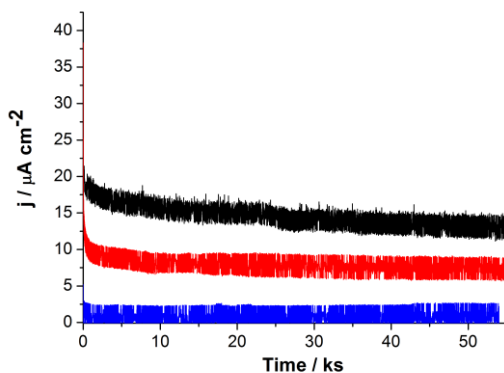
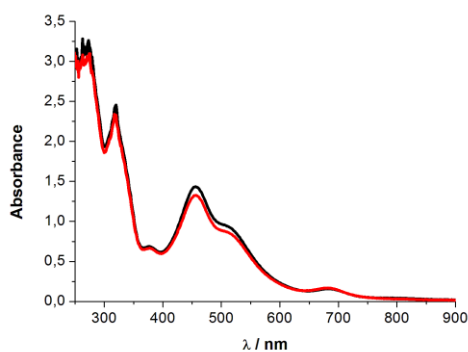
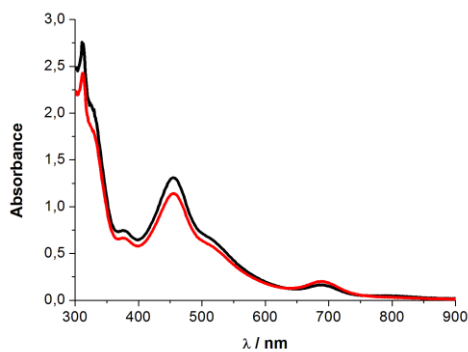


**Figure S 10.** UV-vis spectrums before (black) and after 10 hours (red) controlled potential electrolysis at 1.6 V vs. SSCE of a 0.4 mM solution of  $1^{4+}$  (upper) or  $2^{4+}$  (bottom) in 0.1 M HOTf with a 2 mm optical path length cuvette.



The slight decrease in intensity after the long CPE is due to partial migration of the complexes toward the cathode.





**Figure S 11.** (a) Left, rR spectrum of the reaction product obtained by the reaction of 3 equivalents of CAN with complex  $4^{2+}$  in 0.1 M HOTf after 1255 min (b) Right, overlay of the rR spectra of  $1^{4+}$  (black) in 0.1 M HOTf and (a) (red). The inset shows an enlargement of the fingerprint region.

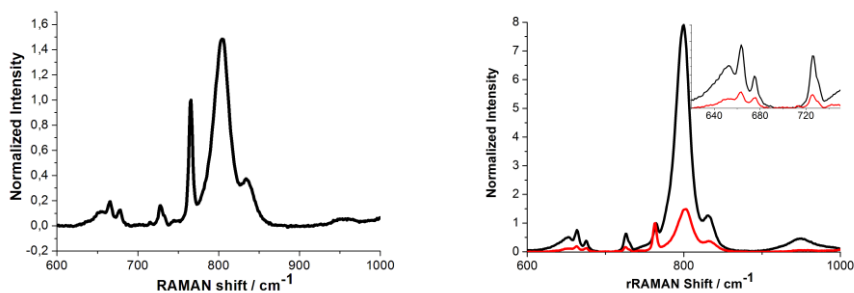


**Figure S 12.** rR spectra before (black) and 1200 min after the addition of 3 equivalents of CAN (red) to complex  $5^{2+}$  in 0.1 M HOTf.

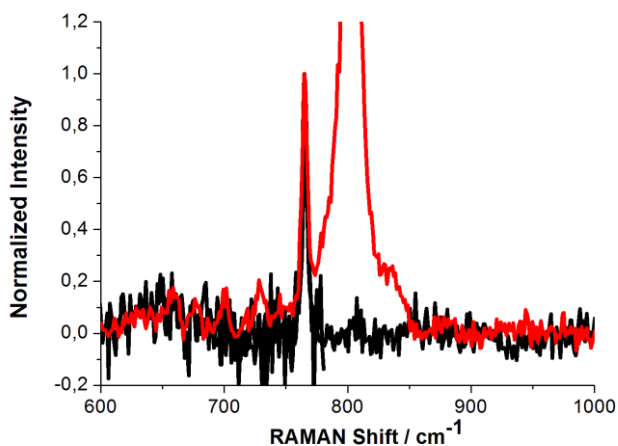


**Table S 1.** Crystal data for **1<sup>4+</sup>**.

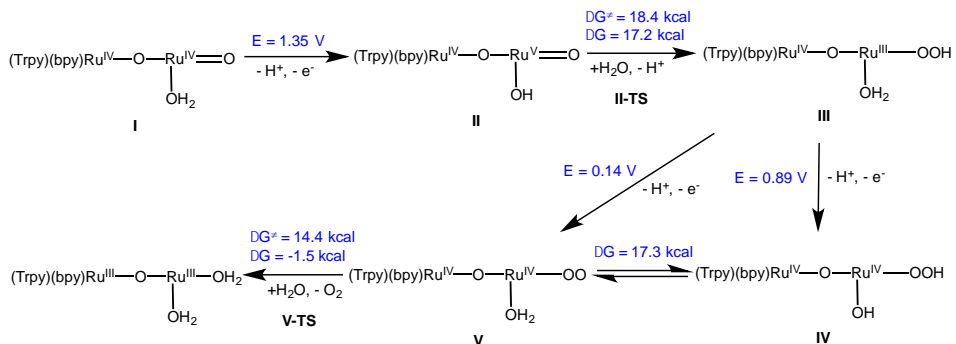
Empirical formula	C <sub>40</sub> H <sub>46</sub> Cl <sub>4</sub> N <sub>8</sub> O <sub>26</sub> Ru <sub>2</sub>
Formula weight	1398.79
Temperature	100(2)K
Wavelength	0.71073 Å
Crystal system	Triclinic
Space group	P-1
Unit cell dimensions	a = 12.4742(7) Å α = 89.112(2) ° b = 13.7076(8) Å β = 78.894(2) ° c = 16.8037(10) Å γ = 67.052(2) °
Volume	2590.7(3) Å <sup>3</sup>
Z	2
Density (calculated)	1.793 Mg/m <sup>3</sup>
Absorption coefficient	0.886 mm <sup>-1</sup>
F(000)	1412
Crystal size	0.15 x 0.10 x 0.02 mm <sup>3</sup>
Theta range for data collection	1.24 to 28.91 °
Index ranges	-16 ≤ h ≤ 11, -18 ≤ k ≤ 17, -21 ≤ l ≤ 22
Reflections collected	17692
Independent reflections	11086 [R(int) = 0.0246]
Completeness to theta = 28.91 °	0.812 %
Absorption correction	Empirical
Max. and min. transmission	0.9825 and 0.8785
Refinement method	Full-matrix least-squares on F <sup>2</sup>
Data / restraints / parameters	11086 / 174 / 799
Goodness-of-fit on F <sup>2</sup>	1.074
Final R indices [I > 2σ(I)]	R1 = 0.0463, wR2 = 0.1249
R indices (all data)	R1 = 0.0659, wR2 = 0.1414
Largest diff. peak and hole	1.686 and -0.976 e.Å <sup>-3</sup>

V

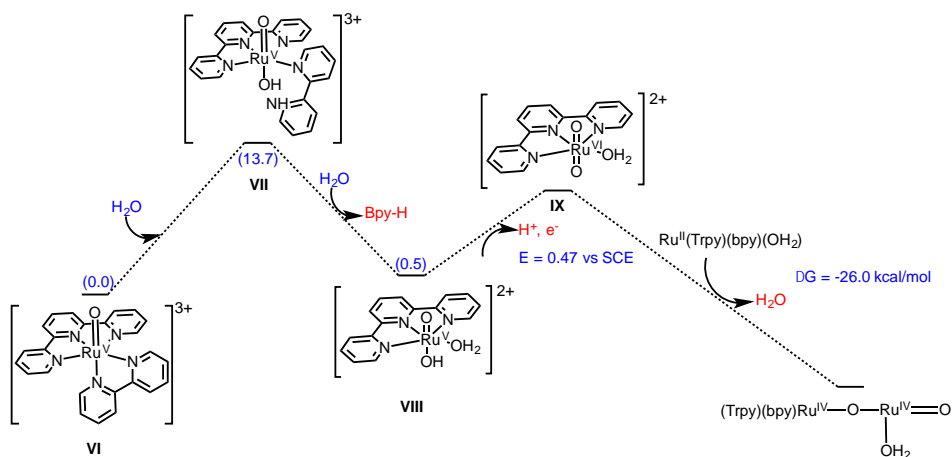
**Table S 2.** Crystal data for  $2^{4+}$ .

Empirical formula	C40 H36.50 F26 N8 O6.25 P4 Ru2
Formula weight	1549.29
Temperature	100(2)K
Wavelength	0.71073 Å
Crystal system	Triclinic
Space group	P-1
Unit cell dimensions	a = 13.872(2) Å $\alpha$ = 87.734(5) ° b = 14.290(2) Å $\beta$ = 67.502(5) ° c = 15.162(2) Å $\gamma$ = 69.971(5) °
Volume	2594.4(7) Å <sup>3</sup>
Z	2
Density (calculated)	1.983 Mg/m <sup>3</sup>
Absorption coefficient	0.856 mm <sup>-1</sup>
F(000)	1529
Crystal size	0.15 x 0.05 x 0.01 mm <sup>3</sup>
Theta range for data collection	1.46 to 26.85 °.
Index ranges	-15 <=h<=17, -17 <=k<=18, -19 <=l<=19
Reflections collected	39040
Independent reflections	11054 [R(int) = 0.0605]
Completeness to theta =26.85 °	0.990 %
Absorption correction	Empirical
Max. and min. transmission	0.9915 and 0.8824
Refinement method	Full-matrix least-squares on F <sup>2</sup>
Data / restraints / parameters	11054 / 343 / 865
Goodness-of-fit on F <sup>2</sup>	1.018
Final R indices [ $I > 2\sigma(I)$ ]	R1 = 0.0510, wR2 = 0.1228
R indices (all data)	R1 = 0.0864, wR2 = 0.1388
Largest diff. peak and hole	1.318 and -0.996 e.Å <sup>-3</sup>

**Scheme S 1.** Proposed mechanism for catalytic water oxidation by  $1^{4+}$  (denoted as I in the scheme) species.



**Scheme S 2.** Proposed mechanism for the generation  $3^{2+}$  (denoted as IX) and its subsequent interconversion to  $1^{4+}$ .



V

UNIVERSITAT ROVIRA I VIRGILI

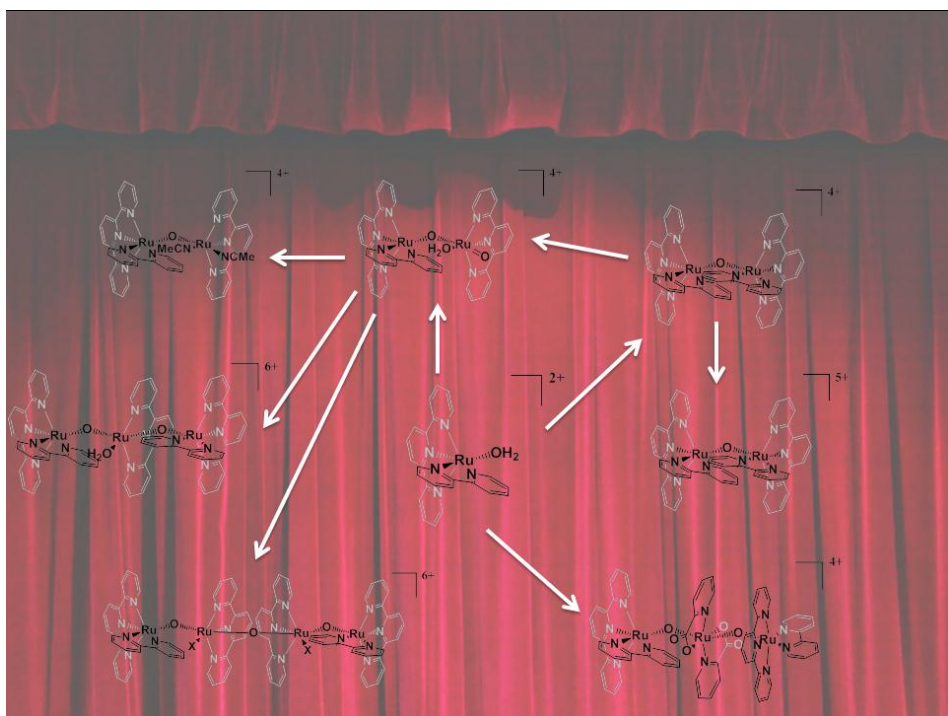
WATER OXIDATION WITH MONONUCLEAR RU COMPLEXES. BELOW THE TIP OF THE

ICEBERG: THE OXO-BRIDGE SCENARIO

Isidoro López Marin

Dipòsit Legal: T. 1505-2013

## Chapter 6. Behind Water Oxidation with Mononuclear Ru Complexes: The Oxo-bridge Scenario.



VI

Water oxidation catalysts (WOCs) based on mononuclear Ru complexes related to  $[\text{Ru}(\text{trpy})(\text{bpy})(\text{H}_2\text{O})]^{2+}$  (where trpy is 2,2':6',2''-terpyridine and bpy is 2,2'-bipyridine) generate dinuclear oxo bridge complexes throughout or after the catalytic cycle which have remained unnoticed. The new dimer compound  $\{[\text{Ru}(\text{trpy})(\text{bpy})]_2 (\mu\text{-O})\}^{4+}$  (**1-dm**<sup>4+</sup>) has been synthesized and completely characterized. The reactivity of this complex and previous known *O*-terminal dinuclear Ru complexes draws an oxo-bridge scenario of interconnected oxo bridge molecules with diverse nuclearity.

UNIVERSITAT ROVIRA I VIRGILI

WATER OXIDATION WITH MONONUCLEAR RU COMPLEXES. BELOW THE TIP OF THE

ICEBERG: THE OXO-BRIDGE SCENARIO

Isidoro López Marin

Dipòsit Legal: T. 1505-2013

**Table of Contents.****Chapter 6. Behind Water Oxidation with Mononuclear Ru complexes: The  
Oxo-bridge Scenario.**

<i>6.1. Introduction.</i>	223
<i>6.2. Experimental Section.</i>	225
<i>6.3. Results and discussion.</i>	229
<i>Oxidation of mononuclear complexes.</i>	230
<i>Reactivity of <b>1-dm</b><sup>4+</sup>.</i>	242
<i>Reactivity of <b>1-dn</b><sup>4+</sup>, <b>2-dn</b><sup>4+</sup> and <b>3-dn</b><sup>4+</sup> with organic     solvents.</i>	245
<i>6.4. Conclusions.</i>	251
<i>6.5. Acknowledgements.</i>	252
<i>6.6. References.</i>	252
<i>6.7. Supporting Information.</i>	257



UNIVERSITAT ROVIRA I VIRGILI

WATER OXIDATION WITH MONONUCLEAR RU COMPLEXES. BELOW THE TIP OF THE

ICEBERG: THE OXO-BRIDGE SCENARIO

Isidoro López Marin

Dipòsit Legal: T. 1505-2013

# Behind Water Oxidation with Mononuclear Ru complexes: The Oxo-bridge Scenario

Isidoro López,<sup>a</sup> Somnath Maji,<sup>a</sup> J. Benet-Buchholz<sup>a</sup> and Antoni Llobet<sup>a,b</sup>

<sup>a</sup> Institute of Chemical Research of Catalonia (ICIQ), Av. Països Catalans, 16, 43007 Tarragona, Spain.

<sup>b</sup> Departament de Química, Universitat Autònoma de Barcelona, Cerdanyola del Vallès, 08193 Barcelona, Spain.

## 6.1. Introduction.

The M-O-M linkage is a ubiquitous motif in bioinorganic chemistry. For instance it can be found in numerous proteins<sup>1-3</sup> with a Fe-O-Fe core or in the oxygen evolving complex (OEC) of photosystem II (PSII). The OEC consists of a Mn<sub>4</sub>CaO<sub>n</sub> cluster responsible for the oxidation of water to dioxygen. This process has gained an increasing interest to achieve an efficient conversion of sunlight into powerful chemical fuels as H<sub>2</sub> or CH<sub>3</sub>OH since water oxidation is one of the most difficult catalytic processes to develop a commercial device.

To mimic OEC, many polynuclear  $\mu$ -oxo high oxidation state metal complexes have been synthesized. The blue dimer was the first reported molecularly well characterized water oxidation catalyst and contains a Ru<sup>III</sup>-O-Ru<sup>III</sup> unit. Later on a di  $\mu$ -oxo dinuclear manganese(III,IV) catalyst was described, although later reports showed that this complex dimerizes in aqueous solution and only evolves oxygen with the help of an oxygen donor reagent.<sup>4</sup> Because oxygen bridges were said to be oxidative unstable, they were gradually replaced by rigid aromatic organic bridge ligands<sup>5-9</sup> or polyoxometalate scaffolds.<sup>10-13</sup>

On the other hand, the recent discovery of single site water oxidation catalyst<sup>6,14,15</sup> has avoided using bridge ligands. The successive pathways that lead to the evolution of dioxygen in complexes related to  $[\text{Ru}(\text{trpy})(\text{bpy})(\text{H}_2\text{O})]^{2+}$  (where trpy is 2,2':6',2''-terpyridine and bpy is 2,2'-bipyridine) have been extensively studied<sup>14,16</sup> and the accepted mechanism considers the key O-O bond forming step to be a water nucleophilic attack on a  $\text{Ru}^{\text{V}}\text{-O}$  moiety. Although the description has been reviewed and extended<sup>17,18</sup> several pathways could have been unnoticed, especially the ones producing deactivation product. In this sense, the dissociation of bpy and later oxidation to 2,2'-bipyridine *N, N*-dioxide has been pointed<sup>19</sup> as a source of catalyst decomposition when a huge excess of CAN is used as sacrificial oxidant at pH=1.

Recently our group has found<sup>20</sup> that mononuclear complexes partially evolve to dinuclear oxo bridge structures of general formula  $[(\text{trpy})(\text{bpy})\text{Ru}^{\text{IV}}(\mu\text{-O})\text{Ru}^{\text{IV}}(\text{trpy})(\text{O})(\text{H}_2\text{O})]^{4+}$  when high oxidation states are achieved. These compounds would explain the release of bpy from the coordination sphere of the initial complex. The formed dinuclear complexes are active and rugged water oxidation catalysts and its presence complements the accepted mechanism, showing that the system is much more complex than originally described (see chapter V). Furthermore, the formation of these  $\mu\text{-O}$  structures denote a trend for the production of oxo bridge scaffolds by mononuclear Ru complexes in high oxidation states like it happens with Fe<sup>2,21</sup> and Cu.<sup>21-23</sup>

In this report we examine the interconnection between  $\mu\text{-oxo}$  species generated after the chemical and electrochemical oxidation of mononuclear complexes related to  $[\text{Ru}(\text{trpy})(\text{bpy})(\text{H}_2\text{O})]^{2+}$  and discuss structural parameters derived from single crystal XRD.

## 6.2. Experimental section.

**Materials.** All reagents used in the present work were obtained from Aldrich Chemical Co. and were used without further purification.  $\text{RuCl}_3 \cdot 3\text{H}_2\text{O}$  was supplied by Alfa Aesar and was used as received. Trifluoromethanesulfonic acid (HOTf) was pursued from CYMIT. Reagent-grade organic solvents were obtained from SDS and high-purity deionized water was obtained by passing distilled water through a nanopure Milli-Q water purification system.

**Preparations.**  $[\text{Ru}(\text{trpy})(\text{bpy})(\text{H}_2\text{O})](\text{PF}_6)_2$  (**1<sup>2+</sup>**),<sup>24</sup>  $[\text{Ru}(\text{trpy})(5,5'\text{-F}_2\text{-bpy})(\text{H}_2\text{O})](\text{PF}_6)_2$  (**2<sup>2+</sup>**),<sup>25</sup>  $[\text{Ru}(\text{trpy})(6,6'\text{-F}_2\text{-bpy})(\text{H}_2\text{O})](\text{PF}_6)_2$  (**3<sup>2+</sup>**),<sup>25</sup>  $[(\text{trpy})(\text{bpy})\text{Ru}^{\text{IV}}(\mu\text{-O})\text{Ru}^{\text{IV}}(\text{trpy})(\text{O})(\text{H}_2\text{O})](\text{ClO}_4)_4$  (**1-dn<sup>4+</sup>**)<sup>20</sup> and  $[(\text{trpy})(5,5'\text{-F}_2\text{-bpy})\text{Ru}^{\text{IV}}(\mu\text{-O})\text{Ru}^{\text{IV}}(\text{trpy})(\text{O})(\text{H}_2\text{O})](\text{ClO}_4)_4$  (**2-dn<sup>4+</sup>**)<sup>20</sup> were prepared as described in the literature.

$\{[\text{Ru}(\text{trpy})(\text{bpy})]_2(\mu\text{-O})\}(\text{ClO}_4)_4 \cdot 7\text{H}_2\text{O}$  (**1-dm<sup>4+</sup>**).  $[\text{Ru}(\text{trpy})(\text{bpy})(\text{H}_2\text{O})](\text{PF}_6)_2$  (101.4 mg, 0.127 mmols) was dissolved in 0.1 M HOTf (127 mL). A amount of 100 equivalents of  $(\text{NH}_4)_2\text{Ce}(\text{NO}_3)_6$  (7.10 g, 12.700 mmols) dissolved in the minimum amount of 0.1 M HOTf was added to the previous stirred solution. The solution is left stirred for approximately 1 week and UV-vis monitored periodically. When the band at 688 nm seemed to achieve a maximum value, a saturated aqueous solution of  $\text{NaClO}_4$  (7 mL) was added. A dark green solid precipitated which was filtered and washed with some drops of cold water. The solid was collected and dried under vacuum overnight. Yield: 39.9 mg (45%). Anal. Calcd for  $\text{C}_{50}\text{H}_{50}\text{Cl}_4\text{N}_{10}\text{O}_{23}\text{Ru}_2$ : C, 39.48; H, 3.45; N, 9.21. Found: C, 39.24; H, 3.24; N, 9.07.

**Equipment and measurements.** UV/Vis spectroscopy was performed on a Cary 50 (Varian) UV/Vis spectrophotometer in 1 cm or 0.2 cm when indicated quartz cuvettes. Cyclic voltammetry (CV) and differential pulse voltammetry

(DPV) experiments were performed on an IJ-Cambria CHI-660 or a Bio-Logic SP-150 potentiostat using a three-electrode cell. Typical CV experiments were carried out at a scan rate of  $100 \text{ mV s}^{-1}$ . DPV experiments were carried out with the parameters: Pulses Height = 50 mV, Pulses Width = 50 ms, Step Height = 4 mV and Step Time = 200 ms. A glassy carbon electrode (3 mm diameter) was used as working electrode, platinum wire as auxiliary electrode, and SSCE as a reference electrode. Working electrodes were polished with 0.05 micron alumina paste, and rinsed with distilled water and acetone followed by blow-drying before each measurement. All cyclic voltammograms presented in this work were recorded in the absence of light and inside a Faradaic cage. The electrochemical experiments were carried out in 0.1 M  $\text{CF}_3\text{SO}_3\text{H}$  (pH 1.0).  $E_{1/2}$  values reported in this work were estimated from CV experiments as the average of the oxidative and reductive peak potentials  $(E_{p,a} + E_{p,c})/2$  or taken as  $E(I_{\text{max}})$  from DPV measurements.

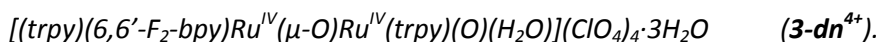
A 400 MHz Bruker Avance II spectrometer and a Bruker Avance 500 MHz were used to carry out NMR spectroscopy at room temperature. Samples were run in 0.1 M DOTf or  $\text{CD}_3\text{CN}$  with internal references (residual protons). Elemental analysis was performed using an EA-1108, CHNS-O elemental analyzer from Fisons Instruments.

Samples for resonance Raman spectroscopy were prepared typically by mixing a 1 mM solution of the starting complex with the desired amount of  $(\text{NH}_4)_2\text{Ce}(\text{NO}_3)_6$  and transferring 100  $\mu\text{L}$  of the reaction solution to a aluminium crucible and subsequently frozen at appropriate times in liquid  $\text{N}_2$ . Then, the crucible was placed into a Linkam THMS 600 temperature controlled cryo stage to keep the temperature at  $-12^\circ\text{C}$ . The rR spectrum was acquired using a Renishaw inVia Reflex RAMAN confocal microscope (Gloucestershire, UK),

equipped with an Ar-ion laser at 514 nm and a Peltier-cooled CCD detector (-70°C) coupled to a Leica DM-2500 microscope. Calibration was carried out daily by recording the Raman spectrum of an internal Si standard. Rayleigh scattered light was appropriately rejected by using edge-type filters. Spectrums were recorded with the accumulation of 5 scans with a 20 s scan time each one. A 10x working distance microscope objective was used to focus 50% of the laser power (25 mW) onto the sample.

On-line manometric O<sub>2</sub> measurements were carried out on a Testo 521 differential pressure manometer with an operating range of 1-100 hPa and accuracy within 0.5 % of the measurement. The manometer was coupled to thermostated reaction vessels for dynamic monitoring of the headspace pressure above each reaction. The manometer's secondary ports were connected to thermostated reaction vessels containing the same solvents and headspace volumes as the sample vials. A typical experiment consists in the addition of 100 equivalents of (NH<sub>4</sub>)<sub>2</sub>Ce(NO<sub>3</sub>)<sub>6</sub> previously dissolved in 100 μL of 0.1 M HOTf upon a solution of the catalyst in 1.850 mL of the same solvent containing the suitable amount of complex to yield 1 mM final concentration. This combination is termed catalytic solution.

#### Single crystal preparation.



Single crystals of **3-dn**<sup>4+</sup> could be grown at RT one week after the addition of some drops of a sat. aq. NaClO<sub>4</sub> solution to a catalytic solution of **3**<sup>2+</sup> in 0.1 M HOTf when oxygen evolution had finished.

$\{[Ru^{III}(trpy)(bpy)]_2(\mu-O)\}(ClO_4)_4 \cdot 4H_2O$  (**1-dm**<sup>4+</sup>). Single crystals could be obtained at RT 2 days after the addition of some drops of a sat. aq. NaClO<sub>4</sub> solution to concentrated solutions of **1-dm**<sup>4+</sup> in 0.1 M HOTf.

$\{[Ru^{III}(trpy)(bpy)(\mu-O)]_2Ru^{IV}(pic)_2\}(ClO_4)_4$  (**4<sup>4+</sup>**). A amount of 10 equivalents of picolinic acid was added to a catalytic solution of **1<sup>2+</sup>** in 0.1 M HOTf when oxygen evolution had finished. The formation of **4<sup>4+</sup>** was tracked by the increase of a band at 688 nm in the UV-vis spectrum. Single crystals could be precipitated at RT 5 days after the addition of some drops of a sat. aq. NaClO<sub>4</sub> solution to the above solution when the increase of the band was negligible.

$\{[Ru^{III.5}(trpy)(bpy)]_2(\mu-O)\}(ClO_4)_4 \cdot 3/2H_2O$  (**1-dm<sup>5+</sup>**). Single crystals of **1-dm<sup>5+</sup>** could be grown at RT 5 days after the addition of some drops of a sat. aq. NaClO<sub>4</sub> solution to a catalytic solution of **1-dm<sup>4+</sup>** in 0.1 M HOTf when oxygen evolution had finished.

$\{(trpy)(bpy)Ru^{III}(\mu-O)Ru^{III}(trpy)(CH_3CN)_2\}(PF_6)_4 \cdot H_2O \cdot CH_3CN$  (**1-dn<sub>CH3CN</sub><sup>4+</sup>**),  
 $\{(trpy)(6,6'-F_2-bpy)Ru^{III}(\mu-O)Ru^{III}(trpy)(CH_3CN)_2\}(PF_6)_4 \cdot CH_3CN$  (**3-dn<sub>CH3CN</sub><sup>4+</sup>**),  
 $\{[(trpy)(bpy)Ru^{II}(\mu-O)Ru^{IV}(trpy)(CH_3CN)]_2(\mu-O)\}(PF_6)_6 \cdot xCH_3CN$  (**1-tn<sup>6+</sup>**),  
 $\{[(trpy)(5,5'-F_2-bpy)Ru^{III}(\mu-O)Ru^{IV}(trpy)(CH_3COO)]_2(\mu-O)\}(ClO_4)_6 \cdot 2H_2O$  (**2-tn<sup>6+</sup>**)  
and  $\{[(trpy)(6,6'-F_2-bpy)Ru^{II}(\mu-O)Ru^{IV}(trpy)(CH_3CN)]_2(\mu-O)\}(PF_6)_4(ClO_4)_2 \cdot 3/2CH_3CN$  (**3-tn<sup>6+</sup>**). Single crystals for all these complexes could be obtained by the same procedure. The compounds were dissolved in CH<sub>3</sub>CN and approximately 10 μL of a sat. aq. solution of NH<sub>4</sub>PF<sub>6</sub> were added. Crystals were grown by slow vapor diffusion of Et<sub>2</sub>O into the solutions.

$\{[Ru^{III}(trpy)(bpy)(\mu-O)]_2Ru^{IV}(trpy)(H_2O)\}(ClO_4)_5(PF_6) \cdot 2H_2O$  (**5<sup>6+</sup>**). Single crystals for this complex were grown at RT 3 days after the addition of acetone to a solution of **1-dn<sup>4+</sup>** in 0.1 M HOTf containing some drops of a sat. aq. solution of NH<sub>4</sub>PF<sub>6</sub>. The ratio acetone/water was approximately 1:1.

**Single-Crystal X-Ray Structure Determination.** All measured crystals were prepared under inert conditions immersed in perfluoropolyether as the protecting oil for manipulation.

*Data collection.* Crystal structure determination was carried out using a Apex DUO Kappa 4-axis goniometer equipped with an APPEX 2 4K CCD area detector, a Microfocus Source E025 IuS using MoK $\alpha$  radiation, Quazar MX multilayer Optics as monochromator and an Oxford Cryosystems low temperature device Cryostream 700 plus ( $T = -173$  °C). Full-sphere data collection was used with  $\omega$  and  $\varphi$  scans. *Programs used:* Data collection APEX-2,<sup>26</sup> data reduction Bruker Saint V/.60A.<sup>27</sup>

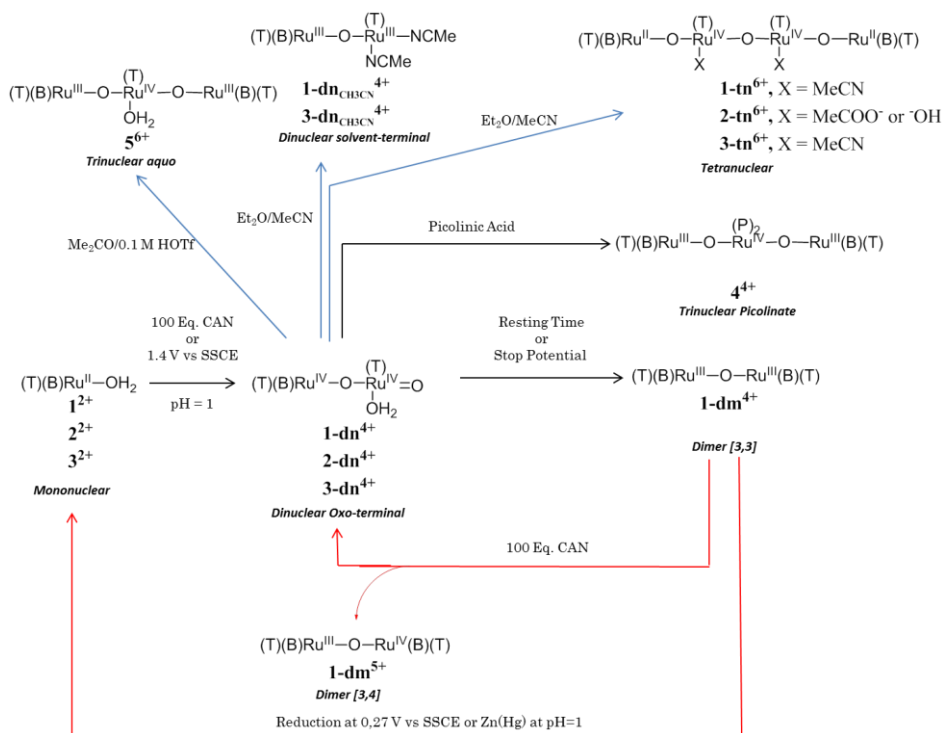
*Structure solution and refinement.* Crystal structure solution was achieved using direct methods as implemented in SHELXTL<sup>28</sup> and visualized using the program XP. Missing atoms were subsequently located from difference Fourier synthesis and added to the atom list. Least-squares refinement on  $F^2$  using all measured intensities was carried out using the program SHELXTL. All non hydrogen atoms were refined including anisotropic displacement parameters. In the case of **1-tn**<sup>6+</sup> the program SQUEEZE<sup>29</sup> was applied in order to avoid the highly disordered solvent molecules leading to a refined model with a R1 value of 6.34 % in which all the solvent molecules were removed. The crystals obtained for **1-tn**<sup>6+</sup> were diffracting extremely weak so that only a completeness of 93.6 % could be reached at a resolution of  $\sin(\theta/\lambda) = 0.6$ .

### 6.3. Results and discussion.

The oxidation of the mononuclear complexes of the general formula  $[\text{Ru}^{\text{II}}(\text{trpy})(n,n'\text{-X}_2\text{-bpy})(\text{H}_2\text{O})]^{2+}$  [ $\text{X} = \text{H}$  (**1**<sup>2+</sup>);  $\text{X} = \text{F}$  and  $n=n'=5$  (**2**<sup>2+</sup>),  $\text{X} = \text{F}$  and  $n=n'=6$  (**3**<sup>2+</sup>)] generates  $\mu$ -oxo species with interesting properties and reactivity outlined in Scheme 1 which are presented below. The resulting oxo-bridge scenario can be divided into three parts according to the starting material used to obtain the derived complexes: 1) The route marked in black in Scheme 1

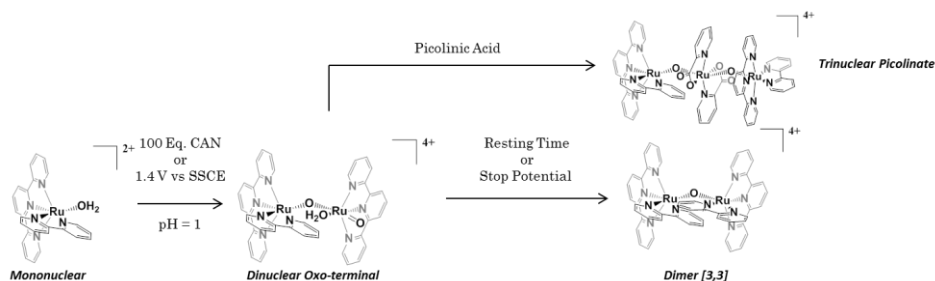


corresponds to the  $\mu$ -oxo species generated directly after the oxidation of the mononuclear complexes; 2) the red arrows indicate the reactivity associated to the dimer  $\{[Ru^{III}(trpy)(bpy)]_2(\mu-O)\}^{4+}$  (**1-dm<sup>4+</sup>**); 3) the processes marked in blue show the formation of polynuclear oxo-bridge structures from the reaction of the indicated organic solvents with the dinuclear oxo-terminal complexes.



**Scheme 1** Oxo bridge scenario derived from oxidation of mononuclear complexes. Abbreviation used for polypyridilic ligands: T = trpy, B = bpy and P = 2-picolinate.

**Oxidation of mononuclear complexes.** The reactivity of high oxidation states of mononuclear complexes is marked in black in Scheme 1 and depicted in Scheme 2.



**Scheme 2.** Reactivity of high oxidation states of mononuclear complexes.

Our group has reported recently<sup>20</sup> the partial conversion of the mononuclear complexes **1**<sup>2+</sup> and **2**<sup>2+</sup> to the dinuclear oxo compounds  $[(\text{trpy})(5,5'\text{-X}_2\text{-bpy})\text{Ru}^{\text{IV}}(\mu\text{-O})\text{Ru}^{\text{IV}}(\text{trpy})(\text{O})(\text{H}_2\text{O})]^{4+}$  (X = H, **1-dn**<sup>4+</sup>; X = F, **2-dn**<sup>4+</sup>) after chemical or electrochemical oxidation. Suitable crystals for XRD analysis of the dinuclear complex  $[(\text{trpy})(6,6'\text{-F}_2\text{-bpy})\text{Ru}^{\text{IV}}(\mu\text{-O})\text{Ru}^{\text{IV}}(\text{trpy})(\text{O})(\text{H}_2\text{O})]^{4+}$  (**3-dn**<sup>4+</sup>) could also be grown after oxidation of a 1 mM solution of complex **3**<sup>2+</sup> in HOTf with 100 equivalents of  $(\text{NH}_4)_2\text{Ce}(\text{NO}_3)_6$  (CAN) (Figure 1).

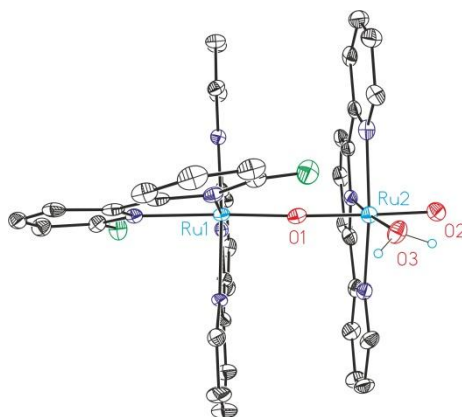


**Figure 1.** Ortep plot (ellipsoid drawn at 50 % probability) of the X-ray structure of **3-dn**<sup>4+</sup>. Color codes: Ru, cyan; O, Red; N, Blue; C, black; F, green. H atoms are not shown except for the aqua ligand that are represented as small light blue circles.

The main structural parameters of this series of dinuclear complexes are indicated in Table 1. The distances Ru(2)-O(terminal) fall in the lower range of

VI

Chapter 6

previous reported<sup>30-36</sup> Ru<sup>IV</sup>=O complexes; indeed, **3-dn**<sup>4+</sup> contains the shortest distance ever reported to the best of our knowledge.<sup>33</sup> The oxo bridge ligand does not lie equally separated from both metallic atoms, the Ru(2)-O<sub>bridge</sub> distance is shorter than the Ru(1)-O<sub>bridge</sub>. This contrasts with previous reported<sup>37-39</sup> Ru<sup>IV</sup>-O-Ru<sup>IV</sup> complexes where the two bonds have the same length (Table 1) and the molecules have a high symmetry. The structural asymmetry in the oxo bridge can be rationalized in terms of the different coordination environments at the metal atoms. The same feature was observed in the crystal structure of the oxidation state III,IV of the blue dimer.<sup>40</sup> On the another hand, the Ru<sup>IV</sup>-O-Ru<sup>IV</sup> angles are slightly bent respect to the ideal 180° found in the previous reported complexes because the steric constraint imposed by the proximity of the bipyridine ligand to the aquo group, thus the less steric demanding unmodified bipyridine in **1-dn**<sup>4+</sup> makes possible a more linear angle (175.5°) than that from **2-dn**<sup>4+</sup> and **3-dn**<sup>4+</sup> (171.5° and 172.6° respectively).

**Table 1.** Comparison of important bond distances (Å) and angles (deg) for several Ru<sup>IV</sup>-O-Ru<sup>IV</sup> and Ru<sup>III</sup>-O-Ru<sup>III</sup> complexes.

Complex <sup>a</sup>	Ru(2)-O <sub>terminal</sub>	Ru(2)-O <sub>bridge</sub>	Ru(1)-O <sub>bridge</sub>	Ru(1)-O-Ru(2)	Ref.
<b>1-dn</b> <sup>4+</sup>	1.747(3) <sup>b</sup>	1.832(3)	1.848(3)	175.43(18)	Tw. <sup>d</sup>
<b>2-dn</b> <sup>4+</sup>	1.738(4) <sup>b</sup>	1.830(3)	1.855(3)	171.5(2)	Tw.
<b>3-dn</b> <sup>4+</sup>	1.731(3) <sup>b</sup>	1.833(3)	1.850(3)	172.63(16)	Tw.
{[(OEP)ClRu <sup>IV</sup> ] <sub>2</sub> O} <sup>c</sup>		1.793(2)	1.793(2)	180	37
{[(OEP)(OH)Ru <sup>IV</sup> ] <sub>2</sub> O} <sup>c</sup>		1.847(13)	1.847(13)	180	38
{[Cl <sub>2</sub> Ru <sup>IV</sup> ] <sub>2</sub> O} <sup>4-c</sup>		1.80	1.80	180	39
Oxidation state III,III					
<b>1-dn</b> <sub>CH<sub>3</sub>CN</sub> <sup>4+e</sup>		1.864(4) <sup>f</sup>	1.865(4)	169.9(2)	Tw.
<b>3-dn</b> <sub>CH<sub>3</sub>CN</sub> <sup>4+</sup>		1.912(5) <sup>f</sup>	1.891(5)	166.1(3)	Tw.

<sup>a</sup>Ligand abbreviation: OEP = octaethylporphinate. <sup>b</sup> Ru(2) corresponds to Ru bound to oxo terminal ligand <sup>c</sup> High symmetry complexes with Ru(1)-O<sub>bridge</sub> = Ru(2)-O<sub>bridge</sub>. <sup>d</sup>This work. <sup>e</sup>The bipyridene and the acetonitrile ligands are disordered interchanging its positions with a ratio of 86:14 which means that Ru(1) and Ru(2) also do it. <sup>f</sup>Ru(2) corresponds to Ru bound to two CH<sub>3</sub>CN ligands.

The UV-vis spectroscopic monitoring of the oxidation of the mononuclear complex **1**<sup>2+</sup> with 100 equivalents of CAN shows an increasing absorption at 688 nm when oxygen evolution finishes (Figure 2) and the color of the solution becomes gradually green. This process consists in the slow dimerization of **1**<sup>2+</sup> into {[Ru<sup>III</sup>(trpy)(bpy)]<sub>2</sub>(μ-O)}<sup>4+</sup> (**1-dm**<sup>4+</sup>). The conversion achieves an 84 % after one week and the pure dimer can be precipitated by addition of sat. aqueous NaClO<sub>4</sub>.

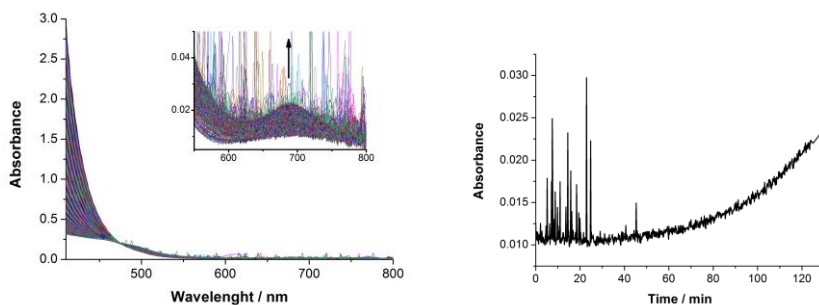


**Figure 2.** Left, UV-vis spectroscopic monitoring of the addition of 100 equivalent of CAN to a 1 mM solution of  $1^{2+}$  in 0.1 M HOTf at 25°C. The inset shows an enlargement of the 550-800 nm region. Right, absorption vs. time profile at 688 nm. A 2 mm optical pass length cuvette was used, the spikes are due to oxygen bubbles.

Suitable crystals for X-Ray diffraction analysis of  $1\text{-dm}^{4+}$  could be obtained by slow diffusion of diethyl ether into a solution of complex in acetonitrile or by addition of some drops of sat. aq.  $\text{NaClO}_4$  to a concentrated solution of complex in 0.1 M HOTf. The ORTEP of the single X-Ray structure of  $1\text{-dm}^{4+}$  is given in Figure 3. The structure consists in two  $[\text{Ru}^{\text{III}}(\text{trpy})(\text{bpy})]$  halves linked by an oxo bridge ligand in which each ruthenium center is in oxidation state III and octahedrally coordinated. The main structural parameters are collected in Table 2.

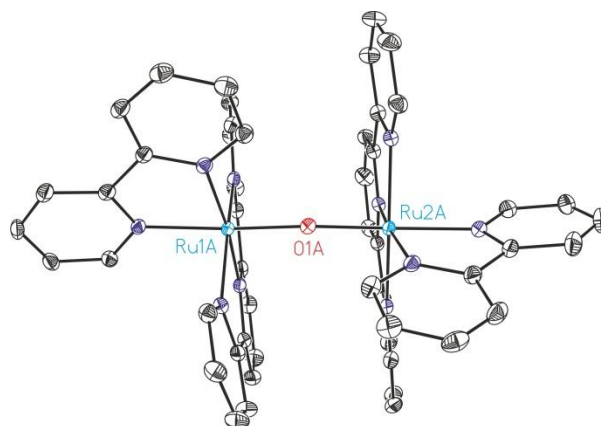


**Figure 3.** ORTEP plot (ellipsoid drawn at 50% probability) of the X-ray structure of complex **1-dm<sup>4+</sup>**. Color codes: Ru, cyan; O, Red; N, Blue; C, black. H atoms omitted for clarity.

The Ru-O distances are practically the same for both metallic atoms and are in the range of previous reported related complexes (see Table 2). However, we have observed that the length of the Ru-O bonds and the Ru-O-Ru angles depend strongly from the ligands coordinated to the Ru(III) atoms.

It is interesting to note the effect of the Ru-O-Ru angle on the magnetic properties of this kind of compounds which has been successfully rationalized<sup>41,42</sup> by Meyer *et al.* and it is showed in the MO diagram of Figure 4. If the Ru-O bond is taken as the z axis for each Ru site, the  $d_{xz}$  and  $d_{yz}$  orbitals from the metal atoms are mixed with two  $\pi$ -type p orbitals from the oxo bridging ligand. This produces three sets of bridge-based orbitals. The first set consists in two bonding orbitals ( $\pi_1^b$ ,  $\pi_2^b$ ) which have a large  $p_o$  character. The next set contains two non-bonding or slightly antibonding orbitals ( $\pi_1^{nb}$ ,  $\pi_2^{nb}$ ) which have a large  $d\pi_{Ru}$  character. Finally, the third set comprises two antibonding orbitals ( $\pi_1^*$ ,  $\pi_2^*$ ) which have also a large  $d\pi_{Ru}$  character. The electronic configuration for a dinuclear oxo bridge  $d^5$  Ru(III) complex depends on the degeneracy of the last set of orbitals. If the Ru-O-Ru angle is close to

$120^\circ$ ,  $\pi_1^*$  and  $\pi_2^*$  are not degenerated and the electronic configuration is  $(\pi_1^b)^2 (\pi_2^b)^2 (\pi_1^{nb})^2 (\pi_2^{nb})^2 (\pi_1^*)^2$ . Therefore, the complex is diamagnetic as it is observed in  $\{[\text{Ru}^{\text{III}}(\text{TAN})]_2(\mu\text{-O})(\mu\text{-CH}_3\text{CO}_2)_2\}^{2+43}$  and  $\{[\text{Ru}^{\text{III}}(\text{tpm})]_2(\mu\text{-O})(\mu\text{-O}_2\text{P}(\text{O})(\text{OH}))_2\}^{42}$ . If the Ru-O-Ru is more linear,  $\pi_1^*$  and  $\pi_2^*$  are degenerated and the complex consequently is paramagnetic since the two electrons arrange unpaired.

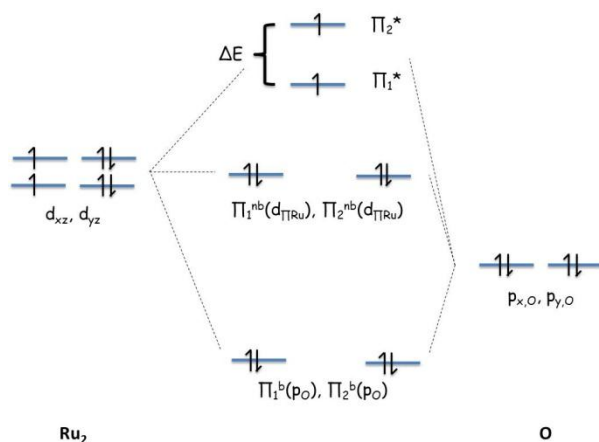


**Figure 4.** Qualitative MO diagram for the  $\pi$  system of Ru-O-Ru complexes.  $\Delta E$  depends on the angle of the moiety, the smaller the angle the larger the energetic separation. The electronic configuration illustrates the case of a  $d^5$ - $d^5$   $\text{Ru}^{\text{III}}$ -O- $\text{Ru}^{\text{III}}$  complex with a linear angle ( $180^\circ$ ).

**Table 2.** Comparison of important bond distances (Å) and angles (deg) for several Ru<sup>III</sup>-O-Ru<sup>III</sup> and Ru<sup>III</sup>-O-Ru<sup>IV</sup> complexes.

Complex <sup>a</sup>	Ru(1)-O <sub>bridge</sub>	Ru(2)-O <sub>bridge</sub>	Ru(1)-O-Ru(2)	Ref.
<b>1-dm<sup>4+</sup></b>	1.8819(12)	1.8810(12)	164.31(7)	Tw. <sup>b</sup>
{[Ru <sup>III</sup> (trpy)(C <sub>2</sub> O <sub>4</sub> )] <sub>2</sub> O}	1.841(8)	1.846(8)	148.5(4)	44
{[Ru <sup>III</sup> (TAN)(acac)] <sub>2</sub> (μ-O)} <sup>2+</sup>	1.913(1)	1.913(1)	180.0(1)	45
{[Ru <sup>III</sup> (bpy) <sub>2</sub> (NH <sub>3</sub> ) <sub>2</sub> (μ-O)] <sup>4+</sup>	1.894(2)	1.894(2)	158.2(4)	46
{[Ru <sup>III</sup> (bpy) <sub>2</sub> (H <sub>2</sub> O)] <sub>2</sub> (μ-O)] <sup>4+</sup>	1.869(1)	1.869(1)	165.4(3)	47
{[Ru <sup>III</sup> (bpy) <sub>2</sub> (NO <sub>2</sub> )] <sub>2</sub> (μ-O)} <sup>2+</sup>	1.890(7)	1.876(6)	157.2(3)	48
{[Ru <sup>III</sup> (TAN)] <sub>2</sub> (μ-O)(μ-CH <sub>3</sub> CO <sub>2</sub> ) <sub>2</sub> } <sup>2+</sup>	1.884(2)	1.884(2)	119.7(2)	43
{[Ru <sup>III</sup> (tpm)] <sub>2</sub> (μ-O)(μ-O <sub>2</sub> P(O)(OH) <sub>2</sub> )}	1.868(2)	1.868(2)	124.7(4)	42
Oxidation state III,IV				
<b>1-dm<sup>5+</sup></b>	1.846(2)	1.848(2)	169.90(13)	Tw.
[(bpy) <sub>2</sub> (H <sub>2</sub> O)Ru <sup>III</sup> ORu <sup>IV</sup> (OH)(bpy) <sub>2</sub> ] <sup>4+</sup>	1.847(12)	1.823(12)	170.0(7)	40
[(bpy) <sub>2</sub> (Cl)Ru <sup>III</sup> ORu <sup>IV</sup> (Cl)(bpy) <sub>2</sub> ] <sup>4+</sup>	1.845(9)	1.805(9)	170.7(5)	40
[(TAN)Ru <sup>III</sup> (O)(CH <sub>3</sub> CO <sub>2</sub> ) <sub>2</sub> Ru <sup>IV</sup> (TAN)] <sup>3+</sup>	1.849(5)	1.837(5)	130.1(3)	43

<sup>a</sup> Ligand abbreviations: TAN = 1, 4, 7-trimethyl-1, 4, 7-triazacyclononane, acac = pentane-2,4-dionate. <sup>b</sup> This work.

Thus the <sup>1</sup>H-NMR of **1-dm<sup>4+</sup>** presents paramagnetically shifted signals in the range of 30 to -20 ppm (Figure S1), similar spectrums can be observed in related Ru<sup>III</sup>-O-Ru<sup>III</sup> complexes.<sup>49</sup> The number of signals agrees with two symmetric [Ru(trpy)(bpy)] halves which indicates that the dimer has certain fluxionality in the solution through the oxo bridge and increases the symmetry respect to the single crystal X-Ray structure. The dinuclear character of **1-dm<sup>4+</sup>** was further corroborated by a DOSY (Diffusion Ordered NMR Spectroscopy)



experiment in CD<sub>3</sub>CN. The calculated hydrodynamic radius of **1-dm**<sup>4+</sup> according to the Stokes-Einstein equation is 1.93 times bigger than that of the mononuclear complex [Ru(trpy)(bpy)(CH<sub>3</sub>CN)]<sup>2+</sup> as it could be expected (Figure 5).

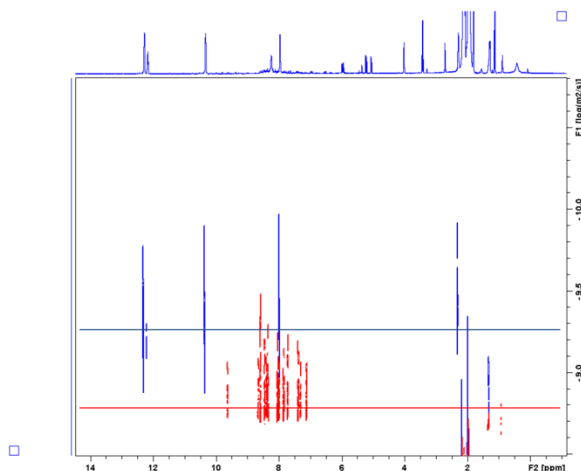
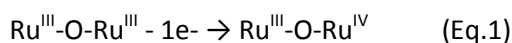
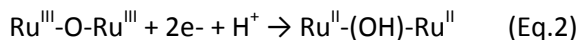


**Figure 5.** DOSY experiment for 1 mM solutions of **1-dm**<sup>4+</sup> (blue) and [Ru(trpy)(bpy)(CH<sub>3</sub>CN)]<sup>2+</sup> (red) in CD<sub>3</sub>CN. The <sup>1</sup>H-NMR experiment on the F2 axis corresponds to **1-dm**<sup>4+</sup>.

The electrochemical behavior of **1-dm**<sup>4+</sup> in 0.1 M HOTf was investigated by means of cyclic (CV) and differential pulse (DPV) voltammetries, Figure 6 shows the CV. The initial anodic scan from the open circuit potential until 1.4 V leads to a reversible wave at E<sup>0</sup> = 1.08 V (ΔE = 55 mV). This electrochemical process is the one electron oxidation in eq. 1 according to previous reported<sup>45,50</sup> related complexes.



After subsequent cathodic scan until 0 V an irreversible wave appears at E<sub>p,c</sub> = 0.22 V which is consistent with the 2 e- reduction in eq. 2. Furthermore protonation of the oxo bridge occurs according to literature.



The wave is irreversible because the formed reduced complex is unstable at  $\text{pH} = 1$  in the CV timescale and dimer cleavage takes place giving the mononuclear compounds. The second cycle of the CV experiment (dashed line in Figure 6) consequently showed a reversible wave at  $E^0 = 0.82 \text{ V}$  and a quasireversible one at  $E^0 = 0.98 \text{ V}$  that belong to  $1^{2+}$ .

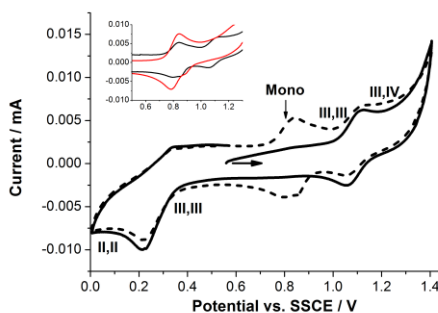


**Figure 6.** CV of  $1\text{-dm}^{4+}$  in 0.1 M HOTf, 1<sup>st</sup> cycle (solid line), 2<sup>nd</sup> cycle (dashed line). The inset shows a comparison of the second cycle (black) and a CV from a solution of  $1^{2+}$  (red) in the same solvent. Polished glassy carbon was used as working electrode, a Pt wire as counter electrode and SSCE as reference electrode. Scan rate =  $100 \text{ mV s}^{-1}$ .

The UV-vis spectrum of  $1\text{-dm}^{4+}$  presents a high intensity, lower energy band at 688 nm (Figure 7). This feature is typical of this kind of complexes (Table S1) and it has been associated to the overlapping of MLCT and bridge-based transitions.<sup>51,52</sup> Interestingly the oxidation of the mononuclear complexes  $1^{2+}$  and  $2^{2+}$  with only 2 or 3 equivalent of CAN produces the gradually increase of a band at the same wavelength observed for  $1\text{-dm}^{4+}$  (Figures S3 and S4), what it can cause misleading with an incipient hydroperoxo complex,<sup>53</sup>  $[\text{Ru}(\text{OOH})]^{2+}$ .

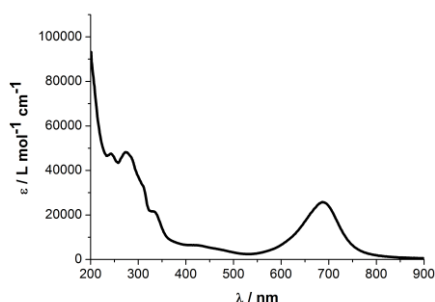
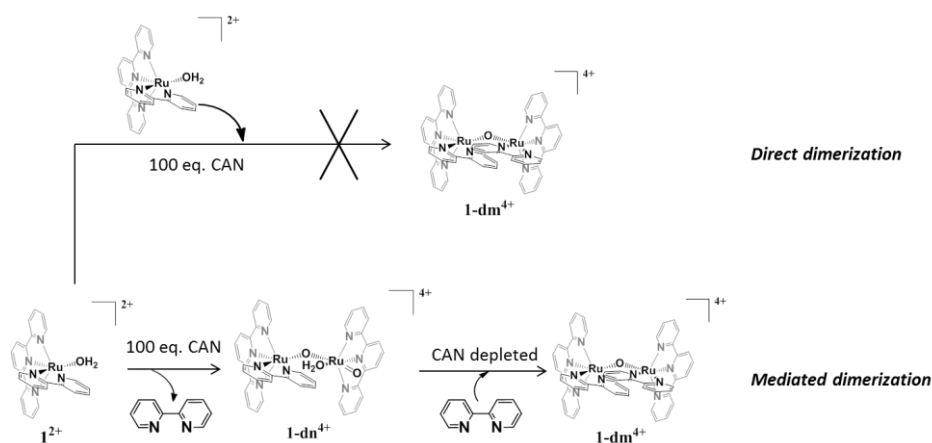


Figure 7. UV-vis spectrum of  $1\text{-dm}^{4+}$  in 0.1 M HOTf.

On the other hand, the possible molecular pathways for the conversion of  $1^{2+}$  into  $1\text{-dm}^{4+}$  have been considered. The dimerization process can occur by direct reaction between two molecules of  $1^{2+}$  (direct dimerization, Scheme 3) or by previous formation of  $1\text{-dn}^{4+}$  and subsequent coordination of free bipyridine (mediated dimerization, Scheme 3).



Scheme 3. Possible molecular pathways for the conversion of  $1^{2+}$  into  $1\text{-dm}^{4+}$ .

In order to get to know the mechanism 10 equivalents of 2-picolinate (pic) were added after catalytic dioxygen evolution by  $1^{2+}$  because in that moment the formation of  $1\text{-dm}^{4+}$  starts according to UV-vis spectroscopy. If  $1\text{-dm}^{4+}$  is produced by previous formation of  $1\text{-dn}^{4+}$  the final complex should be

mostly an oxo bridge asymmetric complex that contains a  $[\text{Ru}^{\text{III}}(\text{trpy})(\text{bpy})]$  half and a  $[\text{Ru}^{\text{III}}(\text{trpy})(\text{pic})]$  half since there is an excess of pic over free bpy, but the new trinuclear complex  $[(\text{trpy})(\text{bpy})\text{Ru}^{\text{III}}-\text{O}-\text{Ru}^{\text{IV}}(\text{pic})_2-\text{O}-\text{Ru}^{\text{III}}(\text{bpy})(\text{trpy})]^{4+}$  ( $4^{4+}$ ) was surprisingly crystallized from the solution (Figure 8).

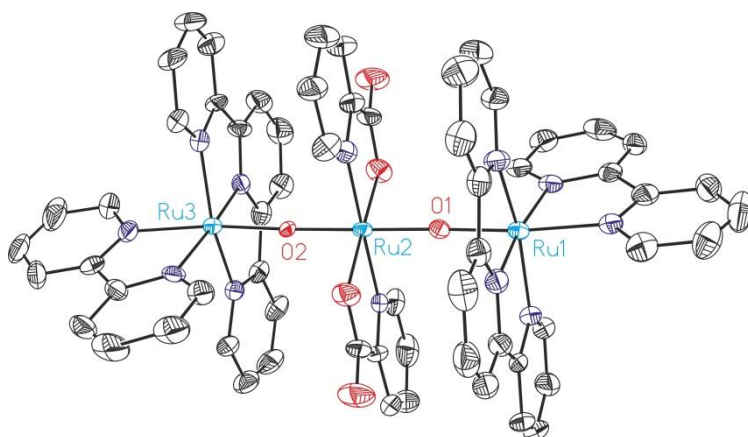


**Figure 8.** Ortep plot (ellipsoid drawn at 50% probability) of the X-ray structure of  $4^{4+}$ . Color codes: Ru, cyan; O, Red; N, Blue; C, black. H atoms are omitted for clarity.

The  $\text{Ru}^{\text{III}}-\text{O}-\text{Ru}^{\text{IV}}-\text{O}-\text{Ru}^{\text{III}}$  moiety was for the first time discovered in the Ruthenium Red,<sup>54</sup>  $\{[(\text{NH}_3)_5\text{Ru}^{\text{III}}(\mu-\text{O})]\text{Ru}^{\text{IV}}(\text{NH}_3)_4\}^{6+}$ . There is a small amount of structurally characterized oxo-bridge trinuclear complexes of ruthenium and some of them are heterometallic complexes<sup>55</sup> where ruthenium occupies the central position in the oxidation state IV. The main structural parameters for  $4^{4+}$  and some compounds are collected in Table 3. It can be observed that the  $\text{Ru}^{\text{IV}}-\text{O}$  distance is considerable shorter than that of  $\text{Ru}^{\text{III}}-\text{O}$  ( $\Delta d = 0.078 \text{ \AA}$ ), the clear difference could suggest a weak or negligible electronic coupling among Ru sites through the oxo ligands, indeed, a XPS experiment<sup>56</sup> on  $\{[(\text{H}_2\text{O})(\text{bpy})_2\text{Ru}^{\text{III}}(\mu-\text{O})]_2\text{Ru}^{\text{IV}}(\text{bpy})_2\}^{6+}$  showed the presence of chemically different sites. Further work about this issue will be carried out. The  $\text{Ru}^{\text{IV}}-\text{O}_{\text{Carboxylate}}$  bond ( $2.034 \text{ \AA}$ ) is shorter than that of reported<sup>57-59</sup> mononuclear

picolinate Ru(II) complexes (2.085-2.102 Å) and similar to that of a described<sup>60</sup> Ru(IV) piridinecarboxylate compound (2.068(3) Å).

The formation of **4<sup>4+</sup>** points out a pathway where **1-dn<sup>4+</sup>** is partly created after oxidation of **1<sup>2+</sup>**. When the oxidant depletes or the imposed potential is stopped the released free pyridine coordinates slowly into **1-dn<sup>4+</sup>** to produce the dimeric complex **1-dm<sup>4+</sup>** (Scheme 3). Pic seems to have a different reactivity compared to bpy mainly due to the carboxylate unit and produces the trinuclear complex instead of the dinuclear expected.

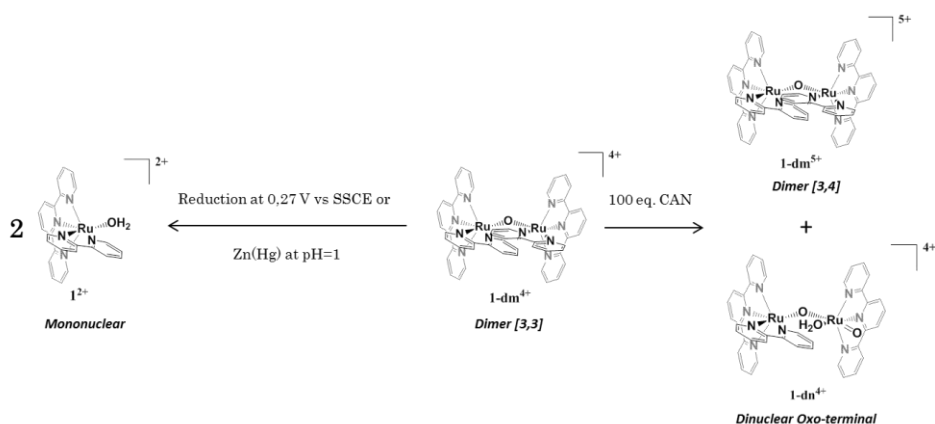
**Table 3.** Comparison of important bond distances (Å) and angles (degree) for several trinuclear M<sup>III</sup>-Ru<sup>IV</sup>-M<sup>III</sup> complexes.

Complex <sup>a</sup>	Ru <sup>IV</sup> -O	M <sup>III</sup> -O	Ru-O-M	Ref. <sup>c</sup>
<b>4<sup>4+</sup></b> <sup>b</sup>	1.799	1.877	175.0	Tw.
<b>5<sup>6+</sup></b>	1.821(3)	1.881(3)	166.0(2)	Tw.
{{(NH <sub>3</sub> ) <sub>5</sub> Ru <sup>III</sup> (μ-O)} <sub>2</sub> Ru <sup>IV</sup> (en) <sub>2</sub> } <sup>6+</sup>	1.850(4)	1.891(4)	177.2(4)	61
{{(BuNH <sub>2</sub> )((DPG)BF <sub>2</sub> ) <sub>2</sub> Fe <sup>III</sup> (μ-O)} <sub>2</sub> Ru <sup>IV</sup> (TPP')} <sup>b</sup>	1.799(11)	1.787(11)	175.0(7)	55
{{(Salmah)Fe <sup>III</sup> (μ-O)} <sub>2</sub> Ru <sup>IV</sup> (TPP)}	1.866(6)	1.848(6)	155.2(5)	62

<sup>a</sup> Ligand abbreviation: en = ethylenediamine, BuNH<sub>2</sub> = *n*-butylamine, (DPG)BF<sub>2</sub> = (difluoroboryl)-diphenylglyoximate, TPP' = tetrakis(4-methoxyphenylporphyrinate), Salmah = *N,N'*-(4-methyl-4-azaheptane-1,7-diyl)bis(salicylaldiminate), TPP = 5,10,15,20-tetraphenylporphyrinate. <sup>b</sup> The complex is noncentrosymmetric and the collected distances and angles correspond to an average. <sup>c</sup> Tw. means this work.

**Reactivity of 1-dm<sup>4+</sup>.** The redox chemistry of **1-dm<sup>4+</sup>** is marked with a red line in Scheme 1 and illustrated in Scheme 4. As it has been previously described, the electrochemical or chemical reduction of **1-dm<sup>4+</sup>** causes the

cleavage of the oxo bridge and generates two equivalents of  $1^{2+}$ . This behaviour is typical for related compounds.<sup>42,50</sup>



**Scheme 4.** Reactivity of  $1\text{-dm}^{4+}$ .

Although  $1\text{-dm}^{4+}$  lacks of an aquo ligand capable of working as active site for catalytic water oxidation, the activity of the dimer was tested using 100 equivalents of CAN as sacrificial oxidant. Surprisingly the dimer produces dioxygen in spite of the TON and TOF are low compare to the mononuclear parent compound  $1^{2+}$  (Figure S5). After the reaction the one electron oxidized form ( $1\text{-dm}^{5+}$ ) of the initial complex was crystallized (Figure S6), thus it seems that the scaffold of  $1\text{-dm}^{4+}$  is largely maintained under the described oxidative conditions.

The average Ru-O distance of the dimer (Table 2) is shortened after the oxidation from III,III to III,IV ( $1.882 - 1.847 = 0.035 \text{ \AA}$ ) which it is in agreement with a higher bond order for Ru-O because removing of an electron from the antibonding orbital  $\pi_2^*$ . Moreover, the two Ru-O bonds in  $1\text{-dm}^{5+}$  present almost the same length confirming that the strong coupling through the oxo bridge between the metallic atoms is preserved.

The catalytic activity by **1-dm**<sup>4+</sup> can be explained by the partial conversion of the dimer to the dinuclear complex **1-dn**<sup>4+</sup>, which has been demonstrated<sup>20</sup> to be an active and stable catalyst for water oxidation. RRAMAN monitoring of the addition of an excess of CAN to **1-dm**<sup>4+</sup> shows two remarkable features (Figure 9). First, the resonance of the highest intensity of the spectrum at 392 cm<sup>-1</sup> observed in **1-dm**<sup>4+</sup> before oxidant addition is shifted at 404 cm<sup>-1</sup>. This band is probably assigned to the  $\nu_s$  Ru-O-Ru mode.<sup>40,52,63</sup> The shift can be explained because the higher bond order of the Ru-O-Ru moiety in **1-dm**<sup>5+</sup>. Secondly, a new resonance appears at 801 cm<sup>-1</sup> which is consistent with the formation of a small amount of **1-dn**<sup>4+</sup>. The generated compound can react with the excess of CAN and produce catalytic water oxidation (Scheme 5).

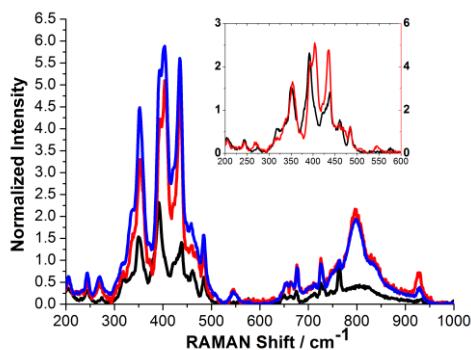
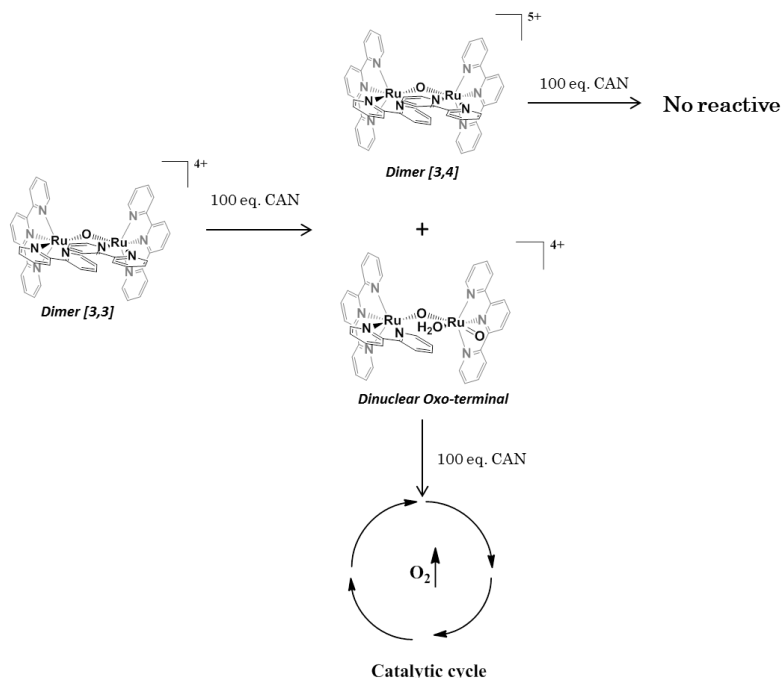


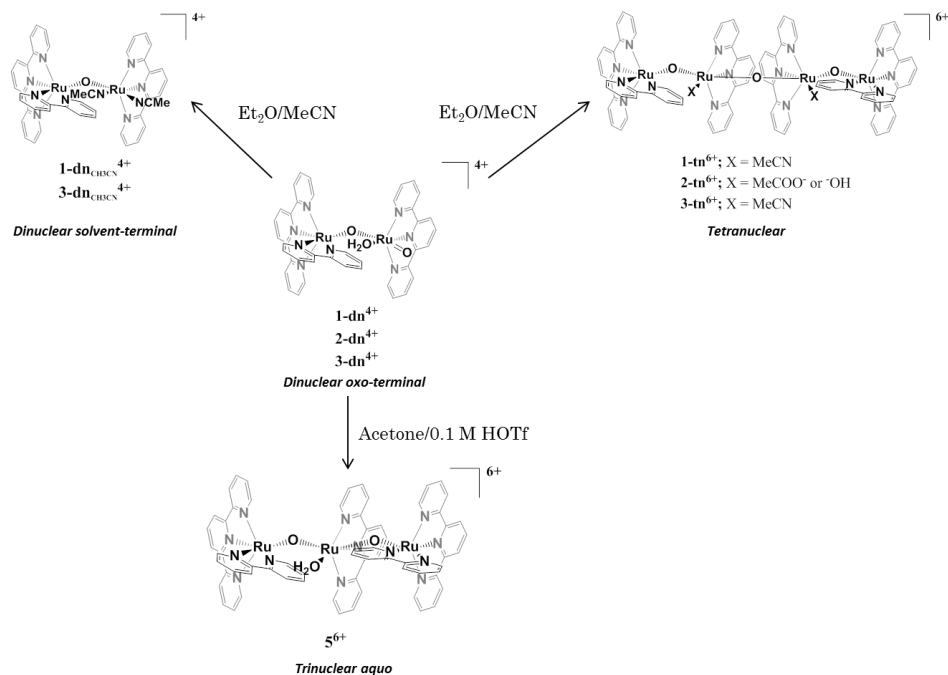
**Figure 9.** RRAMAN spectrums 30 s (red) and 9840 s (blue) after the addition of 100 equivalents of CAN to a 1 mM solution of **1-dm**<sup>4+</sup> in 0.1 M HOTf at 25°C. The spectrum before the reaction is also included (black). The inset shows the shift of the  $\nu_s$  Ru-O-Ru mode.



**Scheme 5.** Underlying processes in the catalytic water oxidation by **1-dm<sup>4+</sup>**.

**Reactivity of 1-dn<sup>4+</sup>, 2-dn<sup>4+</sup> and 3-dn<sup>4+</sup> with organic solvents.** Attempts of crystallization of the oxo terminal dinuclear complexes by slow vapour diffusion of Et<sub>2</sub>O into CH<sub>3</sub>CN solutions of the compounds or by mixtures of acetone and solutions of the complexes in 0.1 M HOTf produced new polynuclear oxo bridge complexes marked in blue in Scheme 1 and depicted in Scheme 6. The transformations can be rationalized in terms of the known high reactivity of Ru(IV) oxo complexes toward oxidation of organic compounds,<sup>34,64-66</sup> in this case the used solvents.





**Scheme 6.** Reactivity of dinuclear oxo-terminal complexes with organic solvents.

Single crystals of two Ru<sup>III</sup>-O-Ru<sup>III</sup> complexes were grown,  $1\text{-dn}_{\text{CH}_3\text{CN}}^{4+}$  and  $3\text{-dn}_{\text{CH}_3\text{CN}}^{4+}$ . The framework of these structures is the same as that from  $1\text{-dn}^{4+}$  and  $3\text{-dn}^{4+}$ , but the aquo and terminal oxo ligands have been replaced by two acetonitrile ligands (Figure 10 and S7). The Ru-O distances are longer than that from the parent dinuclear Ru<sup>IV</sup>-O-Ru<sup>IV</sup> compounds (Table 1) since the antibonding  $\pi_1^*$  and  $\pi_2^*$  orbitals are now partly occupied decreasing the bond order. The bent of the Ru-O-Ru angle is also striking and it has been observed in this work and previous studies (Table 2).

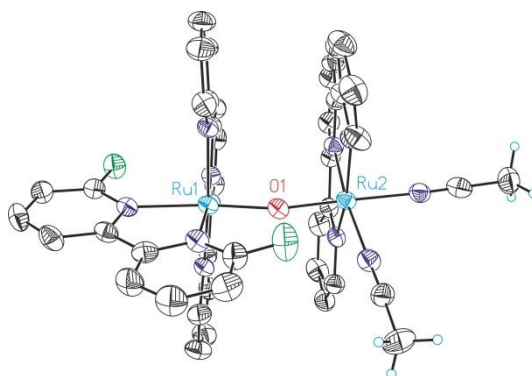


**Figure 10.** Ortep plot (ellipsoid drawn at 50% probability) of the X-ray structure of **3-dn<sup>4+</sup>**. Color codes: Ru, cyan; O, Red; N, Blue; C, black; F, green. H atoms are not shown except for the methyl groups from the acetonitrile ligands that are represented as small light blue circles.

The new aquo coordinated trinuclear complex  $\{[Ru^{III}(trpy)(bpy)(\mu-O)]_2Ru^{IV}(trpy)(H_2O)\}^{6+}$  (**5<sup>6+</sup>**) was also crystallized in organic media (Figure 11). As in the case of **4<sup>4+</sup>**, the Ru<sup>IV</sup>-O and the Ru<sup>III</sup>-O distances are significantly different suggesting a small coupling of the metallic atoms through the oxo bridge ligands (Table 3). The metal coordinated water molecule is disordered around the  $C_2$  axis in two positions (ratio 50:50) and one of the trpy ligands in the half molecule of the complex of the asymmetric unit is also disordered in two orientations (ratio 70:30). **5<sup>6+</sup>** is postulated as an attractive candidate to work as a robust water oxidation catalyst (WOC) considering that it presents a *trans* dioxo O-Ru-O conformation. This motif concedes a great stability to the highest oxidation states species and is the driving force for the formation of the rugged WOCs **1-dn<sup>4+</sup>** and **2-dn<sup>4+</sup>** from its mononuclear counterparts.<sup>20</sup>

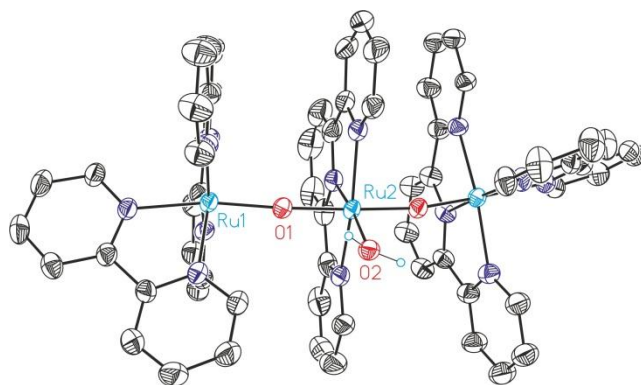


**Figure 11.** ORTEP plot (ellipsoid drawn at 50% probability) of the X-Ray structure of complex  $5^{6+}$ . Color codes: Ru, cyan; O, Red; N, Blue; C, black. H atoms are not shown except for the aqua ligand that are represented as small light blue circles.

On the other hand, the structure of the dinuclear complexes related to  $1\text{-dn}^{4+}$  suggests the possibility of a dimerization process to form tetranuclear oxo bridge complexes; indeed, it has been previously reported<sup>44</sup> that reduction of the mononuclear *trans* dioxo complex  $[\text{Ru}^{\text{VI}}(\text{trpy})(\text{O})_2(\text{H}_2\text{O})]^{2+}$  to  $[\text{Ru}^{\text{IV}}(\text{trpy})(\text{O})(\text{H}_2\text{O})_2]^{2+}$  generates quickly the dimer  $[(\text{trpy})(\text{H}_2\text{O})_2\text{Ru}^{\text{IV}}(\mu\text{-O})\text{Ru}^{\text{IV}}(\text{H}_2\text{O})_2(\text{trpy})]^{6+}$ . Single crystals suitable for X-Ray determination of the tetranuclear compounds  $1\text{-tn}^{6+}$ ,  $2\text{-tn}^{6+}$  and  $3\text{-tn}^{6+}$  could be grown in organic media. The ORTEP plot for  $3\text{-tn}^{6+}$  is presented in Figure 12 and those for  $1\text{-tn}^{6+}$  and  $2\text{-tn}^{6+}$  in Figures S8 and S9. The molecules have  $C_i$  symmetry with the inversion center placed in the central oxo bridge and consist in two  $[(\text{trpy})(\text{X}_2\text{-bpy})\text{Ru}(\mu\text{-O})\text{Ru}(\text{trpy})(\text{L})]$  halves, where  $\text{L} = \text{CH}_3\text{CN}$ ,  $\text{CH}_3\text{COO}^-$  or  $\text{OH}^-$ , linked by an oxo bridge ligand. The coordinated  $\text{CH}_3\text{COO}^-$  and  $\text{OH}^-$  in  $2\text{-tn}^{6+}$  derive probably from the hydrolysis of acetonitrile; this reaction has already been documented<sup>67,68</sup> in mononuclear Ru complexes.

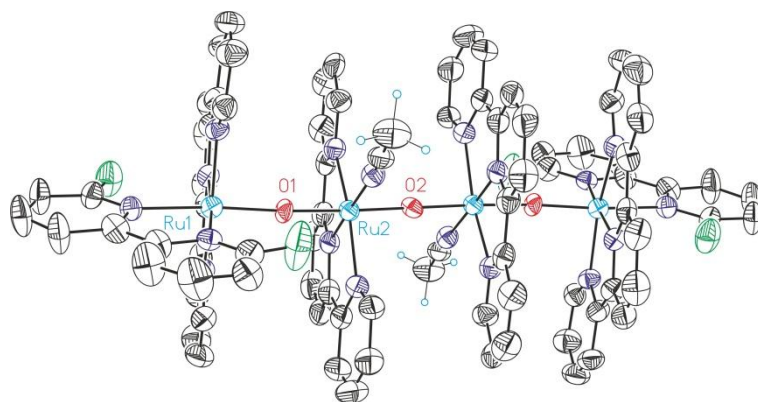


**Figure 12.** Ortep plot (ellipsoid at 50 % probability) of the X-ray structure of **3-tn<sup>6+</sup>**. Color codes: Ru, cyan; O, Red; N, Blue; C, black; F, green. H atoms are not shown except for the methyl groups from the acetonitrile ligands that are represented as small light blue circles.

The assignment of the oxidation states for the Ru atoms is controversial. If a strong coupling through the oxo bridge ligand is assumed the charge balance in **1-tn<sup>6+</sup>** and **3-tn<sup>6+</sup>** indicates that all the metallic atoms are in the oxidation state III,  $[\text{Ru}_2^{\text{III}}(\text{O}_1)\text{Ru}_1^{\text{III}}]_2$ . Because **2-tn<sup>6+</sup>** is a 2 electron oxidized form, the same consideration implies that the Ru atoms in this compound are in the oxidation state III.5,  $[\text{Ru}_2^{\text{III.5}}(\text{O}_1)\text{Ru}_1^{\text{III.5}}]_2$ . However, this distribution does not fit with the observed Ru-O bond distances (Table 4). The two Ru<sub>2</sub>-O bonds are clearly shorter than the Ru<sub>1</sub>-O one ( $\Delta d = 0.035\text{-}0.059 \text{ \AA}$ ) suggesting a different oxidation states for both atoms. If the different valence is taken into account, the charge balance in **1-tn<sup>6+</sup>** and **3-tn<sup>6+</sup>** provides a  $[\text{Ru}_2^{\text{IV}}(\text{O}_1)\text{Ru}_1^{\text{II}}]_2$  system where the central Ru atoms are in the oxidation state IV. However, another intermediate electronic distribution could be viable, for instance  $[\text{Ru}_2^{\text{III.5}}(\text{O}_1)\text{Ru}_1^{\text{II.5}}]_2$ , since the Ru<sup>III.5</sup>-O and Ru<sup>IV</sup>-O bonds cannot be crystallographically distinguished (see Table 1 and Table 2). The comparison of Ru-O distances in **2-tn<sup>6+</sup>** and **3-tn<sup>6+</sup>** supports the assignment  $[\text{Ru}_2^{\text{IV}}(\text{O}_1)\text{Ru}_1^{\text{II}}]_2$ .

Complex **2-tn<sup>6+</sup>** is a 2e<sup>-</sup> oxidized compound respect to **3-tn<sup>6+</sup>**. The oxidation does not affect the length of the Ru<sub>2</sub>-O bonds (Table 4) while shortens remarkably the Ru<sub>1</sub>-O bond (0.027 Å) what it can be interpreted as oxidation only occurring in the terminal Ru atoms. Ru-O bond distances in the formed [Ru<sub>2</sub><sup>IV</sup>(O<sub>1</sub>)Ru<sub>1</sub><sup>III</sup>]<sub>2</sub> complex, **2-tn<sup>6+</sup>**, are consistent with the oxidation states of all the Ru atoms. In contrast, if a completely delocalized through the oxo bridge ligand [Ru<sub>2</sub><sup>III</sup>(O<sub>1</sub>)Ru<sub>1</sub><sup>III</sup>]<sub>2</sub> system is assigned to **3-tn<sup>6+</sup>**, the oxidation should have an effect on all the Ru-O bonds that it is not observed. The presence of Ru atoms in different oxidation states inside an oxo bridge molecule has already been postulated in Ruthenium Reds as it was discussed above. Further work needs to be done in order to corroborate the electronic structure of the tetranuclear complexes. We are currently working in the synthesis of larger amounts of these compounds to carry out electrochemical, spectroscopic and magnetic studies.

**Table 4.** Comparison of important bond distances (Å) and angles (degree) for the tetranuclear complexes discovered in this work.

Complex	Ru <sub>2</sub> -O <sub>2</sub> <sup>a</sup>	Ru <sub>2</sub> -O <sub>1</sub> <sup>b</sup>	Ru <sub>1</sub> -O <sub>1</sub> <sup>c</sup>	Ru <sub>2</sub> -O-Ru <sub>1</sub>
<b>1-tn<sup>6+</sup></b>	1.8496(3)	1.839(2)	1.883(2)	169.67(15)
<b>2-tn<sup>6+</sup></b>	1.8364(3)	1.823(2)	1.865(3)	169.44(16)
<b>3-tn<sup>6+</sup></b>	1.8378(8)	1.829(6)	1.892(6)	168.10(4)

<sup>a</sup> Distance between the central Ru atom and the inner oxo bridge with the inversion center. <sup>b</sup> Distance between the central Ru atom and the outer oxo bridge. <sup>c</sup> Distance between the terminal Ru atom and the outer oxo bridge.

## 6.4. Conclusions.

Catalytic water oxidation by mononuclear Ru complexes affords dinuclear oxo bridge complexes with interesting properties and reactivities which define an intricate and strongly interconnected oxo-bridge scenario (Scheme 1).

The dinuclear compounds **1-dn**<sup>4+</sup>, **2-dn**<sup>4+</sup> and **3-dn**<sup>4+</sup> present an additional O-terminal ligand in *trans* position to the oxo bridge that gives a big stability to the molecules. **1-dn**<sup>4+</sup> and **2-dn**<sup>4+</sup> are active and rugged WOCs as reported<sup>20</sup> previously. The dimer complex **1-dm**<sup>4+</sup> has been isolated in high yield 1 week after the oxygen evolution by **1**<sup>2+</sup> had ceased and it has been completely characterized by analytical, spectroscopic and electrochemical techniques. The conversion of **1**<sup>2+</sup> into **1-dm**<sup>4+</sup> is not a simple bimolecular dimerization process. The crystallization of the Ruthenium Red **4**<sup>4+</sup> suggests that **1-dm**<sup>4+</sup> is formed after coordination of the previously released bpy ligand in the aquo and oxo positions of **1-dn**<sup>4+</sup>.

**1-dm**<sup>4+</sup> can work as WOC using CAN as sacrificial oxidant because partial formation of **1-dn**<sup>4+</sup> according to rRAMAN spectroscopy, although the major product of the process is the one electron oxidized form of the dimer, **1-dm**<sup>5+</sup>, which has been characterized by single crystal XRD.

The crystallization of **1-dn**<sup>4+</sup>, **2-dn**<sup>4+</sup> and **3-dn**<sup>4+</sup> in MeCN/Et<sub>2</sub>O and Me<sub>2</sub>CO/0.1 M HOTf mixtures provided several oxo bridge complexes with diverse nuclearity. The dinuclear compounds **1-dn**<sub>CH<sub>3</sub>CN</sub><sup>4+</sup> and **3-dn**<sub>CH<sub>3</sub>CN</sub><sup>4+</sup> retain the same scaffold that the parent compounds but the oxo terminal and the aquo ligands have been replaced by two acetonitrile ligands. The trinuclear complex **5**<sup>6+</sup> constitutes the second Ruthenium Red described in this work which is relevant due to the low number of structurally characterized examples

of this family in the literature. Finally, the tetranuclear complexes **1-tn<sup>6+</sup>**, **2-tn<sup>6+</sup>** and **3-tn<sup>6+</sup>** have been obtained. The Ru-O bond lengths in these structures suggest two different oxidation states for the Ru atoms inside each molecule which disagrees with the conception of a strong delocalized system through the oxo bridge ligands, however this interpretation is based in merely structural arguments, further electrochemical, spectroscopic and magnetic work must be done once considerable amounts of pure tetranuclear complexes are achieved in order to validate the information obtained by XRD.

The oxo-bridge scenario thoroughly studied in this work shows that mononuclear high oxidation state Ru complexes have a strong preference to form oxo bridge structures provided that no hindered ligands allow it. This reactivity parallels the known one for numerous mononuclear Fe complexes.<sup>21</sup> The resulting oxo bridge complexes are intimately related and can generate interesting molecules with higher nuclearity.

### 6.5. Acknowledgements.

Support from MINECO (CTQ2010-21497 and PRI-PIBIN-2011-1278) is gratefully acknowledged. SM thanks MINECO for a Torres Quevedo contract and IL for a FPU grant.

**Somnath has carried out the synthesis of the mononuclear complexes employed in this work.**

### 6.6. References.

- (1) Bertini, I.; Lalli, D.; Mangani, S.; Pozzi, C.; Rosa, C.; Theil, E. C.; Turano, P. *J. Am. Chem. Soc.* **2012**, *134*, 6169.
- (2) Tshuva, E. Y.; Lippard, S. J. *Chem. Rev. (Washington, DC, U. S.)* **2004**, *104*, 987.

- (3) Vincent, J. B.; Olivier-Lilley, G. L.; Averill, B. A. *Chem. Rev. (Washington, DC, U. S.)* **1990**, *90*, 1447.
- (4) Baffert, C.; Romain, S.; Richardot, A.; Leprêtre, J.-C.; Lefebvre, B.; Deronzier, A.; Collomb, M.-N. *J. Am. Chem. Soc.* **2005**, *127*, 13694.
- (5) Sens, C.; Romero, I.; Rodríguez, M.; Llobet, A.; Parella, T.; Benet-Buchholz, J. *J. Am. Chem. Soc.* **2004**, *126*, 7798.
- (6) Zong, R.; Thummel, R. P. *J. Am. Chem. Soc.* **2005**, *127*, 12802.
- (7) Deng, Z.; Tseng, H.-W.; Zong, R.; Wang, D.; Thummel, R. *Inorg. Chem.* **2008**, *47*, 1835.
- (8) Xu, Y.; Åkermark, T. r.; Gyollai, V.; Zou, D.; Eriksson, L.; Duan, L.; Zhang, R.; Åkermark, B. r.; Sun, L. *Inorg. Chem.* **2009**, *48*, 2717.
- (9) Karlsson, E. A.; Lee, B.-L.; Åkermark, T.; Johnston, E. V.; Kärkäs, M. D.; Sun, J.; Hansson, Ö.; Bäckvall, J.-E.; Åkermark, B. *Angew. Chem. Int. Ed.* **2011**, *50*, 11715.
- (10) Sartorel, A.; Miroñ, P.; Salvadori, E.; Romain, S.; Carraro, M.; Scorrano, G.; Valentin, M. D.; Llobet, A.; Bo, C.; Bonchio, M. *J. Am. Chem. Soc.* **2009**, *131*, 16051.
- (11) Geletii, Y. V.; Botar, B.; Kögerler, P.; Hillesheim, D. A.; Musaev, D. G.; Hill, C. L. *Angew. Chem. Int. Ed.* **2008**, *47*, 3896.
- (12) Yin, Q.; Tan, J. M.; Besson, C.; Geletii, Y. V.; Musaev, D. G.; Kuznetsov, A. E.; Luo, Z.; Hardcastle, K. I.; Hill, C. L. *Science* **2010**, *328*, 342.
- (13) Lv, H.; Geletii, Y. V.; Zhao, C.; Vickers, J. W.; Zhu, G.; Luo, Z.; Song, J.; Lian, T.; Musaev, D. G.; Hill, C. L. *Chem. Soc. Rev.* **2012**, *41*, 7572.
- (14) Concepcion, J. J.; Jurss, J. W.; Templeton, J. L.; Meyer, T. J. *J. Am. Chem. Soc.* **2008**, *130*, 16462.
- (15) Tseng, H.-W.; Zong, R.; Muckerman, J. T.; Thummel, R. *Inorg. Chem.* **2008**, *47*, 11763.
- (16) Concepcion, J. J.; Tsai, M.-K.; Muckerman, J. T.; Meyer, T. J. *J. Am. Chem. Soc.* **2010**, *132*, 1545.
- (17) Wasylenko, D. J.; Ganesamoorthy, C.; Henderson, M. A.; Koivisto, B. D.; Osthoff, H. D.; Berlinguette, C. P. *J. Am. Chem. Soc.* **2010**, *132*, 16094.
- (18) Polyansky, D. E.; Muckerman, J. T.; Rochford, J.; Zong, R.; Thummel, R. P.; Fujita, E. *J. Am. Chem. Soc.* **2011**, *133*, 14649.
- (19) Wasylenko, D. J.; Ganesamoorthy, C.; Koivisto, B. D.; Henderson, M. A.; Berlinguette, C. P. *Inorg. Chem.* **2010**, *49*, 2202.
- (20) Lopez, I.; Ertem, M. Z.; Maji, S.; Benet-Buchholz, J.; Keidel, A.; Kuhlmann, U.; Hildebrandt, P.; Batista, V. S.; Llobet, A. *Angew. Chem. Int. Ed.* **2013**, *submitted*.
- (21) *Activation of Small Molecules*; 1st ed.; Tolman, W. B., Ed.; WILEY-VCH: Weinheim, Germany, 2006.



- (22) Suzuki, M. *Acc. Chem. Res.* **2007**, *40*, 609.
- (23) Cramer, C. J.; Tolman, W. B. *Acc. Chem. Res.* **2007**, *40*, 601.
- (24) Takeuchi, K. J.; Thompson, M. S.; Pipes, D. W.; Meyer, T. J. *Inorg. Chem.* **1984**, *23*, 1845.
- (25) Maji, S.; López, I.; Bozoglian, F.; Benet-Buchholz, J.; Llobet, A. *Inorg. Chem.* **2013**, *52*, 3591.
- (26) Data collection with APEX II version v2009.1-0.2 **2009**. Bruker AXS Inc., Madison, Wisconsin, USA.
- (27) Data reduction with Bruker SAINT version V7.60A **2007**. Bruker AXS Inc., Madison, Wisconsin, USA.
- (28) Sheldrick, G. *Acta Crystallographica Section A* **2008**, *64*, 112.
- (29) Spek, A. J. *Appl. Crystallogr.* **2003**, *36*, 7.
- (30) Welch, T. W.; Ciftan, S. A.; White, P. S.; Thorp, H. H. *Inorg. Chem.* **1997**, *36*, 4812.
- (31) Che, C. M.; Lai, T. F.; Wong, K. Y. *Inorg. Chem.* **1987**, *26*, 2289.
- (32) Cheng, W.-C.; Yu, W.-Y.; Cheung, K.-K.; Che, C.-M. *J. Chem. Soc., Dalton Trans.* **1994**, 57.
- (33) Che, C. M.; Tang, W. T.; Wong, W. T.; Lai, T. F. *J. Am. Chem. Soc.* **1989**, *111*, 9048.
- (34) Kojima, T.; Nakayama, K.; Ikemura, K.; Ogura, T.; Fukuzumi, S. *J. Am. Chem. Soc.* **2011**, *133*, 11692.
- (35) Cheng, W.-C.; Yu, W.-Y.; Zhu, J.; Cheung, K.-K.; Peng, S.-M.; Poon, C.-K.; Che, C.-M. *Inorg. Chim. Acta* **1996**, *242*, 105.
- (36) Aoyagi, K.; Yukawa, Y.; Shimizu, K.; Mukaida, M.; Takeuchi, T.; Kakihana, H. *Bull. Chem. Soc. Jpn.* **1986**, *59*, 1493.
- (37) Masuda, H.; Taga, T.; Osaki, K.; Sugimoto, H.; Mori, M.; Ogoshi, H. *Bull. Chem. Soc. Jpn.* **1982**, *55*, 3887.
- (38) Masuda, H.; Taga, T.; Osaki, K.; Sugimoto, H.; Mori, M.; Ogoshi, H. *J. Am. Chem. Soc.* **1981**, *103*, 2199.
- (39) Deloume, J. P.; Faure, R.; Thomas-David, G. *Acta Crystallogr., Sect. B: Struct. Sci.* **1979**, *35*, 558.
- (40) Schoonover, J. R.; Ni, J.; Roecker, L.; White, P. S.; Meyer, T. J. *Inorg. Chem.* **1996**, *35*, 5885.
- (41) Weaver, T. R.; Meyer, T. J.; Adeyemi, S. A.; Brown, G. M.; Eckberg, R. P.; Hatfield, W. E.; Johnson, E. C.; Murray, R. W.; Untereker, D. *J. Am. Chem. Soc.* **1975**, *97*, 3039.
- (42) Llobet, A.; Curry, M. E.; Evans, H. T.; Meyer, T. J. *Inorg. Chem.* **1989**, *28*, 3131.
- (43) Neubold, P.; Wieghardt, K.; Nuber, B.; Weiss, J. *Inorg. Chem.* **1989**, *28*, 459.

- (44) Lebeau, E. L.; Adeyemi, S. A.; Meyer, T. J. *Inorg. Chem.* **1998**, *37*, 6476.
- (45) Schneider, R.; Weyhermueller, T.; Wieghardt, K.; Nuber, B. *Inorg. Chem.* **1993**, *32*, 4925.
- (46) Ishitani, O.; White, P. S.; Meyer, T. J. *Inorg. Chem.* **1996**, *35*, 2167.
- (47) Gilbert, J. A.; Eggleston, D. S.; Murphy, W. R.; Geselowitz, D. A.; Gersten, S. W.; Hodgson, D. J.; Meyer, T. J. *J. Am. Chem. Soc.* **1985**, *107*, 3855.
- (48) Phelps, D. W.; Kahn, E. M.; Hodgson, D. J. *Inorg. Chem.* **1975**, *14*, 2486.
- (49) Dobson, J. C.; Sullivan, B. P.; Doppelt, P.; Meyer, T. J. *Inorg. Chem.* **1988**, *27*, 3863.
- (50) Llobet, A.; Doppelt, P.; Meyer, T. J. *Inorg. Chem.* **1988**, *27*, 514.
- (51) Liu, F.; Concepcion, J. J.; Jurss, J. W.; Cardolaccia, T.; Templeton, J. L.; Meyer, T. J. *Inorg. Chem.* **2008**, *47*, 1727.
- (52) Jurss, J. W.; Concepcion, J. J.; Butler, J. M.; Omberg, K. M.; Baraldo, L. M.; Thompson, D. G.; Lebeau, E. L.; Hornstein, B.; Schoonover, J. R.; Jude, H.; Thompson, J. D.; Dattelbaum, D. M.; Rocha, R. C.; Templeton, J. L.; Meyer, T. J. *Inorg. Chem.* **2012**, *51*, 1345.
- (53) Wasylenko, D. J.; Ganesamoorthy, C.; Henderson, M. A.; Berlinguette, C. P. *Inorg. Chem.* **2011**, *50*, 3662.
- (54) Fletcher, J. M.; Greenfield, B. F.; Hardy, C. J.; Scargill, D.; Woodhead, J. L. *J. Chem. Soc.* **1961**, *0*, 2000.
- (55) Vernik, I.; Stynes, D. V. *Inorg. Chem.* **1998**, *37*, 10.
- (56) Geselowitz, D. A.; Kutner, W.; Meyer, T. J. *Inorg. Chem.* **1986**, *25*, 2015.
- (57) Barral, M. C.; Jimenez-Aparicio, R.; Royer, E. C.; Saucedo, M. J.; Urbanos, F. A.; Gutierrez-Puebla, E.; Ruiz-valero, C. *J. Chem. Soc., Dalton Trans.* **1991**, *0*, 1609.
- (58) Biswas, M. K.; Patra, S. C.; Maity, A. N.; Ke, S.-C.; Weyhermuller, T.; Ghosh, P. *Chem. Commun. (Cambridge, U. K.)* **2013**, *49*, 4522.
- (59) Carter, L.; Davies, D. L.; Fawcett, J.; Russell, D. R. *Polyhedron* **1993**, *12*, 1599.
- (60) Sahli, Z.; Derrien, N.; Pascal, S.; Demerseman, B.; Roisnel, T.; Barriere, F.; Achard, M.; Bruneau, C. *Dalton Trans.* **2011**, *40*, 5625.
- (61) Earley, J. E.; Smith, P. M.; Fealey, T.; Silverton, J. V. *Inorg. Chem.* **1971**, *10*, 1943.
- (62) Schulz, L. D.; Fallon, G. D.; Moubaraki, B.; Murray, K. S.; West, B. O. *J. Chem. Soc., Chem. Commun.* **1992**, *0*, 971.
- (63) Sanders-Loehr, J.; Wheeler, W. D.; Shiemke, A. K.; Averill, B. A.; Loehr, T. M. *J. Am. Chem. Soc.* **1989**, *111*, 8084.
- (64) Meyer, T. J.; Huynh, M. H. V. *Inorg. Chem.* **2003**, *42*, 8140.
- (65) Mayer, J. M. *Acc. Chem. Res.* **2011**, *44*, 36.

- Chapter 6*
- (66) *Ruthenium Oxidation Complexes: Their Uses as Homogeneous Organic Catalysts*; Griffith, W. P., Ed.; Springer, 2011; Vol. 34.
- (67) Zanella, A. W.; Ford, P. C. *Inorg. Chem.* **1975**, *14*, 42.
- (68) Mola, J.; Pujol, D.; Rodríguez, M.; Romero, I.; Sala, X.; Katz, N.; Parella, T.; Benet-Buchholz, J.; Fontrodona, X.; Llobet, A. *Aust. J. Chem.* **2009**, *62*, 1675.

## Supporting Information for,

# Behind Water Oxidation with Mononuclear Ru Complexes: The Oxo-bridge Scenario

Isidoro López,<sup>a</sup> Somnath Maji,<sup>a</sup> J. Benet-Buchholz<sup>a</sup> and Antoni Llobet<sup>a,b</sup>

<sup>a</sup>Institute of Chemical Research of Catalonia (ICIQ) Av. Països Catalans, 16, 43007 Tarragona, Catalonia, Spain. E-mail: allobet@icicq.cat

<sup>b</sup>Departament de Química, Universitat Autònoma de Barcelona, Cerdanyola del Vallès, 08193 Barcelona, Catalonia, Spain.

Figure S 1.  $^1\text{H-NMR}$  of  $1\text{-dm}^{4+}$  in 0.1 M HOTf (500 MHz).

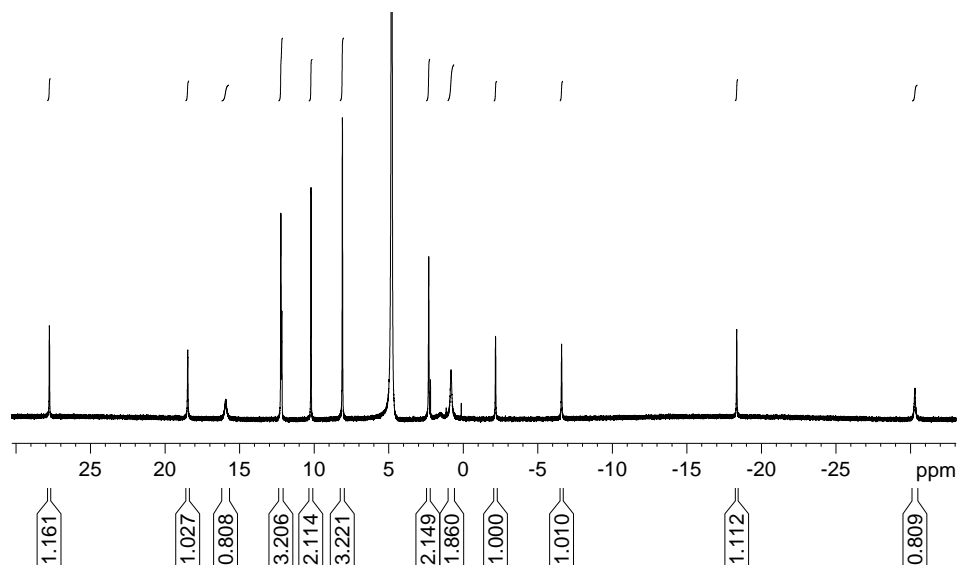
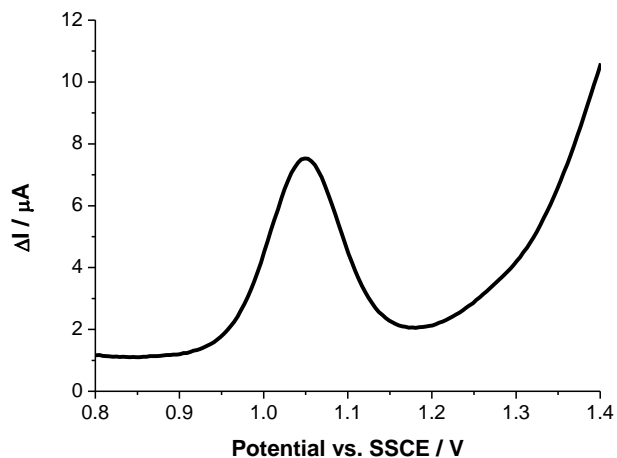


Figure S 2. DPV of  $1\text{-dm}^{4+}$  in 0.1 M HOTf. Polished glassy carbon was used as working electrode, a Pt wire as counter electrode and SSCE as reference electrode. Scan rate =  $20\text{ mV s}^{-1}$ .

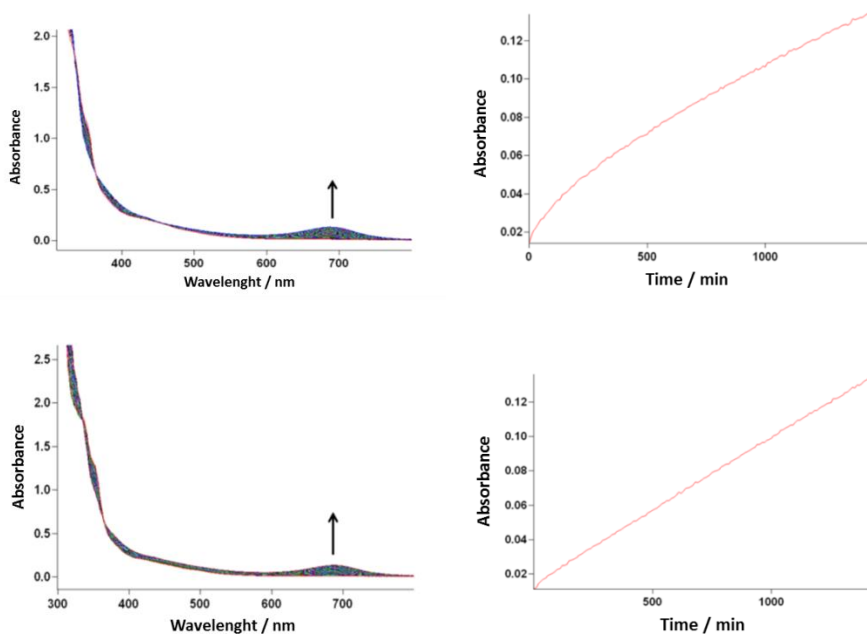


**Table S 1.** Comparison of the highest intensity absorption band in the visible region for several Ru<sup>III</sup>-O-Ru<sup>III</sup> complexes.

Complex <sup>a</sup>	$\lambda_{\max}$ , nm ( $\epsilon$ , L mol <sup>-1</sup> cm <sup>-1</sup> )	Solvent	Ref. <sup>b</sup>
<b>1-dm<sup>4+</sup></b>	689 (25700)	0.1 M HOTf	Tw.
{[Ru <sup>III</sup> (TAN)(acac)] <sub>2</sub> ( $\mu$ -O)} <sup>2+</sup>	596 (12400)	CH <sub>3</sub> CN	1
{[Ru <sup>III</sup> (trpy)(C <sub>2</sub> O <sub>4</sub> )] <sub>2</sub> O}	636 (10500)	pH = 7	2
<i>trans</i> -{[Ru(trpy)(pic)] <sub>2</sub> O} <sup>2+</sup>	682 (13200)	CH <sub>3</sub> CN	3
<i>cis</i> -{[Ru(trpy)(pic)] <sub>2</sub> O} <sup>2+</sup>	698 (16200)	CH <sub>3</sub> CN	3
{[Ru <sup>III</sup> (bpy) <sub>2</sub> (H <sub>2</sub> O)] <sub>2</sub> ( $\mu$ -O)} <sup>4+</sup>	637 (21100)	0.1 M HNO <sub>3</sub>	4

<sup>a</sup> Ligand abbreviation: TAN = 1, 4, 7-trimethyl-1, 4, 7-triazacyclononane, acac = pentane-2,4-dionate, pic = 2-picolinate. <sup>b</sup> This work.

**Figure S 3.** UV-vis monitoring of the reaction of a 0.75 mM solution of **1**<sup>2+</sup> in 0.1 M HOTf with 2 (upper) and 3 (bottom) equivalents of CAN. The absorption profiles at 688 nm are also shown. The reactions are at 25 °C and a cuvette with 2 mm optical pass length was used.



VI

**Figure S 4.** UV-vis monitoring of the reaction of a 0.5 mM solution of  $2^{2+}$  in 0.1 M HOTf with 2 (upper) and 3 (bottom) equivalents of CAN. The absorption profiles at 688 nm are also shown. The reactions are at 25 °C and a cuvette with 2 mm optical pass length was used.

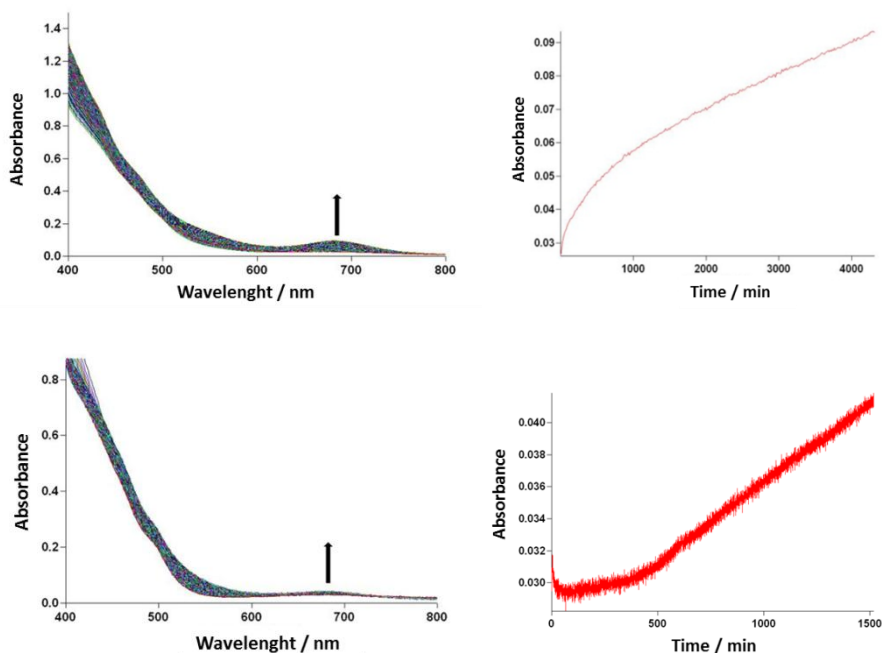


**Figure S 5.** Manometric measurement of dioxygen evolution after the addition of 100 equivalents of CAN to a 1 mM solution of  $1\text{-dm}^{4+}$  in 0.1 M HOTf at 25°C (blue) and the same conditions for  $1^{2+}$  (red).

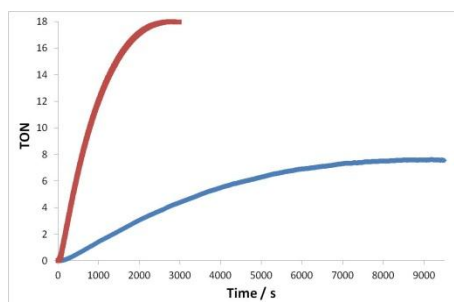


**Figure S 6.** ORTEP plot (ellipsoid drawn at 50% probability) of the X-Ray structure of complex **1-dm**<sup>5+</sup>. Color codes: Ru, cyan; O, Red; N, Blue; C, black. H atoms omitted for clarity.

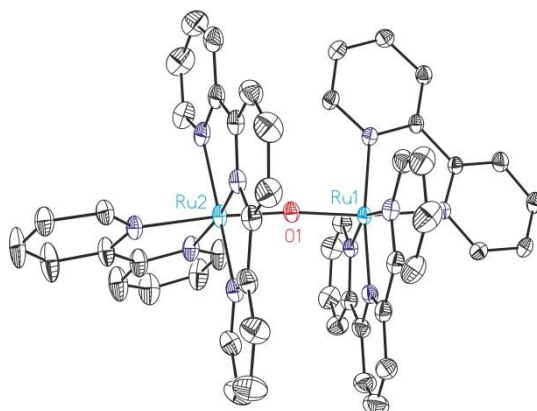
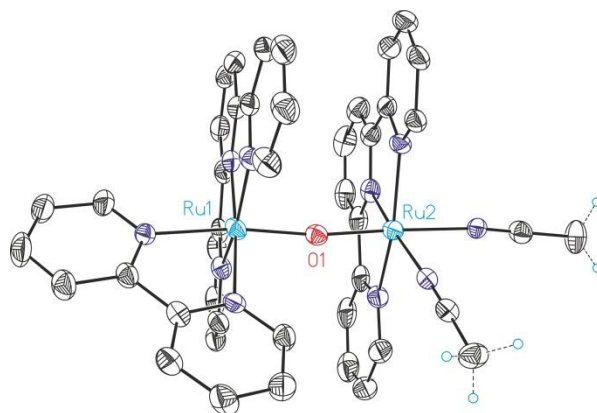


**Figure S 7.** ORTEP plot (ellipsoid drawn at 50% probability) of the X-Ray structure of complex **1-dn<sub>CH3CN</sub>**<sup>4+</sup>. Color codes: Ru, cyan; O, Red; N, Blue; C, black. H atoms are not shown except for the methyl groups from the acetonitrile ligands that are represented as small light blue circles.

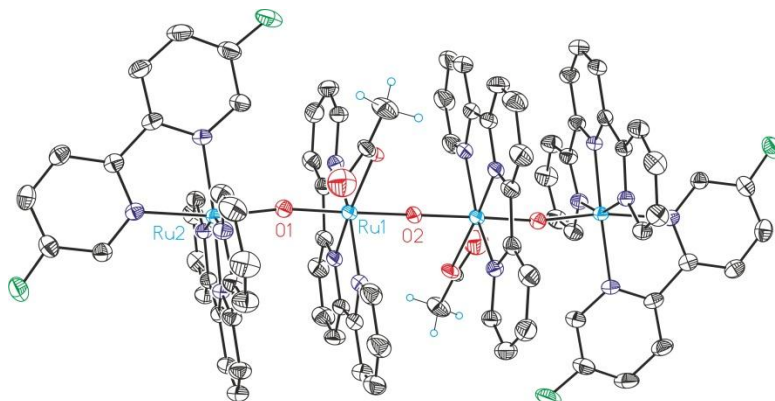


The bipyridene and the acetonitrile ligands are disordered interchanging its positions with a ratio of 86:14.

VI



**Figure S 8.** ORTEP plot (ellipsoid drawn at 50% probability) of the X-Ray structure of complex **2-tn**<sup>6+</sup>. Color codes: Ru, cyan; O, Red; N, Blue; C, black; F, green. H atoms are not shown except for the methyl groups from the acetate ligands that are represented as small light blue circles.



The central Ruthenium atoms of the tetramer are coordinated to disordered acetate/hydroxyl anions with a ratio of respectively 80:20. The acetate complex is shown in the figure.

**Figure S 9.** Ortep plot (ellipsoid drawn at 50% probability) of the X-ray structure of complex **1-tn**<sup>6+</sup>. H atoms are omitted for clarity. Color codes: Ru, cyan; O, Red; N, Blue; C, black. H atoms are not shown except for the methyl groups from the acetonitrile ligands that are represented as small light blue circles.

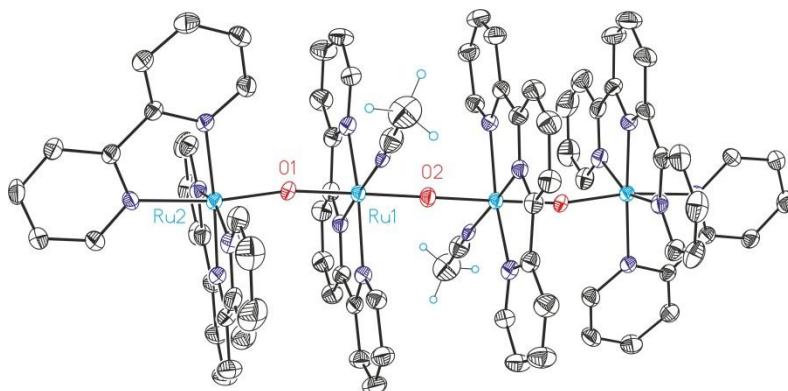


**Table S 2.** Crystal data and structure refinement for **3-dn<sup>4+</sup>**.

Empirical formula	C13.33 H12 Cl1.33 F0.67 N2.67 O7.33 Ru0.67
Formula weight	454.24
Temperature	T100(2)K
Wavelength	0.71073 Å
Crystal system	Triclinic
Space group	P-1
Unit cell dimensions	a = 13.4923(15) Å $\alpha$ = 89.678(4) ° b = 14.3557(15) Å $\beta$ = 65.882(4) ° c = 14.6611(17) Å $\gamma$ = 69.876(4) °
Volume	2403.2(5) Å <sup>3</sup>
Z	6
Density (calculated)	1.883 Mg/m <sup>3</sup>
Absorption coefficient	0.953 mm <sup>-1</sup>
F(000)	1364
Crystal size	0.05 x 0.05 x 0.01 mm <sup>3</sup>
Theta range for data collection	1.54 to 29.95 °
Index ranges	-18 <=h<=18 , -19 <=k<=19 , -20 <=l<=20
Reflections collected	27159
Independent reflections	11628 [R(int) = 0.0568 ]
Completeness to theta =29.95 °	0.833 %
Absorption correction	Empirical
Max. and min. transmission	0.9905 and 0.9539
Refinement method	Full-matrix least-squares on F <sup>2</sup>
Data / restraints / parameters	11628 / 191 / 757
Goodness-of-fit on F <sup>2</sup>	1.002
Final R indices [ $I > 2\sigma(I)$ ]	R1 = 0.0481 , wR2 = 0.0999
R indices (all data)	R1 = 0.0943 , wR2 = 0.1159
Largest diff. peak and hole	0.838 and -0.936 e.Å <sup>-3</sup>

**Table S 3.** Crystal data and structure refinement for **1-dm<sup>4+</sup>**.

Empirical formula	C50 H44.50 Cl4 N10 O20 Ru2
Formula weight	1449.40
Temperature	100(2) K
Wavelength	0.71073 Å
Crystal system	Triclinic
Space group	P-1
Unit cell dimensions	a = 12.3879(8) Å $\alpha$ = 96.503(2) °. b = 13.3477(9) Å $\beta$ = 97.743(2) °. c = 16.7742(11) Å $\gamma$ = 94.440(2) °.
Volume	2718.5(3) Å <sup>3</sup>
Z	2
Density (calculated)	1.771 Mg/m <sup>3</sup>
Absorption coefficient	0.842 mm <sup>-1</sup>
F(000)	1461
Crystal size	0.10 x 0.05 x 0.03 mm <sup>3</sup>
Theta range for data collection	1.67 to 30.05 °.
Index ranges	-17 <=h<=17, -18 <=k<=18, 0 <=l<=23
Reflections collected	23573
Independent reflections	23573 [R(int) = 0.0000]
Completeness to theta =30.05 °	90.3%
Absorption correction	Empirical
Max. and min. transmission	1.00 and 0.88
Refinement method	Full-matrix least-squares on F <sup>2</sup>
Data / restraints / parameters	23573 / 66 / 836
Goodness-of-fit on F <sup>2</sup>	1.050
Final R indices [I>2sigma(I)]	R1 = 0.0311, wR2 = 0.0783
R indices (all data)	R1 = 0.0386, wR2 = 0.0845
Largest diff. peak and hole	0.807 and -0.716 e.Å <sup>-3</sup>

**Table S 4.** Crystal data and structure refinement for **4<sup>4+</sup>**.

Empirical formula	C62 H54 Cl4 N12 O26 Ru3
Formula weight	1828.18
Temperature	100(2)K
Wavelength	0.71073 Å
Crystal system	Monoclinic
Space group	P2(1)/n
Unit cell dimensions	a = 13.2783(17) Å $\alpha$ = 90.00 °. b = 22.367(3) Å $\beta$ = 100.173(5) °. c = 22.842(3) Å $\gamma$ = 90.00 °.
Volume	6677.4(15) Å <sup>3</sup>
Z	4
Density (calculated)	1.819 Mg/m <sup>3</sup>
Absorption coefficient	0.926 mm <sup>-1</sup>
F(000)	3672
Crystal size	0.12 x 0.05 x 0.01 mm <sup>3</sup>
Theta range for data collection	1.28 to 27.80 °.
Index ranges	-17 <=h<=15, -29 <=k<=29, -22 <=l<=29
Reflections collected	67999
Independent reflections	15714 [R(int) = 0.0967 ]
Completeness to theta =27.80 °	0.994 %
Absorption correction	Empirical
Max. and min. transmission	0.9908 and 0.8970
Refinement method	Full-matrix least-squares on F <sup>2</sup>
Data / restraints / parameters	15714 / 344 / 1086
Goodness-of-fit on F <sup>2</sup>	1.090
Final R indices [I>2sigma(I)]	R1 = 0.0777 , wR2 = 0.1734
R indices (all data)	R1 = 0.1423 , wR2 = 0.2045
Largest diff. peak and hole	2.667 and -1.366 e.Å <sup>-3</sup>

**Table S 5.** Crystal data and structure refinement for **1-dm<sup>5+</sup>**.

Empirical formula	C50 H41 Cl5 N10 O22.50 Ru2
Formula weight	1521.32
Temperature	100(2)K
Wavelength	0.71073 Å
Crystal system	Triclinic
Space group	P-1
Unit cell dimensions	a = 11.624(3) Å α = 89.670(7) °. b = 13.136(3) Å β = 84.478(8) °. c = 20.002(5) Å γ = 65.182(7) °.
Volume	2757.3(11) Å <sup>3</sup>
Z	2
Density (calculated)	1.832 Mg/m <sup>3</sup>
Absorption coefficient	0.885 mm <sup>-1</sup>
F(000)	1528
Crystal size	0.12 x 0.08 x 0.02 mm <sup>3</sup>
Theta range for data collection	1.71 to 30.04 °.
Index ranges	-16 ≤ h ≤ 16, -18 ≤ k ≤ 18, -27 ≤ l ≤ 27
Reflections collected	97252
Independent reflections	14633 [R(int) = 0.0393]
Completeness to theta = 30.04 °	0.906 %
Absorption correction	Empirical
Max. and min. transmission	0.9825 and 0.9013
Refinement method	Full-matrix least-squares on F <sup>2</sup>
Data / restraints / parameters	14633 / 299 / 859
Goodness-of-fit on F <sup>2</sup>	1.046
Final R indices [I > 2σ(I)]	R1 = 0.0418, wR2 = 0.1026
R indices (all data)	R1 = 0.0585, wR2 = 0.1135
Largest diff. peak and hole	1.642 and -1.685 e.Å <sup>-3</sup>

**Table S 6.** Crystal data and structure refinement for **1-dn<sub>CH3CN</sub><sup>4+</sup>**.

Empirical formula	C <sub>46</sub> H <sub>41</sub> F <sub>24</sub> N <sub>11</sub> O <sub>2</sub> P <sub>4</sub> Ru <sub>2</sub>
Formula weight	1561.92
Temperature	100(2)K
Wavelength	0.71073 Å
Crystal system	Triclinic
Space group	P-1
Unit cell dimensions	a = 10.7906(12) Å α = 80.416(4) ° b = 12.8062(13) Å β = 77.861(5) ° c = 22.219(3) Å γ = 66.514(3) °
Volume	2741.4(5) Å <sup>3</sup>
Z	2
Density (calculated)	1.892 Mg/m <sup>3</sup>
Absorption coefficient	0.802 mm <sup>-1</sup>
F(000)	1548
Crystal size	0.30 x 0.10 x 0.02 mm <sup>3</sup>
Theta range for data collection	0.94 to 29.80 °
Index ranges	-14 ≤ h ≤ 15, -17 ≤ k ≤ 10, -29 ≤ l ≤ 30
Reflections collected	41002
Independent reflections	13755 [R(int) = 0.0519]
Completeness to theta = 29.80 °	0.877 %
Absorption correction	Empirical
Max. and min. transmission	0.9841 and 0.7949
Refinement method	Full-matrix least-squares on F <sup>2</sup>
Data / restraints / parameters	13755 / 1009 / 1057
Goodness-of-fit on F <sup>2</sup>	1.051
Final R indices [I > 2σ(I)]	R <sub>1</sub> = 0.0719, wR <sub>2</sub> = 0.1788
R indices (all data)	R <sub>1</sub> = 0.1118, wR <sub>2</sub> = 0.2018
Largest diff. peak and hole	2.224 and -1.787 e.Å <sup>-3</sup>

**Table S 7.** Crystal data and structure refinement for **3-dn<sub>CH3CN</sub><sup>4+</sup>**.

Empirical formula	C <sub>46</sub> H <sub>37</sub> F <sub>26</sub> N <sub>11</sub> O <sub>4</sub> Ru <sub>2</sub>
Formula weight	1579.89
Temperature	273(2)K
Wavelength	0.71073 Å
Crystal system	Triclinic
Space group	P-1
Unit cell dimensions	a = 13.240(3) Å α = 95.23(3) °. b = 14.214(3) Å β = 96.87(3) °. c = 18.518(4) Å γ = 116.81(3) °.
Volume	3046.6(10) Å <sup>3</sup>
Z	2
Density (calculated)	1.722 Mg/m <sup>3</sup>
Absorption coefficient	0.726 mm <sup>-1</sup>
F(000)	1560
Crystal size	0.15 x 0.10 x 0.05 mm <sup>3</sup>
Theta range for data collection	1.12 to 27.67 °.
Index ranges	-17 ≤ h ≤ 17, -18 ≤ k ≤ 15, -23 ≤ l ≤ 23
Reflections collected	41412
Independent reflections	ln13608 [R(int) = 0.0733 ]
Completeness to theta = 27.67 °	.956 %
Absorption correction	Empirical
Max. and min. transmission	0.9646 and 0.8989
Refinement method	Full-matrix least-squares on F <sup>2</sup>
Data / restraints / parameters	13608 / 512 / 903
Goodness-of-fit on F <sup>2</sup>	1.018
Final R indices [I > 2σ(I)]	R1 = 0.0693, wR2 = 0.1970
R indices (all data)	R1 = 0.1097, wR2 = 0.2205
Largest diff. peak and hole	1.584 and -1.433 e.Å <sup>-3</sup>

**Table S 8.** Crystal data and structure refinement for  $5^{6+}$ .

Empirical formula	C65 H55 Cl5 F6 N13 O25 P Ru3
Formula weight	2043.65
Temperature	100(2) K
Wavelength	0.71073 Å
Crystal system	Monoclinic
Space group	C2/c
Unit cell dimensions	a = 15.580(3) Å $\alpha$ = 90.00 °. b = 21.323(3) Å $\beta$ = 101.034(6) °. c = 22.581(4) Å $\gamma$ = 90.00 °.
Volume	7363(2) Å <sup>3</sup>
Z	4
Density (calculated)	1.844 Mg/m <sup>3</sup>
Absorption coefficient	0.917 mm <sup>-1</sup>
F(000)	4088
Crystal size	0.10 x 0.10 x 0.02 mm <sup>3</sup>
Theta range for data collection	1.64 to 30.01 °.
Index ranges	-21 <=h<=21, -26 <=k<=29, -30 <=l<=31
Reflections collected	112958
Independent reflections	10255 [R(int) = 0.0405 ]
Completeness to theta =30.01 °	95.4%
Absorption correction	Empirical
Max. and min. transmission	0.9730 and 0.8379
Refinement method	Full-matrix least-squares on F <sup>2</sup>
Data / restraints / parameters	10255 / 582 / 754
Goodness-of-fit on F <sup>2</sup>	1.054
Final R indices [I>2sigma(I)]	R1 = 0.0644 , wR2 = 0.1669
R indices (all data)	R1 = 0.0867 , wR2 = 0.1860
Largest diff. peak and hole	3.276 and -1.681 e.Å <sup>-3</sup>



**Table S 9.** Crystal data and structure refinement for **1-tn<sup>6+</sup>**.

Empirical formula	C84 H66 F36 N18 O3 P6 Ru4
Formula weight	2649.65
Temperature	100(2)K
Wavelength	0.71073 Å
Crystal system	Monoclinic
Space group	C2/c
Unit cell dimensions	a = 20.078(2) Å α = 90.00 °. b = 19.058(2) Å β = 101.484(3) °. c = 28.627(3) Å γ = 90.00 °.
Volume	10735(2) Å <sup>3</sup>
Z	4
Density (calculated)	1.639 Mg/m <sup>3</sup>
Absorption coefficient	0.758 mm <sup>-1</sup>
F(000)	5240
Crystal size	0.30 x 0.10 x 0.02 mm <sup>3</sup>
Theta range for data collection	1.49 to 33.24 °.
Index ranges	-30 ≤ h ≤ 30, -29 ≤ k ≤ 20, -42 ≤ l ≤ 42
Reflections collected	50782
Independent reflections	19621 [R(int) = 0.0554]
Completeness to theta = 33.24 °	0.950 %
Absorption correction	Empirical
Max. and min. transmission	0.9850 and 0.8046
Refinement method	Full-matrix least-squares on F <sup>2</sup>
Data / restraints / parameters	19621 / 846 / 984
Goodness-of-fit on F <sup>2</sup>	1.076
Final R indices [I > 2σ(I)]	R1 = 0.0634, wR2 = 0.1709
R indices (all data)	R1 = 0.0965, wR2 = 0.1835
Largest diff. peak and hole	1.893 and -0.960 e.Å <sup>-3</sup>

**Table S 10.** Crystal data and structure refinement for **2-tn<sup>6+</sup>**.

Empirical formula	C83.20 H65.20 Cl6 F4 N16 O32.60 Ru4
Formula weight	2503.69
Temperature	296(2)K
Wavelength	0.71073 Å
Crystal system	Triclinic
Space group	P-1
Unit cell dimensions	a = 12.6065(8) Å $\alpha$ = 91.810(3) °. b = 13.6669(9) Å $\beta$ = 112.224(2) °. c = 15.8222(11) Å $\gamma$ = 116.112(2) °.
Volume	2200.7(3) Å <sup>3</sup>
Z	1
Density (calculated)	1.889 Mg/m <sup>3</sup>
Absorption coefficient	0.964 mm <sup>-1</sup>
F(000)	1251
Crystal size	0.20 x 0.10 x 0.03 mm <sup>3</sup>
Theta range for data collection	1.43 to 29.87 °.
Index ranges	-17 <=h<=17, -18 <=k<=19, -20 <=l<=21
Reflections collected	44428
Independent reflections	11330 [R(int) = 0.0350]
Completeness to theta =29.87 °	0.892 %
Absorption correction	Empirical
Max. and min. transmission	0.9717 and 0.8306
Refinement method	Full-matrix least-squares on F <sup>2</sup>
Data / restraints / parameters	11330 / 228 / 737
Goodness-of-fit on F <sup>2</sup>	1.043
Final R indices [I>2sigma(I)]	R1 = 0.0452, wR2 = 0.1130
R indices (all data)	R1 = 0.0602, wR2 = 0.1255
Largest diff. peak and hole	3.677 and -0.976 e.Å <sup>-3</sup>

**Table S 11.** Crystal data and structure refinement for **3-tn<sup>6+</sup>**.

Empirical formula	C87 H66.50 Cl2 F28 N19.50 O11 P4 Ru4
Formula weight	2692.16
Temperature	100(2) K
Wavelength	0.71073 Å
Crystal system	Triclinic
Space group	P-1
Unit cell dimensions	a = 13.410(2) Å $\alpha$ = 74.839(7) °. b = 14.433(2) Å $\beta$ = 66.059(7) °. c = 15.012(3) Å $\gamma$ = 80.026(5) °.
Volume	2555.6(7) Å <sup>3</sup>
Z	1
Density (calculated)	1.749 Mg/m <sup>3</sup>
Absorption coefficient	0.813 mm <sup>-1</sup>
F(000)	1335
Crystal size	0.15 x 0.10 x 0.05 mm <sup>3</sup>
Theta range for data collection	1.52 to 24.64 °.
Index ranges	-15 <=h<=15, -14 <=k<=16, -17 <=l<=17
Reflections collected	25220
Independent reflections	8078 [R(int) = 0.0499]
Completeness to theta =24.64 °	93.6%
Absorption correction	Empirical
Max. and min. transmission	0.9605 and 0.8878
Refinement method	Full-matrix least-squares on F <sup>2</sup>
Data / restraints / parameters	8078 / 530 / 850
Goodness-of-fit on F <sup>2</sup>	1.075
Final R indices [I>2sigma(I)]	R1 = 0.0801, wR2 = 0.2222
R indices (all data)	R1 = 0.1242, wR2 = 0.2618
Largest diff. peak and hole	2.068 and -1.408 e.Å <sup>-3</sup>

## References

- (1) Schneider, R.; Weyhermueller, T.; Wieghardt, K.; Nuber, B. *Inorg. Chem.* **1993**, *32*, 4925.
- (2) Lebeau, E. L.; Adeyemi, S. A.; Meyer, T. J. *Inorg. Chem.* **1998**, *37*, 6476.
- (3) Llobet, A.; Doppelt, P.; Meyer, T. J. *Inorg. Chem.* **1988**, *27*, 514.
- (4) Jurss, J. W.; Concepcion, J. J.; Butler, J. M.; Omberg, K. M.; Baraldo, L. M.; Thompson, D. G.; Lebeau, E. L.; Hornstein, B.; Schoonover, J. R.; Jude, H.; Thompson, J. D.; Dattelbaum, D. M.; Rocha, R. C.; Templeton, J. L.; Meyer, T. J. *Inorg. Chem.* **2012**, *51*, 1345.

UNIVERSITAT ROVIRA I VIRGILI

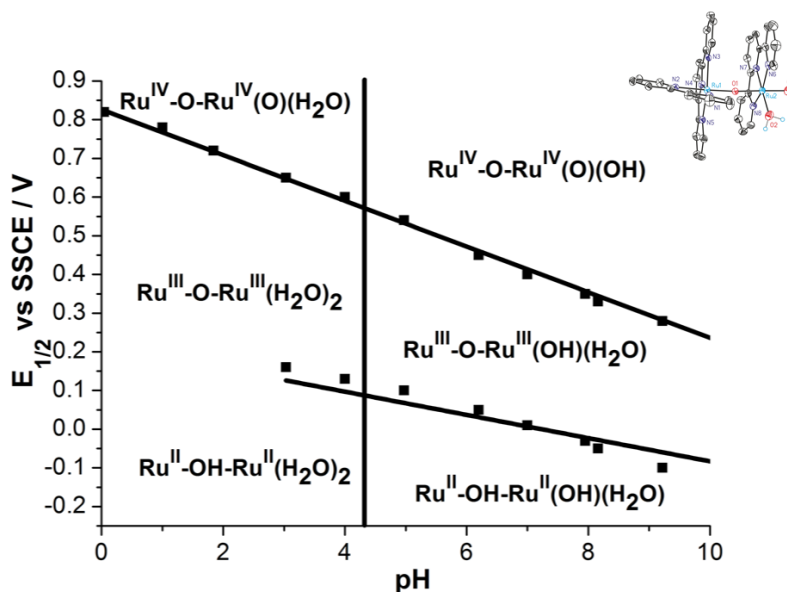
WATER OXIDATION WITH MONONUCLEAR RU COMPLEXES. BELOW THE TIP OF THE

ICEBERG: THE OXO-BRIDGE SCENARIO

Isidoro López Marin

Dipòsit Legal: T. 1505-2013

## Chapter 7. Exploring the properties of rugged oxo-bridge dinuclear water oxidation catalysts and its relationship with mononuclear catalysts.



The complete electrochemical and spectroscopic characterization of the dinuclear complexes  $[(\text{trpy})(5,5'\text{-X}_2\text{-bpy})\text{Ru}^{\text{IV}}(\mu\text{-O})\text{Ru}^{\text{IV}}(\text{trpy})(\text{O})(\text{H}_2\text{O})]^{4+}$  ( $\text{X} = \text{H}$ , **1-dn**<sup>4+</sup>;  $\text{X} = \text{F}$ , **2-dn**<sup>4+</sup>) has been accomplished. Additionally new rRAMAN spectroscopic studies evidence the conversion of the high oxidation states of the mononuclear complexes  $[\text{Ru}(\text{trpy})(5,5'\text{-F}_2\text{-Bpy})(\text{H}_2\text{O})]^{2+}$  ( $\text{X} = \text{H}$ , **1**<sup>2+</sup>;  $\text{X} = \text{F}$ , **2**<sup>2+</sup>) into its dinuclear counterparts, **1-dn**<sup>4+</sup> and **2-dn**<sup>4+</sup> respectively, *via* the formation of *trans*- $[\text{Ru}^{\text{VI}}(\text{trpy})(\text{O})_2(\text{H}_2\text{O})]^{2+}$  (**3**<sup>2+</sup>). This feature strongly supports our earlier hypothesis about two interconnected cycles leading to dioxygen under chemical or electrochemical catalytic conditions. Intermediates from different cycles interact each other producing a synergic effect in the evolution of dioxygen.

UNIVERSITAT ROVIRA I VIRGILI

WATER OXIDATION WITH MONONUCLEAR RU COMPLEXES. BELOW THE TIP OF THE

ICEBERG: THE OXO-BRIDGE SCENARIO

Isidoro López Marin

Dipòsit Legal: T. 1505-2013

**Table of Contents.****Chapter 7. Exploring the properties of rugged oxo-bridge dinuclear water  
oxidation catalysts and its relationship with mononuclear catalysts.**

<i>7.1. Introduction.</i>	279
<i>7.2. Experimental Section.</i>	282
<i>7.3. Results and discussion.</i>	285
<i>Synthesis of the dinuclear complexes.</i>	285
<i>Electrochemical and spectroscopic properties.</i>	286
<i>Evolution of the mononuclear complexes.</i>	294
<i>Two interconnected cycles.</i>	299
<i>7.4. Conclusions.</i>	304
<i>7.5. Acknowledgements.</i>	306
<i>7.6. References.</i>	306
<i>7.7. Supporting Information.</i>	309



UNIVERSITAT ROVIRA I VIRGILI

WATER OXIDATION WITH MONONUCLEAR RU COMPLEXES. BELOW THE TIP OF THE

ICEBERG: THE OXO-BRIDGE SCENARIO

Isidoro López Marin

Dipòsit Legal: T. 1505-2013

## Exploring the properties of rugged oxo-bridge dinuclear water oxidation catalysts and its relationship with mononuclear catalysts

Isidoro López,<sup>a</sup> Somnath Maji,<sup>a</sup> Anke Keidel,<sup>b</sup> Jordi Benet-Buchholz,<sup>a</sup> Uwe Kuhlmann,<sup>b</sup> Peter Hildebrandt<sup>b</sup> and Antoni Llobet<sup>a,c</sup>

<sup>a</sup> Institute of Chemical Research of Catalonia (ICIQ), Av. Països Catalans, 16, 43007 Tarragona, Spain.

<sup>b</sup> Technische Universität Berlin, Institut für Chemie, Sekr. PC14, Straße des 17. Juni 135, D-10623 Berlin, Germany.

<sup>c</sup> Departament de Química, Universitat Autònoma de Barcelona, Cerdanyola del Vallès, 08193 Barcelona, Spain.

### 7.1. Introduction.

Single-site water oxidation catalysts (WOC) are currently receiving an increased interest since Thummel *et al.* found<sup>1</sup> the first active mononuclear ruthenium complexes. Extensive mechanistic<sup>2-4</sup> studies have been carried out by Meyer *et al.* The proposed catalytic pathway is shown in the left side of Figure 1, where the key O-O bond formation step is a water nucleophilic attack (WNA) on the the Ru<sup>V</sup>=O unit. Later reports by Berlinguette *et al.*<sup>5</sup> and Sakai *et al.*<sup>6</sup> added a pathway where an O-atom from (NH<sub>4</sub>)<sub>2</sub>Ce(NO<sub>3</sub>)<sub>6</sub> (CAN) is incorporated to the final dioxygen product via a radical coupling with the Ru<sup>V</sup>=O unit.

The mechanism has been proposed for a large number of mononuclear Ru catalyst from [Ru(trpy)(bpy)(H<sub>2</sub>O)]<sup>2+</sup> (**1**<sup>2+</sup>) (where trpy is 2,2':6',2''-terpyridine and bpy is 2,2'-bipyridine) analogues<sup>5,7</sup> to single site Ru

polyoxometalates.<sup>8</sup> Furthermore, this description has also been extended to iridium<sup>9</sup> and other first-row transition metals molecular catalysts.<sup>10,11</sup>

Strong efforts have been dedicated to identify and characterize the proposed intermediates and possible side products. *Meyer et al.* provided the first UV-vis spectroscopic and electrochemical evidences<sup>3</sup> for the hydroperoxo  $[\text{Ru}-\text{OOH}]^{2+}$  intermediate. After that, *Berlinguette et al.* employed ESI-MS<sup>5</sup> to gain a deeper insight into the mechanism and discovered the  $\{[\text{Ru}^{\text{IV}}(\text{trpy})(\text{bpy})(\text{O})][\text{Ce}^{\text{IV}}(\text{NO}_3)_5]\}^+$  and  $[\text{Ru}^{\text{III}}(\text{trpy})(\text{bpy})\text{O}_2]^+$  cations which proceed from an side reaction where Ce(IV) activates a N-O bond of a nitrate ligand and the O-atom is then transferred to the  $[\text{Ru}^{\text{IV}}=\text{O}]^{2+}$  unit. Interestingly the  $[\text{Ru}^{\text{V}}=\text{O}]$  complex could not be observed by this technique. Later on *Fujita et al.* reported an exhaustive study of the intermediates of the catalytic cycle. They achieved a complete spectroscopic and electrochemical characterization of a peroxo complex  $[\text{Ru}^{\text{IV}}-\text{OO}]^{2+}$ . However, the rRAMAN spectrum lacks a band for the indicative O-O stretching mode although the Ru-O mode is observed after labeling experiments.

The proposed mechanism has been also indirectly validated by subtle modifications in the ligands of the  $\mathbf{1}^{2+}$  complex. *Fujita et al.* have examined<sup>12</sup> the effect of a pendant base in catalytic water oxidation. They found a drastic decrease of the activity when the base is placed next to the aquo ligand while the stereoisomeric complex with a distant pendant base is a better catalyst than  $\mathbf{1}^{2+}$ . We have also studied<sup>7</sup> the remarkable effect exerted by a proximal fluorine atom. The modified bipyridine ligand forms a hydrogen bond with the active site which lowers the activity. It is also worth mentioning that 2,2'-bipyridine *N,N*-dioxide has been observed as the main deactivation product<sup>13</sup>

after catalysis with  $1^{2+}$  and a huge excess of CAN which points out that dissociation of bpy ligand is an important pathway for catalyst decomposition.

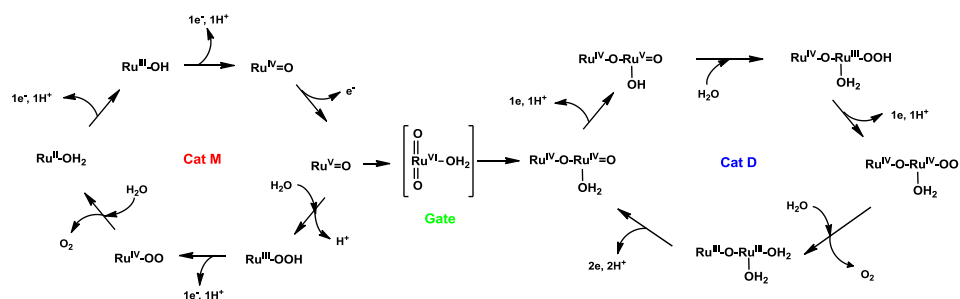


**Figure 1.** Interconnected cycles for water oxidation by mononuclear (left) and dinuclear (right) complexes.

Recently our group has demonstrated<sup>14</sup> that  $1^{2+}$  and the structurally related complex  $[\text{Ru}(\text{trpy})(5,5'\text{-F}_2\text{-Bpy})(\text{H}_2\text{O})]^{2+}$  (where 5,5'-F<sub>2</sub>-Bpy is 5,5'-difluoro-2,2'-bipyridine,  $2^{2+}$ ) are partly converted into the new oxidatively rugged and active dinuclear catalysts  $[(\text{trpy})(5,5'\text{-X}_2\text{-bpy})\text{Ru}^{\text{IV}}(\mu\text{-O})\text{Ru}^{\text{IV}}(\text{trpy})(\text{O})(\text{H}_2\text{O})]^{4+}$  (X = H,  $1\text{-dn}^{4+}$ ; X = F,  $2\text{-dn}^{4+}$ ) under catalytic conditions (see chapter V). This evolution draws a complete and deep description at the molecular level of the activity by single-site WOCs behind the current accepted mechanistic proposal. Two catalytic cycles run concurrently and are interconnected by the gate  $[\text{Ru}^{\text{VI}}(\text{trpy})(\text{O})_2(\text{H}_2\text{O})]^{2+}$  ( $3^{2+}$ ). Additionally, intermediates of different cycles could interact each other making difficult to establish the pathways leading to oxygen.

In this work, we study thoroughly the spectroscopic and electrochemical properties of  $1\text{-dn}^{2+}$  and  $2\text{-dn}^{4+}$  including its pH dependency. New spectroscopic evidences for the conversion of the mononuclear complexes into the dinuclear ones will be also discussed. All these features provide a complete, consistent and comprehensive understanding of the electronic

VII

structure of the dinuclear complexes and the mechanism of water oxidation by single-site Ru catalysts.

## 7.2. Experimental Section.

**Materials.** All reagents used in the present work were obtained from Aldrich Chemical Co. and were used without further purification.  $\text{RuCl}_3 \cdot 3\text{H}_2\text{O}$  was supplied by Alfa Aesar and was used as received. Trifluoromethanesulfonic acid (HOTf) was purchased from CYMIT. Reagent-grade organic solvents were obtained from SDS and high-purity deionized water was obtained by passing distilled water through a nanopure Milli-Q water purification system.

**Preparations.**  $[\text{Ru}(\text{trpy})(\text{bpy})(\text{H}_2\text{O})](\text{PF}_6)_2$  (**1**<sup>2+</sup>),<sup>15</sup>  $[\text{Ru}(\text{trpy})(5,5'\text{-F}_2\text{-bpy})(\text{H}_2\text{O})](\text{PF}_6)_2$  (**2**<sup>2+</sup>),<sup>7</sup> *trans*- $[\text{Ru}^{\text{VI}}(\text{trpy})(\text{O})_2(\text{H}_2\text{O})]^{2+}$  (**3**<sup>2+</sup>),<sup>16</sup>  $[(\text{trpy})(\text{bpy})\text{Ru}^{\text{IV}}(\mu\text{-O})\text{Ru}^{\text{IV}}(\text{trpy})(\text{O})(\text{H}_2\text{O})](\text{ClO}_4)_4$  (**1-dn**<sup>4+</sup>)<sup>14</sup> and  $[(\text{trpy})(5,5'\text{-F}_2\text{-bpy})\text{Ru}^{\text{IV}}(\mu\text{-O})\text{Ru}^{\text{IV}}(\text{trpy})(\text{O})(\text{H}_2\text{O})](\text{ClO}_4)_4$  (**2-dn**<sup>4+</sup>)<sup>14</sup> were prepared as described in the literature.

**Equipment and measurements.** UV/Vis spectroscopy was performed on a Cary 50 (Varian) UV/Vis spectrophotometer in 1 cm or 0.2 cm when indicated quartz cuvettes. Cyclic voltammetry (CV) and differential pulse voltammetry (DPV) experiments were performed on an IJ-Cambria CHI-660 or a Bio-Logic SP-150 potentiostat using a three-electrode cell. Typical CV experiments were carried out at a scan rate of  $100 \text{ mV s}^{-1}$ . DPV experiments were carried out with the parameters: Pulses Height = 50 mV, Pulses Width = 50 ms, Step Height = 4 mV and Step Time = 200 ms. A glassy carbon electrode (3 mm diameter) was used as working electrode, platinum wire as auxiliary electrode, and a SSCE or  $\text{Hg}/\text{Hg}_2\text{SO}_4$ ,  $\text{K}_2\text{SO}_4$  (sat) as reference electrode. Working electrodes were polished with 0.05 micron alumina paste, and rinsed with distilled water and acetone followed by blow-drying before each measurement. When glassy

carbon electrodes were activated, a procedure described by Meyer *et al.* was used.<sup>17</sup> All cyclic voltammograms presented in this work were recorded in the absence of light and inside a Faradaic cage. The electrochemical experiments were carried out in 1 M CF<sub>3</sub>SO<sub>3</sub>H (pH = 0.0), 0.1 M CF<sub>3</sub>SO<sub>3</sub>H (pH = 1.0), NaH<sub>2</sub>PO<sub>4</sub>/H<sub>3</sub>PO<sub>4</sub> buffers (pH range: 2.0 – 4.0), Na<sub>2</sub>HPO<sub>4</sub>/NaH<sub>2</sub>PO<sub>4</sub> buffers (pH range: 4.0 – 8.0) or sodium tetraborate buffers (pH range: 8.0 - 9.5) with *I* = 0.1 M. *E*<sub>1/2</sub> values reported in this work were estimated from CV experiments as the average of the oxidative and reductive peak potentials (*E*<sub>p,a</sub> + *E*<sub>p,c</sub>)/2 or taken as *E*(*I*<sub>max</sub>) from DPV measurements.

A 400 MHz Bruker Avance II spectrometer and a Bruker Avance 500 MHz were used to carry out NMR spectroscopy at room temperature. Samples were run in 0.1 M DOTf with internal references (residual protons). Elemental analysis was performed using an EA-1108, CHNS-O elemental analyzer from Fisons Instruments.

Samples for resonance Raman spectroscopy using a 514 nm laser were prepared by mixing a 1 mM solution of **1-dn**<sup>4+</sup> with two equivalents of (NH<sub>4</sub>)<sub>2</sub>Fe(SO<sub>4</sub>)<sub>2</sub> and transferring 100 μL of the reaction solution to a aluminium crucible and subsequently frozen at appropriate times in liquid N<sub>2</sub>. Then, the crucible was placed into a Linkam THMS 600 temperature controlled cryo stage to keep the temperature at -12°C. The rR spectrum was acquired using a Renishaw inVia Reflex RAMAN confocal microscope (Gloucestershire, UK), equipped with an Ar-ion laser at 514 nm and a Peltier-cooled CCD detector (-70°C) coupled to a Leica DM-2500 microscope. Calibration was carried out daily by recording the Raman spectrum of an internal Si standard. Rayleigh scattered light was appropriately rejected by using edge-type filters. Spectra were recorded with the accumulation of 5 scans with a 20 s scan time each

one. A 10x working distance microscope objective was used to focus 50% of the laser power (25 mW) onto the sample.

On-line manometric O<sub>2</sub> measurements were carried out on a Testo 521 differential pressure manometer with an operating range of 1-100 hPa and accuracy within 0.5 % of the measurement. The manometer was coupled to thermostated reaction vessels for dynamic monitoring of the headspace pressure above each reaction. The manometer's secondary ports were connected to thermostated reaction vessels containing the same solvents and headspace volumes as the sample vials. Composition of the gaseous phase was determined by online mass-spectrometry with an OmniStar GSD 301 C (Pfeiffer) quadrupole mass-spectrometer.

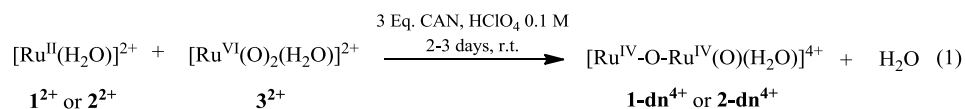
**Single-Crystal X-Ray Structure Determination.** Single crystals for the oxidation state IV of **2**<sup>2+</sup> were grown 4 days after the addition of some drops of an aqueous saturated NH<sub>4</sub>PF<sub>6</sub> solution to a reaction mixture of 3 equivalents of CAN and **2**<sup>2+</sup> in 0.1 M HOTf that was previously left reacting one day. All measured crystals were prepared under inert conditions immersed in perfluoropolyether as the protecting oil for manipulation.

*Data collection.* Crystal structure determination was carried out using a Apex DUO Kappa 4-axis goniometer equipped with an APPEX 2 4K CCD area detector, a Microfocus Source E025 luS using MoK<sub>α</sub> radiation, Quazar MX multilayer Optics as monochromator and an Oxford Cryosystems low temperature device Cryostream 700 plus (*T* = -173 °C). Full-sphere data collection was used with  $\omega$  and  $\varphi$  scans. *Programs used:* Data collection APEX-2,<sup>18</sup> data reduction Bruker Saint<sup>19</sup> V/.60A.

**Structure Solution and Refinement.** Crystal structure solution was achieved using direct methods as implemented in SHELXTL<sup>20</sup> and visualized using the program XP. Missing atoms were subsequently located from difference Fourier synthesis and added to the atom list. Least-squares refinement on F2 using all measured intensities was carried out using the program SHELXTL. All non hydrogen atoms were refined including anisotropic displacement parameters.

### 7.3. Results and discussion.

**Synthesis of the dinuclear complexes.** Complexes **1-dn**<sup>4+</sup> and **2-dn**<sup>4+</sup> were prepared in moderate yields (40 – 50 %) by reacting equimolar amounts of *trans*-[Ru<sup>VI</sup>(trpy)(O)<sub>2</sub>(H<sub>2</sub>O)]<sup>2+</sup> (**3**<sup>2+</sup>) and the corresponding mononuclear complex, **1**<sup>2+</sup> or **2**<sup>2+</sup>, in the presence of CAN (Eq 1, polypyridilic ligands not shown) as previously reported.



**1-dn**<sup>4+</sup> and **2-dn**<sup>4+</sup> were thoroughly characterized by the usual analytic, spectroscopic and electrochemical techniques (see Chapter V). The X-ray structure obtained for **1-dn**<sup>4+</sup> is depicted in Figure 2 and it has been discussed in detail in previous works<sup>14</sup> (see chapter V and VI). The complex contains two octahedrally distorted coordinated Ru atoms linked by an oxo bridge, where one of the metallic centers bears a terminal oxo ligand in the *trans* position to the oxo bridge and an aquo ligand.



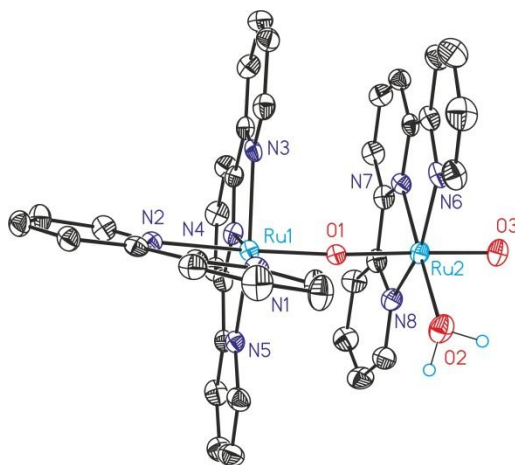
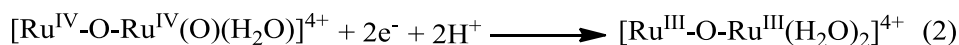
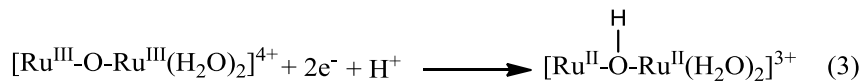


**Figure 2.** Ortep plot (ellipsoids drawn at 50 % probability) of the X-ray structure of  $\mathbf{1}^{4+}$ . Color codes: Ru, cyan; O, Red; N, Blue, C, black. H atoms are not shown except for the aqua ligands that are represented as small light blue circles.

**Electrochemical and spectroscopic properties.** In order to characterize more completely its various oxidation states, the electrochemical properties of the dinuclear complexes were studied under several conditions. The cyclic voltammeteries (CVs) of  $\mathbf{1-dn}^{4+}$  and  $\mathbf{2-dn}^{4+}$  in 0.1 M triflic acid (pH = 1) show an electrochemical and chemical reversible wave followed by a chemically irreversible wave (Figure 3). The first one is attributed to the 2 electron reduction, determined by coulometry, from the oxidation state IV,IV to III,III which is accompanied with double protonation on the oxo terminal group according to



From relative peak height, the second wave is consistent with another 2 electron reduction process from the oxidation state III,III to II,II which is associated with protonation on the oxo bridge in agreement with related dinuclear III,III complexes<sup>21-23</sup> (see chapter VI also).



The oxidation state II,II is unstable at acidic pH and is cleaved through the oxo bridge generating the corresponding mononuclear complexes, thus new waves attributed to  $3^{2+}$  and  $1^{2+}$  ( or  $2^{2+}$ ) can be observed after a subsequent anodic scan. At pH > 4 the reduction wave becomes chemically reversible suggesting that the hydroxo bridge complex is stable in the time scale of a CV experiment (Figure S1).

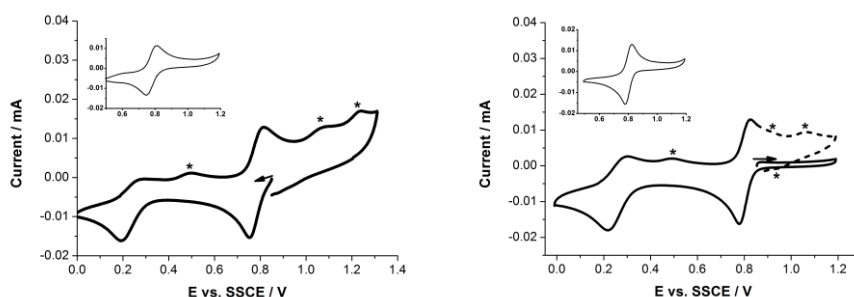
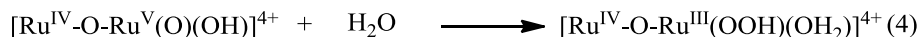


**Figure 3.** CVs of 0.5 mM solutions in 0.1 M triflic acid (pH = 1.0) for complexes **1-dn<sup>4+</sup>**(left) and **2-dn<sup>4+</sup>**(right). The insets show CV experiments where the potential was switched before the irreversible reduction,  $E_{\text{SW}} = 0.5$  V. The asterisks mark electrochemical features for the mononuclear complexes. Scan rate =  $100 \text{ mV s}^{-1}$ . Glassy Carbon (GC) was used as working electrode, a Pt wire as counter electrode and Hg/Hg<sub>2</sub>SO<sub>4</sub>, K<sub>2</sub>SO<sub>4</sub> (sat.) as reference electrode.

**1-dn<sup>4+</sup>** and **2-dn<sup>4+</sup>** present also a large electrocatalytic increase of the current intensity in the anodic part which is associated to the oxidation of water as previously described (see chapter V). The electrochemical process is assigned to the one electron oxidation of IV,IV to IV,V (eq. 3) followed by a water nucleophilic attack on the Ru<sup>V</sup>=O to form a hydroperoxo intermediate (eq. 4) which evolves oxygen after a sequence of reactions.

VII



A compilation of the standard potentials for **1-dn**<sup>4+</sup>, **2-dn**<sup>4+</sup> and several dinuclear and mononuclear complexes is collected in Table 1. The potentials for **1-dn**<sup>4+</sup> and **2-dn**<sup>4+</sup> are quite similar (entry **1** vs. **2**), although the electron withdrawing fluorine atoms in the bpy ring of **2-dn**<sup>4+</sup> increase slightly the potentials (20-30 mV). The absence of the mixed valence state III,IV (it should be considered that this distribution of formal oxidation states is a convenience, since strong electronic coupling through the oxo bridge has been demonstrated<sup>21,24,25</sup> for structurally related complexes. A more suitable oxidation state description would be III.5,III.5) in the electrochemical experiments suggests that  $E^0(\text{III,IV}/\text{III,III}) > E^0(\text{IV,IV}/\text{III,IV})$ , i. e. the oxidation state III,IV is unstable with respect to disproportionation. In sharp contrast, the complex  $\{[\text{Ru}(\text{trpy})(\text{bpy})]_2(\mu\text{-O})\}^{4+}$  where the oxo terminal and the aquo ligands have been replaced by a bpy shows only the III,IV/III,III couple in the anodic region and at higher potential (entry **5** vs **1** or **2**). The wave corresponding to the IV,IV/III,IV lies probably in a very high potential region where the surface of the electrode is seriously damaged. These dramatically different electrochemical properties reveal that the two aquo ligands in the oxidation state III,III of **1-dn**<sup>4+</sup> or **2-dn**<sup>4+</sup> play a crucial role in lowering the potentials through proton coupled electron transfer processes (PCET) which avoid the buildup of positive charge after oxidation. Furthermore, the *trans* dioxo coordination in the oxidation state IV,IV stabilizes<sup>16,26</sup> this specie contributing to lower the potentials.

The two electron reduction wave assigned to the III,III/II,II couple in **1-dn**<sup>4+</sup> and **2-dn**<sup>4+</sup> indicates that  $E^0(\text{II,III}/\text{II,II}) > E^0(\text{III,III}/\text{II,III})$  so that the mixed

valence state II,III is unstable with respect to disproportionation. This behavior in water has already been observed for previous reported dinuclear oxo bridge complexes<sup>21,22</sup> (entries **1** or **2** vs. **5**). The pH-dependence of the potential for this couple shows that a proton is added in the reduction (*vide infra*), probably it protonates the oxo bridge group to form the corresponding hydroxo bridge in the oxidation state II,II. Because the  $\mu$ -oxo group is strongly basic in that species, the protonation stabilizes it and consequently increases the potential for the non-observed II,III/II,II couple. The basicity of the lower oxidation states of dinuclear oxo bridge complexes can be rationalize in terms of the MO diagram presented in chapter VI. The reduction of the oxidation state III,III causes a gradual rise of population into the  $\pi^*$  levels and the added protons stabilize the electron rich Ru-O-Ru moiety. The standard potentials for this couple in **1-dn**<sup>4+</sup> and **2-dn**<sup>4+</sup> are pretty similar to the one in  $\{[\text{Ru}(\text{trpy})(\text{bpy})]_2(\mu\text{-O})\}^{4+}$  pointing out that the electrochemical process concerns mainly the Ru-O-Ru core. On the other hand the well-known oxo bridge water oxidation catalyst  $\{[\text{Ru}(\text{bpy})_2(\text{H}_2\text{O})]_2(\mu\text{-O})\}^{4+}$ , the blue dimer, differs from the previous discussed structurally related complexes (entry **3** vs. **1**, **2** or **5**). It exhibits an one electron irreversible reduction from the oxidation state III,III to II,III where the latter is unstable towards the oxo bridge cleavage.

The complex  $\{[\text{Ru}(\text{trpy})(\text{H}_2\text{O})]_2(\mu\text{-bpp})\}^{3+}$  illustrates that the exchange of the oxo bridge by a rigid aromatic organic one has drastic consequences in each standard potential. The comparison of  $\{[\text{Ru}(\text{trpy})(\text{H}_2\text{O})]_2(\mu\text{-bpp})\}^{3+}$  and **1-dn**<sup>4+</sup> or alternatively **2-dn**<sup>4+</sup> (entry **4** vs. **1** or **2**) shows that the standard potentials for the IV,IV/III,III and III,III/II,II couples of the former are higher. This trend can be explained by simple electrostatic arguments, since  $\mu\text{-bpp}$  constitutes a monoanionic bridge ligand while  $\mu\text{-O}$  owns formally two negative

charges. The difference is more noticeable for  $E^0(\text{III,III/II,II})$  than for  $E^0(\text{IV,IV/III,III})$ ; indeed, the low value of the potential for the couple III,III/II,II explains why oxo bridge dinuclear complexes are usually isolated in high oxidation states, usually III,III.

The standard potentials for the IV,IV/III,III couple in **1-dn**<sup>4+</sup> and **2-dn**<sup>4+</sup> are slightly lower than the potentials for the IV/III or IV/II couples of the related mononuclear complexes **1**<sup>2+</sup> and **2**<sup>2+</sup> respectively (entry **1** vs. **6** and entry **2** vs **7**). However, the onset potential for the electrocatalytic increase of the current is quite similar.

**Table 1.** Summary of reduction potentials (V vs. SSCE) for various dinuclear and mononuclear complexes at pH = 1.

Dinuclears						
Entry	Complex <sup>a</sup>	E <sup>0</sup>			E <sub>onset</sub> <sup>b</sup>	Ref.
		III,IV/III,III	IV,IV/III,III	III,III/II,II		
1	1-dn <sup>4+</sup>	---	0.78 <sup>d</sup>	0.18 <sup>d,e</sup>	1.45	Tw. <sup>c</sup>
2	2-dn <sup>4+</sup>	---	0.80 <sup>d</sup>	0.21 <sup>d,e</sup>	1.47	Tw.
3	{[Ru(bpy) <sub>2</sub> (H <sub>2</sub> O)] <sub>2</sub> (μ-O)} <sup>4+</sup>	0.79	> 1.17 <sup>f</sup>	< 0.06 <sup>g</sup>	---	23
4	{[Ru(trpy)(H <sub>2</sub> O)] <sub>2</sub> (μ-bpp)} <sup>3+</sup>	0.88	0.98 <sup>h</sup>	0.62	1.30	27,28
5	{[Ru(trpy)(bpy)] <sub>2</sub> (μ-O)} <sup>4+</sup>	1.08	---	0.21 <sup>d,e</sup>	---	C. VI <sup>j</sup>

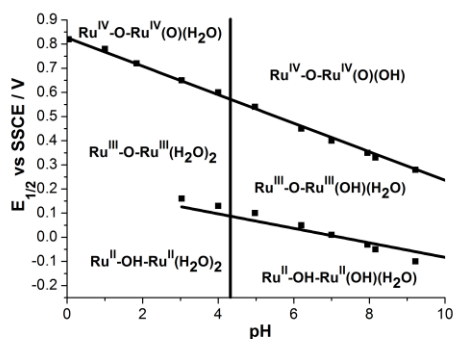
  

Mononuclears							
Entry	Complex	E <sup>0</sup>				E <sub>onset</sub>	Ref.
		III/II	IV/III	IV/II	V/IV		
6	1 <sup>2+</sup>	0.82	0.98	0.90	1.62	1.45	7,15
7	2 <sup>2+</sup>	---	---	0.87 <sup>d</sup>	1.68	1.48	7
8	3 <sup>2+</sup>	0.47	0.87	0.67	> 1.03 <sup>i</sup>	---	16

<sup>a</sup> Ligand abbreviation: bpp = bis(2-pyridyl)-3,5-pyrazolate. <sup>b</sup> Potential refers the value where electrocatalysis starts. <sup>c</sup> TW. means this work. <sup>d</sup> Two electron process. <sup>e</sup> Chemically irreversible process, the indicated potential corresponds to E<sub>p,c</sub> -0.015 V. <sup>f</sup> The oxidation state IV,IV is unstable with respect to disproportionation, so this E<sup>0</sup> is estimated considering that E<sup>0</sup>(IV,IV/III,IV) > E<sup>0</sup>(V,V/III,IV) where the latter is 1.22 V. <sup>g</sup> The oxidation state II,III suffers oxo bridge cleavage in the time scale of CV, however E<sup>0</sup>(III,III/II,II) cannot be lower than E<sup>0</sup>(III,III/II,III). <sup>h</sup> The wave associated to the IV,IV/III,IV couple is electrochemically irreversible, so its E<sub>1/2</sub> was estimated taking E<sub>p,a</sub> -0.03 V. <sup>i</sup> The oxidation state V is unstable with respect to disproportionation, thus this E<sup>0</sup> must be bigger than E<sup>0</sup>(VI/IV) = 1.03 V. <sup>j</sup> C.VI means chapter VI.

The potentials for the reductions of **1-dn**<sup>4+</sup> depend on the pH due to the acid-base properties of the different oxidation states (eq. 2 and 3). This dependency was studied over a broad pH range and is shown in the Pourbaix diagram depicted in Figure 4. The figure contains the  $E_{1/2}$ -pH values obtained from CV. The  $E_{1/2}$  values are equal to the formal potentials of the couples in a particular media under the assumption that  $D_{Ox} = D_{Red}$ .

The straight line corresponding to the IV,IV/III,III couple displays a constant slope of 59 mV/pH unit in the whole studied pH range (0 - 9). This value is consistent with a 2 electron reduction with the addition of 2 protons. On the other hand, a slope of approximately 30 mV/pH unit is observed for the couple III,III/II,II in agreement with a 2 electron reduction accompanied by the inclusion of 1 proton. Because both couples exhibit a constant slope in the whole pH range, spectrophotometric determinations of the  $pK_a$  values for the oxidation states IV,IV and III,III were carried out (Figures S2 and S3). The acid-base titration of IV,IV showed clear isosbestic points at 363, 415, 481 and 707 nm and a  $pK_a(IV,IV) = 4.4$  was calculated. The same titration for III,III, obtained by coulometric reduction of the initial IV,IV form provided  $pK_a(III,III) = 4.3$ . In this case, the changes in the UV-vis spectra are smaller as it has been previously observed in the oxidation state III,III of the blue dimer.<sup>23</sup> The close similarity between both  $pK_a$  values explains why the slopes for the two couples remain unmodified in the whole pH range. **1-dn**<sup>4+</sup> is unstable above pH = 9.50 probably because dimerization reactions occur which preclude obtaining reliable data from this pH.



**Figure 4.** Pourbaix diagram for **1-dn<sup>4+</sup>**. The potential-pH regions where the various oxidation states are the dominant forms are indicated. The vertical line represents the narrow region where the pK<sub>a</sub>s values are found. E<sub>1/2</sub> values were obtained by CV using an activated glassy carbon as working electrode, a Pt wire as counter electrode and a SSCE or Hg/Hg<sub>2</sub>SO<sub>4</sub>, K<sub>2</sub>SO<sub>4</sub> (sat.) reference electrodes. Scan rate = 100 mV s<sup>-1</sup>.

The pK<sub>a</sub> for the oxidation state IV,IV of **2-dn<sup>4+</sup>** was also spectrophotometrically determined in order to gain an insight of the influence of the bpy ligand onto the acid-base properties of the dinuclear complexes (Figure S4). The calculated pK<sub>a</sub> (4.0) is lower than the found in **1-dn<sup>4+</sup>** as expected from the electron-withdrawing effect of the F atoms substituents in the bpy ligand. The same behavior has been reported<sup>7</sup> for the mononuclear complexes **1<sup>2+</sup>** and **2<sup>2+</sup>**, however the effect size is smaller in the dinuclear complexes because the nature of the bpy ligand has a weaker influence upon the electronic structure of the complex as evidenced in the standard potentials (Table 1) and in the UV-vis spectroscopic features (Figure S5 and table S1).

On the other hand, the pK<sub>a</sub> value associated to the oxidation state II,II must be similar to the one for III,III in order to account for the constant slope for this couple. We could not determine it due to the previous discussed instability of this oxidation state towards the oxo bridge cleavage. The release



of the proton takes place in one of the aquo ligands, since deprotonation of the hydroxo group has not been observed<sup>21</sup> in structurally related complexes.

The oxidation states IV,IV and III,III of **1-dn**<sup>4+</sup> has been previously characterized by UV-vis spectroscopy (see chapter V and table S1). Low energy resonance Raman spectroscopy for both oxidation states was also carried out. The spectrum of IV,IV presents a band at 800 cm<sup>-1</sup> of very high intensity as main feature. It was assigned to a Ru=O<sub>terminal</sub> stretching mode on the basis that was <sup>18</sup>O-sensitive and the obtained shift (40 cm<sup>-1</sup>) (Figure 5). Resonance Raman spectrum of III,III could be acquired after the addition of 2 equivalents of Mohr's salt, (NH<sub>4</sub>)<sub>2</sub>Fe(SO<sub>4</sub>)<sub>2</sub>, to the IV,IV form. The spectrum lacks of the band of high intensity at 800 cm<sup>-1</sup> what confirms the earlier assignment and the absence of a Ru=O group in this oxidation state (Figure 5).

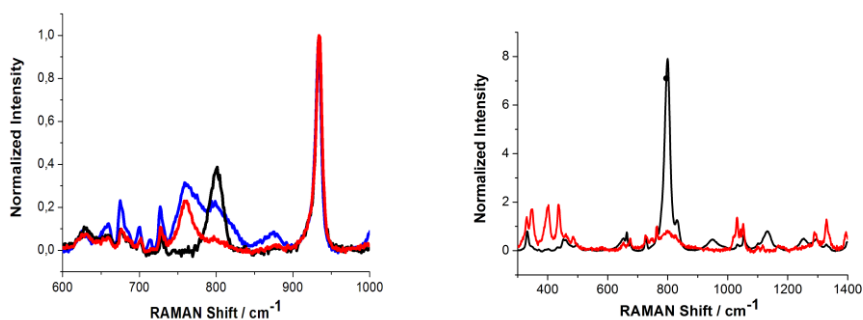


**Figure 5.** Left; overlay of the RR spectra obtained for the formation of **2-dn**<sup>4+</sup> in 0.1 M HClO<sub>4</sub> in H<sub>2</sub><sup>16</sup>O (black), H<sub>2</sub><sup>18</sup>O (red) and 1:1 H<sub>2</sub><sup>16</sup>O/ H<sub>2</sub><sup>18</sup>O (blue). Right; overlay of the RR spectra of the oxidation state IV,IV (black) and III,III (red) of **1-dn**<sup>4+</sup> in 0.1 M HOTf. The III,III form was generated after the addition of 2 equivalents of (NH<sub>4</sub>)<sub>2</sub>Fe(SO<sub>4</sub>)<sub>2</sub> to the IV,IV form. A 514 nm laser was used.

**Evolution of the mononuclear complexes.** The conversion of the mononuclear complexes **1**<sup>2+</sup> and **2**<sup>2+</sup> into the dinuclear ones **1-dn**<sup>4+</sup> and **2-dn**<sup>4+</sup>

was unambiguously demonstrated previously by UV-vis spectroelectrochemistry and rRAMAN spectroscopy using a 514 nm laser (see chapter V). Further rRAMAN experiments using a 413 nm laser were carried out in order to be able to observe species or stretching modes that do not appear with the 514 nm laser.

It has been extensively accepted that the addition of 3 equivalents of CAN to mononuclear complexes structurally related to  $\mathbf{1}^{2+}$  produces a hydroperoxo intermediate<sup>3,5</sup> (see Figure 1, left side). We decided to monitor this reaction with  $\mathbf{1}^{2+}$  and  $\mathbf{2}^{2+}$  by rRAMAN spectroscopy using a 413 nm laser (Figure 6 and S6). Additionally the addition of 2 equivalents of CAN to the mononuclear compounds was also monitored. Interestingly any remarkable difference could be observed in both experiments. This close similarity leads us to think that the species formed under both conditions are the same unless there are compounds non-observable by rRAMAN spectroscopy under one of the conditions. However, the CV of a solution containing 3 equivalents of CAN and  $\mathbf{2}^{2+}$  showed that the main product after 4 days of reaction was the  $\text{Ru}^{\text{IV}}=\text{O}$  complex (see chapter IV, figure S20). These evidences point out that the rRAMAN spectra correspond fundamentally to the  $\text{Ru}^{\text{IV}}=\text{O}$  complex.

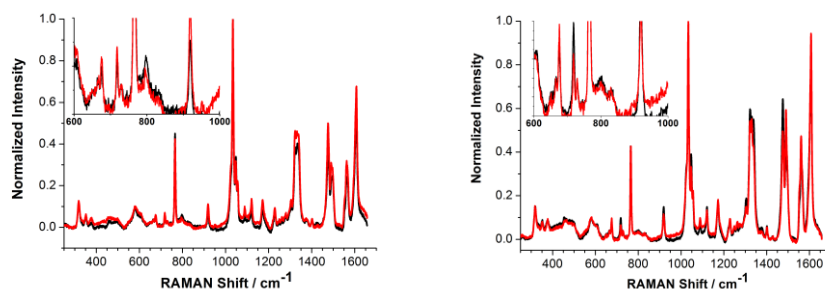


**Figure 6.** RR monitoring of the reaction of 2 (red) or 3 (black) equivalents of CAN with a 1 mM solution of  $1^{2+}$  in 0.1 M HOTf immediately (left) or 20 hours after the addition of CAN (right).

A band of small intensity appears at  $800\text{ cm}^{-1}$  which corresponds to the formation of  $1\text{-dn}^{4+}$  and  $2\text{-dn}^{4+}$  in agreement with previous studies using a 514 nm laser (see chapter V). Labelling experiments with  $\text{H}_2^{18}\text{O}$  lead to a downshift of this mode to  $760\text{ cm}^{-1}$  as expected. A new  $^{18}\text{O}$ -sensitive broad band was also observed at  $614\text{ cm}^{-1}$  in  $\text{H}_2^{16}\text{O}$  which is shifted at  $573\text{ cm}^{-1}$  in  $\text{H}_2^{18}\text{O}$  ( $\Delta\nu = 41\text{ cm}^{-1}$ ). Spectra taken in 50 %  $^{18}\text{O}$ -labelled water exhibited only two bands in both cases discarding that they are associated to some O-O stretching mode. The big width and downshift of the band at  $614\text{ cm}^{-1}$  somehow remind the broad band at 688 nm found<sup>29-31</sup> by Hurst *et. al* in CAN oxidized solutions of blue dimer in 0.1 M  $\text{HNO}_3$  or HOTf. The band only appeared in solutions containing  $\text{Ce}^{\text{IV}}$  and  $\text{NO}_3^-$ , thus it was proposed that the band proceeded from an intermediate which is related to  $\text{O}_2$  evolution by an oxidized form of the blue dimer and a nitrate anion previously activated by ceric coordination. The precise nature of the intermediate is currently unknown. Our experiments could indicate that the same anomalous cerium reactivity can occur in mononuclear catalysts as suggested in previous MS, UV-vis spectroscopic and computational studies.<sup>5,6</sup> However it is worth to mention that the rRAMAN

spectra obtained<sup>32</sup> for the electrolysis in 10 mM sodium phosphate buffer of the mononuclear complex  $[\text{Ru}(\text{NMP})(4\text{-Mepy})_2(\text{H}_2\text{O})]^{2+}$  (where 4-Mepy is 4-picoline and NMP is 4-*t*-butyl-2,6-di-(1',8'-naphthyrid-2'-yl)-pyridine) displayed a band at  $547\text{ cm}^{-1}$  which was shifted at  $535\text{ cm}^{-1}$  ( $\Delta\nu = 12\text{ cm}^{-1}$ ) after labelling with  $\text{H}_2^{18}\text{O}$ . The band was assigned to the peroxo intermediate  $[\text{Ru}^{\text{IV}}\text{-OO}]^{2+}$ . Although the band arose in  $\text{Ce}^{\text{IV}}$ ,  $\text{NO}_3^-$  free-conditions, it is sharp and suffers a low downshift in contrast to our findings. The clear difference precludes the identification of both resonances with the same kind of compound. Further rRAMAN experiments are required in order to check if the band at  $614\text{ cm}^{-1}$  also appears in the absence of nitrate anions.

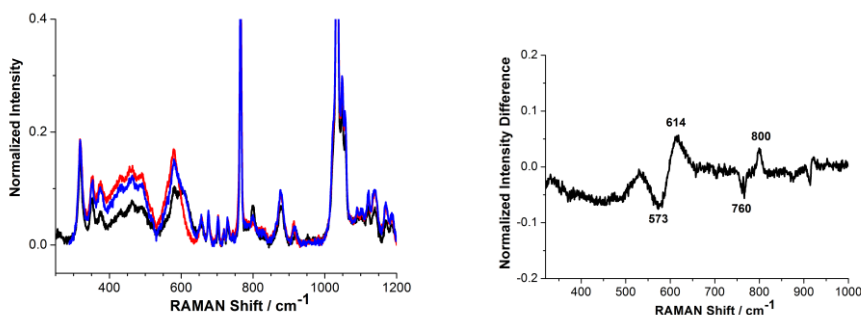


**Figure 7.** Left, overlay of RR spectra obtained in the first 5 minutes of the reaction of 2 equivalents of CAN with a 1 mM solution of  $2^{2+}$  in 0.1 M HOTf in  $\text{H}_2^{16}\text{O}$  (black),  $\text{H}_2^{18}\text{O}$  (red) and  $\text{H}_2^{16}\text{O}:\text{H}_2^{18}\text{O}$  (1:1) (blue). Right, differential spectrum of  $\text{H}_2^{16}\text{O} - \text{H}_2^{18}\text{O}$ .

The catalytic water oxidation by  $1^{2+}$  and  $2^{2+}$  using CAN as sacrificial oxidant was also studied by rRAMAN spectroscopy. The first spectrum taken 300 s after the addition of CAN exhibits a new band at  $835\text{ cm}^{-1}$  which gradually increases its intensity (Figure 8). The band assigned to  $1\text{-dn}^{4+}$  ( $800\text{ cm}^{-1}$ ) is not so clearly discernible in the beginning of the catalysis, but it grows faster than the previous one. The band at  $835\text{ cm}^{-1}$  corresponds to the symmetric stretching mode of the  $[\text{O}=\text{Ru}^{\text{VI}}=\text{O}]$  group of  $3^{2+}$  and is the most

prominent rRAMAN spectral feature of this compound in 0.1 M HOTf (Figure 8). Therefore, our experiments confirm unambiguously the formation of  $3^{2+}$  from the very beginning of the catalysis. The *trans*-dioxo complex plays the role of a gate giving access to the catalytic cycle driven by the more robust catalyst  $1\text{-dn}^{4+}$ . When  $2^{2+}$  is used as catalyst instead of  $1^{2+}$  the rRAMAN spectra follow the same trend but the changes are slower in agreement with the lower catalytic activity of  $2^{2+}$  (Figure S7).

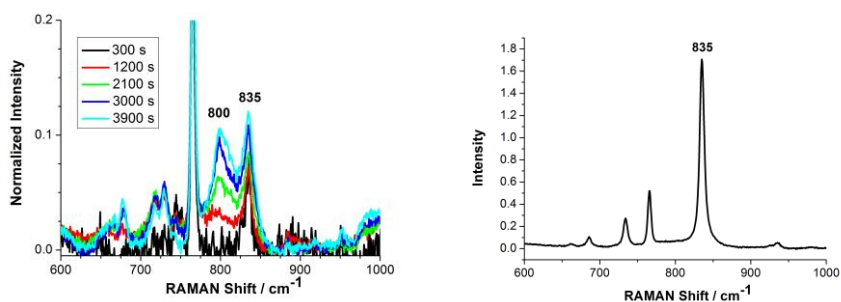
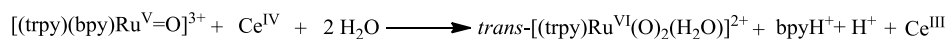


**Figure 8.** Left, spectroscopic rRAMAN monitoring of the reaction of 100 equivalents of CAN with a 1 mM solution of  $1^{2+}$  in 0.1 M HOTf. Right, rR spectrum of  $3^{2+}$  in 0.1 M HOTf.

The generation of  $3^{2+}$  and consequently the dinuclear complexes is conceived as a general process in catalytic water oxidation by mononuclear complexes, so it is of great interest to understand the reasons that drive this transformation at the molecular level. The conversion of  $1^{2+}$  or  $2^{2+}$  into  $3^{2+}$  has been proposed to occur due to bpy ligand loss from the single-site catalysts potentially in the oxidation state V (see chapter V),



The strong *trans* effect exerted by the  $\text{Ru}^{\text{V}}=\text{O}$  group weakens one of the Ru-N bpy bonds that eventually leads to the loss of the bpy ligand. This

phenomenon has already been pointed out by Berlinguette *et al.*<sup>13</sup> and us<sup>14</sup> based on DFT calculations. We could successfully get crystals suitable for X-ray analysis of the oxidation state IV of  $\mathbf{2}^{2+}$  which corroborate the calculated predictions. The structure consists in an octahedrally distorted coordinated ruthenium (IV) metal center which bears an oxo ligand in addition to the trpy and bpy ligands (Figure 9). The Ru-O distance (1.85 Å) falls in the longer range of values reported for Ru<sup>IV</sup>=O groups<sup>33-38</sup> (see also chapter VI). A water molecule crystallized with the complex is making an Hydrogen Bond to the oxygen atom linked to the Ruthenium atom. However the most remarkable feature is the elongation of the *trans* Ru-N bpy bond (2.14 Å) with regard to the same bond in the aquo complex in the oxidation state II (2.02 Å). The striking difference (0.12 Å) suggests that bpy decooordination is a feasible scenario for the formation of  $\mathbf{3}^{2+}$ .

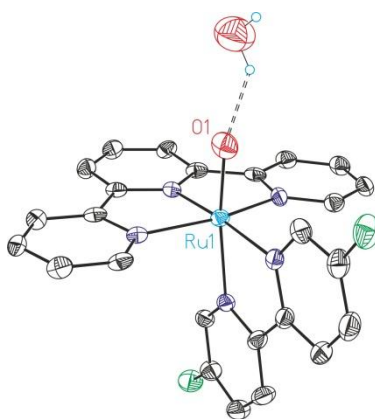


**Figure 9.** ORTEP plot (ellipsoid drawn at 50% probability) of the X-ray structure of complex  $\mathbf{2}^{2+}$  in the oxidation state IV. Color codes: Ru, cyan; O, Red; N, Blue; C, black; F, green. H atoms are not shown except for a crystallized water molecule forming a H-bond with the oxo group.

**Two interconnected cycles.** Complexes  $\mathbf{1-dn}^{4+}$  and  $\mathbf{2-dn}^{4+}$  are rugged and active electrocatalysts for the oxidation of water to dioxygen (see chapter V).

The catalytic activity has also been evaluated using CAN as sacrificial oxidant and compared to the one of its mononuclear counterparts  $1^{2+}$  and  $2^{2+}$ . The oxygen production was monitored manometrically (Figure 10) and the nature of the evolved gases was analyzed by mass spectrometry confirming that dioxygen was the only generated gas (Figure S8). As can be observed in the graph, the initial activity of the dinuclear complexes is practically the same as the one of the mononuclear compounds, nonetheless the production of oxygen by the dinuclears decays before and as a consequence the TON achieves a lower value.

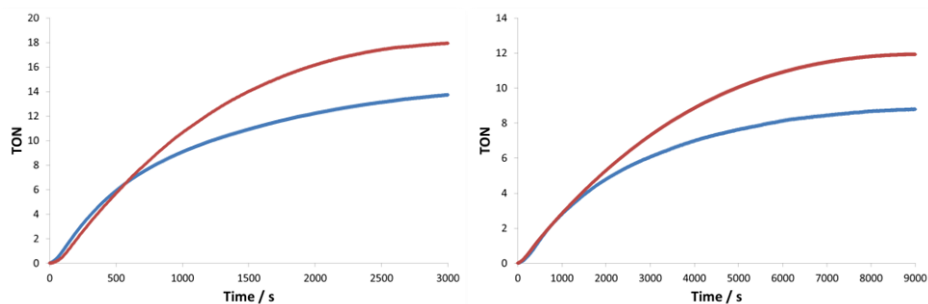


**Figure 10.** Overlay of oxygen evolution profiles for 1 mM solutions of dinuclear (blue) and mononuclears (red) complexes under 1:100 Cat/CAN ratios in 0.1 M HOTf (pH = 1). Left,  $1\text{-dn}^{4+}$  vs.  $1^{2+}$ ; right,  $2\text{-dn}^{4+}$  vs.  $2^{2+}$ .

In order to know if decomposition pathways had destroyed the dinuclear catalysts UV-vis spectroscopy was carried out upon catalytic solutions when the oxygen evolution had ceased. The spectrum for the reaction with  $1\text{-dn}^{4+}$  exhibits a slight decrease of the band at 455 nm (457 nm for  $2\text{-dn}^{4+}$ ) accompanied by an enhancement of a band at 691 nm (687 nm for  $2\text{-dn}^{4+}$ ) (Figure 11 and figure S9). The latter feature could be attributed to the formation of the known dimeric complex  $\{[\text{Ru}(\text{trpy})(\text{bpy})]_2(\mu\text{-O})\}^{4+}$  ( $1\text{-dm}^{4+}$ ). However, the loss of absorbance at 455 nm indicates that only a 5 % of the

initial  $\mathbf{1-dn}^{4+}$  disappears. If this small amount would be fully transformed into  $\mathbf{1-dm}^{4+}$ , this complex should have a extinction coefficient at 691 nm of  $104000 \text{ M}^{-1} \text{ cm}^{-1}$  which is clearly larger than the observed value of  $25600 \text{ M}^{-1} \text{ cm}^{-1}$  (Figure 11 and chapter VI).

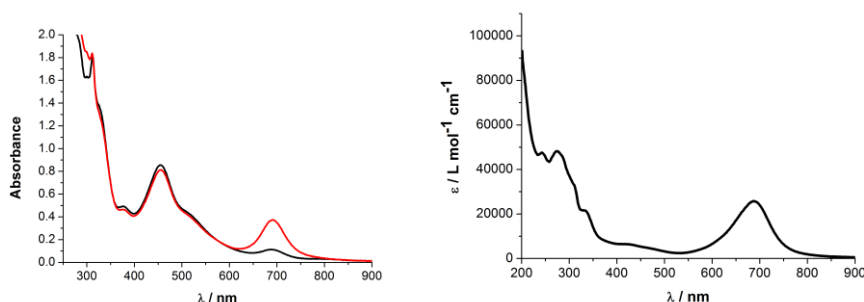


**Figure 11.** Left; overlay of UV-visible spectra of a 1 mM solution of complex  $\mathbf{1-dn}^{4+}$  in 0.1 M HOTf before (black) and after oxygen evolution induced by the addition of 100 equivalents of CAN (red). The samples were previously 20 times diluted. Right, UV-vis spectrum of  $\mathbf{1-dm}^{4+}$  in 0.1 M HOTf.

Therefore, the increase of the band at 691 nm must proceed from the generation of another compound; probably the tetranuclear complex  $\{[(\text{trpy})(\text{bpy})\text{Ru}^{\text{II}}(\mu\text{-O})\text{Ru}^{\text{IV}}(\text{trpy})(\text{H}_2\text{O})]_2(\mu\text{-O})\}^{6+}$  ( $\mathbf{1-tn}^{6+}$ ) whose acetonitrile coordinated analogue was structurally characterized in chapter VI.  $\mathbf{1-tn}^{6+}$  comprises two  $\mathbf{1-dn}^{4+}$  halves linked by a central oxo bridge and is formally a dimerization product from the condensation of two  $\mathbf{1-dn}^{4+}$  molecules (Figure 12). The large extinction coefficient attributed to  $\mathbf{1-tn}^{6+}$  is consistent with a common trend in structurally related oligomers stating that the higher the nuclearity the larger the extinction coefficients in the visible region<sup>39</sup> of the UV-vis spectrum; which means that the produced amount of tetranuclear complex observed by UV-vis spectroscopy is considerably small. Hence, the dinuclear catalysts survive the harsh oxidative conditions in catalytic water



oxidation using CAN as sacrificial oxidant, only a small part is converted to tetranuclear complexes that preserve the scaffold of the dinuclear compounds. This ruggedness has already been found in electrocatalytic water oxidation<sup>14</sup> where exposure of the dinuclear catalysts at 1.6 V vs. SSCE for 10 hours did not show any evidence of decomposition (chapter V).

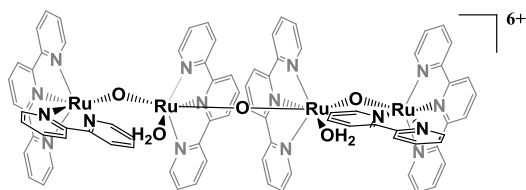


**Figure 12.** Structure of the tetranuclear complex **1-tn<sup>6+</sup>**.

The conversion of mononuclear complexes into dinuclears under catalytic conditions establishes the coexistence of two cycles that lead to dioxygen. The different intermediates could interact and speed up the generation of dioxygen with regard to two completely independent cycles. The activity of a 1:1 catalytic solution of **1-dn<sup>4+</sup>** and **1<sup>2+</sup>** was compared with the one of each separated complex at the same concentration of catalyst and CAN. The mixture of catalysts produced a bigger amount of O<sub>2</sub> in a faster rate with regard to each separated component (Figure 13). This behavior points out clearly the existence of a synergic effect between the two interconnected catalytic cycles.

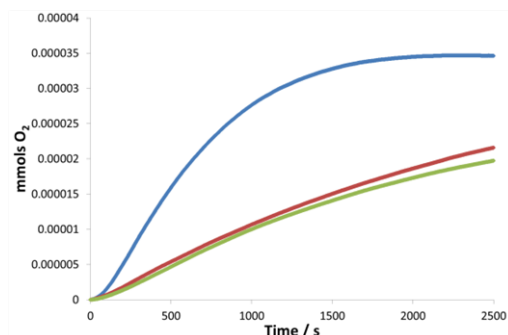
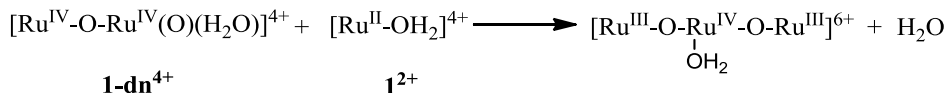
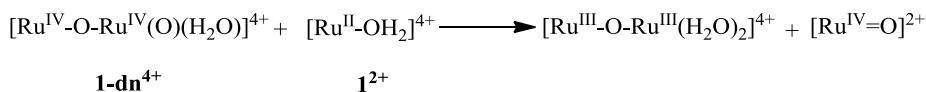


**Figure 13.** Overlay of oxygen evolution profiles resulting of the addition of a 100 mM solution of CAN to a solution mixture of  $1^{2+}$  and  $1\text{-dn}^{4+}$ , both at 0.5 mM concentration, (blue), a 0.5 mM solution of only  $1^{2+}$  (red) or only  $1\text{-dn}^{4+}$  (green).

The formation of the trinuclear complex  $\{[\text{Ru}^{\text{III}}(\text{trpy})(\text{bpy})(\mu\text{-O})]_2\text{Ru}^{\text{IV}}(\text{trpy})(\text{H}_2\text{O})\}^{6+}$  which was structurally characterized in a previous report (see chapter VI), could explain the increase of activity observed in the mixture of catalysts if the new compound would be a high active WOC,



However, the UV-vis spectroscopic monitoring of the reaction of a 1:1 mixture of  $1\text{-dn}^{4+}$  and  $1^{2+}$  showed spectral changes consistent with the slow reduction of the oxidation state IV,IV of  $1\text{-dn}^{4+}$  to the oxidation state III,III as the uniquely occurring process, discarding the formation of a new species like the trinuclear complex (Figure S10),



Therefore, the synergic effect observed in the catalysis must proceed from the interaction of intermediates from different cycles. Additional

mechanistic studies will be developed in order to clarify the nature of such interactions.

#### 7.4. Conclusions.

In a previous study we demonstrated that single-site WOCs structurally related to  $\mathbf{1}^{2+}$  evolved to oxo-bridge dinuclear complexes which are rigger catalysts (chapter V). The presented work constitutes a mandatory continuation where the electrochemical and acid-base properties of the dinuclear compounds  $\mathbf{1-dn}^{4+}$  and  $\mathbf{2-dn}^{4+}$  have been thoroughly examined.  $\mathbf{1-dn}^{4+}$  shows two pH-dependent 2 electron waves in cyclic voltammetry. The wave attributed to the IV,IV/III,III is associated to double protonation of the oxo terminal ligand of IV,IV according to the Pourbaix diagram. The conversion of the oxo ligand into an aquo group in the oxidation state III,III is consistent with the rRAMAN spectrum of III,III that lacks the Ru=O stretching mode. The second wave proceeds from the III,III/II,II couple and is associated to protonation in the oxo bridge ligand according to its pH-dependency. The electrochemical process is irreversible at pH < 4 because oxo-bridge cleavage occurs in the oxidation state II,II. The pK<sub>a</sub>s of the aquo ligands in IV,IV and III,III were spectrophotometrically determined. Both values are quite similar (pK<sub>a</sub>(IV,IV) = 4.4 and pK<sub>a</sub>(III,III) = 4.3), what explains the constant slope for the two couples in the Pourbaix diagram. Additionally, the pK<sub>a</sub> for the oxidation state IV,IV of  $\mathbf{2-dn}^{4+}$  was obtained. The value is slightly lower than the found for  $\mathbf{1-dn}^{4+}$  (4.0 vs. 4.4) which is consistent with the electron withdrawing effect exerted by the F atoms of the bpy ligand.

The conversion of  $\mathbf{1}^{2+}$  into  $\mathbf{1-dn}^{4+}$  was studied previously by rRAMAN spectroscopy using a device equipped with a 514 nm laser (see chapter V). Herein, we have carried out the same method using a rRAMAN

spectrophotometer equipped with a 413 nm laser. We have observed that the reaction of the mononuclear complexes with 2 or 3 equivalents of CAN produces significantly the same features in the rRAMAN spectra, suggesting that both processes generate the same compounds. Two  $^{18}\text{O}$ -sensitive bands could be observed: 1) a band at  $800\text{ cm}^{-1}$  which corresponds to the formation of the dinuclear complexes and is  $40\text{ cm}^{-1}$  downshifted as expected, 2) a broad band around 614 nm that is  $41\text{ cm}^{-1}$  downshifted. This band presents similar characteristics to the band found at 688 nm by Hurst *et. al.*<sup>31</sup> in the study of catalytic water oxidation by high oxidation states of the blue dimer. It has been attributed to an unknown intermediate that proceeds from nitrate activation by  $\text{Ce}^{\text{IV}}$  and subsequent reaction with some oxidation state of the blue dimer. Our observations could point out the existence of a similar route in single-site WOCs. Catalytic water oxidation by  $\mathbf{1}^{2+}$  and  $\mathbf{2}^{2+}$  using 100 equivalents of CAN was also followed by rRAMAN spectroscopy. The spectra showed unambiguously the formation of the *trans*-dioxo compound  $\mathbf{3}^{2+}$  immediately after the addition of the sacrificial oxidant and the gradual increase of the band associated to the dinuclear complexes. These evidences support our first proposal where the formation of  $\mathbf{3}^{2+}$  plays the critical role of a *gate* giving access to the formation of the dinuclear complexes (see chapter V and Figure 1).

$\mathbf{1-dn}^{4+}$  and  $\mathbf{2-dn}^{4+}$  are good WOCs using CAN as sacrificial oxidant. The most remarkable property of these catalysts is its impressive robustness, proved by UV-vis spectroscopy, under the harsh oxidative environment imposed by the huge excess of oxidant. The same ruggedness was observed previously under electrocatalytic conditions (see chapter V). On the other hand, the coexistence of two catalytic cycles suggests that intermediates from

different cycles could interact and speed up the evolution of dioxygen. This synergic effect was corroborated by manometric experiments. The formation of the trinuclear complex  $\{[\text{Ru}^{\text{III}}(\text{trpy})(\text{bpy})(\mu\text{-O})]_2\text{Ru}^{\text{IV}}(\text{trpy})(\text{H}_2\text{O})\}^{6+}$  from the reaction of  $\mathbf{1-dn}^{4+}$  and  $\mathbf{1}^{2+}$  was discarded as responsible for the synergic effect, since UV-vis monitoring of the aforementioned reaction only exhibited spectral changes consistent with the reduction of the oxidation state IV,IV of  $\mathbf{1-dn}^{4+}$  to III,III.

The rRAMAN spectra taken with the device equipped with a 413 nm laser were carried out in the Max-Volmer-Laboratory (MVL) for Biophysical Chemistry of the Technische Universität Berlin by Anke Keidel under the supervision of Dr. Uwe Kuhlmann and Prof. Peter Hildebrandt.

## 7.5. Acknowledgement.

Support from MINECO (CTQ2010–21497 and PRI-PIBIN-2011-1278) and FPU grant to IL and Torres Quevedo contract to SM are gratefully acknowledged. Support has also been received from the Cluster of Excellence (UniCat).

## 7.6. References.

- (1) Zong, R.; Thummel, R. P. *J. Am. Chem. Soc.* **2005**, *127*, 12802.
- (2) Concepcion, J. J.; Jurss, J. W.; Templeton, J. L.; Meyer, T. J. *J. Am. Chem. Soc.* **2008**, *130*, 16462.
- (3) Concepcion, J. J.; Tsai, M.-K.; Muckerman, J. T.; Meyer, T. J. *J. Am. Chem. Soc.* **2010**, *132*, 1545.
- (4) Concepcion, J. J.; Jurss, J. W.; Norris, M. R.; Chen, Z.; Templeton, J. L.; Meyer, T. J. *Inorg. Chem.* **2010**, *49*, 1277.
- (5) Wasylenko, D. J.; Ganesamoorthy, C.; Henderson, M. A.; Koivisto, B. D.; Osthoff, H. D.; Berlinguette, C. P. *J. Am. Chem. Soc.* **2010**, *132*, 16094.
- (6) Yoshida, M.; Masaoka, S.; Abe, J.; Sakai, K. *Chem. Asian J.* **2010**, *5*, 2369.

- (7) Maji, S.; López, I.; Bozoglian, F.; Benet-Buchholz, J.; Llobet, A. *Inorg. Chem.* **2013**, *52*, 3591.
- (8) Murakami, M.; Hong, D.; Suenobu, T.; Yamaguchi, S.; Ogura, T.; Fukuzumi, S. *J. Am. Chem. Soc.* **2011**, *133*, 11605.
- (9) Blakemore, J. D.; Schley, N. D.; Balcells, D.; Hull, J. F.; Olack, G. W.; Incarvito, C. D.; Eisenstein, O.; Brudvig, G. W.; Crabtree, R. H. *J. Am. Chem. Soc.* **2010**, *132*, 16017.
- (10) Wasylenko, D. J.; Palmer, R. D.; Schott, E.; Berlinguette, C. P. *Chem. Commun. (Cambridge, U. K.)* **2012**, *48*, 2107.
- (11) Zhang, M.-T.; Chen, Z.; Kang, P.; Meyer, T. J. *J. Am. Chem. Soc.* **2013**, *135*, 2048.
- (12) Boyer, J. L.; Polyansky, D. E.; Szalda, D. J.; Zong, R.; Thummel, R. P.; Fujita, E. *Angew. Chem. Int. Ed.* **2011**, *50*, 12600.
- (13) Wasylenko, D. J.; Ganesamoorthy, C.; Koivisto, B. D.; Henderson, M. A.; Berlinguette, C. P. *Inorg. Chem.* **2010**, *49*, 2202.
- (14) Lopez, I.; Ertem, M. Z.; Maji, S.; Benet-Buchholz, J.; Keidel, A.; Kuhlmann, U.; Hildebrandt, P.; Batista, V. S.; Llobet, A. *Angew. Chem. Int. Ed.* **2013**, *submitted*.
- (15) Takeuchi, K. J.; Thompson, M. S.; Pipes, D. W.; Meyer, T. J. *Inorg. Chem.* **1984**, *23*, 1845.
- (16) Adeyemi, S. A.; Dovletoglou, A.; Guadalupe, A. R.; Meyer, T. J. *Inorg. Chem.* **1992**, *31*, 1375.
- (17) Cabaniss, G. E.; Diamantis, A. A.; Murphy, W. R.; Linton, R. W.; Meyer, T. J. *J. Am. Chem. Soc.* **1985**, *107*, 1845.
- (18) Data collection with APEX II version v2009.1-0.2 **2009**. Bruker AXS Inc., Madison, Wisconsin, USA.
- (19) Data reduction with Bruker SAINT version V7.60A **2007**. Bruker AXS Inc., Madison, Wisconsin, USA.
- (20) Sheldrick, G. *Acta Crystallographica Section A* **2008**, *64*, 112.
- (21) Llobet, A.; Doppelt, P.; Meyer, T. J. *Inorg. Chem.* **1988**, *27*, 514.
- (22) Llobet, A.; Curry, M. E.; Evans, H. T.; Meyer, T. J. *Inorg. Chem.* **1989**, *28*, 3131.
- (23) Gilbert, J. A.; Eggleston, D. S.; Murphy, W. R.; Geselowitz, D. A.; Gersten, S. W.; Hodgson, D. J.; Meyer, T. J. *J. Am. Chem. Soc.* **1985**, *107*, 3855.
- (24) Schneider, R.; Weyhermueller, T.; Wieghardt, K.; Nuber, B. *Inorg. Chem.* **1993**, *32*, 4925.
- (25) Jurss, J. W.; Concepcion, J. J.; Butler, J. M.; Omberg, K. M.; Baraldo, L. M.; Thompson, D. G.; Lebeau, E. L.; Hornstein, B.; Schoonover, J. R.; Jude, H.; Thompson, J. D.; Dattelbaum, D. M.; Rocha, R. C.; Templeton, J. L.; Meyer, T. J. *Inorg. Chem.* **2012**, *51*, 1345.

- (26) Mayer, J. M. *Comments Inorg. Chem.* **1988**, *8*, 125.
- (27) Bozoglian, F.; Romain, S.; Ertem, M. Z.; Todorova, T. K.; Sens, C.; Mola, J.; Rodri guez, M.; Romero, I.; Benet-Buchholz, J.; Fontrodona, X.; Cramer, C. J.; Gagliardi, L.; Llobet, A. *J. Am. Chem. Soc.* **2009**, *131*, 15176.
- (28) Roeser, S., Universitat Rovira i Virgili, 2011.
- (29) Yamada, H.; Hurst, J. K. *J. Am. Chem. Soc.* **2000**, *122*, 5303.
- (30) Moonshiram, D.; Jurss, J. W.; Concepcion, J. J.; Zakharova, T.; Alperovich, I.; Meyer, T. J.; Pushkar, Y. *J. Am. Chem. Soc.* **2012**, *134*, 4625.
- (31) Stull, J. A.; Britt, R. D.; McHale, J. L.; Knorr, F. J.; Lyman, S. V.; Hurst, J. K. *J. Am. Chem. Soc.* **2012**, *132*, 19973.
- (32) Polyansky, D. E.; Muckerman, J. T.; Rochford, J.; Zong, R.; Thummel, R. P.; Fujita, E. *J. Am. Chem. Soc.* **2011**, *133*, 14649.
- (33) Welch, T. W.; Ciftan, S. A.; White, P. S.; Thorp, H. H. *Inorg. Chem.* **1997**, *36*, 4812.
- (34) Che, C. M.; Lai, T. F.; Wong, K. Y. *Inorg. Chem.* **1987**, *26*, 2289.
- (35) Cheng, W.-C.; Yu, W.-Y.; Cheung, K.-K.; Che, C.-M. *J. Chem. Soc., Dalton Trans.* **1994**, 57.
- (36) Che, C. M.; Tang, W. T.; Wong, W. T.; Lai, T. F. *J. Am. Chem. Soc.* **1989**, *111*, 9048.
- (37) Kojima, T.; Nakayama, K.; Ikemura, K.; Ogura, T.; Fukuzumi, S. *J. Am. Chem. Soc.* **2011**, *133*, 11692.
- (38) Cheng, W.-C.; Yu, W.-Y.; Zhu, J.; Cheung, K.-K.; Peng, S.-M.; Poon, C.-K.; Che, C.-M. *Inorg. Chim. Acta* **1996**, *242*, 105.
- (39) Lebeau, E. L.; Adeyemi, S. A.; Meyer, T. J. *Inorg. Chem.* **1998**, *37*, 6476.

## Supporting Information for,

# Exploring the properties of rugged oxo-bridge dinuclear water oxidation catalyst and its relationship with mononuclear catalysts

Isidoro López,<sup>a</sup> Somnath Maji,<sup>a</sup> Anke Keidel,<sup>b</sup> Jordi Benet-Buchholz,<sup>a</sup> Uwe Kuhlmann,<sup>b</sup> Peter Hildebrandt<sup>b</sup> and Antoni Llobet<sup>a,c</sup>

<sup>a</sup> Institute of Chemical Research of Catalonia (ICIQ), Av. Països Catalans, 16, 43007 Tarragona, Spain.

<sup>b</sup> Technische Universität Berlin, Institut für Chemie, Sekr. PC14, Straße des 17. Juni 135, D-10623 Berlin, Germany.

<sup>c</sup> Departament de Química, Universitat Autònoma de Barcelona, Cerdanyola del Vallès, 08193 Barcelona, Spain.



**Figure S 1.** CVs of complex **1-dn**<sup>4+</sup> at different pHs. 0.3 mM complex concentration. Activated glassy carbon was used as working electrode, a Pt wire as counter electrode and SSCE as reference electrode. Scan rate=100 mV s<sup>-1</sup>.

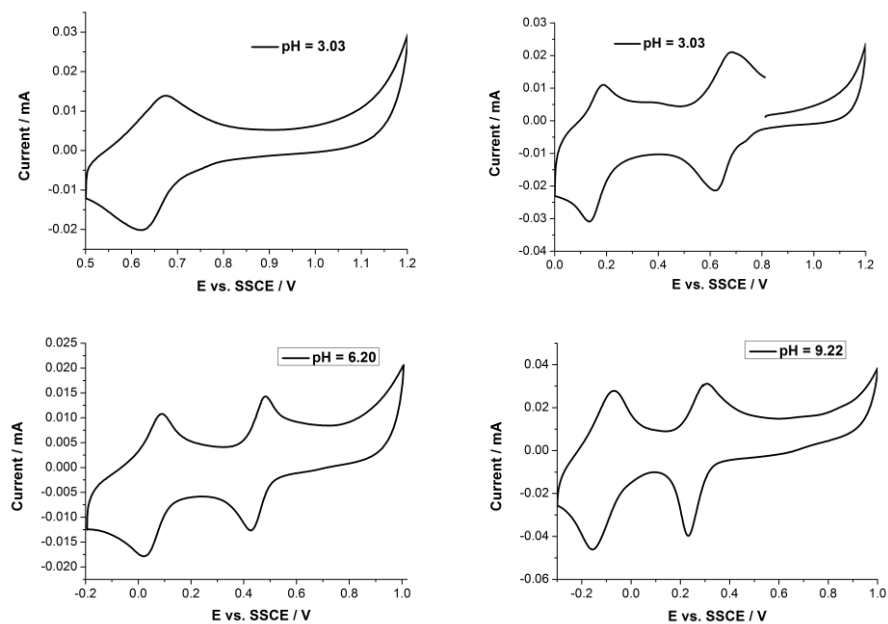


**Figure S 2.** (Upper) Acid-base spectrophotometric titration of the oxidation state IV,IV of **1-dn**<sup>4+</sup> after consecutive additions of 1-5  $\mu\text{L}$  of 6.16 M NaOH to a 25  $\mu\text{M}$  solution of the complex in 0.1 M  $\text{H}_3\text{PO}_4$  /  $\text{NaH}_2\text{PO}_4$  buffer at pH = 2.15. pH changes: 2.32, 2.52, 2.78, 3.29, 3.41, 3.70, 4.04, 4.26, 4.60, 4.79, 5.03, 5.21, 5.44, 5.73 and 5.95. (Bottom) Plot for the calculation of the  $\text{pK}_a$  value.

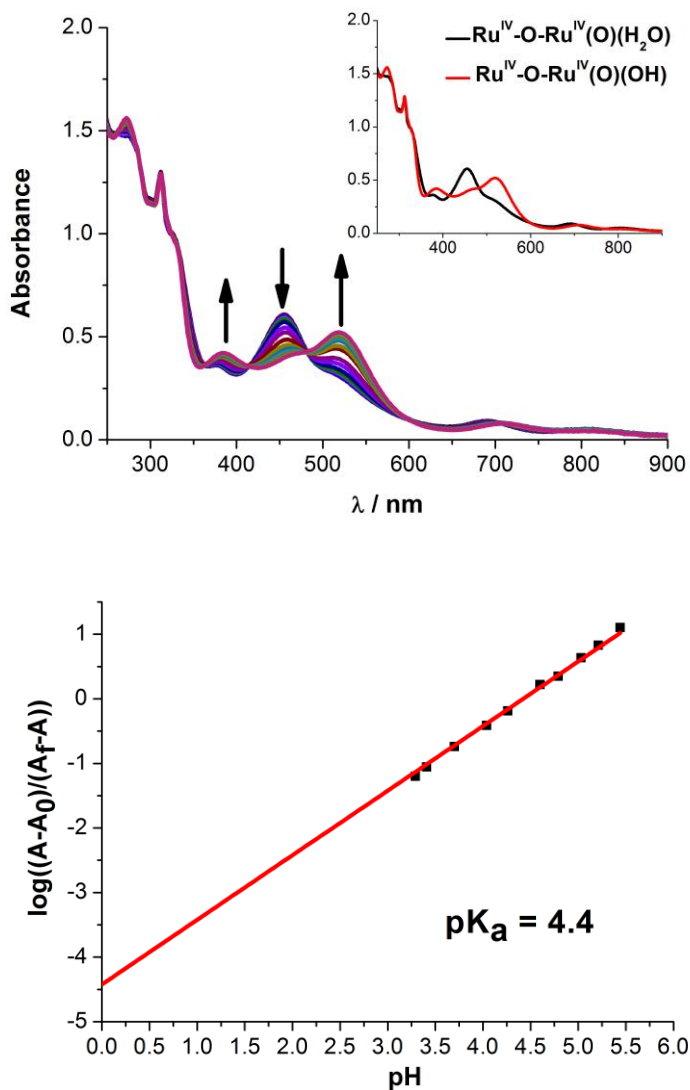


**Figure S 3.** (Upper) Acid-base spectrophotometric titration of the oxidation state III,III of **1-dn**<sup>4+</sup> after consecutive additions of 1-5  $\mu\text{L}$  of 6.16 M NaOH to a 25  $\mu\text{M}$  solution of the complex in 0.1 M  $\text{H}_3\text{PO}_4 / \text{NaH}_2\text{PO}_4$  buffer at pH = 2.15. pH changes: 2.94, 3.33, 3.52, 3.78, 4.65 and 5.22. (Bottom) Plot for the calculation of the  $\text{pK}_a$  value.

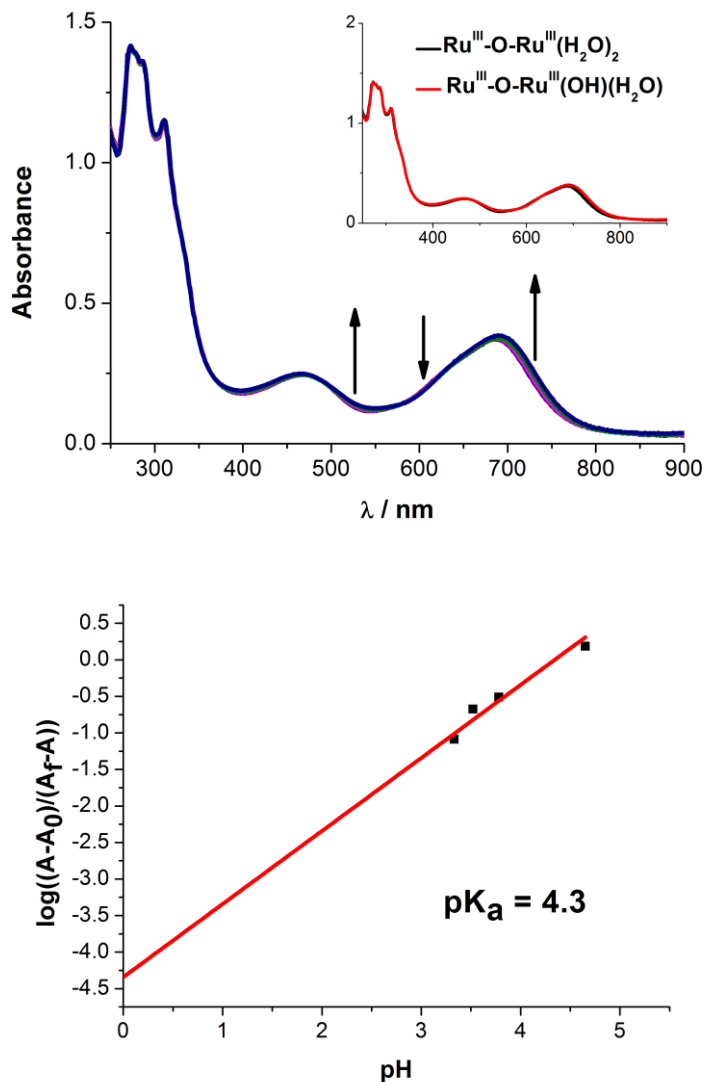
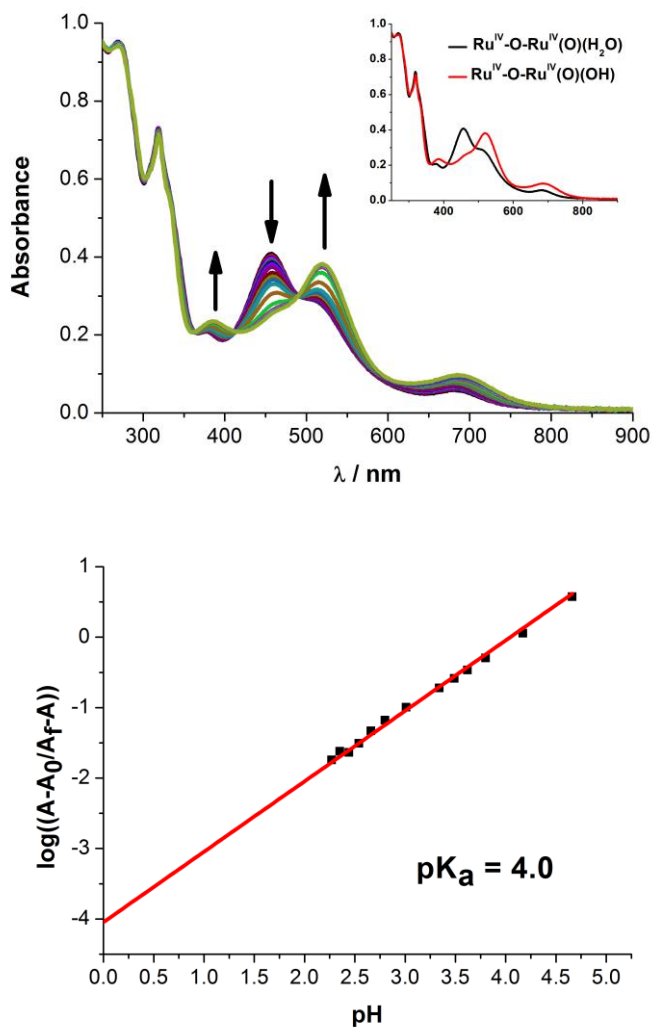


**Figure S 4.** (Upper) Acid-base spectrophotometric titration of the oxidation state IV,IV of **2-dn**<sup>4+</sup> after consecutive additions of 1-5  $\mu\text{L}$  of 6.16 M NaOH to a 25  $\mu\text{M}$  solution of the complex in 0.1 M  $\text{H}_3\text{PO}_4$  /  $\text{NaH}_2\text{PO}_4$  buffer at pH = 2.15. pH changes: 2.20, 2.27, 2.35, 2.44, 2.54, 2.66, 2.80, 3.01, 3.34, 3.49, 3.62, 3.80, 4.17, 4.66, 5.02, 5.24, 5.38 and 5.57. (Bottom) Plot for the calculation of the  $\text{pK}_a$  value.



VII

**Figure S 5.** UV-vis spectra of **1-dn<sup>4+</sup>** and **2-dn<sup>4+</sup>** in 0.1 M HOTf.

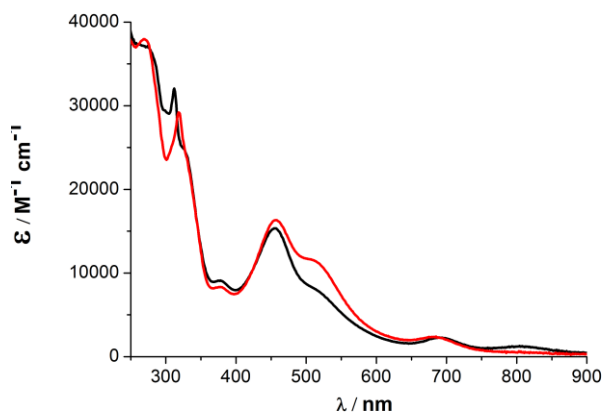


**Table S 1.** UV-vis spectroscopic signatures of dinuclear complexes in 0.1 M HOTf.

Complex	Oxidation State	$\lambda$ ( $\epsilon$ ) / nm ( $M^{-1} cm^{-1}$ )
<b>1-dn<sup>4+</sup></b>	IV,IV	274 (37000), 312 (32000), 378 (9000), 455 (15300), 515sh (8000), 691 (2200)
	III,III	445 (5200), 638sh (10400), 684 (13100)
<b>2-dn<sup>4+</sup></b>	IV,IV	268 (3800), 317 (29200), 379 (8300), 457 (16300), 511sh (11500), 682 (2400)

**Figure S 6.** RR monitoring of the reaction of 2 (red) or 3 (black) equivalents of CAN with a 1 mM solution of  $\mathbf{2}^{2+}$  in 0.1 M HOTf immediately (upper) or 20 hours after the addition of CAN (bottom).

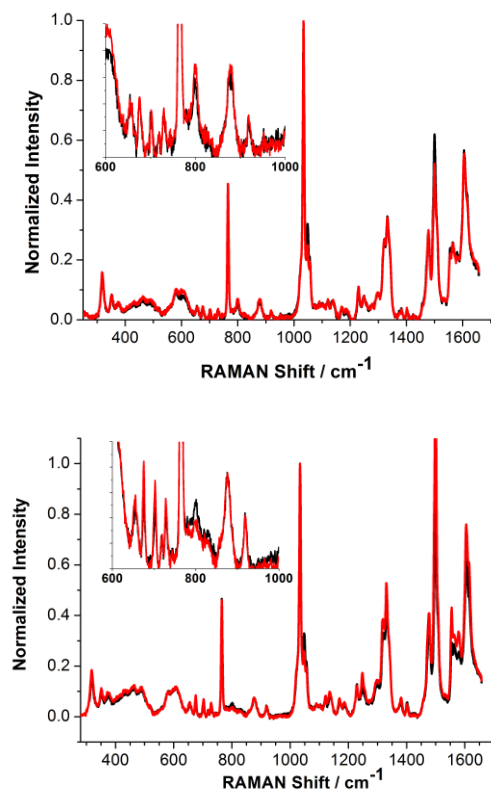


**Figure S 7.** Spectroscopic rRAMAN monitoring of the reaction of 100 equivalents of CAN with a 1 mM solution of  $\mathbf{2}^{2+}$  in 0.1 M HOTf.

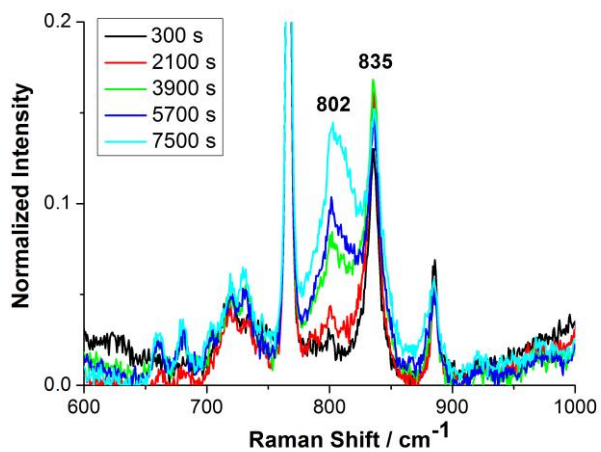


**Table S 2.** Crystal data for the oxidation state IV of  $2^{2+}$ .

Empirical formula	C <sub>25</sub> H <sub>19</sub> F <sub>14</sub> N <sub>5</sub> O <sub>2</sub> P <sub>2</sub> Ru
Formula weight	850.46
Temperature	100(2)K
Wavelength	0.71073 Å
Crystal system	Triclinic
Space group	P-1
Unit cell dimensions	a = 8.5407(7) Å $\alpha$ = 88.479(5) ° b = 12.7401(9) Å $\beta$ = 79.089(4) ° c = 13.6574(13) Å $\gamma$ = 79.697(5) °
Volume	1435.6(2) Å <sup>3</sup>
Z	2
Density (calculated)	1.967 Mg/m <sup>3</sup>
Absorption coefficient	0.786 mm <sup>-1</sup>
F(000)	840
Crystal size	0.20 x 0.10 x 0.01 mm <sup>3</sup>
Theta range for data collection	1.62 to 27.63 °
Index ranges	-11 <=h<=11, -16 <=k<=16, -17 <=l<=17
Reflections collected	15045
Independent reflections	6622 [R(int) = 0.1054]
Completeness to theta =27.63 °	0.991 %
Absorption correction	Empirical
Max. and min. transmission	0.9922 and 0.8586
Refinement method	Full-matrix least-squares on F <sup>2</sup>
Data / restraints / parameters	6622 / 3 / 448
Goodness-of-fit on F <sup>2</sup>	1.014
Final R indices [ $I > 2\sigma(I)$ ]	R1 = 0.0661, wR2 = 0.1575
R indices (all data)	R1 = 0.0955, wR2 = 0.1862
Largest diff. peak and hole	2.113 and -2.154 e.Å <sup>-3</sup>



**Figure S 8.** Online MS monitoring of the composition of the gas phase in the catalytic reactions of 1 mM solutions of complex **1-dn**<sup>4+</sup> (upper) and **2-dn**<sup>4+</sup> (bottom) in 0.1 M HOTf at RT.

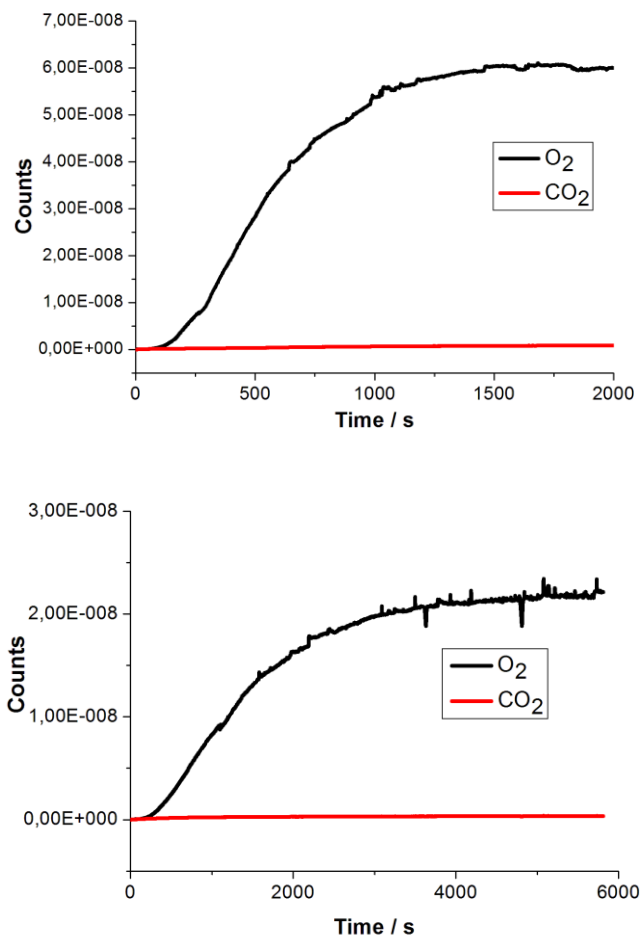


**Figure S 9.** Overlay of UV-visible spectra of a 1 mM solution of the dinuclear complex **2-dn<sup>4+</sup>** in 0.1 M HOTf before (black) and after oxygen evolution induced by the addition of 100 equivalents of CAN (red). The samples were previously 100 times diluted.

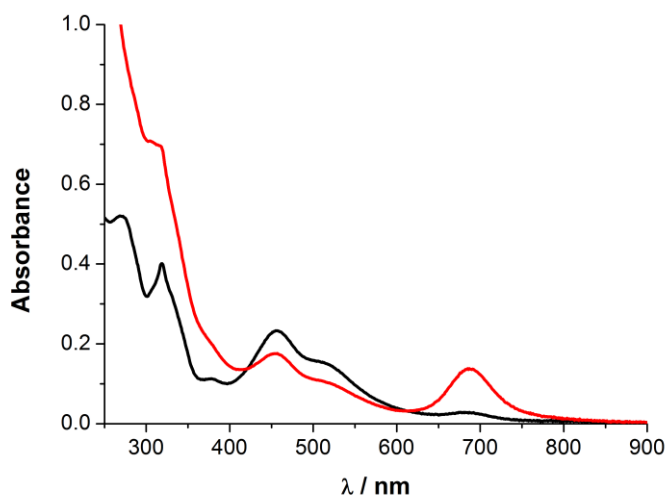
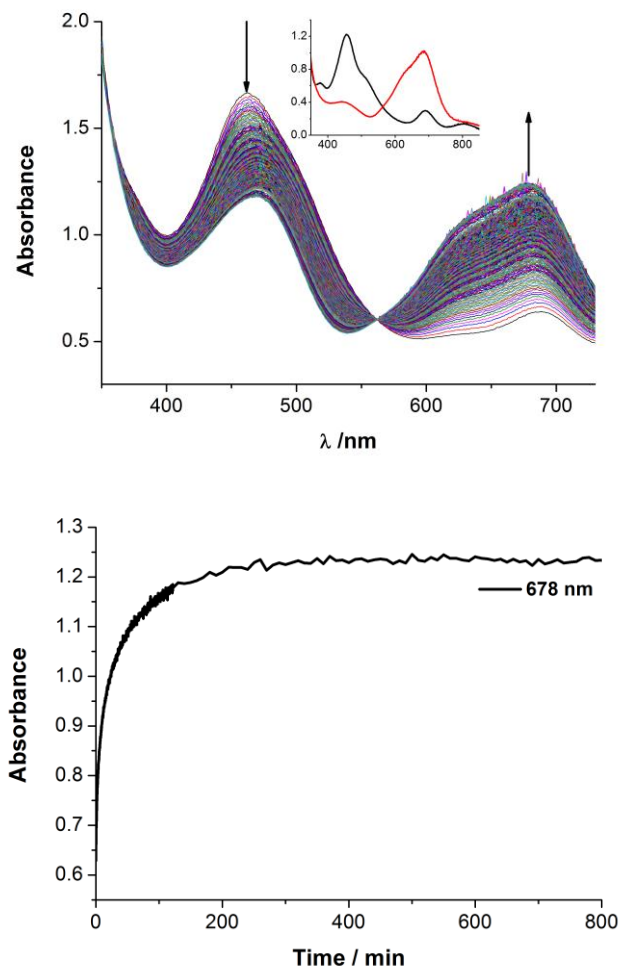


**Figure S 10.** (Upper) UV-vis time-course of the 1:1 reaction of 0.5 mM solutions of **1-dn**<sup>4+</sup> and **1**<sup>2+</sup> in 0.1 M HOTf at 25°C. The inset shows the UV-vis spectra for the oxidation states IV,IV (black) and III,III (red) of **1-dn**<sup>4+</sup> in the same solvent. (Bottom) Absorption vs. time profile at 678 nm indicating the formation of the oxidation state III,III. A 2 mm path length quartz cuvette was used.



---

## ***Chapter 8. Summary and Conclusions.***



---

“The absolute truth is never achieved, but you never are completely away from it”.

*Aristotle, Greek Philosopher.*

---

UNIVERSITAT ROVIRA I VIRGILI

WATER OXIDATION WITH MONONUCLEAR RU COMPLEXES. BELOW THE TIP OF THE

ICEBERG: THE OXO-BRIDGE SCENARIO

Isidoro López Marin

Dipòsit Legal: T. 1505-2013

The contribution of this thesis to the field of single-site water oxidation catalysts can be summarized as follows:

### Chapter 3.

- The tetradentate ligand 2,7-bipyridil-1,8-diazaanthracene (bipan) has been successfully prepared by means of a six steps synthesis and characterized by  $^1\text{H-NMR}$  and single crystal XRD.
- The two new stereoisomeric chloro mononuclear Ru complexes containing the bipan ligand *in*-[Ru(trpy)(bipan)Cl] $^+$  (**1-*in* $^+$** ) and *out*-[Ru(trpy)(bipan)Cl] $^+$  (**1-*out* $^+$** ) have been synthesized and fully characterized by the usual analytical, spectroscopic and electrochemical techniques. Furthermore, the structure of the *out*-isomer could be confirmed by single crystal XRD.
- The difference in the Ru(III/II) standard potentials for the two isomers is lower than in previous structurally related complexes. This feature is due to the particular electronic distribution in the bipan ligand.
- The *in*- isomer is a good catalyst for water oxidation whereas the *out*-isomer exhibits a poor activity because it is insoluble under catalytic conditions.

### Chapter 4.

- The two new aquo mononuclear Ru complexes [Ru $^{\text{II}}$ (trpy)(5,5'-F $_2$ -bpy)(H $_2$ O)] $^{2+}$  (**5 $^{2+}$** ) and [Ru $^{\text{II}}$ (trpy)(6,6'-F $_2$ -bpy)(H $_2$ O)] $^{2+}$  (**6 $^{2+}$** ) have been prepared and thoroughly characterized by the usual analytical, spectroscopic and electrochemical techniques.
- The electrochemical and acid/base properties of the new compounds were compared with that from the parent compound [Ru $^{\text{II}}$ (trpy)

(bpy)(H<sub>2</sub>O)]<sup>2+</sup> (**2**<sup>2+</sup>). The electron-withdrawing effect of the F atoms in **5**<sup>2+</sup> decreases the pK<sub>a,II</sub> by 0.8 log units with regard to **2**<sup>2+</sup>, in contrast the pK<sub>a,II</sub> of **6**<sup>2+</sup> is increased 0.6 log units because hydrogen bonding of the aquo ligand with the nearby F atom.

- The complexes were evaluated as WOCs. The initial turn over frequency (TOFi) decreases by a factor near to 4 when comparing **2**<sup>2+</sup> and **5**<sup>2+</sup> (the purely electronic scenario), and by a factor bigger than 2 when comparing **5**<sup>2+</sup> and **6**<sup>2+</sup> (the purely hydrogen-bonding scenario).
- Kinetic studies establish a rate determining step where the [Ru<sup>IV</sup>-OO]<sup>2+</sup> intermediate is oxidized to [Ru<sup>V</sup>-OO]<sup>2+</sup> and is preceded by a fast equilibrium step involving the oxidation of [Ru<sup>V</sup>=O]<sup>3+</sup> to [Ru<sup>IV</sup>-OO]<sup>2+</sup>.

## Chapter 5.

- The new dinuclear oxo bridge Ru complexes [(trpy)(5,5'-X<sub>2</sub>-bpy)Ru<sup>IV</sup>(μ-O)Ru<sup>IV</sup>(trpy)(O)(H<sub>2</sub>O)]<sup>4+</sup> (X = H for **1**<sup>4+</sup> and X = F for **2**<sup>4+</sup>) were prepared and fully characterized by analytic, spectroscopic and electrochemical techniques as well as by single crystal XRD. The compounds contain an oxo terminal ligand defined by the short Ru-O distance.
- The new complexes are robust and active electrocatalysts for water oxidation.
- DFT calculations provide a complete catalytic cycle where the rds is the O-O bond formation step through water nucleophilic attack to the intermediate [Ru<sup>IV</sup>-O-Ru<sup>V</sup>(O)(OH)]<sup>4+</sup>.
- The mononuclear Ru complexes [Ru<sup>II</sup>(trpy)(bpy)(H<sub>2</sub>O)]<sup>2+</sup> (**4**<sup>2+</sup>) and [Ru<sup>II</sup>(trpy)(5,5'-F<sub>2</sub>-bpy)(H<sub>2</sub>O)]<sup>2+</sup> (**5**<sup>2+</sup>) are converted into its dinuclear counterparts **1**<sup>4+</sup> and **2**<sup>4+</sup> respectively, under catalytic conditions as evidenced by rRAMAN spectroscopy and UV-vis

spectroelectrochemistry. The transformation is mediated by previous formation of  $[\text{Ru}^{\text{VI}}(\text{trpy})(\text{O})_2(\text{H}_2\text{O})]^{2+}$  (**3<sup>2+</sup>**). DFT calculations prove that this conversion is feasible.

## Chapter 6.

- The single crystal XRD structure of  $[(\text{trpy})(6,6'\text{-X}_2\text{-bpy})\text{Ru}^{\text{IV}}(\mu\text{-O})\text{Ru}^{\text{IV}}(\text{trpy})(\text{O})(\text{H}_2\text{O})]^{4+}$  (**3-dn<sup>4+</sup>**) has been successfully determined and compared with those from the previous described structurally related complexes.
- The new dinuclear oxo bridge Ru complex  $\{[\text{Ru}(\text{trpy})(\text{bpy})]_2(\mu\text{-O})\}^{4+}$  (**1-dm<sup>4+</sup>**) was synthesized and fully characterized by analytic, spectroscopic and electrochemical techniques as well as by single crystal XRD.
- **1-dm<sup>4+</sup>** is formed after catalytic water oxidation by the mononuclear complex  $[\text{Ru}^{\text{II}}(\text{trpy})(\text{bpy})(\text{H}_2\text{O})]^{2+}$  (**1<sup>2+</sup>**) when the sacrificial oxidant is depleted or the applied potential stopped. The conversion of **1<sup>2+</sup>** into **1-dm<sup>4+</sup>** occurs *via* previous formation of  $[(\text{trpy})(\text{bpy})\text{Ru}^{\text{IV}}(\mu\text{-O})\text{Ru}^{\text{IV}}(\text{trpy})(\text{O})(\text{H}_2\text{O})]^{4+}$  (**1-dn<sup>4+</sup>**) and coordination of free bipyridine ligand.
- **1-dm<sup>4+</sup>** can act as a WOC because the complex is partly transformed into **1-dn<sup>4+</sup>** under the oxidative catalytic conditions as found by rRAMAN spectroscopy. However, the main product after the oxidation is the one electron oxidized form **1-dm<sup>5+</sup>**, which was characterized by single crystal XRD.
- Attempts of crystallization of **1-dn<sup>4+</sup>** and **3-dn<sup>4+</sup>** in MeCN/Et<sub>2</sub>O solvent mixtures lead to the formation of the dinuclear complexes  $[(\text{trpy})(\text{bpy})\text{Ru}^{\text{III}}(\mu\text{-O})\text{Ru}^{\text{III}}(\text{trpy})(\text{CH}_3\text{CN})_2]^{4+}$  (**1-dn<sub>CH3CN</sub><sup>4+</sup>**) and  $[(\text{trpy})(6,6'$



$F_2\text{-bpy}Ru^{III}(\mu\text{-O})Ru^{III}(\text{trpy})(\text{CH}_3\text{CN})_2]^{4+}$  (**3-dn**<sup>4+</sup>). These compounds preserve the scaffold from **1-dn**<sup>4+</sup> and **3-dn**<sup>4+</sup> respectively, although in the oxidation state III,III.

- Attempts of crystallization of **1-dn**<sup>4+</sup>, **2-dn**<sup>4+</sup> and **3-dn**<sup>4+</sup> in MeCN/Et<sub>2</sub>O solvent mixtures also produced the tetranuclear oxo bridge Ru complexes  $\{[(\text{trpy})(\text{bpy})Ru^{II}(\mu\text{-O})Ru^{IV}(\text{trpy})(\text{CH}_3\text{CN})_2(\mu\text{-O})]^{6+}$  (**1-tn**<sup>6+</sup>),  $\{[(\text{trpy})(5,5'\text{-F}_2\text{-bpy})Ru^{III}(\mu\text{-O})Ru^{IV}(\text{trpy})(\text{CH}_3\text{COO})_2(\mu\text{-O})]^{6+}$  (**2-tn**<sup>6+</sup>) and  $\{[(\text{trpy})(6,6'\text{-F}_2\text{-bpy})Ru^{II}(\mu\text{-O})Ru^{IV}(\text{trpy})(\text{CH}_3\text{CN})_2(\mu\text{-O})]^{6+}$  (**3-tn**<sup>6+</sup>). A structural comparative study suggests that the metal coupling through the oxo bridge atoms is weak or negligible.
- Two new Ruthenium Red-type of complexes were successfully crystallized,  $\{[Ru^{III}(\text{trpy})(\text{bpy})(\mu\text{-O})]_2Ru^{IV}(\text{pic})_2\}^{4+}$  (**4**<sup>4+</sup>) and  $\{[Ru^{III}(\text{trpy})(\text{bpy})(\mu\text{-O})]_2Ru^{IV}(\text{trpy})(\text{H}_2\text{O})\}^{6+}$  (**5**<sup>6+</sup>). As in the previous case, the Ru-O bond distances indicate that the Ru centers coupling is weak or negligible.

## Chapter 7.

- The Pourbaix diagram of the dinuclear complex  $[(\text{trpy})(\text{bpy})Ru^{IV}(\mu\text{-O})Ru^{IV}(\text{trpy})(\text{O})(\text{H}_2\text{O})]^{4+}$  (**1-dn**<sup>4+</sup>) was built. The compound presents two 2-electrons PCET processes.
- The pK<sub>a</sub> for the oxidation state IV,IV of **1-dn**<sup>4+</sup> is slightly bigger than that from the complex  $[(\text{trpy})(5,5'\text{-F}_2\text{-bpy})Ru^{IV}(\mu\text{-O})Ru^{IV}(\text{trpy})(\text{O})(\text{H}_2\text{O})]^{4+}$  (**2-dn**<sup>4+</sup>) due to the electron-withdrawing effect exerted by the F atoms on the bipyridine ligand (pK<sub>a</sub> = 4.4 for **1-dn**<sup>4+</sup> and pK<sub>a</sub> = 4.0 for **2-dn**<sup>4+</sup>).
- rRAMAN experiments prove that the reaction of 2 and 3 equivalents of CAN with the mononuclear complexes  $[Ru^{II}(\text{trpy})(\text{bpy})(\text{H}_2\text{O})]^{2+}$  (**1**<sup>2+</sup>) or  $[Ru^{II}(\text{trpy})(5,5'\text{-F}_2\text{-bpy})(\text{H}_2\text{O})]^{2+}$  (**2**<sup>2+</sup>) generate the same spectroscopic

features, in clear contrast to the current accepted mechanism for single-site catalysts.

- rRAMAN monitoring of the reaction of 100 equivalents of CAN with  $\mathbf{1}^{2+}$  or  $\mathbf{2}^{2+}$  shows a characteristic resonance associated to  $[\text{Ru}^{\text{VI}}(\text{trpy})(\text{O})_2(\text{H}_2\text{O})]^{2+}$  ( $\mathbf{3}^{2+}$ ), confirming our mechanistic proposal about two intimately interconnected catalytic cycles where  $\mathbf{3}^{2+}$  plays the critical role of a *gate* giving access to the formation of  $\mathbf{1-dn}^{4+}$  or  $\mathbf{2-dn}^{4+}$ .
- The XRD structure of the oxidation state  $[\text{Ru}^{\text{IV}}=\text{O}]$  of  $\mathbf{2}^{2+}$  exhibits an elongation of the Ru-N bond *trans* to the oxo ligand, suggesting that bpy decoordination is a viable scenario for the formation of  $\mathbf{3}^{2+}$ .
- $\mathbf{1-dn}^{4+}$  and  $\mathbf{2-dn}^{4+}$  are active and rugged WOCs. UV-vis spectroscopy shows that the scaffold of the complexes is largely maintained after the catalysis.
- A synergic effect that speeds up the oxygen production was found between  $\mathbf{1}^{2+}$  and  $\mathbf{1-dn}^{4+}$ .

We have drawn a complete picture of dioxygen evolution from water by single-site catalysts. Our findings represent a revolutionary advance in the field in the sense that expands radically the current accepted mechanistic proposal.

UNIVERSITAT ROVIRA I VIRGILI

WATER OXIDATION WITH MONONUCLEAR RU COMPLEXES. BELOW THE TIP OF THE

ICEBERG: THE OXO-BRIDGE SCENARIO

Isidoro López Marin

Dipòsit Legal: T. 1505-2013

UNIVERSITAT ROVIRA I VIRGILI

WATER OXIDATION WITH MONONUCLEAR RU COMPLEXES. BELOW THE TIP OF THE

ICEBERG: THE OXO-BRIDGE SCENARIO

Isidoro López Marin

Dipòsit Legal: T. 1505-2013

*Appendix: Contributions to Congress*

---

***Appendix: Contributions to Congress.***

UNIVERSITAT ROVIRA I VIRGILI

WATER OXIDATION WITH MONONUCLEAR RU COMPLEXES. BELOW THE TIP OF THE


ICEBERG: THE OXO-BRIDGE SCENARIO

Isidoro López Marin

Dipòsit Legal: T. 1505-2013

Solar H<sub>2</sub>-European Project Meeting. Cambrills (Spain), 2009.


## O-O Bond Formation Strategies with Ru<sub>2</sub>-complexes



ICIQ

S. Romain,<sup>1</sup> F. Bozoglian,<sup>1</sup> S. Röser,<sup>1</sup> N. Planas,<sup>1</sup> C. D'Inoi,<sup>1</sup> I. Lopez,<sup>1</sup> C. Di Giovanni,<sup>1</sup>  
 L. Vaquer,<sup>1</sup> J. Mola,<sup>3</sup> L. Francàs,<sup>2</sup> X. Sala,<sup>1</sup> A. Llobet<sup>1,2</sup>

<sup>1</sup>Institut Català d'Investigació Química (ICIQ), Av. Països Catalans, n°16, E-43007, Tarragona, Spain  
<sup>2</sup>Departament de Química, Universitat Autònoma de Barcelona, Bellaterra, E-08193, Barcelona, Spain  
<sup>3</sup>Departament de Química, Universitat de Girona, E-17003, Girona, Spain  
 allobet@iciq.es



SOLAR-H

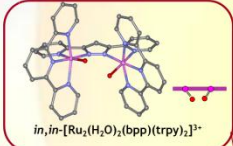
### Introduction

The biological generation of dioxygen from water during photosynthesis (eq 1) occurring through photosystem II (PSII) is one of the most important and fundamental chemical processes in nature. In PS II, this four-electron oxidation is catalyzed by the Oxygen Evolving Center (OEC) containing a manganese tetramer associated with Ca<sup>2+</sup> and Cl<sup>-</sup> ions.<sup>1</sup>

$$2 \text{H}_2\text{O} \rightarrow \text{O}_2 + 4\text{H}^+ + 4\text{e}^- \quad (\text{eq.1})$$

To mimic this natural active center, many complexes have been synthesized. However, few of them are capable of catalytically oxidizing water to molecular dioxygen<sup>2</sup>. Among these, dinuclear Ru polypyridyl complexes with different bridging ligands present the best performance. The majority of these Ru complexes are based on the system Ru-OH<sub>2</sub>/Ru=O.<sup>3</sup> In the present work we describe a family of RuII complexes, active toward water oxidation, focusing on different possible mechanistic pathways.

### Ruthenium catalysts studied and their possible reaction mechanisms



*in,in*-[Ru<sub>2</sub>(H<sub>2</sub>O)<sub>2</sub>(bpp)(trpy)]<sup>3+</sup>

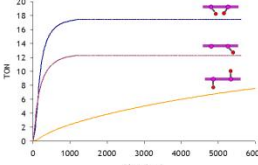
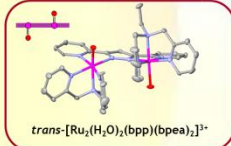


Figure 2: Catalytic performance of *in,in*-Ru<sub>2</sub>(H<sub>2</sub>O)<sub>2</sub> and *trans*-Ru<sub>2</sub>(H<sub>2</sub>O)<sub>2</sub> under identical reaction conditions.

Cat	TON	Initial O <sub>2</sub> formation rate (mol.s <sup>-1</sup> )
<i>in,in</i> -Ru <sub>2</sub> (H <sub>2</sub> O) <sub>2</sub>	18.6	9.0·10 <sup>-4</sup>
<i>out</i> -Ru <sub>2</sub> (H <sub>2</sub> O) <sub>2</sub>	14.0	9.0·10 <sup>-4</sup>
<i>trans</i> -Ru <sub>2</sub> (H <sub>2</sub> O) <sub>2</sub>	11.2	8.0·10 <sup>-4</sup>



*trans*-[Ru<sub>2</sub>(H<sub>2</sub>O)<sub>2</sub>(bpp)(bpea)]<sup>3+</sup>

**Homogeneous**

☹ + ☹ → ☺ = ☺

**Heterogeneous**

**Intramolecular**

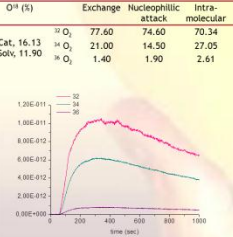
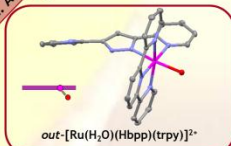


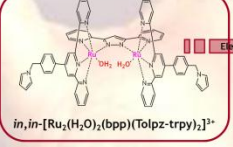
Figure 1: Mass spectra obtained during the first turnover and relative intensity of the ratio <sup>10</sup>/<sup>100</sup>.

**Bimolecular or Nucleophilic attack**



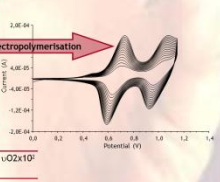
*out*-[Ru<sub>2</sub>(H<sub>2</sub>O)<sub>2</sub>(Hbpp)(trpy)]<sup>3+</sup>

**Intramol.**



*in,in*-[Ru<sub>2</sub>(H<sub>2</sub>O)<sub>2</sub>(bpp)(Tolpz-trpy)]<sup>3+</sup>

**Nucleoph. attack?**

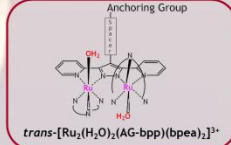


Electropolymerisation

**Intramol.**

Cat	nmols Ru	nmols Ce(IV)	Ratio	TON	λO <sub>2</sub> ·10 <sup>4</sup>
FTO/poly-(3-co-4)	0.5	1.8	3600	250	1.1

**Anchoring Group**



*trans*-[Ru<sub>2</sub>(H<sub>2</sub>O)<sub>2</sub>(AG-bpp)(bpea)]<sup>3+</sup>

### Conclusions

A family of mono- and dinuclear polypyridyl ruthenium complexes has been synthesized and thoroughly characterized. We put in evidence that through the choice of appropriate ligands, the mechanistic pathway of O-O bond formation can be influenced. Some more experiments are in progress, in order to determine the nature of the "intermediates" involved.


### References

- Yano, J.; Kern, J.; Sauer, K.; Latimer, M. J.; Pushkar, Y.; Blesiadka, J.; Loll, B.; Seeger, W.; Messinger, J.; Zouni, A.; Yachandra, V. K. *Science*, 2006, 314, 821.
- Romero, I.; Rodríguez, M.; Serró, C.; Mola, J.; Saso Kollipara, M. R.; Francàs, L.; Mas-Marzá, E.; Escriche, L.; Llobet, A. *Inorg. Chem.* 2008, 47, 1815-1823.
- Huyth, M. H. B.; Meyer, T. J. *Chem. Rev.* 2007, 107, 5004.
- Romain, S.; Bozoglian, F.; Sala, X.; Llobet, A. *J. Am. Chem. Soc.*, 2009, 131(8), 2769-2769.
- Mola, J.; Mas-Marzá, E.; Sala, X.; Romero, I.; Rodríguez, M.; Parella, T.; Llobet, A. *Angew.*, 2008, 47, 5830.
- Mola, J.; D'Inoi, C.; Sala, X.; Romero, I.; Rodríguez, M.; Parella, T.; Fontrodona, X.; Llobet, A. submitted.

### Acknowledgments

Support from MEC of Spain (CSO2006-0003, CTQ2007-67918, CTQ2007-60476/PPQ), from Generalitat de Catalunya through the SGR program, SOLARH2 and from ICIQ are gratefully acknowledged.


Solar H<sub>2</sub>-European Project Meeting. Berlin (Germany), 2010.



**ICIQ**

## Complexes of Ru and Mn as Water Oxidation Catalyst

Isidoro López, Somnath Maji, Sukanta Mandal and Antoni Llobet  
 Institut Català d'Investigació Química (ICIQ), Av. Països Catalans, n°16, E-43007, Tarragona, Spain  
 allobet@iciq.es



### Introduction

The biological generation of dioxygen from water during photosynthesis (eq 1) occurring through photosystem II (PSII) is one of the most important and fundamental chemical processes in nature. In PS II, this four-electron oxidation is catalyzed by the Oxygen Evolving Center (OEC) containing a manganese tetramer associated with Ca<sup>2+</sup> and Cl<sup>-</sup> ions.<sup>1</sup>

$$2 \text{H}_2\text{O} \rightarrow \text{O}_2 + 4\text{H}^+ + 4\text{e}^- \quad (\text{eq. 1})$$

To mimic this natural active center, many complexes have been synthesized. However, few of them are capable of catalytically oxidizing water to molecular dioxygen<sup>2</sup>. Most of them are mononuclear and dinuclear complexes of Ruthenium and Manganese. In the present work, we study the catalytic activity of several complexes to gain insight into the relationship between structure and activity.

### Mononuclear Complexes

	2.682 Å	2.695 Å	2.533 Å	
X-Ray Structures				
	[Ru(tpyy)(bpy)(H <sub>2</sub> O)] <sup>2+</sup>	[Ru(tpyy)(Fbpy)(H <sub>2</sub> O)] <sup>2+</sup>	[Ru(tpyy)(Mebpy)(H <sub>2</sub> O)] <sup>2+</sup>	[Ru(tpyy)(MebpyCOO)] <sup>+</sup>
Oxygen Evolution <sup>a</sup>	17 TONs	2.5 TONs	No O <sub>2</sub> Evolution	No O <sub>2</sub> Evolution
	Only O <sub>2</sub> Production	Ratio O <sub>2</sub> /CO <sub>2</sub> at 22 min. =12.8	No O <sub>2</sub> Evolution	No O <sub>2</sub> Evolution
	😊☹️	😊☹️	😞😞	😞☹️

### Polynuclear Complexes

X-Ray Structures			
	<i>m,n</i> -[[Ru(tpyy)(H <sub>2</sub> O)] <sub>2</sub> (μ-bpp)] <sup>2+</sup>	[[Ru(tpyy)] <sub>2</sub> (μ-bpp)(μ-OAc)] <sup>2+</sup>	[[Ru(tpyy)]Mn(tpyy)(μ-Cl)] <sup>2+</sup>
Oxygen Evolution <sup>a</sup>	18.3 TONs	17.9 TONs	?
	Only O <sub>2</sub> Production		Makes O <sub>2</sub> !
	😊☹️	😊☹️	😊☹️

<sup>a</sup>Activity was quantified by means of manometric measures. Complex (1 mM) was dissolved in 1.850 mL of 0.1 M Triflic Acid (pH=1.1) and an excess of 100 equivalents of Cerium (IV) ammonium nitrate (dissolved in 150 μL of Triflic Acid) was added. The higher possible turnover is TON=25. Evolved gases was analyzed by Mass Spectrometry under the same conditions.

### Conclusions

A family of mono- and polynuclear polypyridyl ruthenium and Manganese complexes has been synthesized and tested as water oxidation catalyst. In the case of the mononuclear complexes, we put in evidence that through the choice of appropriate ligands, the activity is radically modified.

Some more deep experiments are in progress in order to determinate the most influential elements in the catalytic activity for water oxidation.

### References

- 1) Yano, J.; Kern, J.; Sauer, K.; Latimer, M. J.; Puhkar, Y.; Blesiadka, J.; Loll, B.; Saenger, W.; Messinger, J.; Zouni, A.; Yachandra, V. K. *Science*, 2006, 314, 821.
- 2) Sala, X.; Romero, I.; Rodriguez, M.; Escriche, LL.; Llobet, A. *Angew Chem. Int. Ed.* 2009, 48, 2-13.
- 3) Qvortrup, K.; McKenzie, C. J.; Bond, A. D. *Acta Cryst.* 2007, 63, 1400-1401

### Acknowledgments

Support from MEC of Spain (CSO2006-0003, CTQ2007-67918, CTQ2007-60476/PPQ), from Generalitat de Catalunya through the SGR program SOLARH2 and from ICIQ are gratefully acknowledged.

1<sup>st</sup> Proton Coupled Electron Transfer Congress. Chaveignes ( France ), 2011.

New Polypyridilic Ruthenium Complexes As Water Oxidation Catalysts



Isidoro López<sup>a</sup>, Somnath Maji<sup>a</sup>, Sven Neudeck<sup>b</sup>, Franc Meyer<sup>b</sup> and Antoni Llobet<sup>a</sup>

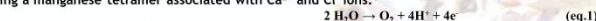
<sup>a</sup>Institut Català d'Investigació Química (ICIQ), Av. Països Catalans, n°16, E-43007, Tarragona, Spain

<sup>b</sup>Institut für Anorganische Chemie, Georg-August-Universität Göttingen, Tammannstraße, 4, 37007, Göttingen, Germany

allobet@icq.es

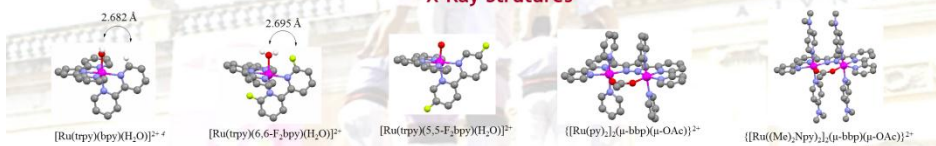
Introduction

The biological generation of dioxygen from water during photosynthesis (eq 1) occurring through photosystem II (PSII) is one of the most important and fundamental chemical processes in nature. In PS II, this four-electron oxidation is catalyzed by the Oxygen Evolving Center (OEC) containing a manganese tetramer associated with Ca<sup>2+</sup> and Cl<sup>-</sup> ions.<sup>1</sup>



To mimic this natural active center, many complexes have been synthesized. Although several of them are capable of catalytically oxidizing water to molecular dioxygen<sup>2</sup>, the catalytic mechanism is known only in some Ruthenium Complexes<sup>3</sup>. In the present work, we study the catalytic activity of several complexes to gain insight into the relationship between structure and catalytic mechanism.

X-Ray Structures



Electrochemical Properties

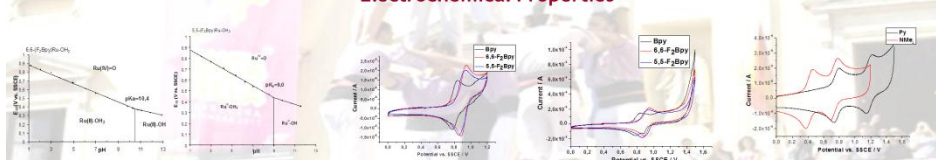


**Figure 1.** Pourbaix Diagrams for complexes [Ru(trpy)(6,6-F<sub>2</sub>-bpy)(H<sub>2</sub>O)]<sup>2+</sup> and [Ru(trpy)(5,5-F-bpy)(H<sub>2</sub>O)]<sup>2+</sup>. E<sub>1/2</sub>(V) taken from CV (0-0.1 M, glassy carbon working electrode, scan rate=100 mV/s).

**Figure 2.** Cyclic Voltammograms of 1 mM complex solutions in 0.1 M CF<sub>3</sub>SO<sub>3</sub>H, pH=1 (scan rate=100 mV/s, glassy carbon working electrode).

**Figure 3.** Cyclic voltammetry of dinuclear complexes in CH<sub>2</sub>Cl<sub>2</sub> (Bu<sub>4</sub>NPF<sub>6</sub>, 0.1 M, scan rate=100 mV/s, glassy carbon working electrode).

H-bond between the aquo ligand and the F atom of the bipyridine in 6,6-F<sub>2</sub>-BpyRu-OH<sub>2</sub> complex makes the deprotonation harder than in the case of 5,5-F<sub>2</sub>-BpyRu-OH<sub>2</sub> and even in BpyRu-OH<sub>2</sub> (pK<sub>a</sub>≈9.7).  
 As expected 5,5-F<sub>2</sub>-BpyRu-OH<sub>2</sub> has a pK<sub>a</sub> value smaller than BpyRu-OH<sub>2</sub> because the electro-withdrawing F atom.

6,6-F<sub>2</sub>-BpyRu-OH<sub>2</sub> and 5,5-F<sub>2</sub>-BpyRu-OH<sub>2</sub> present a two electron wave for the Ru(IV)/Ru(II) couple at lower E<sub>1/2</sub> than the Ru(IV)/Ru(II) couple of BpyRu-OH<sub>2</sub> complex. However, the onset of the catalytic water oxidation (associated to the Ru(V)/Ru(IV) couple) is lower in BpyRu-OH<sub>2</sub> (-1.1 V vs. SCE) than in 6,6-F<sub>2</sub>-BpyRu-OH<sub>2</sub> (-1.35 V vs. SCE) and 5,5-F<sub>2</sub>-BpyRu-OH<sub>2</sub> (-1.35 V vs. SCE).

Electron donating -NMe<sub>2</sub> groups decrease E<sub>1/2</sub> for the III(IV)/III and III(III)/II complexes respect to unsubstituted pyridines.

Catalytic Water Oxidation<sup>a</sup>

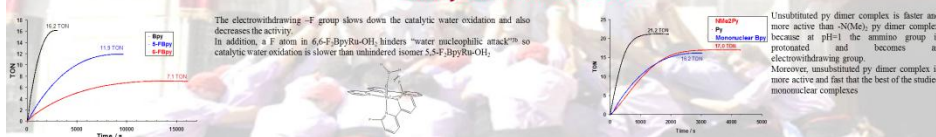


**Figure 5.** Catalytic water oxidation for the mononuclear complexes at 1 mM concentration in 0.1 M CF<sub>3</sub>SO<sub>3</sub>H at 25°C.

**Figure 6.** Catalytic water oxidation for the dinuclear complexes at 1 mM concentration in 0.1 M CF<sub>3</sub>SO<sub>3</sub>H at 25°C.

<sup>a</sup>Activity was quantified by means of manometric measures. Complex (1 mM) was dissolved in 1.850 mL of 0.1 M Triflic Acid (pH=1) and an excess of 100 equivalents of Cerium (IV) ammonium nitrate (solved in 150 µL of Triflic Acid) was added. The higher possible turnover is TOF=25. Evolved gases was analyzed by Mass-Spectrometry under the same conditions. In the case of dinuclear complexes, the catalytic reaction was carried out in 5 % (v/v) of CH<sub>2</sub>Cl<sub>2</sub> in 0.1 M Triflic acid due to solubility problems.

Conclusions

A family of mono- and dinuclear polypyridilic ruthenium complexes has been synthesised and tested as water oxidation catalyst. In the case of the mononuclear complexes, we put in evidence that through the choice of appropriate ligands, the activity is radically modified.

Some more deep experiments are in progress in order to determinate the most influential elements in the catalytic activity for water oxidation.

References

- 1) Unuma, Y.; Kawasumi, K.; Shen, J. R.; Kawanishi, S. *Nature*, 2011, 474, 821.
- 2) (a) Saha, X.; Romero, I.; Rodriguez, M.; Escobedo, J.; Llobet, A. *Angew Chem, Int. Ed.*, 2009, 48, 2-43; (b) Roman, S.; Vignola, J.; Llobet, A. *Acc. Chem. Res.*, 2009, 42, 1040-1051; (c) Durr, H.; Lammig, C.; Peter, T.; Bock, M.; Regus, S.; Steiner, F. *Chem. Commun.*, 2008, 7, 724-741; (d) Benisek, L.; Labadie, R.; Oghata, W.; Muehle-Bauer, H.; Vignola, J.; Llobet, A.; Albrecht, M. *Chem. Commun.*, 2011, 47, 8058-8060.
- 3) (a) Boiocchi, F.; Roman, S.; Estrem, M. Z.; Todros, T. K.; Sen, C.; Mola, J.; Rodriguez, M.; Romero, I.; Bosc-Bakkhal, J.; Fontrodona, J.; Cranner, C.; Oghata, L.; Llobet, A. *J. Am. Chem. Soc.*, 2009, 131, 15126-15137; (b) Concepcion, J. J.; Tam, M.-S.; Mielke, J. T.; Meyer, T. *J. Am. Chem. Soc.*, 2009, 131, 1545-1557; (c) Liu, F.; Concepcion, J. J.; Sen, S. W.; Cardelino, T.; Tomer, J. L.; Meyer, T. *J. Inorg. Chem.*, 2009, 47, 1727-1732.
- 4) Quastrop, K.; Mikkelsen, C. J.; Bond, A. D. *Acc. Chem. Res.*, 2007, 40, 1400-1411.
- 5) Takemachi, K.; Thompson, M. S.; Papp, D. W.; Meyer, T. *J. Inorg. Chem.*, 1994, 32, 1845.

Acknowledgments

Support from MICINN (CTQ2010-21497, Consolider-Ingenio 2010 (CSD2006-003) and Euro-investigacion, EU02009-04139, is gratefully acknowledged. It is grateful for a MICINN doctoral grant and SM for a Torres Quevedo grant.



UNIVERSITAT ROVIRA I VIRGILI

WATER OXIDATION WITH MONONUCLEAR RU COMPLEXES. BELOW THE TIP OF THE

ICEBERG: THE OXO-BRIDGE SCENARIO

Isidoro López Marin

Dipòsit Legal: T. 1505-2013

UNIVERSITAT ROVIRA I VIRGILI

WATER OXIDATION WITH MONONUCLEAR RU COMPLEXES. BELOW THE TIP OF THE

ICEBERG: THE OXO-BRIDGE SCENARIO

Isidoro López Marin

Dipòsit Legal: T. 1505-2013

UNIVERSITAT ROVIRA I VIRGILI

WATER OXIDATION WITH MONONUCLEAR RU COMPLEXES. BELOW THE TIP OF THE

ICEBERG: THE OXO-BRIDGE SCENARIO

Isidoro López Marin

Dipòsit Legal: T. 1505-2013